



**HAL**  
open science

# The role of subducting heterogeneities and fluids on the Northern Lesser Antilles margin deformation and seismogenesis

Kingsley Chimaobi Ezenwaka

► **To cite this version:**

Kingsley Chimaobi Ezenwaka. The role of subducting heterogeneities and fluids on the Northern Lesser Antilles margin deformation and seismogenesis. Earth Sciences. Université Côte d'Azur, 2023. English. NNT : 2023COAZ4054 . tel-04238234

**HAL Id: tel-04238234**

**<https://theses.hal.science/tel-04238234v1>**

Submitted on 12 Oct 2023

**HAL** is a multi-disciplinary open access archive for the deposit and dissemination of scientific research documents, whether they are published or not. The documents may come from teaching and research institutions in France or abroad, or from public or private research centers.

L'archive ouverte pluridisciplinaire **HAL**, est destinée au dépôt et à la diffusion de documents scientifiques de niveau recherche, publiés ou non, émanant des établissements d'enseignement et de recherche français ou étrangers, des laboratoires publics ou privés.



# THÈSE DE DOCTORAT

Le rôle des hétérogénéités et des fluides en subduction sur la déformation et la sismogenèse de la marge nord des Petites Antilles

**Kingsley Chimaobi EZENWAKA**

GéoAzur UMR 7329

**Présentée en vue de l'obtention du grade de docteur en Sciences de la Terre et de l'Univers d'Université Côte d'Azur**

**Dirigée par :** Boris Marcaillou

**Co-dirigée par :** Mireille Laigle

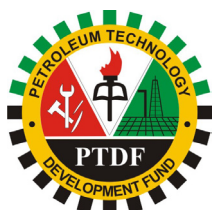
**Soutenue le :** 12.07.2023

**Devant le jury, composé de :**

Marc-André Gutscher, DR CNRS, Geo-Ocean Brest  
Mélody Philippon, McF HDR, Géosciences Montpellier, Université Antilles

Sylvie Leroy, DR CNRS, Istep Sorbonne Université Paris

Matthias Delescluse, McF HDR, ENS Paris



# **The role of subducting heterogeneities and fluids on the Northern Lesser Antilles margin deformation and seismogenesis**

**Thèse présentée devant le jury composé de**

Rapporteurs :

Marc-André Gutscher, DR CNRS, (UMR Geo-Ocean Brest) : Rapporteur

Mélody Philippon, McF HDR, (Géosciences Montpellier, Université Antilles) : Rapportrice

Examineurs :

Sylvie Leroy DR CNRS, (UMR Istep Sorbonne Université Paris) : Examinatrice

Matthias Delescluse McF HDR, (UMR Laboratoire de Géologie - ENS Paris) : Examineur

Directeur de thèse :

Boris Marcaillou, Professor, Université Côte d'Azur (UMR GeoAzur)

Mireille Laigle, DR CNRS (UMR GeoAzur)

## Résumé

La zone de subduction des Petites Antilles est considérée comme étant très hydratée et par conséquent très particulière. Cette thèse porte sur l'étude de l'impact des hétérogénéités structurales en subduction et de la circulation associée des fluides sur la déformation tectonique de la marge et l'activité sismique. Pour ce faire, des données sismiques multitraces à haute résolution, bathymétriques, de flux de chaleur et de sismicité acquises au cours des campagnes Manta-Ray, Antithesis et Sismantilles ont été utilisées. Les données de flux thermique révèlent l'advection de chaleur par des fluides liés à une circulation ventilée et isolée dans le nord et le centre des Petites Antilles respectivement, et mettent en évidence un contrôle thermique de la localisation de la sismicité. Ainsi, au large de Saint-Martin, les faibles valeurs du flux de chaleur dans la fosse et positives dans l'avant-arc, comparées aux valeurs conductrices globales, mettent en évidence la percolation descendante de fluides froids dans la fosse et la migration ascendante de fluides chauds dans l'avant-arc. À l'inverse, au large de la Martinique, un flux thermique positif dans la fosse révèle une migration ascendante de fluides chauds le long de l'interplaque jusqu'à la fosse. Les données de sismicité offshore montrent que la distribution des séismes de profondeurs intermédiaires est corrélée aux réactions de déshydratation profondes de la lithosphère plongeante. Ainsi, la migration de ces fluides vers la surface pourrait expliquer le faible couplage interplaque et la rareté des grandes ruptures cosismiques, favorisant des comportements de glissement lents à asismiques et augmentant le temps de retour des grands événements sismiques dans cette marge.

Les données sismiques et bathymétriques ont mis en évidence dans le nord des Petites Antilles un segment de croûte océanique, appelé "Jacksonville Patch", qui est en partie constitué de roches mantelliques exhumées et hydratées, formées le long de grandes failles de détachement. Ces failles pourraient avoir été réactivées lors de la flexure avant-fosse de la plaque plongeante, facilitant la percolation des fluides froids en profondeur et un nouvel épisode de serpentinitisation. La subduction de ce socle faillé, hydraté et serpentinitisé génère probablement une variation des propriétés mécaniques sur l'interplaque, pouvant également contribuer à expliquer la faible sismicité du méga-chevauchement.

Au nord de la ride de Barracuda, cette étude révèle par ailleurs une marge globalement érosive, avec des phases d'accrétion mineures qui diminuent vers le nord. L'érosion frontale est documentée par une diminution de la largeur du prisme vers le nord, probablement liée à la subduction des rides topographiques et un socle océanique rugueux dans une fosse dépourvue de sédiments. Au niveau de l'avant-arc, la distribution de failles normales subparallèles à la ride de Barracuda est cohérente avec l'âge Quaternaire de formation de ce relief sous le domaine avant-arc. Les failles imagées sont par ailleurs associées à des hauts de socle et sont profondément enracinées, potentiellement sur l'interplaque, formant des voies possibles de migration ascendante des fluides, potentiellement liés à la zone de fracture 15-20 en subduction. Les anomalies de flux de chaleur, les polarités inverses des réflecteurs, les figures de cheminées de fluides sur les profils, associés aux pockmarks et à des volcans de boue sur le plancher océanique concourent à souligner la circulation de fluides au travers de cette marge. Cette étude documente également une subsidence généralisée de la marge et un amincissement du socle qui est largement supérieure au déplacement le long des failles profondes. Ainsi, l'érosion tectonique basale long-terme de cette marge profondément fracturée semble dominée par la circulation de fluides libérés en profondeur par les portions de lithosphère océanique constituées

de manteau exhumé et par les zones de fracture, et aurait été récemment amplifiée par la déformation récente induite pas la ride de Barracuda formée depuis 2,3 millions d'années.

**Mots clés** : Zone de subduction, tectonique, sismogenèse, flux de chaleur, modélisation thermique, Petites Antilles.

## Abstract

At subduction zones, the nature of the subducting plate, fluid circulation, and temperature contribute significantly to the tectonic pattern and seismogenic potential. The Lesser Antilles is an end-member subduction zone, which undergoes the subduction of trans-oceanic fracture zones (FZ) bounded by topographic ridges, and large-scale patches of tectonically dominated oceanic crust that is prone to produce high water budget. This thesis focuses on investigating the impact of subducting heterogeneities and related fluid circulation on the margin tectonic deformation and seismic activity. For this purpose, newly and previously acquired multichannel (MCS) and high-resolution seismic, bathymetric, heat-flow, and seismicity data during the Manta-Ray, Antithesis, and Sismantilles campaigns were employed. The heat-flow data reveal heat advection by fluids related to a ventilated and an insulated circulation in the northern and central Lesser Antilles respectively, and further highlight the thermal control of seismicity location. Along Saint Martin, low heat-flow values in the trench and high values in the forearc compared to global conductive values highlight downward percolation of cold fluids in the trench and upward migration of warm fluids at the forearc. Contrastingly, along Martinique, high heat-flow values in the trench reveals warm fluid up dip migration along the plate interface from subduction depths up to the trench. There, the offshore seismicity data shows that the locations of the interplate, intraslab, and supraslab earthquakes have a close relationship with temperature dehydration reactions. Thus, the presence of fluids likely explains the low interplate coupling and the scarce large co-seismic ruptures, favouring aseismic slip behaviours, and increasing time return of large seismic events in this margin.

In addition, the MCS and bathymetric data in the northern Lesser Antilles imaged an oceanic tectonic fabric named the Jacksonville Patch, which is partly made of exhumed and hydrated mantle rocks, formed along pervasive detachment faults. During plate bending, the faults could be reactivated and allow deep fluid circulation and further serpentinization. The subduction of this faulted, hydrated and serpentinized basement likely generates interplate patchiness of contrasting frictional properties, which contributes to the megathrust weakness and low interplate seismicity.

North of the Barracuda ridge, this study further reveals a globally erosive margin, with minor accretion phases that decrease northwards. Evidence of frontal erosion is recorded by a northward decrease in the width of the prism favoured by the subduction of topographic ridges and a rough oceanic basement within a sediment-starved trench. At the forearc, normal faults subparallel to the southward sweeping Barracuda ridge, a Quaternary oceanic basement high, highlight its possible earliest onset beneath the forearc, at the eastern flank of the Antigua Valley. Some of the imaged faults are associated with basement highs and are deeply rooted, potentially down to the interplate, forming pathways for fluid upward migrations. Reverse polarity reflectors and fluid pipes, both collocated with pockmarks and mud-volcanoes on the seafloor, and with the 15-20 FZ at depth, highlight the potential of fluid flow occurrence at this margin forearc, in agreement with heat-flow observations. This study also documents widespread margin subsidence and basement thinning consistent with previous estimates north of the study area, which cannot be accounted for by the displacement along the deep-rooted faults. Thus, long-term basal tectonic erosion of this deeply fractured margin has been dominated by circulating fluids from subducted exhumed mantle patches and FZs as the

Fifteen-twenty, and has been recently increased by the uplift and southward sweeping of the ~ 2.3 Ma old Barracuda Ridge.

**Keywords:** Subduction zone, tectonics, seismogenesis, heat-flow, thermal modelling, Lesser Antilles.

## **Acknowledgements**

I would like to start by thanking the Petroleum Technology Development Fund (PTDF) of Nigeria, who in partnership with Campus France provided the funding of my studies. I am grateful for believing in me and awarding me the scholarship for my PhD.

Special thanks go to my supervisors, Boris Marcaillou and Mireille Laigle. Your support, encouragement and guidance throughout the period of my studies made a tremendous impact in my academics and has made me a better geoscientist. Working under your tutelage for the past three years, I could not have asked for better supervisors. Even though the start of my PhD was met with the covid pandemic and lockdowns, the numerous calls and check-ups from Mireille were priceless, and Boris volunteering to pick me at my apartment to the lab with him in his car, are days that I can never forget. Arriving from a foreign country, you made here feel like home. I want to thank you both for the opportunities and the amount of time that you constantly invested in me even with your busy schedules. You were always ready to listen to me and provide every assistance and directions necessary. I am grateful for the opportunity to be part of the MANTA-RAY oceanographic campaign. It was indeed a great learning moment for me, and an avenue to interact with many interesting scientists. For the references that you both provided for me that made me secure the SEG grant twice during my studies, I say a big thank you. I can say that I enjoyed beautiful relationships with you both that transcends academic or professional life, and for which I am very grateful.

My thanks go to Jean-Frederic Lebrun, Elia d'Acremont, and Frederique Leclerc for being part of my thesis committee. Thank you for all the suggestions and advise that helped me develop and improve the different segments of the thesis. I am also grateful for how quickly you always respond to my emails and agreeing to the fixing of our meetings even with your busy schedules.

Many thanks to you Laure Schenini for everything that you taught me about seismic processing using Geovation. You were always kind and available to listen and answer my numerous questions with a smile. I am very grateful that our paths crossed.

I want to thank all the scientific teams and engineers at Genavir with whom I embarked on the Manta-Ray cruise. I am grateful for all the times we shared and the scientific discussions that we had onboard. To Yannick, Estelle, Pauline and Laure with whom I shared most time with during the processing of the seismic data, thank you very much for everything that I learned from you.



My appreciation goes to every staff (permanent and contract), and students of GeoAzur lab for the great atmosphere and learning environment at the lab. Thank you, Alex, Albane, Sébastien, Sara, and numerous others too many to mention for all the good times, your explanations with administrative requirements, and interpretations where my French fails. I am very grateful to you Sébastien for the many times you brought me to the lab from Nice in your car during the strikes, and the times you did not allow me to sleep at the lab in the days I miss my bus working late.

Finally, my sincere gratitude goes to my entire family for all the love and support. To my wife Gabriella, thank you for all your understanding, encouragements and love especially during the stressful days. Big thanks to my parents Michael and Chikaodi Ezenwaka. Dad, it is sad that you are not here to see the end of my PhD, but all your advice were key to everything that I have accomplished, and I am very grateful for all the support I received from you growing up. Thank you, mum, for all your encouragements and prayers that has kept me going all these years. To my siblings, I love you all and I am grateful for your understanding and supports.

# Contents

|   |             |
|---|-------------|
| <b>Résumés</b>  | <b>ii</b>   |
| <b>Acknowledgements</b>   | <b>vi</b>   |
| <b>Contents</b>   | <b>viii</b> |
| <b>Chapter 1 Introduction</b>                                       | <b>1</b>    |
| 1.0 Thesis background .....   | 1           |
| 1.1 Thesis question and objectives .....                            | 5           |
| 1.2 Thesis plan .....   | 6           |
| 1.3 Subduction zones .....  | 7           |
| 1.4 Subduction zone geometry and tectonic deformations .....        | 10          |
| 1.4.1 Nature and structure of the oceanic crust .....               | 10          |
| 1.4.2 Tectonic accretion and erosion .....                          | 13          |
| 1.5 Seismic activities at subduction zones .....                    | 14          |
| 1.5.1 Seismic cycle .....   | 15          |
| 1.5.2 The seismogenic zone .....                                    | 15          |
| 1.5.3 Slab temperature and fluids .....                             | 17          |
| 1.5.4 The interplate patchiness .....                               | 17          |
| 1.6 Geodynamic context of the Lesser Antilles subduction zone ..... | 18          |
| 1.7 Seismic activity in the Lesser Antilles .....                   | 22          |
| 1.7.1 Geodetic coupling .....                                       | 22          |
| 1.7.2 Seismicity .....  | 23          |
| References .....  | 26          |
| <b>Chapter 2 Method of data acquisition and analysis</b>            | <b>40</b>   |
| 2.1 Dataset .....   | 40          |
| 2.2 MCS data processing .....                                       | 40          |
| 2.2.1 Resampling .....  | 43          |
| 2.2.2 Spherical divergence correction .....                         | 43          |
| 2.2.3 Noise Attenuation .....                                       | 44          |

|   |            |
|---|------------|
| 2.2.4 Surface related multiple and Adaptive model subtraction .....   | 45         |
| 2.2.5 Deconvolution .....   | 46         |
| 2.2.6 Velocity Analysis .....   | 48         |
| 2.2.7 Normal Move Out correction (NMO) .....  | 50         |
| 2.2.8 Dip Move Out correction (DMO) and stacking .....  | 50         |
| 2.2.9 Post-stack (f,k) time migration .....   | 52         |
| 2.3 Seismic interpretation methods .....  | 56         |
| 2.3.1 Structural Interpretations .....  | 56         |
| 2.3.2 Stratigraphic Interpretations .....   | 56         |
| 2.3.3 Seismic Attribute Analysis .....  | 57         |
| 2.4 Heat-flow data acquisition and thermal modelling .....  | 58         |
| References .....  | 68         |
| <b>Chapter 3 Nature of the oceanic crust, Fluid circulation and thermal structure<br/>of the margin</b>         | <b>73</b>  |
| 3.1 The nature of the subducting oceanic crust .....  | 73         |
| 3.2 Thermal structure and fluid circulation in the LA subduction zone .....                                     | 96         |
| <b>Chapter 4 The tectonic impact of fluids and subducting ridges on the Northern<br/>Lesser Antilles margin</b> | <b>126</b> |
| 4.1 Mechanism of subduction erosion at the Lesser Antilles subduction zone;<br>Ezenwaka et al., (in prep) ..... | 128        |
| Supplementary material for Ezenwaka et al., (in prep) .....   | 165        |
| <b>Chapter 5 Summary and Conclusions</b>  | <b>172</b> |
| 5.0.1 Tectonically-dominated oceanic crust in the Northern Lesser Antilles...                                   | 173        |
| 5.0.2 Thermal structure of the margin .....   | 173        |
| 5.0.3 Impact of subducting heterogeneities and associated fluids on<br>seismogenesis .....                      | 174        |
| 5.0.4 Tectonic impact of structural heterogeneities and associated fluids .....                                 | 175        |
| 5.1 Future work .....   | 177        |
| References .....  | 178        |

# Chapter 1

## Introduction

### 1.0 Thesis background

Subduction zones host most of the tectonic deformation and seismic activity in the world, making them excellent sites to investigate tectonic evolutions of our planet and telluric risks that threaten numerous populated coastal areas. At convergent margins, the forearc amongst other subduction zone morphologies reflects most of the subduction dynamics, and may be impacted by various geometrical and structural characteristics such as the slab dip (e.g. Hyndman & Wang, 1995; Lallemand et al., 2005; Gutscher et al., 2000; McCaffrey, 2009), the subduction obliquity (Chemenda et al., 2000; Laurencin et al., 2019), the nature and roughness of the subducting plate (e.g. Cloos, 1992; Ranero & Von Huene, 2000; Graindorge et al., 2008), the subducting sediment thickness (e.g. Tsuru et al., 2002; Clift & Hartley, 2007), and the pore or bound water content of the slab material (e.g. Calahorrano et al., 2008; Moreno et al., 2014; Hacker et al., 2003). For the latter, the thermal structure of the margin forms a key parameter, as thermally controlled metamorphic reactions of the oceanic plate (e.g. Peacock, 2001; Hacker et al., 2003) and mantle wedge materials (e.g. Ulmer & Trommsdorff, 1995; Ferrand, 2019) generate fluids, which may trigger upper plate deformation while percolating upwards. Depending on the impact of these features, tectonic deformation may be localized, generating phenomena such as accretion or tectonic erosion of the seaward edge of the forearc domain (e.g. Clift & Vannucchi, 2004). They may also be extensive, occurring over a large area, for instance, leading to the opening of back-arc basins such as the Lau Basin in New Zealand (Zellmer & Taylor, 2001). On the other hand, they may result in large megathrust seismic events and tsunamogenic hazards like the Mw 9.0 Tohoku event in 2011 (Hirose et al., 2011).

Most destructive seismic events that occur along subduction zones nucleate at the interface between the down-going and overriding plate. These events originate in a part of the megathrust known as the seismogenic zone, located at depths beneath the forearc. The magnitude of these events depends on the coseismic amount of slip and on the size of the rupture area, which in turn depends on the frictional properties of the interplate contact (e.g. McGarr & Fletcher, 2003). Amongst the parameters that controls the interplate seismic behaviours, temperature and fluids play a predominant role. The distribution of temperature along the plate interface may control the extent of the seismogenic limit of the megathrust (e.g. Hyndman et al., 1997), as the transition from stable sliding (aseismic) to stick-slip (seismic) behaviour could depend on

temperature (e.g. Moore & Saffer, 2001; Tse & Rice, 1986). Moreover, fluid circulation may affect the thermal and mechanical evolution of the interplate sliding behaviour, generating patchiness of contrasting frictional properties (e.g. Moreno et al., 2014), promoting moderate-sized-Mw, slow-slip and/or very low frequency earthquakes (Saffer & Wallace, 2015), and reducing the time return of large co-seismic ruptures.

In addition to fluids impacting the seismogenic behaviour along the megathrust, studies have shown that fluid circulation along the interplate can increase pore-fluid pressure (Moreno et al., 2014) and induce hydrofracturing of the upper plate (e.g. von Huene et al., 2004). Together with other subducting heterogeneities like seamount, ridges, horst and graben structures, fluids can dislodge upper plate materials, causing subduction erosion, and inducing subsidence of the forearc (e.g. Hilde, 1983; Von Huene & Culotta, 1989; Von Huene & Lallemand, 1990; Von Huene et al., 2004).

Thus, fluid play a significant role in impacting subduction dynamics. It is therefore important to investigate the processes by which fluids enter the subduction zone, and their role in seismic activities and tectonic deformation along subduction zones.

The Lesser Antilles subduction zone is one of the few areas in the world where oceanic crust formed at a slow-spreading Mid-Oceanic Ridge, hosting several fracture zones, and topographic ridges, is actively subducting. This endmember subduction zone is therefore a good site to make this kind of study. At the Lesser Antilles subduction zone, the North America Plate underthrusts the Caribbean Plate at a convergence rate of 20 mm/yr in a S74°W direction (DeMets et al., 2010). The convex shape of the Caribbean margin results in plate convergence obliquity that increases northwards from 0° offshore of the Central Lesser Antilles Islands to > 70° to the North of the Virgin Islands (Figure 1.0.1). To the West of Hispaniola, the subduction changes to a suture and strike-slip deformation. This convex shape of the margin results in a northward decrease in slab dip angle at shallow depths, from Barbuda to the Virgin Islands (Laurencin et al., 2018). The trench sediments thickness decreases drastically northwards from ~2 km in the Central Antilles (Pichot et al., 2012) to less than 0.5 km in the Northern Antilles (Laurencin et al., 2019). These features are likely to impact tectonic deformation patterns and seismicity at least in the Northern Lesser Antilles.

In addition, two topographic Barracuda and Tiburon Ridges, probably originated as flanking transforms at the Mid-Atlantic Ridge, and likely related to the North and South American plate boundary (Patriat et al., 2011) are obliquely oriented with respect to the convergence direction.

Their subducted portions are thus, sweeping southwards along the margin and impinging its whole structure at crustal scale. Subduction of these ridges likely impact tectonic deformation and seismic activities. The ridge imprint onto the forearc basins and spur has been investigated in the Central Antilles (De Min et al., 2015) and imaged at depth (Laigle et al., 2013) but remains widely unknown in the Northern margin segment. Thus, the evolution of the Barracuda Ridge beneath the forearc and its tectonic impact on the Northern Lesser Antilles margin needs to be investigated.

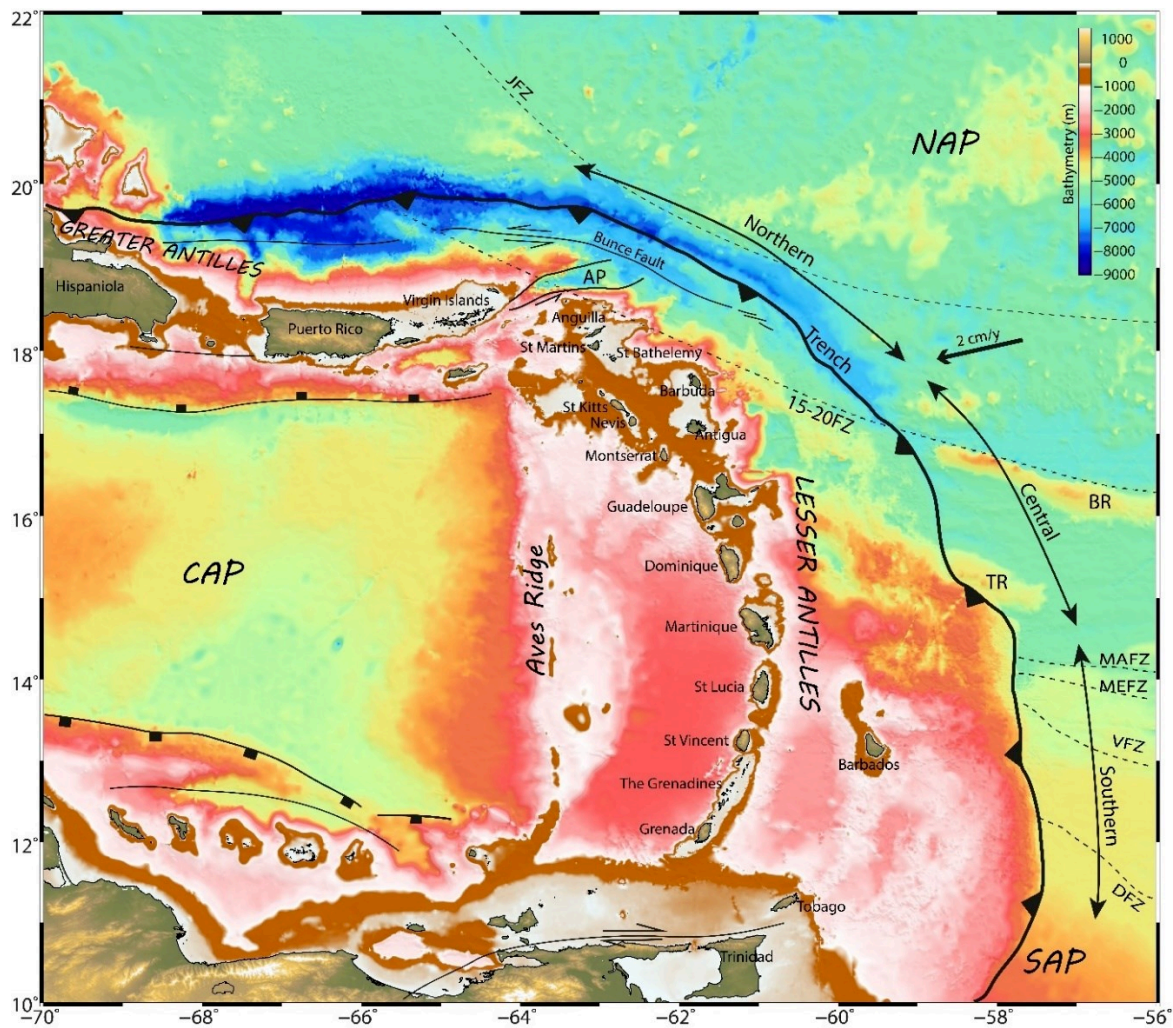


Figure 1.0.1: Bathymetric map of the eastern Caribbean plate and the Lesser Antilles subduction zone. The map shows the trench and major tectonic boundaries, the different fracture zones and the ridges of the oceanic lithosphere of the North and South American plates, the active internal arc and the inactive external arcs of the Caribbean Upper plate. CAP: Caribbean Plate, NAP: North American Plate, SAP: South American Plate, BR: Barracuda Ridge, TR: Tiburon Ridge, JFZ: Jacksonville Fracture zone, MAFZ: Marathon Fracture zone, MEFZ: Mercurius Fracture zone, VFZ: Vema Fracture zone, DFZ: Doldrums Fracture zone (after Cooper et al., 2020); Faults after (Feuillet et al., 2010; Gomez et al., 2018) ; Boucard et al., 2021); AP: Anegada Passage. Bathymetry and topography from GEBCO 2014 dataset. Map made with GMT.

The subducting oceanic basement formed at slow-spreading Mid-Atlantic Ridge, where episodic low magma production favours the formation of tectonically-dominated crust patches (e.g. Escartín et al., 2008). In these patches, the basement consists of discrete gabbro bodies hosted by hydrated mantle peridotite (Cannat, 1996), exhumed along detachment faults (Smith et al., 2006), and oceanic core complexes (e.g. Ildefonse et al., 2007). Moreover, trans-oceanic fracture zones, possibly highly hydrated, subduct below the forearc down to great depths (e.g. Copper et al., 2020; Paulatto et al., 2017; Schlarphorst et al., 2016; Bie et al., 2020). These features of the subducting crust signal a highly hydrated oceanic crust. At great depths in the subduction, increased temperature and pressure will become favourable for the release of fluids from the subducted crust through metamorphic dehydration (e.g. Hacker et al., 2003) and deserpentinization reactions (e.g. Wunder & Schreyer, 1997). This scenario will likely introduce an increased volume of fluids into the subduction system. The presence of these fluids in constant circulation will impact the thermal structure of the margin, and in-turn have an effect on the tectonic and seismogenic behaviour of this subduction zone.

Seismic activities recorded during the instrumental period in the Lesser Antilles subduction zone to date show very few interplate thrust earthquakes with magnitude greater than 5. Most of these events are aggregated in two nests; in the central Antilles and at the Virgin Island Platform, very few of them in the Saint Martin segment in between, raising the question of seismic gaps (Hayes et al., 2013). A study based on coral micro-atolls over the 20th century (Philibosian et al., 2022) propose that the Lesser Antilles subduction interface maybe coupled at large depths (30-70 km). Other studies based on geodetic data over the past 25 years reveal low interplate coupling, but suggest that a high interplate slip deficit may be the sign of a high seismogenic potential (Manaker et al., 2008), or strong interplate decoupling possibly leading to a very long interseismic phase (Symithe et al., 2015). However, recent geodetic studies (van Rijsingen et al., 2021; van Rijsingen et al., 2022) suggest a very low interplate coupling for the Lesser Antilles subduction zone. These uncertainties raise questions to the seismic potential of this margin especially in the Northern Lesser Antilles.

Indeed, fluids and temperature play a significant role in the seismogenic behaviour of the megathrust along subduction zones (e.g. Hyndman et al., 1993; Bangs et al., 2015). Moreover, the subduction of an oceanic basement at least partly made of serpentinite affects the crustal strength (e.g. Escartin et al., 1997; Escartín et al., 2001) and thus likely, the seismic behaviour of the megathrust. Therefore, it is necessary to investigate the thermal impact of circulating fluids along this subduction margin, its tectonic and seismic consequences, as well as those of

the subducting patches of tectonically-dominated crust and potentially weak and fluid-rich fracture zones.

### **1.1 Thesis questions and objectives**

The complex nature of the incoming oceanic plate along this obliquely subducting margin, and the different geodynamic characteristics that abound the Northern Lesser Antilles raise several questions addressed in this thesis.

1. How does fluid circulation occur in this subduction zone at;
  - a. The trench and oceanic domain
  - b. The forearc margin and the plate interface
2. What is the impact of fluid circulation on;
  - a. The thermal structure of the margin and seismogenesis
  - b. The margin's tectonic deformation
3. What are the tectonic consequences of the Barracuda Ridge on the margin's deformation?

To answer these questions, we have developed these specific objectives;

1. To investigate the nature and structures of the subducting oceanic crust at the Northern Lesser Antilles subduction zone.
2. Model the thermal state of the margin using heat-flow data as constraints. This will enable us to:
  - a. Identify the effects of the fluids on the thermal anomaly and locate areas with fluid circulation.
  - b. Estimate the temperatures along the plate interface and define the possible limits of the seismogenic zone.
  - c. Identify the depths of metamorphic dehydration and deserpentinization in the subduction zone.
  - d. Establish relationships between fluids, temperature, and seismicity in the subduction zone.
3. To assess the impact of circulating fluids and subducting Barracuda Ridge on the margin's tectonic deformations. This will be achieved by;
  - a. Mapping the fault-related structures on the seismic and bathymetric data.
  - b. Interpreting forearc stratigraphy and other subduction environments.



- c. Highlighting the tectonic imprints of the Barracuda Ridge from the seismic and bathymetric data.
- d. Describing the fluid migration pathways on the seismic data and fluid-related features on the seafloor.
- e. Drawing regional tectono-morpho-structural map and 3D models of the subduction zone.

In order to achieve these objectives, I have used multichannel seismic (MCS), bathymetric, heat-flow, and seismicity data acquired during 3 different oceanographic campaigns. The MCS and bathymetric data were acquired during the Antithesis 1 and 3 (Marcaillou & Klingelhoefer, 2013a; Marcaillou & Klingelhoefer, 2013b; Marcaillou & Klingelhoefer, 2016), Sismantilles 2 (Laigle et al., 2007), and Manta-Ray projects (Klingelhoefer & Marcaillou, 2022). They cover the central and northern Lesser Antilles from Martinique to Puerto Rico, and extend from the trench to the inner forearc. The seismicity data were obtained by a 5.5-year-long OBS deployment as part of the Sismantilles project (Laigle et al., 2007; Laigle et al., 2013; Ruiz et al., 2013). The heat-flow data was acquired during the Antithesis 3 campaign along two transects in the northern and central Antilles, that are perpendicular to the trench. More details about the datasets are provided in chapter 2.

## **1.2 Thesis plan**

To discuss effectively the different challenges and questions that we have raised, we structure this thesis into 5 chapters as follows:

The first chapter introduces the rationale behind this thesis and the main objectives that I adopt to answer the questions raised in the study area. This is followed by an overview of the recent knowledge of subduction zones, their geometries and the dominant characteristics that may impact their deformations and seismicity. I then review the geodynamics, tectonics, and seismic characteristics of the Lesser Antilles subduction zone in order to understand its evolution through time.

The second chapter describes the different datasets I have used for the study and their locations. This is followed by the MCS processing steps carried out to improve the overall quality of the imaged structures from sea-bottom to crustal depths, and the effects of the processing shown using data examples before and after the application of the procedures. The structural and stratigraphic interpretation workflow adopted for the MCS data is also provided. I conclude this

chapter with the method of the heat-flow data acquisition, and the process of 2D finite element method that we used for the thermal modelling.

Chapter three has two sections. The first section discusses the nature of the subducting oceanic crust and its impact on the megathrust seismogenic zone in the Northern Lesser Antilles. It is presented in the form of a paper published in *Nature Communications Earth and Environment* in 2021 and to which I participated (Marcaillou et al., 2021). The second section focuses on the modelling of the thermal structure of the margin I have carried out with heat-flow data. The results reveal the temperature along the plate interface, and the depths of metamorphic dehydration reactions. This is followed by describing interpreted fluid migrations within the subduction zone. I then conclude the chapter by establishing the relationship between fluids, temperature, and seismic activities in this subduction zone. This part of the work is also presented in the form a paper that is published on *EPSL* in 2022 (Ezenwaka et al., 2022).

After establishing the presence of fluids and their circulation, I proceed in the fourth chapter to investigate the impact of the circulating fluids on the tectonic deformations of the Lesser Antilles subduction zone. I show the tectonic deformation pattern based on interpretations from the MCS, High-resolution, and bathymetric data. In addition, the imprints of the subducting Barracuda Ridge and the extent of its impact on the margin deformation are also shown. With all this evidence, I document a dominant process of tectonic erosion in the Northern Lesser Antilles, and proposed a mechanism for the subduction erosion.

In the final chapter, I describe the most important outcomes of the studies carried out, highlight the contributions of this PhD research to the body of knowledge, and make propositions for future work.

### **1.3 Subduction zones**

At convergent plate boundaries, subduction zones are areas where lithospheric plates subduct beneath each other into the mantle (Figure 1.3.1). The subduction process is responsible for the recycling of oceanic lithospheres at depth, the creation of continental lithosphere by arc magmatism, and in maintaining convection processes in the mantle (Hofmann, 1997; Stern, 2010). During subduction, increasing temperature and pressure trigger dehydration reactions of the downgoing slab and subsequent release of fluids into the upper plate's mantle to cause partial melting. The generated magma rises vertically to the surface to form volcanic arcs along which new continental crusts form (e.g. Stern, 2002).

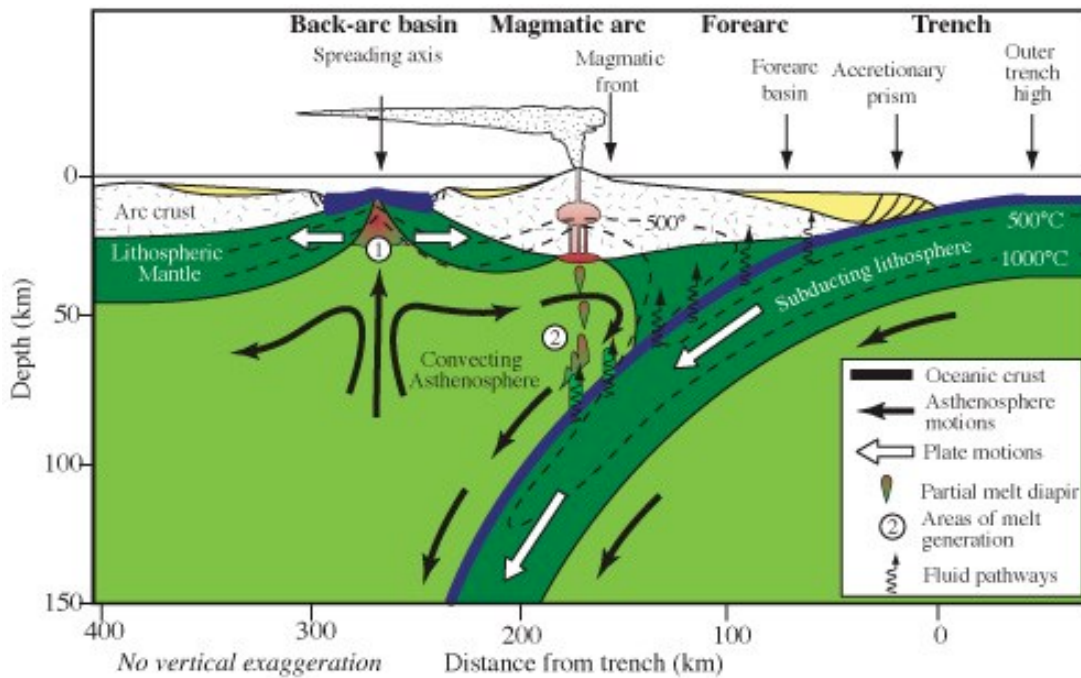


Figure 1.3.1: Cross-section of a subduction zone (Stern, 2002), showing the incoming oceanic crust subducting beneath the overlying plate. It also shows the different morphologies that forms along a convergent margin, which includes the trench, accretionary prism, forearc, volcanic arc, and the backarc domains.

A typical subduction zone model involves the sliding of a denser oceanic lithosphere beneath a less dense continental lithosphere at the trench (e.g. the subduction of the Nazca plate under the South America). This scenario accounts for 67% of subduction cases. Other types of subduction zone models include oceanic to oceanic convergence (e.g. subduction of the Pacific plate beneath the Philippine plate), which account for 15% of subduction type, and continent-to-continent subduction (e.g. the Indian and Eurasian plate subduction), that make up 17% of subduction zone. Altogether, subduction zones are located along 55,000 km of convergent plate boundaries (Lallemand, 1999) (Figure 1.3.2), which is almost equal in length to the mid-oceanic ridge with cumulative 60,000 km (Kearey et al., 2009).

Different structural units and morphologies make up the subduction zone, and they include; the plunging oceanic plate, the outer rise, the trench, the subduction channel, the accretionary prism, the forearc basin, the volcanic arc, and the backarc basin and the mantle wedge (Figure 1.3.1). The slab is the lithospheric plate that subducts at the point of convergence and is formed at a mid-oceanic ridge. Before reaching the trench, the slab flexes at the outer rise and is characterised by normal faults that develop between the outer rise and the trench due to plate bending (Ranero et al., 2003).

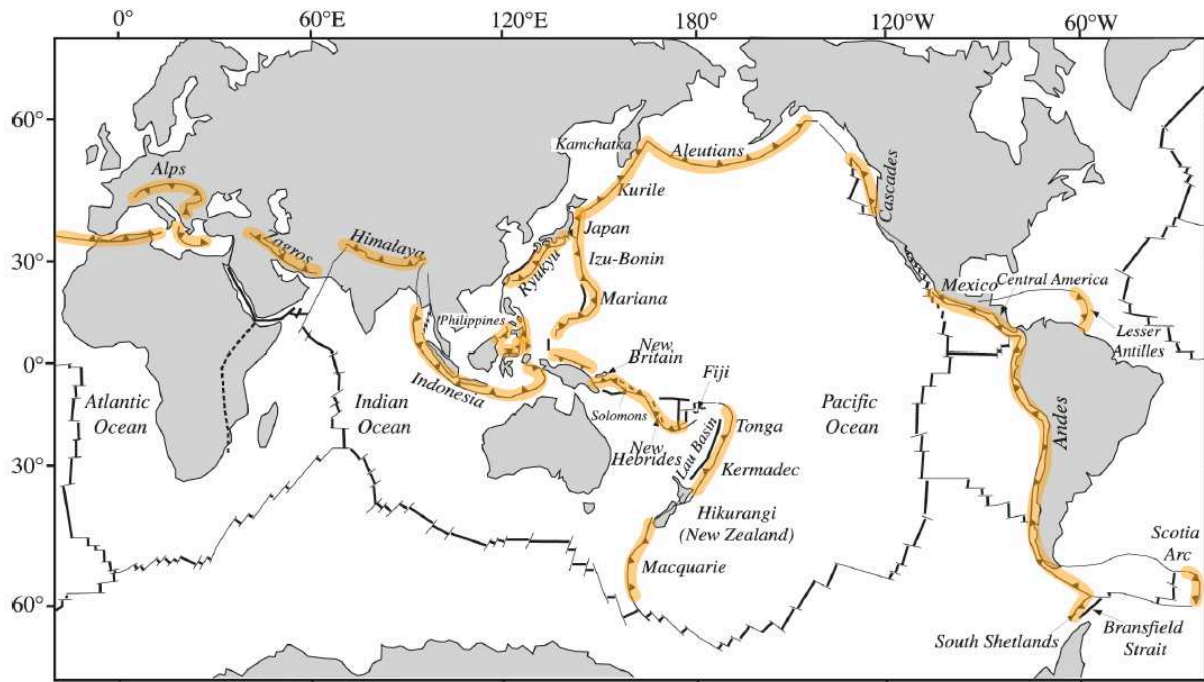


Figure 1.3.2: Plate tectonic boundaries around the world showing areas where the plates are subducting (subduction zone – thick yellow lines), and the Mid-oceanic ridges where rifting and creation of new oceanic crusts occur (thick black lines offset by thin black lines) (Lallemand, 1999).

The trench is a long, steep depression at the ocean floor that results from the flexing of the slab (with few exceptions, e.g. Greece, Makran, and southern Lesser Antilles subduction zones). They may exceed 6 km in depth and can reach up to 11 km e.g. the Mariana trench (Gardner et al., 2014). Sediment accumulation occur in the trench and some of the sediments subduct within the subduction channel.

The subduction channel is a relatively thin and weak layer with coherent kinematics that exists between the overlying plate and subducting plate. This layer is filled with sediments carried into the subduction by the downgoing plate (Cloos & Shreve, 1988), and/or fragments of the upper-plate materials scrapped off by the subduction process (Von Huene et al., 2004). The sediments of the subduction channel are separated from the upper plate by the decollement fault. In seismic lines, this fault has been imaged more than 4 decades ago as high amplitude reflector showing sometimes reverse polarity relative to the seafloor (e.g. Lesser Antilles, Westbrook & Smith, 1983; Moore et al., 1995; Bangs & Westbrook, 1991) and has been used since then in few 3D acquisitions to examine fault zone properties (e.g. Bangs et al., 2015).

The forearc is the region between the oceanic trench and the corresponding volcanic arc. Forearc region comprises the accretionary prism, the forearc basins, and the outer-arc high. The

accretionary prism forms immediately after the trench from sediments scrapped off the downgoing plate. The accretion occurs by offscraping of sediments and rocks at the front of the prism, and/or by underplating. Deformations occurring in the accretionary prism are large and fast, thus, rocks in this region are usually disrupted and mixed, forming melanges (Moore, 2001). Between the accretionary prism and the volcanic arc are the inner and outer forearc regions. They are usually dominated by forearc basins which can accumulate thick sediment deposits (Fuller et al., 2006; Mannu et al., 2017; Noda, 2016). The forearc basins architecture reflect subduction dynamics, making them suitable for studying the tectonic evolutions and seismic activities across subduction zones.

Volcanic arcs are lines of volcanoes formed above the upper plate in a subduction zone. They are usually aligned parallel to the trench. These volcanic arcs are formed by the partial melting of the overlying mantle caused by the dehydration of hydrous minerals in the downgoing plate, and release of fluids into the upper plate mantle. Behind the volcanic arcs is the back-arc region within which back-arc basins may form.

## **1.4 Subduction zone geometry and tectonic deformations**

Subduction zones worldwide exhibit different subduction geometry, tectonic framework, seismicity, and erosional or accretionary behaviour. These features and processes are primarily controlled by slab's temperature, age, dip and dynamics, the plate convergence rate, sediment thickness, and the nature and structure of both the lower and upper plate lithospheres. For instance, old, cold and thick oceanic crust are usually denser and have steeper dipping interplate interface, and deeper trenches (Hu & Gurnis, 2020; Lallemand et al., 2005b). They have intraslab seismicity that occur to the depth of up to 600 km (e.g. Frohlich, 2006; Houston, 2007) and are characterized by extensional back-arc crust due to slab roll-back such as in the Mariana subduction zone (e.g. Deschamps & Fujiwara, 2003; Dasgupta et al., 2021). On the other hand, subduction zones of young, hot, and thinner oceanic crusts usually have shallow trenches and shallow dipping plate interface. They also exhibit shallow intraslab seismicity and a compressional back-arc region (e.g. Stern, 2002).

### **1.4.1 Nature and structure of the oceanic crust**

Oceanic crusts are formed at mid-oceanic ridges. Their nature depends on the kind of spreading ridges where they form, i.e. either fast spreading, with spreading rate of more than 40 - 90 mm/yr, or slow spreading, with spreading rates of less than 40 mm/yr (Macdonald, 2019). Based on the Penrose type (Penrose Conference Participants, 1972), the oceanic crust is divided into

3 layers (Figure 1.4.1). Layer 1 consist of unconsolidated or semi-consolidated sediments, about 0.4 km thick, with velocity of approximately 2 km/s. Layer 2 is made up of pillow basalt and sheeted dikes with an average thickness of 2 km and velocity of approximately 5 km/s. Layer 3 consist of isotropic and layered gabbro, with ultramafic rocks. They have a thickness of up to 5 km and an approximate velocity of 6.7 km/s (Boudier & Nicolas, 1985; White et al., 1992; Dick et al., 2006; Christeson et al., 2019).

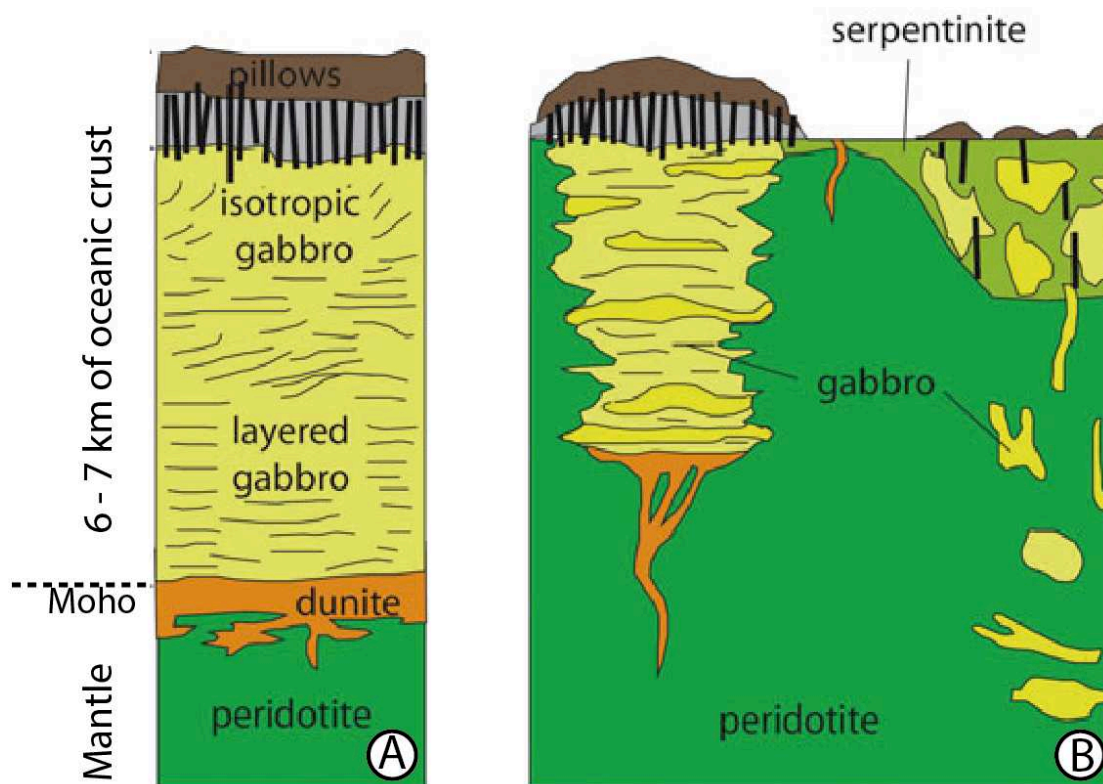


Figure 1.4.1: Schematic diagram showing the two models of oceanic crust. (A) The Penrose type showing crust with defined layers generated at fast spreading ridge. (B) The Cannat model, representing crust formed at slow-spreading ridge, consisting of poorly developed gabbros and dykes, mostly hydrated serpentinite rock. The diagram is adopted from (Kendrick, 2018), as modified after Dick et al., 2006.

The Penrose model is usually consistent at fast spreading ridges, however, at slow spreading ridges like the Mid-Atlantic-Ridge with spreading rate of  $\sim 2.5$  cm/yr (Fleischer et al., 1968), in situ studies has shown a more heterogenous nature in the formation of the crust (e.g. Juteau et al., 1990). Instead of the typical layer 2/3 structure, gabbro and peridotite expose directly to the surface to form large bodies of exhumed, hydrated and serpentinized upper mantle rocks (Cannat et al., 2006). This model is known as the “plum-pudding” model (Figure 1.4.1). The heterogenous crust formation is linked to the tectonically-dominated segment of the slow-

spreading ridge where the crust is stretched and thinned, e.g. at oceanic core complexes and detachment faults (Escartín et al., 2008) (Figure 1.4.2). Where oceanic crusts of this type subducts along convergent margins, they are likely to contribute to reduced interplate seismicity by weakening the megathrust due to low-temperature serpentinite minerals that make up the composition (e.g. Hirauchi et al., 2010).

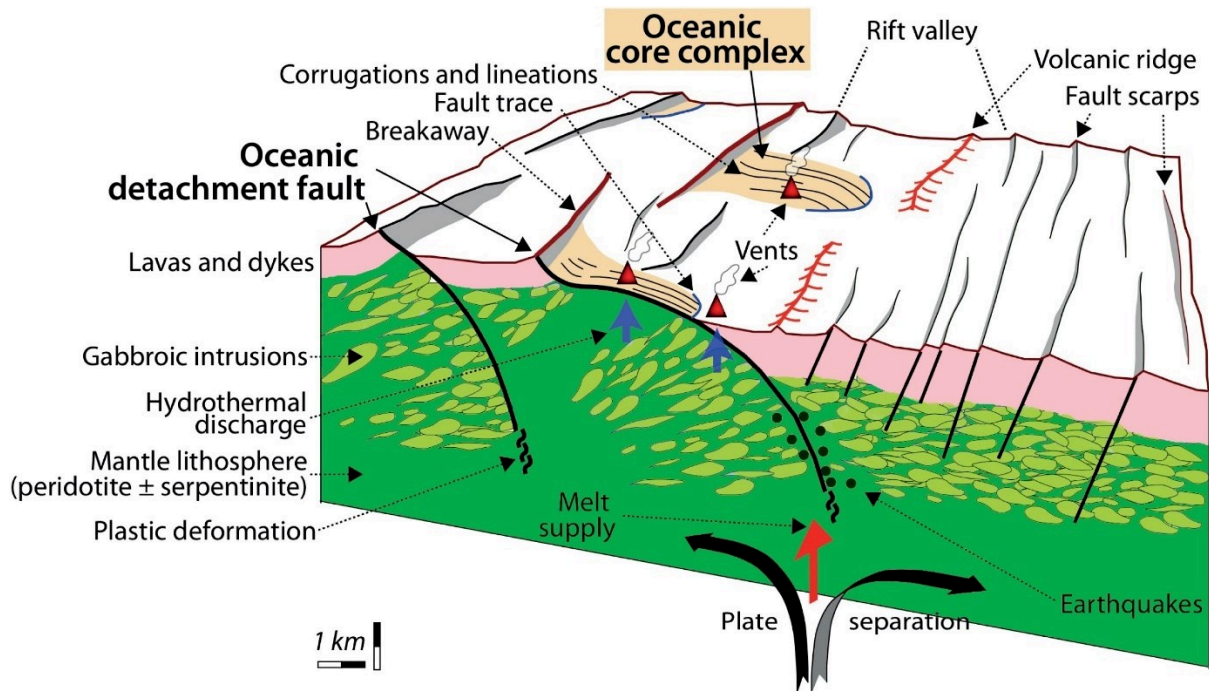


Figure 1.4.2: Schematic diagram showing oceanic core complex dominated by detachment faulting formed along slow-spread mid oceanic ridge (Escartín & Canales, 2011).

Oceanic crusts are also affected by numerous structural heterogeneities (seamounts, ridges, and faults). These heterogeneities, which end up in the subduction system will potentially impact the frictional properties on the megathrust fault, and consequently seismicity and long-term margin tectonic deformations. The fracture zones, when deep, pervasive and outcropping at sea-floor, may allow for fluid percolation, rock alteration, and serpentinitization reactions. At depths in the subduction, they might therefore release high volume of fluid through dehydration process.

Subduction of seamounts, aseismic ridges, and volcanic plateaus significantly deform the overriding plate during subduction (Von Huene et al., 1995; Moore & Sender, 1995; Dominguez et al., 1998 and Dominguez et al., 2000). For instance, seamount subduction in active margins such as Costa Rica Trench (Fisher et al., 1998; Ranero & Von Huene, 2000) appears to be responsible for a significant tectonic erosion across this margin. They may

influence seismicity and magmatic activity across the subduction zone and the volcanic arc respectively (Thatcher, 1989). They have also been found to favour the initiation of strong earthquakes by modifying seismic coupling (Scholz & Campos, 2012; Cloos, 1992), and could sometimes fracture the surrounding oceanic crusts, or produce landslides (Ruh, 2016) when large seamounts are subducted. During seamount subduction, the inner and outer accretionary wedge undergo significant deformation including frontal margin erosion, removal and underplating of large volumes of sediment, indentation, and basal erosion of the cohesive part of the margin (Dominguez et al., 2000). There may also be fluid expulsion due to intense fracturing of the margin, which may lead to a possible change in the mechanical coupling (Dominguez et al., 2000). In contrast, seamounts and ridges can also be a barrier to propagation of the rupture during earthquakes and participate in the segmentation of subduction zone large earthquakes (e.g. van Rijnsingen et al., 2018; Wang & Bilek, 2011; Kodaira et al., 2000; Kelleher & McCann, 1976).

#### **1.4.2 Tectonic accretion and erosion**

Plate convergence velocity and the subducting sediments thickness control frontal and basal tectonic accretion and erosion (Clift & Vannucchi, 2004) (Figure 1.4.3). According to Clift & Vannucchi, (2004), long-term accretion usually occurs when the relative convergence rate is low ( $< 5$  cm/yr) and the incoming sediment thickness is large ( $>1$  km). Accretion involves the transfer of materials by offscraping of the lower plate at the deformation front, as observed in the southern Antilles – Barbados Ridge Complex (Westbrook et al., 1988), or underplating at depth as proposed for Central Japan by (Kimura et al., 2010). Accretionary convergent margins around the world are often associated with forearc growth and widening over time (e.g. Cascadia and Aleutians). On the other hand, high convergence rates, exceeding 6 cm/yr, thin incoming sediment volume ( $< 1$  km), and a rough seafloor frequently generate margin tectonic erosion. This erosion occurs by frontal prism removal, for example observed in the Middle America convergent margin (Ranero & Von Huene, 2000) and/or removal of upper plate material at depth by basal erosion, as proposed by (von Huene et al., 2004). Erosive margins constitute about 75% of convergent margins (Stern, 2011), thus, making it an important process in the evolution of subduction zones.



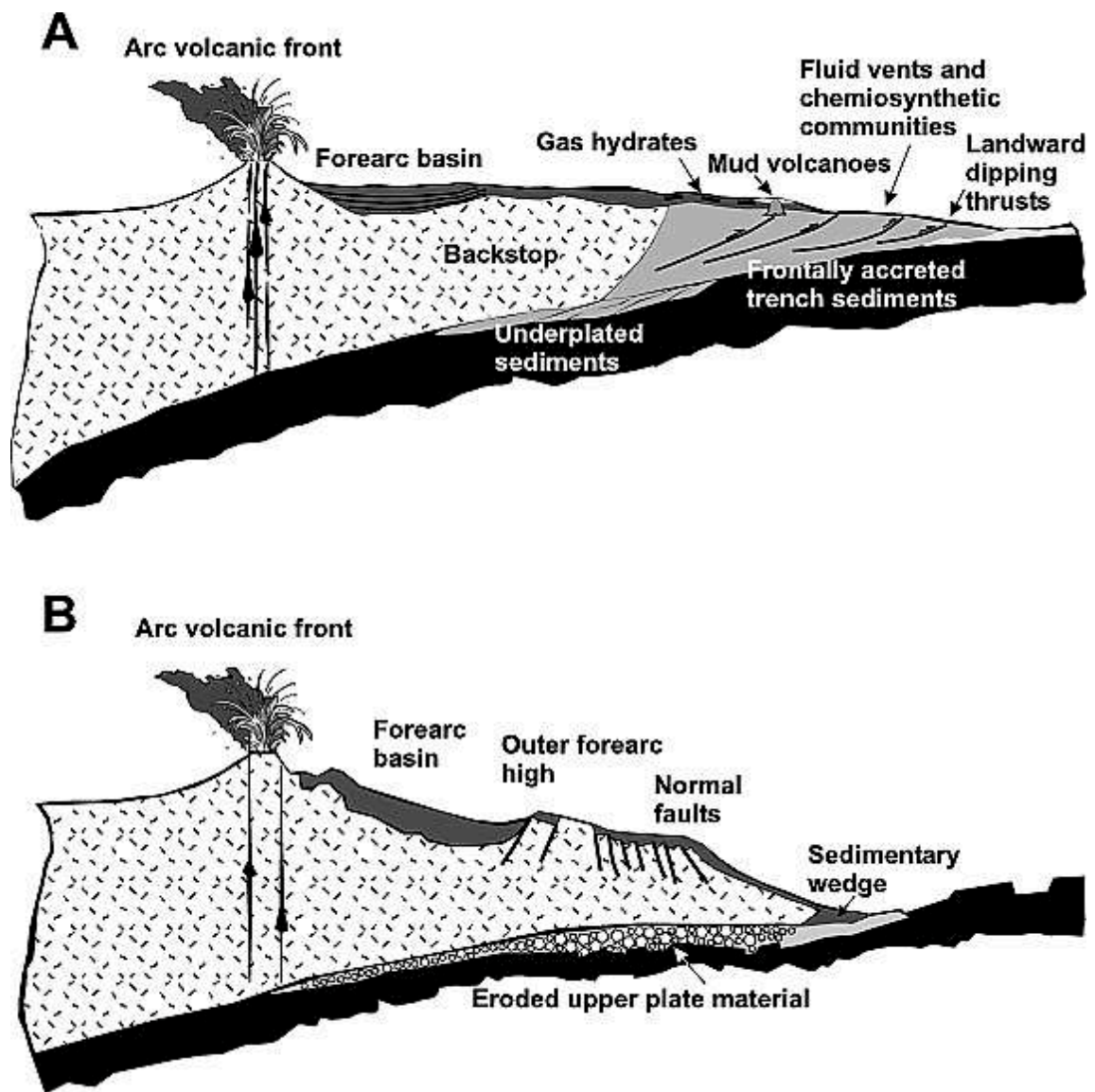


Figure 1.4.3: Schematic diagram showing (A) Accretionary margin and (B) Erosive margin (Clift & Vannucchi, 2004). The accretionary type margin allows the offscraping of materials to form an accretionary prism at the margin front, and underplating of material at the toe of the prism. Erosive margins have very short prisms with erosion occurring in the front of the margin and/or at the base of the overriding plate.

### 1.5 Seismic activities at subduction zones

At subduction zones, the sliding between the down-going and overriding plates causes the accumulation of elastic strain over time due to coupling. When the amount of accumulated strain exceeds the frictional forces that are preventing slip, the fault ruptures. This process generates most of the large and destructive earthquakes and tsunamis that occur around the world. Earthquake occurrence at subduction zones is characterised in phases known as seismic cycle.

### 1.5.1 Seismic cycle

The seismic cycle is divided into three periods, namely inter-seismic, co-seismic, and post-seismic (Scholz, 2002) (Figure 1.5.1). The interseismic phase is the period of slow accumulation of elastic strain along the locked portion of a fault since its last rupture (Kanamori & Brodsky, 2004). During this phase along the megathrust fault-plane, rocks closer to the locked zone accumulate a slip deficit with respect to the plate convergence. The elastic strain accumulation occurs over a long period until the elastic strain build-up exceeds the ability of the frictional forces that lock the fault to prevent slip. The coseismic phase is the period when the locked patch of the fault ruptures and slips causing an earthquake. At this phase, the strain built-up is released, and all the plate movement is concentrated along the fault. The post-seismic phase corresponds to a period of days or months after the earthquake when the adjacent portions to the fault's patch that suddenly slipped adapt to catch up with the slip, as well as to the modified state of stress (Scholz, 2002).

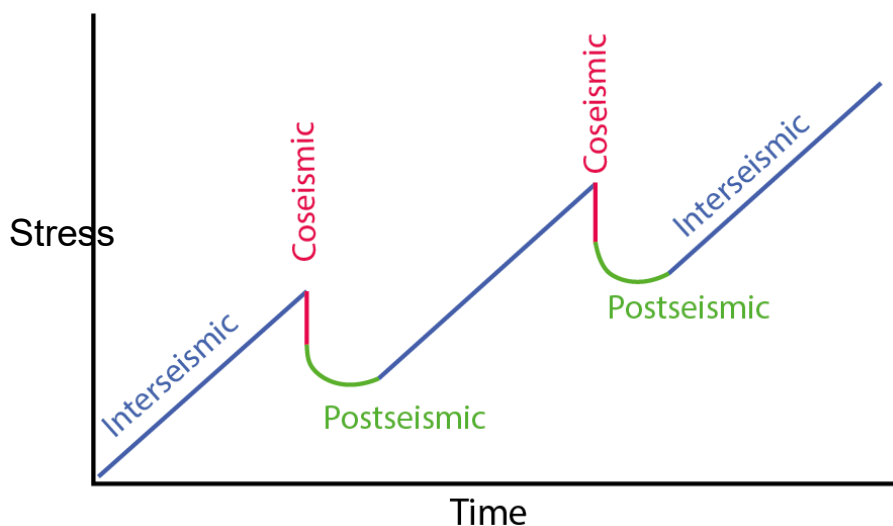


*Figure 1.5.1: Seismic cycle showing strain accumulation and release with time during the interseismic, coseismic, and post seismic periods. (Modified from Wright, 2013)*

### 1.5.2 The seismogenic zone

Destructive earthquakes nucleate from a part of the megathrust known as the seismogenic zone. Interseismic coupling (ISC) quantify the amount of sliding deficit between two plates, compared to the convergence rate. The fault's frictional sliding behaviour can be either stable, conditionally stable, or unstable (Scholz, 1998; Pacheco et al., 1993) (Figure 1.5.2). When a region undergoes stable sliding, it slips freely and no elastic energy is accumulated. Contrastingly, when a region experiences unstable sliding, it accumulates elastic energy.

However, between these two ends, the subduction zone is partially unstable. Earthquakes nucleate in the unstable regions and may propagate also into the conditionally stable regions, for instance, the 2011  $M_w$  9.0 Tohoku earthquake (e.g. Ito et al., 2011). The unstable and conditionally stable zone defines the extent of the seismogenic zone, which is the area that slips co-seismically during subduction earthquake rupture. However, since the large interplate events of the previous decade (Sumatra, Maule, Tohoku), improved observations by densified geodetic and seismological networks revealed that the spatio-temporal occurrences of events with contrasted slip behaviour may show that a distribution of these frictional properties are more complex than between an updip and downdip limit. Since the early 90s, the limits of this seismogenic zone have been considered to be controlled by many parameters of the subduction zone such as temperature, which correspond to phase changes of mineral (Hyndman et al., 1997), rheology, sediment properties, fluids, and the subducting plate fabric (e.g. Saffer & Marone, 2003; Byrne et al., 1988; Bilek et al., 2003; Hyndman & Wang, 1995; Oleskevich et al., 1999).

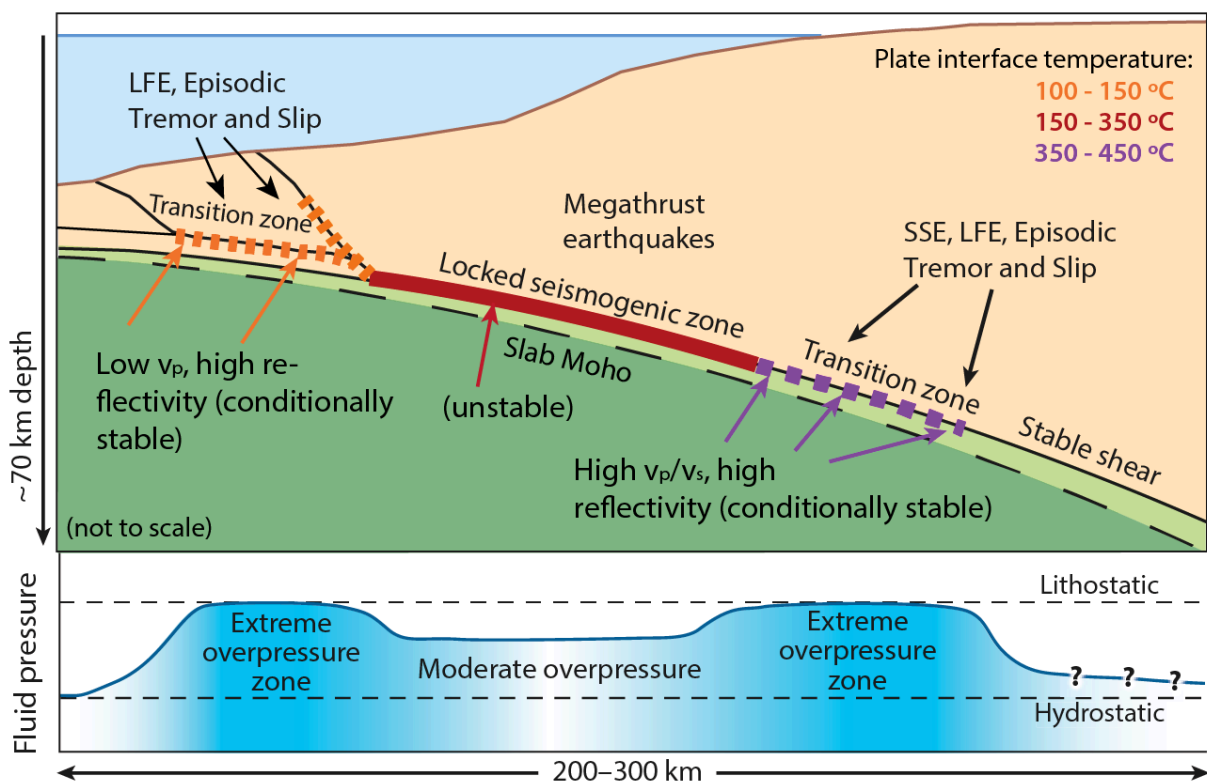


Figure 1.5.2: Sketch diagram of a subduction zone showing the shallow plate interface, highlighting the locked seismic portion sandwiched between the transitional zones (Saffer & Tobin, 2011). The limits of the different zones correspond to certain temperature limits signifying the updip and downdip limits of the potential seismogenic portions as stated in Hyndman et al., (1997).

### **1.5.3 Slab temperature and fluids**

Amongst the physical properties of the plate interface that control the seismogenic behaviour of the megathrust, temperature-fluid interaction plays a predominant role. Studies have shown that the transition from shallow stable (aseismic) to a stick-slip (seismogenic) behaviour along the plate interface occur at 60°-150°C, linked to the chemical and mechanical changes associated with clay mineral transition from smectite to illite (Moore & Saffer, 2001; Vrolijk, 1990). Downdip, the onset of stable sliding at greater depth occurs at temperatures of 350°-450°C, loosely described as brittle-ductile transition (Blanpied et al., 1995; Tse & Rice, 1986). The deeper stable sliding zone or isolated patches may also occur at the interaction of the interplate with the serpentinized mantle wedge of the upper plate if it occurs before the 350°C temperature (Hyndman et al., 1997) (Figure 1.4.4).

In addition, slab dehydration and fluid release related to metamorphic reactions especially during crustal eclogitisation and mantle deserpentinisation occur at depths in the subduction zone due to increasing temperature and pressure (Kirby et al., 1996; Hacker et al., 2003); (Ferrand, 2019). These temperature-related dehydration reactions have been linked to the locations of intraslab, supraslab and interplate seismicity occurring at subduction zones (e.g. Peacock & Wang, 1999; Ulmer & Trommsdorff, 1995). Moreover, fluid circulations at depth affect thermally and mechanically the evolution of the interplate sliding behaviour, as pore fluid overpressure has been correlated with patches of low interseismic coupling or with repeating slow slip earthquakes (SSEs) (e.g. Moreno et al., 2014). Thus, studying the temperature and fluid interactions at subduction zones has become key to understanding the mechanical behaviour of the megathrust seismogenic zone.

### **1.5.4 The interplate patchiness**

The subduction zone is a very complex zone with numerous heterogeneities such as the subduction of seamounts, ridges, varying trench sediment thickness, volume of fluids, etc. occurring at different locations. Thus, the mechanical behaviour and interplate frictional properties significantly vary laterally in a subduction zone. This variation may result in patchiness along the interplate contact (Figure 1.5.3), and lead to heterogenous (high and low) interseismic coupling. As a result, coseismic slips along the plate interface occur heterogeneously in patches as either stable sliding slip (aseismic), episodic slow-slip, or stick-slip with various rupture size behaviour. This interplate patchiness, depending on the relative proportion of the locked and unlocked zones may impede large-scale zones of full interplate

coupling (Hirauchi et al., 2010), and promote slow-slips and/or very-low frequency earthquakes (Saffer & Wallace, 2015).

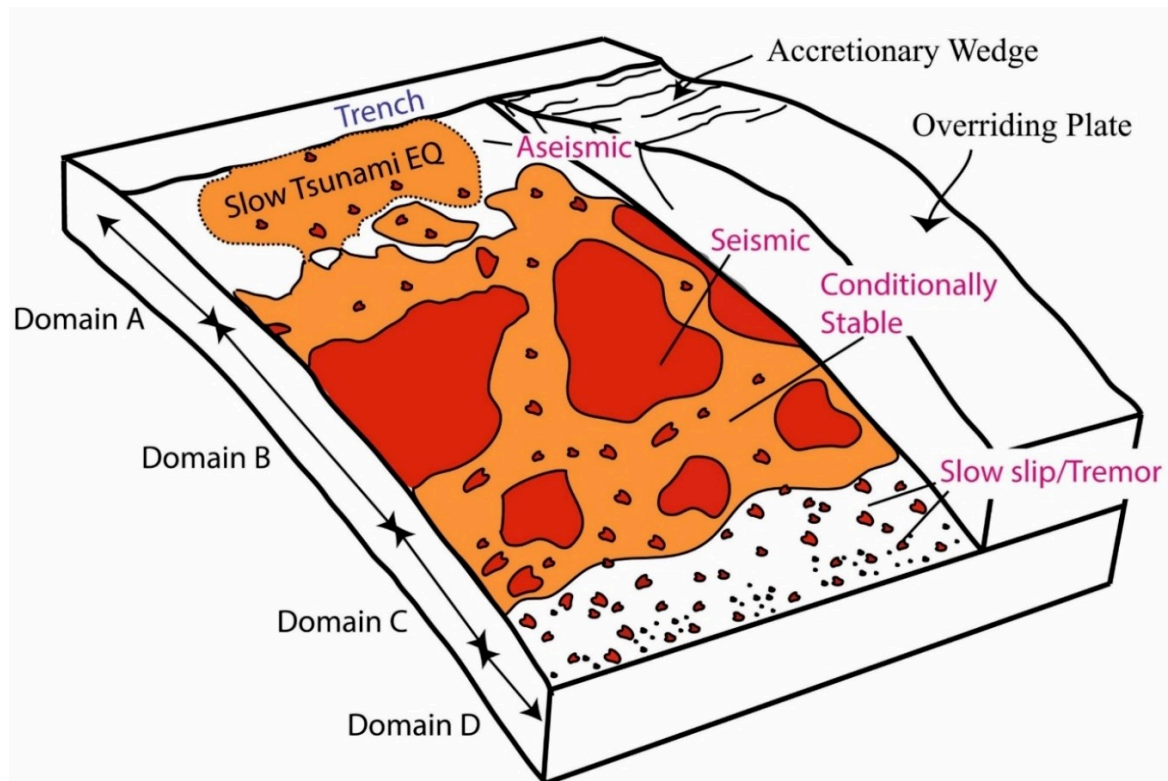


Figure 1.5.3: Schematic diagram characterizing the mechanical and frictional variations along the interplate (Lay & Nishenko, 2022). The diagram shows regions of unstable sliding (seismic), stable (aseismic) sliding, episodic slow-slips, and conditionally stable regions.

## 1.6 Geodynamic context of the Lesser Antilles subduction zone

The Lesser Antilles subduction zone forms at the eastern part of the Caribbean where the North and South American plates subduct beneath the Caribbean plate. The plates converge at a velocity of  $20 \text{ mmyr}^{-1}$  in a  $S74^\circ W$  direction (DeMets et al., 2010). Subduction along this margin is traced back to the Late Cretaceous (approximately 75-80 Ma) during the subduction polarity reversal, when the Caribbean Oceanic plateau failed to subduct beneath the eastward-dipping slab of the Great Arc of the Caribbean (Burke, 1988). The subduction reversal that resulted in a change in the subduction to a westward-dipping slab led to the Greater Arc of the Caribbean entering the Caribbean region. Subsequently, the oceanic crust of the Proto-Caribbean and the Atlantic subducted beneath the Caribbean plate (Burke, 1988), and the North and South American plate subducts to present (Figure 1.6.1).

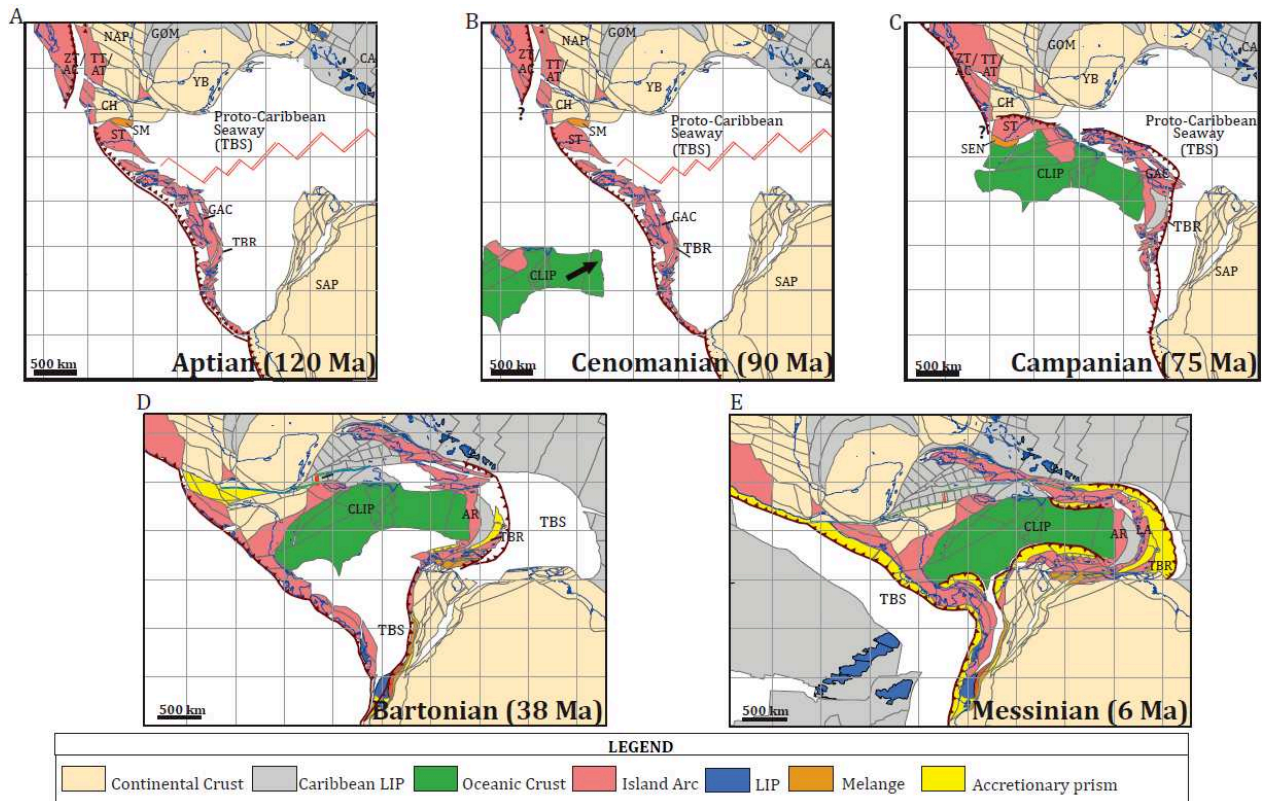


Figure 1.6.1: Plate tectonic reconstruction of the eastern Caribbean from the Early Cretaceous – Recent (Gomez, 2018) as modified from Sanchez et al., (2016). NAP: North American Plate, CA: Central America, GAC: Great Arc of the Caribbean, SAP: South American Plate, GOM: Gulf of Mexico, AV: Aves Ridge, CLIP: Caribbean Large Igneous Province, YB: Yucatan Block, CH: Chortis Block, ST: Siuna Terrane, SM: Siuna Melange, ZT: Zihuatanejo Terrane, LIP: Large Igneous Province, LA: Lesser Antilles Island arc, TT: Teloloapan terrane. TBS represents the area that is to be subducted.

During the Paleocene, the Bahamas Bank collision with the Northern Caribbean margin has blocked the subduction of the Atlantic lithosphere to the north and has resulted in a major plate boundary reorganization (e.g. Pindell & Barrett, 1991). The Caribbean margin has bended in an eastward convex shape (Mann, 1999), and since the late Eocene, the Puerto Rico to Northern Lesser Antilles block has recorded a counterclockwise rotation of 40° to 45° (Reid et al., 1991; Van Fossen et al., 1989; Mann et al., 2005; Philippon et al., 2020; Montheil et al., 2023). In the Greater Antilles, the plate boundary relocated along the left lateral Cayman Trough that propagated from west to east, to transpressive fault zones across Hispaniola and possibly to the left-lateral strike-slip Anegada Passage (e.g. Leroy et al., 2000; Pindell & Barrett, 1991; Laurencin et al., 2017). At the Lesser Antilles, due to the convex shape of the margin,

convergence obliquity increases northwards from  $0^\circ$  - subduction normal to the margin offshore Central Antilles - to greater than  $75^\circ$  north of the Virgin Islands. A trench-parallel left-lateral strike-slip Bunce Fault that extends over approximately 850 km in the Northern Lesser Antilles, highlights an increase in plate obliquity and accommodates strain partitioning associated to the left-lateral component of the plate convergence (Laurencin et al., 2017). Since the Eocene-Miocene, the Northern Lesser Antilles margin has undergone two successive tectonic phases (Laurencin et al., 2017, Boucard et al., 2021; Legendre et al., 2018; Philippon et al., 2020; Montheil et al., 2023)). During the Miocene, a N-S to NW-SE extensive phase, accommodated by trench-parallel extension along  $N40^\circ$ -  $N90^\circ$  trending normal faults, has resulted in the opening of V-shaped basins. This event was accompanied by tectonic uplift, which ended up in a regional emersion phase (Philippon et al., 2020; Cornée et al., 2021). From the latest Miocene to present, SW-NE extension, perpendicular to the margin, has generated the major normal Tintamarre Fracture zone, margin basal erosion and subsidence (Boucard et al., 2021).

In the Lesser Antilles, based on magnetic anomaly C34 of the North American Plate, the age of the incoming oceanic plate at the trench is calculated to range from 83 Ma east of Barbuda to 98 Ma east of southern Martinique (Carpentier et al., 2008). The oceanic crust, formed at the slow-spreading Mid-Atlantic Ridge (MAR), shows occurrences of tectonically-dominated basement patches. Evidence of stretched and thinned crust hosting large bodies of exhumed, hydrated mantle rocks has been observed near the MAR as Oceanic Core-Complexes (e.g. Ildefonse et al., 2007; Szitkar et al., 2019) and between the MAR and the Lesser Antilles trench (Davy et al., 2020). During my PhD, we observed a tectonically-dominated patch that we named the Jacksonville patch, in the trench (Cf Chapter 3) (Marcaillou et al., 2021). In addition, the oceanic basement is incised by several fracture zones, namely; the Vema, Marathon, Mercurius, and Doldrums Fracture Zones in the south, and the 15-20, and Jacksonville Fracture Zones in the north (see Figure 1.0.1).

Numerous seamounts and topographic ridges exist eastward of the trench on the oceanic crust especially within the Northern Lesser Antilles. The two most prominent ridges, Tiburon Rise and Barracuda Ridge, lie parallel to each other between latitudes  $15^\circ$  and  $17^\circ$  and have been described and studied by (Birch, 1970; Roest & Collette, 1986; Muller & Smith, 1993). This is only a decade ago that more detailed geophysical studies constrained their formation and evolution (e.g. Patriat et al., 2011b; Pichot et al., 2012). These ridges were uplifted as a result of the convergence between the North and South American Plates during the Mid-Late Miocene

and Pleistocene respectively (Pichot et al., 2012b), and are identified on the bathymetry beyond the trench, beneath the accretionary prism (Laigle, et al., 2013) and the forearc.

At the trench, sediment thickness decreases northwards from ~3 km in the south offshore Martinique (Pichot et al., 2012) to less than 0.5 km in the north of the Barracuda Ridge (Laurencin et al., 2019). The sediments consist of terrigenous materials that are transported from the South American river sources since the Eocene (e.g. Wright, 1984; Xie et al., 2010). Thus, the uplift of the oceanic ridges has been proposed to form barrier to the northward propagation of these sediments (Westbrook, 1982). The margin has one of the largest accretionary prisms in the world known as the Barbados prism, which is located in the southern Lesser Antilles, measuring up-to ~300-400 km wide and ~12 – 18 km thick (Westbrook et al., 1988). This prism volume decreases progressively northward to become less than 30 km wide to the north of the Barracuda Ridge (Laurencin et al., 2019).

The Lesser Antilles forearc consist of upper plate igneous basement up to ~24 km thick (e.g. (Kopp et al., 2011; Evain, 2011; Paulatto et al., 2017), covered with sedimentary basins. The forearc crust is characterised by three layers based on wide angle seismic profile analysed across southern Guadeloupe (Kopp et al., 2011). The uppermost layer has variable velocities (3 - 5.5  $\text{kms}^{-1}$ ) and thickness of few kilometres, the middle layer consists of felsic to intermediate crust, with an average velocity of  $6.4 \pm 0.2 \text{ kms}^{-1}$  and thickness up-to 10 km, while the lower layer consists of plutonic rocks, with velocity up-to  $7.3 \text{ kms}^{-1}$  and thickness reaching 12 km (Kopp et al., 2011). Similar observations of crustal thickness and structures were also observed further south (e.g. Christeson et al., 2008) and in the Northern Lesser Antilles (Laurencin et al., 2018; Padron et al., 2021). The upper plate crust is thought to be of oceanic origin and formed due to crustal thickening by flood basalts, magmatic intrusions, and crustal underplating during its drift over the Galapagos hotspot in the Mesozoic (Evain, 2011; Kopp et al., 2011; Christenson et al., 2008). In the outer forearc, this upper plate basement transitions to a damaged or imbricated and underplated igneous basement, and are covered with deep forearc sedimentary basins (Evain et al., 2013; Laigle et al., 2013; Bangs et al., 2003; Christeson et al., 2003). Landward, north-south sequences of basins and spurs characterize the inner forearc from the Anegada Passage to Karukera Spur (Boucard et al., 2021). The sedimentary units are best preserved within these forearc basins, and consist of two deep and two shallow units (Boucard et al., 2021), separated by a regional late Eocene unconformity (Philippon et al., 2020; Cornée et al., 2021).



Volcanic activity in this margin dates as far back as the Eocene when the active volcanic arc of the Great arc of the Caribbean migrated eastwards to form the volcanic arc of the Lesser Antilles (Bouysse, 1983; Bouysse et al., 1988; Neill et al., 2011). This volcanic arc was active during the Eocene to Oligocene time before its migration westward to the present-day active arc in the Northern Lesser Antilles (Bouysse & Westercamp, 1990; Carpentier et al., 2008) from Guadeloupe to the Anegada Passage. The inactive arcs in the east lie parallel to the active arcs in the west, until the two arcs meet in the south of Guadeloupe to form a single active arc up-to Venezuela (see Figure 1.0.1).

## **1.7 Seismic activity in the Lesser Antilles**

### **1.7.1 Geodetic coupling**

Different studies based on geodetic data (Manaker et al., 2008; Symithe et al., 2015) has evaluated the Caribbean plate velocity field and proposed a heterogeneous seismic coupling along the Caribbean margin from the north of Hispaniola to Martinique. These studies proposed a strong coupling along the subduction interface north of Hispaniola and a weak interplate coupling north of Puerto Rico. Between the north of Puerto Rico to the Central Antilles, Symithe et al., (2015) propose a weak seismic coupling along the plate interface (Figure 1.7.1a). Contrastingly, Manaker et al., (2008) show a different coupling result for this segment of the margin. They proposed a partial interplate coupling between the Virgin Islands and Barbuda, then no coupling between Barbuda and northern Guadeloupe, and again a partial coupling to the south of Guadeloupe (Figure 1.7.1b). However, a recent study using GPS measurements in the Caribbean has re-evaluated the plate velocity field and proposed a very low interplate coupling along the Puerto-Rico and Lesser Antilles subduction zone (van Rijsingen et al., 2021). In a different study based on some coral micro-atolls along the island arcs (Philibosian et al., 2022), the authors suggest a local increase in interseismic coupling at great depth and argue that models based on GPS may be limited in its time scale measurements. However, in a more recent study using geodetic data, (van Rijsingen et al., 2022) concludes that a locked or partially locked interplate would produce uplift of the island arcs (Figure 1.7.1c). In contrast, their study shows subsidence of the arcs at the same rate consistent with the ~100-yr trend derived from coral micro-atolls, suggesting a low interplate coupling for the Lesser Antilles subduction zone.

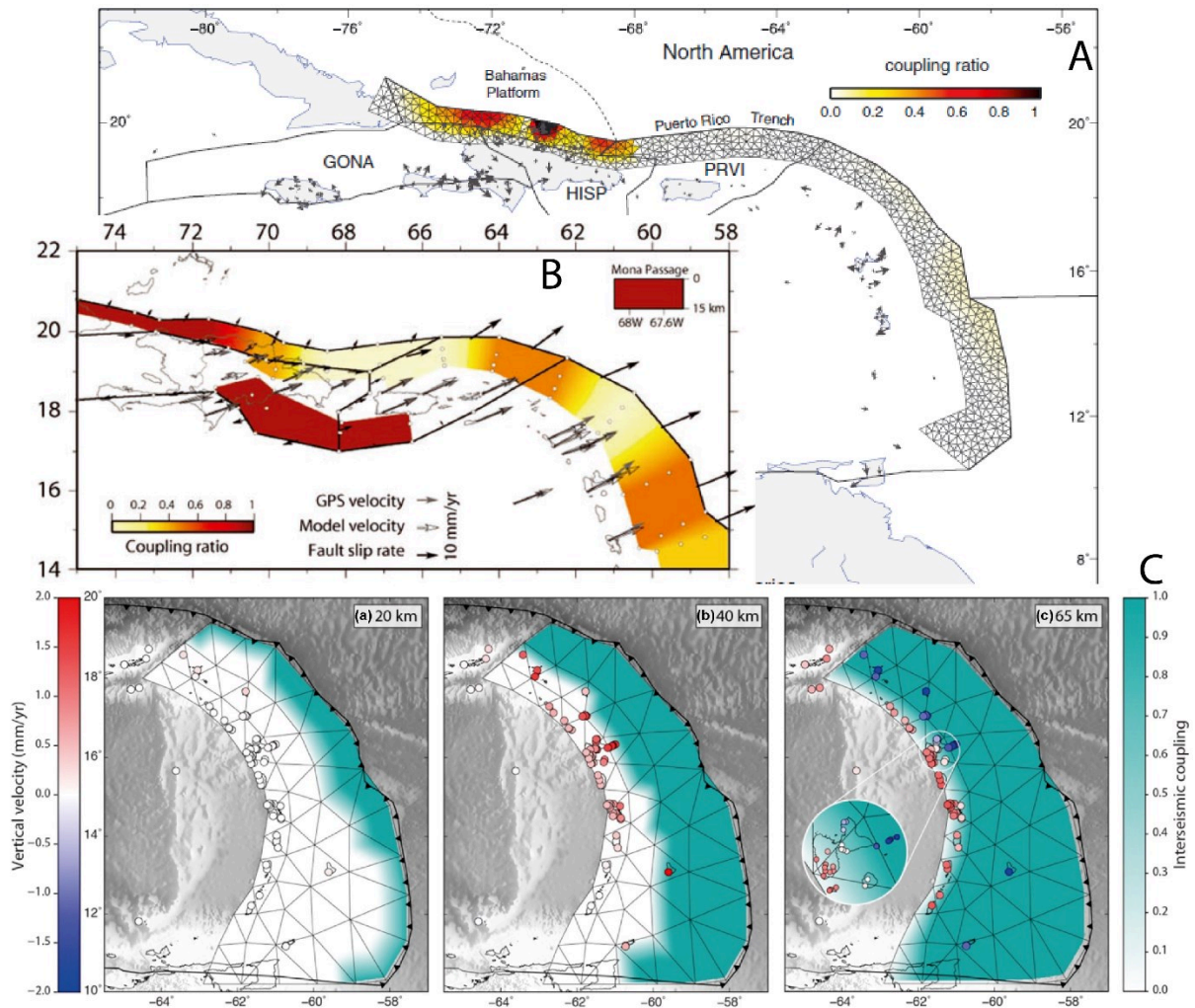


Figure 1.7.1: Estimated seismic coupling of the plate interface based on geodetic measurement along the Lesser Antilles. (A) Symithe et al., 2015, and (B) Manaker et al., 2008. The model in (C) are predicted vertical motions of interseismic coupling based on different downdip locking limits from van Rijnsingen et al., (2022). Models show uplift of the islands in contrast to subsidence recorded by GNSS and Coral Microatolls, indicating a poorly coupled margin.

## 1.7.2 Seismicity

Seismicity in the Lesser Antilles subduction zone is generally low, and few great historical earthquakes have been recorded since the settlement of these islands before the 16<sup>th</sup> century. Among those interpreted as subduction earthquakes, there are two significant events of 1839 and 1843 that occurred to the east of Martinique and Antigua respectively (Dorel, 1981; Bernard & Lambert, 1988). The 1839 earthquake that destroyed Fort-de-France in Martinique island had a magnitude estimated to be greater than 8.0 (Feuillet et al., 2011), while that of the 1843 ranges between 7.0 (Bernard & Lambert., 1988) and 8.4 (Feuillet et al., 2011; Ten Brink et al., 2011).

Other historical earthquakes located along normal and strike-slip faults with magnitudes between 7 – 7.5 has also occurred. They include those of 1690 which occurred off Nevis (Feuillet et al., 2010), and the 1867 earthquake that was located at shallow depth close to St Kitts & Nevis, and on the northern edge of the Virgin Island basin respectively (Figure 1.7.2).

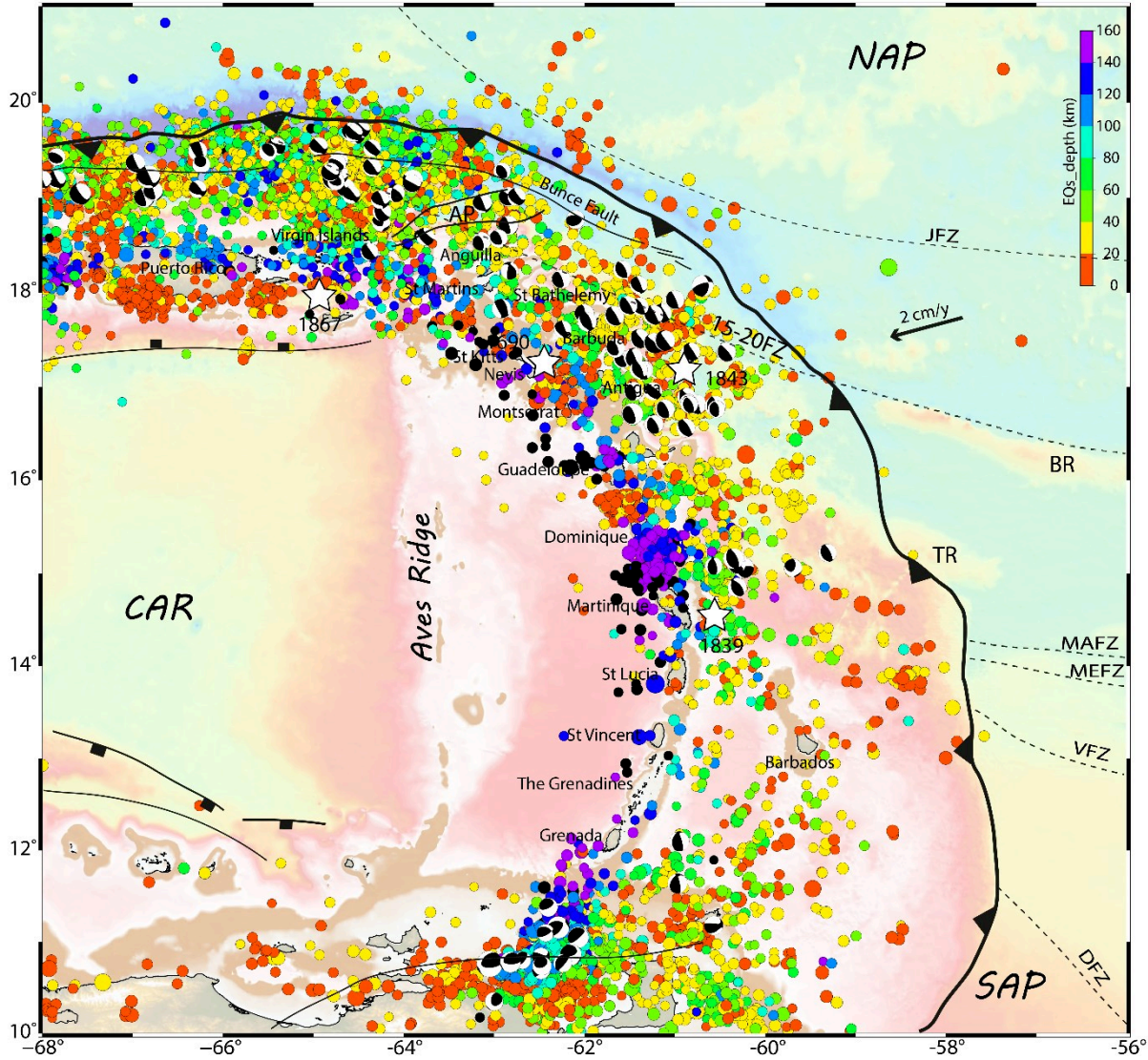


Figure 1.7.2: Earthquake map of the eastern Caribbean showing seismicity distribution. The black focal mechanism are thrust-type earthquakes with  $M_w > 5$  from gCMT catalogue (1976 – 2023). Coloured circles are earthquakes from USGS catalogue with  $M_w > 3.5$  from 1900 – 2023. The size of the circles is consistent with the magnitude of the events, while the colours represent the depth. The white stars are locations of historical events. Abbreviations are the same as in Figure 1.0.1.

Seismicity distribution of the instrumental period based on CMT catalogue (Dziewonski et al., 1981; Ekström et al., 2012) includes only a few interplate thrust events in the area. Since 1973 to date, only about 70 earthquakes with  $M_w < 6$  and focal mechanisms that represents flat thrust event occurring along the plate interface has been recorded (Figure 1.7.2). In the northern Lesser Antilles, these earthquakes are aggregated in two clusters and display a possible seismic gap between Barbuda and the Anegada Passage (Figure 1.7.2). In all, the Lesser Antilles subduction interface has long been considered as slipping aseismically due to the lack of interplate earthquakes at least greater than  $M_w 7.0$  (Stein et al., 1982), compared to other subduction zones (e.g. Chile, Cascadia or around Japan) where earthquakes of  $M_w > 9.0$  have been observed. However, the presence of patches of low magnitude interplate earthquakes, and the historical 1839 and 1843 events that possibly ruptured the interplate raises question to the possibility of future greater magnitude events along the megathrust, especially since the 2004 Sumatra event (Hough, 2013).

## References

- Bangs, N. L. B., & Westbrook, G. K. (1991). Seismic modeling of the decollement zone at the base of the Barbados Ridge accretionary complex. *Journal of Geophysical Research*, 96(B3), 3853–3866. <https://doi.org/10.1029/90JB02138>
- Bangs, N. L., Christeson, G. L., & Shipley, T. H. (2003). Structure of the Lesser Antilles subduction zone backstop and its role in a large accretionary system. *Journal of Geophysical Research: Solid Earth*, 108(B7). <https://doi.org/10.1029/2002jb002040>
- Bangs, N. L., McIntosh, K. D., Silver, E. A., Kluesner, J. W., & Ranero, C. R. (2015). Fluid accumulation along the Costa Rica subduction thrust and development of the seismogenic zone. *Journal of Geophysical Research: Solid Earth*, 120(1), 67–86. <https://doi.org/10.1002/2014JB011265>
- Bernard, P., & Lambert, J. (1988). Subduction and seismic hazard in the northern Lesser Antilles: revision of the historical seismicity. *Bulletin - Seismological Society of America*, 78(6), 1965–1983.
- Bie, L., Rietbrock, A., Hicks, S., Allen, R., Blundy, J., Clouard, V., Collier, J., Davidson, J., Garth, T., Goes, S., Harmon, N., Henstock, T., van Hunen, J., Kendall, M., Krüger, F., Lynch, L., Macpherson, C., Robertson, R., Rychert, K., Tait, S., Wilkinson, J., Wilson, M. (2019) Along-Arc Heterogeneity in Local Seismicity across the Lesser Antilles Subduction Zone from a Dense Ocean-Bottom Seismometer Network. *Seismological Research Letters*. 91 (1): 237–247. <http://doi.org/10.1785/0220190147>
- Bilek, S. L., Schwartz, S. Y., & DeShon, H. R. (2003). Control of seafloor roughness on earthquake rupture behavior. *Geology*, 31(5), 455–458. <https://doi.org/10.1130/0091-7613>
- Birch, F. S. (1970). *The Barracuda Fault Zone in the western North Atlantic: geological and geophysical studies* (Vol. 17). Pergamon Press.
- Blanpied, M. L., Lockner, D. A., & Byerlee, J. D. (1995). Frictional slip of granite at hydrothermal conditions. *Journal of Geophysical Research*, 100(B7). <https://doi.org/10.1029/95jb00862>
- Boucard, M., Marcaillou, B., Lebrun, J. F., Laurencin, M., Klingelhoefer, F., Laigle, M., Lallemand, S., Schenini, L., Graindorge, D., Cornée, J. J., Münch, P., Philippon, M., & the, A. (2021). Paleogene V-Shaped Basins and Neogene Subsidence of the Northern Lesser Antilles Forearc. *Tectonics*, 40(3), 1–18. <https://doi.org/10.1029/2020TC006524>
- Boudier, F., & Nicolas, A. (1985). Harzburgite and lherzolite subtypes in ophiolitic and oceanic environments. *Earth and Planetary Science Letters*, 76(1–2), 84–92. [https://doi.org/10.1016/0012-821X\(85\)90150-5](https://doi.org/10.1016/0012-821X(85)90150-5)
- Bouysse, P. (1983). The Lesser Antilles Island arc: structure and geodynamic evolution. *Atlantic*, 83–103.
- Bouysse, P., Mascle, A., Mauffret, A., De Lepinay, B. M., Jany, I., Leclere-Vanhoeve, A., & Montjaret, M. C. (1988). Reconnaissance de structures tectoniques et volcaniques sous-marines de l'arc récent des Petites Antilles (Kick'em Jenny, Qualibou, Montagne Pelee,

- nordouest de la Guadeloupe). *Marine Geology*, 81(1–4), 261–287. [https://doi.org/10.1016/0025-3227\(88\)90031-X](https://doi.org/10.1016/0025-3227(88)90031-X)
- Bouysson, P., & Westercamp, D. (1990). Subduction of Atlantic aseismic ridges and Late Cenozoic evolution of the Lesser Antilles Island arc. *Tectonophysics*, 175(4). [https://doi.org/10.1016/0040-1951\(90\)90180-G](https://doi.org/10.1016/0040-1951(90)90180-G)
- Britannica, T. (2018). *Subduction Zone*. Britannica Encyclopædia. <https://www.britannica.com/science/subduction-zone/images-videos#/media/1/570643/151217>
- Burke, K. (1988). Tectonic Evolution of the Caribbean. *Annual Review of Earth and Planetary Sciences*, 16, 201–230.
- Byrne, E., Davis, M., & Sykes, R. (1988). Loci and Maximum size of thrust earthquakes and the mechanics of the shallow region of subduction zones. *Tectonics*, 7(4), 833–857.
- Calahorrano B., A., Sallarès, V., Collot, J. Y., Sage, F., & Ranero, C. R. (2008). Nonlinear variations of the physical properties along the southern Ecuador subduction channel: Results from depth-migrated seismic data. *Earth and Planetary Science Letters*, 267(3–4), 453–467. <https://doi.org/10.1016/j.epsl.2007.11.061>
- Cannat, M. (1996). How thick is the magmatic crust at slow spreading oceanic ridges? Melt Migration in the Axial Lithosphere of Slow Spreading Ridges: Constraints from Ultramafic and Gabbroic Samples. *Journal of Geophysical Research: Solid Earth*, 101, 2847–2857.
- Cannat, M., Sauter, D., Mendel, V., Ruellan, E., Okino, K., Escartin, J., Combier, V., & Baala, M. (2006). Modes of seafloor generation at a melt-poor ultraslow-spreading ridge. *Geology*, 34(7), 605–608. <https://doi.org/10.1130/G22486.1>
- Carpentier, M., Chauvel, C., & Mattielli, N. (2008a). Pb-Nd isotopic constraints on sedimentary input into the Lesser Antilles arc system. *Earth and Planetary Science Letters*, 272(1–2), 199–211. <https://doi.org/10.1016/j.epsl.2008.04.036>
- Carpentier, M., Chauvel, C., & Mattielli, N. (2008b). Pb-Nd isotopic constraints on sedimentary input into the Lesser Antilles arc system. *Earth and Planetary Science Letters*, 272(1–2), 199–211. <https://doi.org/10.1016/j.epsl.2008.04.036>
- Chemenda, A., Lallemand, S., & Bokun, A. (2000). Strain partitioning and interplate friction in oblique subduction zones: Constraints provided by experimental modeling. *Journal of Geophysical Research: Solid Earth*, 105(B3), 5567–5581. <https://doi.org/10.1029/1999jb900332>
- Christeson, G. L., Bangs, N. L., & Shipley, T. H. (2003). Deep structure of an island arc backstop, Lesser Antilles subduction zone. *Journal of Geophysical Research: Solid Earth*, 108(B7). <https://doi.org/10.1029/2002jb002243>
- Christeson, G. L., Goff, J. A., & Reece, R. S. (2019). Synthesis of Oceanic Crustal Structure from Two-Dimensional Seismic Profiles. In *Reviews of Geophysics* (Vol. 57, Issue 2, pp. 504–529). Blackwell Publishing Ltd. <https://doi.org/10.1029/2019RG000641>

- Christeson, G. L., Mann, P., Escalona, A., & Aitken, T. J. (2008). Crustal structure of the Caribbean - Northeastern South America arc-continent collision zone. *Journal of Geophysical Research: Solid Earth*, *113*(8), 1–19. <https://doi.org/10.1029/2007JB005373>
- Clift, P. D., & Hartley, A. J. (2007). Slow rates of subduction erosion and coastal underplating along the Andean margin of Chile and Peru. *Geology*, *35*(6), 503–506. <https://doi.org/10.1130/G23584A.1>
- Clift, P., & Vannucchi, P. (2004). Controls on tectonic accretion versus erosion in subduction zones: Implications for the origin and recycling of the continental crust. *Reviews of Geophysics*, *42*(2). <https://doi.org/10.1029/2003RG000127>
- Cloos, M. (1992). Thrust-type subduction-zone earthquakes and seamount asperities: A physical model for seismic rupture. *The Geological Society of America*, *20*, 601–604. [https://doi.org/10.1130/0091-7613\(1992\)020<0601](https://doi.org/10.1130/0091-7613(1992)020<0601)
- Cornée, J. J., Münch, P., Philippon, M., BouDagher-Fadel, M., Quillévéré, F., Melinte-Dobrinescu, M., Lebrun, J. F., Gay, A., Meyer, S., Montheil, L., Lallemand, S., Marcaillou, B., Laurencin, M., Legendre, L., Garroq, C., Boucard, M., Beslier, M. O., Laigle, M., Schenini, L., ... Marivaux, L. (2021). Lost islands in the northern Lesser Antilles: possible milestones in the Cenozoic dispersal of terrestrial organisms between South-America and the Greater Antilles. *Earth-Science Reviews*, *217*(October 2020). <https://doi.org/10.1016/j.earscirev.2021.103617>
- Dasgupta, R., Sen, J., & Mandal, N. (2021). Bending curvatures of subducting plates: old versus young slabs. *Geophysical Journal International*, *225*(3), 1963–1981. <https://doi.org/10.1093/gji/ggab070>
- Davy, R. G., Collier, J. S., Henstock, T. J., Rietbrock, A., Goes, S., Blundy, J., Harmon, N., Rychert, C., Macpherson, C. G., Van Hunen, J., Kendall, M., Wilkinson, J., Davidson, J., Wilson, M., Cooper, G., Maunder, B., Bie, L., Hicks, S., Allen, R., ... Labahn, E. (2020). Wide-Angle Seismic Imaging of Two Modes of Crustal Accretion in Mature Atlantic Ocean Crust. *Journal of Geophysical Research: Solid Earth*, *125*(6), 1–21. <https://doi.org/10.1029/2019JB019100>
- De Min, L., Lebrun, J. F., Cornée, J. J., Münch, P., Léticée, J. L., Quillévéré, F., Melinte-Dobrinescu, M., Randrianasolo, A., Marcaillou, B., & Zami, F. (2015). Tectonic and sedimentary architecture of the Karukéra spur: A record of the Lesser Antilles fore-arc deformations since the Neogene. *Marine Geology*, *363*, 15–37. <https://doi.org/10.1016/j.margeo.2015.02.007>
- DeMets, C., Gordon, R. G., & Argus, D. F. (2010). Geologically current plate motions. *Geophysical Journal International*, *181*(1), 1–80. <https://doi.org/10.1111/j.1365-246X.2009.04491.x>
- Deschamps, A., & Fujiwara, T. (2003). Asymmetric accretion along the slow-spreading Mariana Ridge. *Geochemistry, Geophysics, Geosystems*, *4*(10), 1–11. <https://doi.org/10.1029/2003GC000537>

- Dick, H. J. B., Natland, J. H., & Ildefonse, B. (2006). Past and future impact of deep drilling in the oceanic crust and mantle. *Oceanography*, 19(SPL.ISS. 4), 72–80. <https://doi.org/10.5670/oceanog.2006.06>
- Dominguez, S., Lallemand, S. E., Malavieille, J., & Von Huene, R. (1998). Upper plate deformation associated with seamount subduction. *Tectonophysics*, 293(3–4), 207–224. [https://doi.org/10.1016/S0040-1951\(98\)00086-9](https://doi.org/10.1016/S0040-1951(98)00086-9)
- Dominguez, S., Malavieille, J., & Lallemand, S. E. (2000). Deformation of accretionary wedges in response to seamount subduction: Insights from sandbox experiments. *Tectonics*, 19(1), 182–196. <https://doi.org/10.1029/1999TC900055>
- Dorel, J. (1981). Seismicity and seismic gap in the Lesser Antilles arc and earthquake hazard in Guadeloupe. *Geophysical Journal of the Royal Astronomical Society*, 67(3), 679–695. <https://doi.org/10.1111/j.1365-246X.1981.tb06947.x>
- Dziewonski, A. M., Chou, T. A., & Woodhouse, J. H. (1981). Determination of earthquake source parameters from waveform data for studies of global and regional seismicity. *Journal of Geophysical Research*, 86(B4), 2825–2852. <https://doi.org/10.1029/JB086iB04p02825>
- Ekström, G., Nettles, M., & Dziewoński, A. M. (2012). The global CMT project 2004–2010: Centroid-moment tensors for 13,017 earthquakes. *Physics of the Earth and Planetary Interiors*, 200–201, 1–9. <https://doi.org/10.1016/j.pepi.2012.04.002>
- Escartín, J., & Canales, J. P. (2011). Detachments in Oceanic Lithosphere: Deformation, Magmatism, Fluid Flow, and Ecosystems. *Eos, Transactions American Geophysical Union*, 92(4), 31. <https://doi.org/10.1029/2011EO040003>
- Escartín, J., Hirth, G., & Evans, B. (2001). Strength of slightly serpentized peridotites: Implications for the tectonics of oceanic lithosphere. *Geology*, 29(11), 1023–1026. <https://doi.org/10.1130/0091-7613>
- Escartin, J., Hirth, J. G., & Evans, B. (1997). Effects of serpentization on the lithospheric strength and the style of normal faulting at slow-spreading ridges. *Earth and Planetary Science Letters*, 151, 181–189.
- Escartín, J., Smith, D. K., Cann, J., Schouten, H., Langmuir, C. H., & Escrig, S. (2008). Central role of detachment faults in accretion of slow-spreading oceanic lithosphere. *Nature*, 455(7214), 790–794. <https://doi.org/10.1038/nature07333>
- Evain, M. (2011). *Structure de la zone de subduction des Petites Antilles : implications sur les dimensions de la zone sismogène interplaque*. Université Nice Sophia Antipolis.
- Ferrand, T. P. (2019). Seismicity and mineral destabilizations in the subducting mantle up to 6 GPa, 200 km depth. *Lithos*, 334–335, 205–230. <https://doi.org/10.1016/j.lithos.2019.03.014>
- Fleischer, R. L., J. R. M. Viertl, P. B. Price, and F. Aumento. “Mid-Atlantic Ridge: Age and Spreading Rates.” *Science* 161, no. 3848 (1968): 1339–42. <http://www.jstor.org/stable/1725701>.



- Feuillet, N., Beauducel, F., & Tapponnier, P. (2011). Tectonic context of moderate to large historical earthquakes in the Lesser Antilles and mechanical coupling with volcanoes. *Journal of Geophysical Research: Solid Earth*, 116(10), 1–26. <https://doi.org/10.1029/2011JB008443>
- Fisher, D. M., Gardner, T. W., Marshall, J. S., Sak, P. B., & Protti, M. (1998). Effect of subducting sea-floor roughness on fore-arc kinematics, Pacific coast, Costa Rica. *Geology*, 26(5), 467–470. <https://doi.org/10.1130/0091-7613>
- Frohlich, C. (2006). *Deep Earthquakes*. Cambridge University Press.
- Fuller, C. W., Willett, S. D., & Brandon, M. T. (2006). Formation of forearc basins and their influence on subduction zone earthquakes. *Geology*, 34, 65–68.
- Gardner, J. V., Armstrong, A. A., Calder, B. R., & Beaudoin, J. (2014). So, How Deep Is the Mariana Trench? *Marine Geodesy*, 37(1), 1–13. <https://doi.org/10.1080/01490419.2013.837849>
- Gomez, S. (2018). *Tectonostratigraphic Evolution of The Barbados Accretionary Prism and Surrounding Sedimentary Basins within the Southeastern Caribbean- South America Plate Boundary Zone*. University of Houston.
- Gomez, S., Bird, D., & Mann, P. (2018). Deep crustal structure and tectonic origin of the Tobago-Barbados ridge. *Interpretation*, 6(2), T471–T484. <https://doi.org/10.1190/INT-2016-0176.1>
- Graindorge, D., Klingelhoefer, F., Sibuet, J. C., McNeill, L., Henstock, T. J., Dean, S., Gutscher, M. A., Dessa, J. X., Permana, H., Singh, S. C., Leau, H., White, N., Carton, H., Malod, J. A., Rangin, C., Aryawan, K. G., Chaubey, A. K., Chauhan, A., Galih, D. R., ... Shankar, U. (2008). Impact of lower plate structure on upper plate deformation at the NW Sumatran convergent margin from seafloor morphology. *Earth and Planetary Science Letters*, 275(3–4), 201–210. <https://doi.org/10.1016/j.epsl.2008.04.053>
- Gutscher, M.-A., Spakman, W., Bijwaard, H., & Engdahl, E. R. (2000). Geodynamics of flat subduction: Seismicity and tomographic constraints from the Andean margin. *Tectonics*, 19(5), 814–833.
- Hacker, B. R., Abers, G. A., & Peacock, S. M. (2003). Subduction factory 1. Theoretical mineralogy, densities, seismic wave speeds, and H<sub>2</sub>O contents. *Journal of Geophysical Research: Solid Earth*, 108(B1), 1–26. <https://doi.org/10.1029/2001jb001127>
- Hacker, B. R., Peacock, S. M., Abers, G. A., & Holloway, S. D. (2003). Subduction factory 2. Are intermediate-depth earthquakes in subducting slabs linked to metamorphic dehydration reactions? *Journal of Geophysical Research: Solid Earth*, 108(B1). <https://doi.org/10.1029/2001jb001129>
- Hayes, G. P., McNamara, D. E., Seidman, L., & Roger, J. (2013). Quantifying potential earthquake and tsunami hazard in the Lesser Antilles subduction zone of the Caribbean region. *Geophysical Journal International*, 196(1), 510–521. <https://doi.org/10.1093/gji/ggt385>

- Hilde, T. W. C. (1983). Sediment subduction versus accretion around the Pacific. *Tectonophysics*, 99, pp. 381-397
- Hirauchi, K. I., Katayama, I., Uehara, S., Miyahara, M., & Takai, Y. (2010). Inhibition of subduction thrust earthquakes by low-temperature plastic flow in serpentine. *Earth and Planetary Science Letters*, 295(3–4), 349–357. <https://doi.org/10.1016/j.epsl.2010.04.007>
- Hirose, F., Miyaoka, K., Hayashimoto, N., Yamazaki, T., & Nakamura, M. (2011). Outline of the 2011 off the pacific coast of tohoku earthquake (M w 9.0) -seismicity: Foreshocks, mainshock, aftershocks, and induced activity. *Earth, Planets and Space*, 63(7), 513–518. <https://doi.org/10.5047/eps.2011.05.019>
- Hofmann, A. W. (1997). Mantle geochemistry: the message from oceanic volcanism. In *Nature* (Vol. 385, Issue 6613, pp. 219–229). <https://doi.org/10.1038/385219a0>
- Hough, S. E. (2013). Missing great earthquakes. *Journal of Geophysical Research: Solid Earth*, 118(3), 1098–1108. <https://doi.org/10.1002/jgrb.50083>
- Houston, H. (2007). Deep earthquakes. *Earthquake Seismology*, 4, 321–350.
- Hu, J., & Gurnis, M. (2020). Subduction Duration and Slab Dip. *Geochemistry, Geophysics, Geosystems*, 21(4), 1–24. <https://doi.org/10.1029/2019GC008862>
- Hyndman, R. D., & Wang, K. (1995). The rupture of Cascadia great earthquakes from current deformation and the thermal regime. *Journal of Geophysical Research*, 100(22), 133–154.
- Hyndman, R. D., Wang, K., Yuan, T., & Spence, G. D. (1993). Tectonic sediment thickening, fluid expulsion, and the thermal regime of subduction zone accretionary prisms: the Cascadia margin off Vancouver Island. *Journal of Geophysical Research*, 98(B12). <https://doi.org/10.1029/93jb02391>
- Hyndman, R. D., Yamano, M., & Oleskevich, D. A. (1997). The seismogenic zone of subduction thrust faults. *Island Arc*, 6(3), 244–260. <https://doi.org/10.1111/j.1440-1738.1997.tb00175.x>
- Ildefonse, B., Blackman, D. K., John, B. E., Ohara, Y., Miller, D. J., MacLeod, C. J., Abe, N., Abratis, M., Andal, E. S., Andréani, M., Awaji, S., Beard, J. S., Brunelli, D., Charney, A. B., Christie, D. M., Delacour, A. G., Delius, H., Drouin, M., Einaudi, F., ... Zhao, X. (2007). Oceanic core complexes and crustal accretion at slow-spreading ridges. *Geology*, 35(7), 623–626. <https://doi.org/10.1130/G23531A.1>
- Ito, Y., Tsuji, T., Osada, Y., Kido, M., Inazu, D., Hayashi, Y., Tsushima, H., Hino, R., & Fujimoto, H. (2011). Frontal wedge deformation near the source region of the 2011 Tohoku-Oki earthquake. *Geophysical Research Letters*, 38(15), 1–5. <https://doi.org/10.1029/2011GL048355>
- Juteau, T., Berger, E., & Cannat, M. (1990). Serpentinized, Residual Mantle Peridotites from the M.A.R. Median Valley, ODP hole 670A (21°10'N, 45°02'W, leg 109): primary mineralogy and geothermometry. *Proceedings of the Ocean Drilling Program Scientific Results*, 106/109, 27–43.
- Kanamori, H., & Brodsky, E. E. (2004). “The physics of earthquakes”. *Reports on Progress in Physics*. 67 1429. <http://doi.org/10.1088/0034-4885/67/8/R03>

- Kearey, P., Klepeis, K. A., & Vine, F. J. (2009). *Global tectonics*. Wiley.
- Kelleher, J., Sykes, L., & Oliver, J. (1973). Possible criteria for predicting earthquake locations and their application to major plate boundaries of the Pacific and the Caribbean. *Journal of Geophysical Research*, *78*(14), 2547. <https://doi.org/10.1029/JB078i014p02547>
- Kendrick, M. A. (2018). *Halogens in Seawater, Marine Sediments and the Altered Oceanic Lithosphere*. [https://doi.org/10.1007/978-3-319-61667-4\\_9](https://doi.org/10.1007/978-3-319-61667-4_9)
- Kimura, H., Takeda, T., Obara, K., & Kasahara, K. (2010). Seismic Evidence for Active Underplating Below the Megathrust Earthquake Zone in Japan. *Science*, *329*(5988), 210–212. <https://doi.org/10.1126/science.1187115>
- Kirby, S., Engdahl, E. R., & Denlinger, R. (1996). Intermediate-depth intraslab earthquakes and arc volcanism as physical expressions of crustal and uppermost mantle metamorphism in subducting slabs. *Geophysical Monograph Series*, *96*, 195–214. <https://doi.org/10.1029/GM096p0195>
- Klingelhofer, F., & Marcaillou, B. (2022). *MANTA-RAY cruise, RV L'Atalante*. <https://doi.org/https://doi.org/10.17600/18002498>
- Kodaira, S., Takahashi, N., Nakanishi, A., Miura, S., & Kaneda, Y. (2000). Subducted seamount imaged in the rupture zone of the 1946 Nankaido earthquake. *Science*, *289*(5476), 104–106. <https://doi.org/10.1016/j.tecto.2012.12.037>
- Kopp, H., Weinzierl, W., Becel, A., Charvis, P., Evain, M., Flueh, E. R., Gailler, A., Galve, A., Hirn, A., Kandilarov, A., Klaeschen, D., Laigle, M., Papenberg, C., Planert, L., & Roux, E. (2011). Deep structure of the central Lesser Antilles Island Arc: Relevance for the formation of continental crust. *Earth and Planetary Science Letters*, *304*(1–2), 121–134. <https://doi.org/10.1016/j.epsl.2011.01.024>
- Laigle, M., Becel, A., de Voogd, B., Sachpazi, M., Bayrakci, G., Lebrun, J. F., & Evain, M. (2013). Along-arc segmentation and interaction of subducting ridges with the Lesser Antilles Subduction forearc crust revealed by MCS imaging. *Tectonophysics*, *603*, 32–54. <https://doi.org/10.1016/j.tecto.2013.05.028>
- Laigle, M., Hirn, A., Sapin, M., Bécél, A., Charvis, P., Flueh, E., Diaz, J., Lebrun, J. F., Gesret, A., Raffaele, R., Galvé, A., Evain, M., Ruiz, M., Kopp, H., Bayrakci, G., Weinzierl, W., Hello, Y., Lépine, J. C., Viodé, J. P., ... Nicolich, R. (2013). Seismic structure and activity of the north-central Lesser Antilles subduction zone from an integrated approach: Similarities with the Tohoku forearc. In *Tectonophysics* (Vol. 603, pp. 1–20). <https://doi.org/10.1016/j.tecto.2013.05.043>
- Laigle, M., Lebrun, J.-F., & Hirn, A. (2007). *SISMANTILLES 2 cruise, RV L'Atalante*. <https://doi.org/https://doi.org/10.17600/7010020>
- Lallemand, S. (1999). *La subduction océanique SB - 90-5699-205-8*. Gordon and Breach science, Amsterdam.
- Lallemand, S., Heuret, A., & Boutelier, D. (2005). On the relationships between slab dip, back-arc stress, upper plate absolute motion, and crustal nature in subduction zones. *Geochemistry, Geophysics, Geosystems*, *6*(9). <https://doi.org/10.1029/2005GC000917>

- Laurencin, M., Graindorge, D., Klingelhofer, F., Marcaillou, B., & Evain, M. (2018). Influence of increasing convergence obliquity and shallow slab geometry onto tectonic deformation and seismogenic behavior along the Northern Lesser Antilles zone. *Earth and Planetary Science Letters*, 492, 59–72. <https://doi.org/10.1016/j.epsl.2018.03.048>
- Laurencin, M., Marcaillou, B., Graindorge, D., Klingelhofer, F., Lallemand, S., Laigle, M., & Lebrun, J. F. (2017). The polyphased tectonic evolution of the Anegada Passage in the northern Lesser Antilles subduction zone. *Tectonics*, 36(5), 945–961. <https://doi.org/10.1002/2017TC004511>
- Laurencin, M., Marcaillou, B., Graindorge, D., Lebrun, J. F., Klingelhofer, F., Boucard, M., Laigle, M., Lallemand, S., & Schenini, L. (2019). The Bunce Fault and Strain Partitioning in the Northern Lesser Antilles. *Geophysical Research Letters*, 46(16), 9573–9582. <https://doi.org/10.1029/2019GL083490>
- Lay, T., & Nishenko, S. (2022). Updated concepts of seismic gaps and asperities to assess great earthquake hazard along South America. *Earth, Atmospheric, and Planetary Sciences*, 119(51), 1–9. <https://doi.org/10.1073/pnas>
- Legendre, L., Philippon, M., Münch, P., Leticee, J.L., Noury, M., Maincent, G., Cornée, J.J., Caravati, A., Lebrun, J.F., Mazabraud, Y. (2018). Trench bending initiation: upper plate strain pattern and volcanism. Insights from the Lesser Antilles Arc, St. Barthelemy Island, French West Indies. *Tectonics* 37 (9), 2777–2797
- Leroy, S., Mau, A., Patriat, P., & Le, B. M. De. (2000). *An alternative interpretation of the Cayman trough evolution from a reidentification of magnetic anomalies*. 539–557.
- Macdonald, K. C. (2019). Mid-ocean ridge tectonics, volcanism, and geomorphology. In *Encyclopedia of Ocean Sciences: Vol. v* (Issue January). Elsevier Inc. <https://doi.org/10.1016/B978-0-12-409548-9.11065-6>
- Manaker, D. M., Calais, E., Freed, A. M., Ali, S. T., Przybylski, P., Mattioli, G., Jansma, P., Prépetit, C., & De Chabaliér, J. B. (2008). Interseismic plate coupling and strain partitioning in the Northeastern Caribbean. *Geophysical Journal International*, 174(3), 889–903. <https://doi.org/10.1111/j.1365-246X.2008.03819.x>
- Mann, P. (1999). Chapter 1 Caribbean sedimentary basins: classification and tectonic setting from jurassic to present. In P. B. T.-S. B. of the W. Mann (Ed.), *Caribbean Basins* (Vol. 4, pp. 3–31). Elsevier. [https://doi.org/https://doi.org/10.1016/S1874-5997\(99\)80035-5](https://doi.org/https://doi.org/10.1016/S1874-5997(99)80035-5)
- Mann, P., Hippolyte, J.-C., Grindlay, N. R., & Abrams, L. J. (2005). Neotectonics of southern Puerto Rico and its offshore margin. In P. Mann (Ed.), *Active Tectonics and Seismic Hazards of Puerto Rico, the Virgin Islands, and Offshore Areas* (Vol. 385, p. 0). Geological Society of America. <https://doi.org/10.1130/0-8137-2385-X.173>
- Mannu, U., Ueda, K., Willett, S. D., Gerya, T. V., & Strasser, M. (2017). Stratigraphic signatures of forearc basin formation mechanisms. *Geochemistry, Geophysics, Geosystems*, 18, 2388–2410. <https://doi.org/10.1002/2017GC006810>
- Marcaillou, B., & Klingelhofer, F. (2013a). *ANTITHESIS-1-Leg1 Cruise, RV L'Atalante*. <https://doi.org/doi:10.17600/13010070>

- Marcaillou, B., & Klingelhoefer, F. (2013b). *ANTITHESIS-1-Leg2 Cruise, RV Pourquoi Pas?* <https://doi.org/doi:10.17600/13030100>
- Marcaillou, B., & Klingelhoefer, F. (2016). *ANTITHESIS-3 Cruise, RV Pourquoi Pas?* <https://doi.org/doi:10.17600/16001700>
- Marcaillou, B., Klingelhoefer, F., Laurencin, M., Lebrun, J.-F., Laigle, M., Lallemand, S., Schenini, L., Gay, A., Boucard, M., Ezenwaka, K., & Graindorge, D. (2021). Pervasive detachment faults within the slow spreading oceanic crust at the poorly coupled Antilles subduction zone. *Communications Earth & Environment*, 2(1). <https://doi.org/10.1038/s43247-021-00269-6>
- McCaffrey, R. (2009). The tectonic framework of the Sumatran subduction zone. *Annual Review of Earth and Planetary Sciences*, 37, 345-366. <https://doi.org/10.1146/annurev.earth.031208.100212>
- McGarr, A., Fletcher, J. B. (2003). Maximum Slip in Earthquake Fault Zones, Apparent Stress, and Stick-Slip Friction. *Bulletin of the Seismological Society of America*. 93 (6): 2355–2362. <http://doi.org/10.1785/0120030037>
- Montheil, L., Philippon, M., Münch, P., Camps, P., Vaes, B., Cornée, J.-J., Poidras, T., van Hinsbergen D.J.J. (2023). Paleomagnetic rotations in the northeastern Caribbean region reveal major intraplate deformation since the Eocene. *Tectonics*, 42, e2022TC007706. <https://doi.org/10.1029/2022TC007706>
- Moore, G. F., & Sender, K. L. (1995). Fracture zone collision along the South Panama margin. *Special Paper of the Geological Society of America*, 295(September), 201–212. <https://doi.org/10.1130/SPE295-p201>
- Moore, J. C. (2001). Accretionary Prisms (J. K. Cochran, H. J. Bokuniewicz, & P. L. B. T.-E. of O. S. (Third E. Yager, Eds.; pp. 275–281). Academic Press. <https://doi.org/https://doi.org/10.1016/B978-0-12-813081-0.00465-1>
- Moore, J. C., & Saffer, D. (2001). Updip limit of the seismogenic zone beneath the accretionary prism of Southwest Japan: An effect of diagenetic to low-grade metamorphic processes and increasing effective stress. *Geology*, 29(2), 183–186. <https://doi.org/10.1130/0091-7613>
- Moore, J. C., Shipley, T. H., Goldberg, D., Ogawa, Y., Filice, F., Fisher, A., Jurado, M.-J., Moore, G. F., Rabaute, A., Yin, H., Zwart, G., Brückmann, W., Henry, P., Ashi, J., Blum, P., Meyer, A., Housen, B., Kastner, M., Labaume, P., ... Zheng, Y. (1995). Abnormal fluid pressures and fault-zone dilation in the Barbados accretionary prism: Evidence from logging while drilling. *Geology*, 23(7), 605–608. <https://doi.org/10.1130/0091-7613>
- Moreno, M., Haberland, C., Oncken, O., Rietbrock, A., Angiboust, S., & Heidbach, O. (2014). Locking of the Chile subduction zone controlled by fluid pressure before the 2010 earthquake. *Nature Geoscience*, 7(4), 292–296. <https://doi.org/10.1038/ngeo2102>
- Muller, R. D., & Smith, W. H. F. (1993). Deformation of the oceanic crust between the North American and South American plates. *Journal of Geophysical Research*, 98(B5), 8275–8291. <https://doi.org/10.1029/92JB02863>

- Neill, I., Kerr, A. C., Hastie, A. R., Stanek, K.-P., & Millar, I. L. (2011). Origin of the Aves Ridge and Dutch–Venezuelan Antilles: interaction of the Cretaceous ‘Great Arc’ and Caribbean–Colombian Oceanic Plateau?’ *Journal of the Geological Society*, *168*(2), 333–348. <https://doi.org/10.1144/0016-76492010-067>
- Noda, A. (2016). Forearc basins: Types, geometries, and relationships to subduction zone dynamics. *GSA Bulletin*, *128*, 879–895.
- Oleskevich, D. A., Hyndman, R. D., & Wang, K. (1999). The updip and downdip limits to great subduction earthquakes: Thermal and structural models of Cascadia, south Alaska, SW Japan, and Chile. *Geophysical Research*, *104*, 965–991.
- Pacheco, J. F., Sykes, L. R., & Scholz, C. H. (1993). Nature of seismic coupling along simple plate boundaries of the subduction type. *Journal of Geophysical Research*, *98*(B8). <https://doi.org/10.1029/93jb00349>
- Padron, C., Klingelhoefer, F., Marcaillou, B., Lebrun, J., Lallemand, S., Garroq, C., Laigle, M., Roest, W. R., Beslier, M., Schenini, L., Graindorge, D., Gay, A., Audemard, F., & Münch, P. (2021). Deep Structure of the Grenada Basin from Wide-Angle Seismic, Bathymetric and Gravity Data. *Journal of Geophysical Research: Solid Earth*, *126*(2). <https://doi.org/10.1029/2020JB020472>
- Patriat, M., Pichot, T., Westbrook, G. K., UMBER, M., Deville, E., Bénard, F., Roest, W. R., & Loubrieu, B. (2011a). Evidence for Quaternary convergence across the North America–South America plate boundary zone, east of the Lesser Antilles. *Geology*, *39*(10), 979–982. <https://doi.org/10.1130/G32474.1>
- Patriat, M., Pichot, T., Westbrook, G. K., UMBER, M., Deville, E., Bénard, F., Roest, W. R., & Loubrieu, B. (2011b). Evidence for Quaternary convergence across the North America–South America plate boundary zone, east of the Lesser Antilles. *Geology*, *39*(10), 979–982. <https://doi.org/10.1130/G32474.1>
- Paulatto, M., Laigle, M., Galve, A., Charvis, P., Sapin, M., Bayrakci, G., Evain, M., & Kopp, H. (2017). Dehydration of subducting slow-spread oceanic lithosphere in the Lesser Antilles. *Nature Communications*, *8*(m), 62. <https://doi.org/10.1038/ncomms15980>
- Peacock, S. M. (2001). Are the lower planes of double seismic zones caused by serpentine dehydration in subducting oceanic mantle? *Geology*, *29*(4), 299–302. <https://doi.org/10.1130/0091-7613>
- Peacock, S. M., & Wang, K. (1999). Seismic Consequences of Warm Versus Cool Subduction Metamorphism: Examples from Southwest and Northeast Japan. *Science*, *286*, 937–939.
- Penrose Conference Participants. (1972). *Penrose Field Conference: Ophiolites*. *Geotimes*. 24–25.
- Philibosian, B., Feuillet, N., Weil-Accardo, J., Jacques, E., Guihou, A., Mériaux, A. S., Anglade, A., Saurel, J. M., & Deroussi, S. (2022). 20th-century strain accumulation on the Lesser Antilles megathrust based on coral microatolls. *Earth and Planetary Science Letters*, *579*, 117343. <https://doi.org/10.1016/j.epsl.2021.117343>

- Philippon, M., van Hinsbergen, D. J. J., Boschman, L. M., Gossink, L. A. W., Cornée, J. J., BouDagher-Fadel, M., Léticée, J. L., Lebrun, J. F., & Munch, P. (2020). Caribbean intra-plate deformation: Paleomagnetic evidence from St. Barthélemy Island for post-Oligocene rotation in the Lesser Antilles forearc. *Tectonophysics*, 777. <https://doi.org/10.1016/j.tecto.2020.228323>
- Pichot, T., Patriat, M., Westbrook, G. K., Nalpas, T., Gutscher, M. A., Roest, W. R., Deville, E., Moulin, M., Aslanian, D., & Rabineau, M. (2012a). The Cenozoic tectonostratigraphic evolution of the Barracuda Ridge and Tiburon Rise, at the western end of the North America-South America plate boundary zone. *Marine Geology*, 303–306, 154–171. <https://doi.org/10.1016/j.margeo.2012.02.001>
- Pichot, T., Patriat, M., Westbrook, G. K., Nalpas, T., Gutscher, M. A., Roest, W. R., Deville, E., Moulin, M., Aslanian, D., & Rabineau, M. (2012b). The Cenozoic tectonostratigraphic evolution of the Barracuda Ridge and Tiburon Rise, at the western end of the North America-South America plate boundary zone. *Marine Geology*, 303–306, 154–171. <https://doi.org/10.1016/j.margeo.2012.02.001>
- Pindell, J. L., & Barrett, S. F. (1991). Geological evolution of the Caribbean region; A plate-tectonic perspective. In G. Dengo & J. E. Case (Eds.), *The Caribbean Region: Vol. H* (p. 0). Geological Society of America. <https://doi.org/10.1130/DNAG-GNA-H.405>
- Ranero, C. R., Morgan, J. P., McIntosh, K. D., & Reichert, C. (2003). Bending-related faulting and mantle serpentinization at the Middle America trench. *Nature*, 425, 367–373.
- Ranero, C. R., & Von Huene, R. (2000). Subduction erosion along the Middle America convergent margin. *Nature*, 404(6779), 748–752. <https://doi.org/10.1038/35008046>
- Reid, J.A., Plumley, P.W., Schellekens, J.H. (1991). Paleomagnetic evidence for late Miocene counterclockwise rotation of north coast carbonate sequence, Puerto Rico. *Geophys. Res. Lett.* 18 (3), 565–568
- Roest, W. R., & Collette, B. J. (1986). The Fifteen Twenty Fracture Zone and the North American-South American plate boundary. *Journal of the Geological Society, London*, 9, 833–843.
- Ruh, J. B. (2016). Submarine landslides caused by seamounts entering accretionary wedge systems. *Terra Nova*, 28(3), 163–170. <https://doi.org/10.1111/ter.12204>
- Ruiz, M., Galve, A., Monfret, T., Sapin, M., Charvis, P., Laigle, M., Evain, M., Hirn, A., Flueh, E., Gallart, J., Diaz, J., & Lebrun, J. F. (2013). Seismic activity offshore Martinique and Dominica islands (Central Lesser Antilles subduction zone) from temporary onshore and offshore seismic networks. *Tectonophysics*, 603, 68–78. <https://doi.org/10.1016/J.TECTO.2011.08.006>
- Saffer, D. M., & Marone, C. (2003). Comparison of smectite- and illite-rich gouge frictional properties: Application to the updip limit of the seismogenic zone along subduction megathrusts. *Earth and Planetary Science Letters*, 215(1–2), 219–235. [https://doi.org/10.1016/S0012-821X\(03\)00424-2](https://doi.org/10.1016/S0012-821X(03)00424-2)

- Saffer, D. M., & Tobin, H. J. (2011). Hydrogeology and mechanics of subduction zone forearcs: Fluid flow and pore pressure. *Annual Review of Earth and Planetary Sciences*, 39, 157–186. <https://doi.org/10.1146/annurev-earth-040610-133408>
- Saffer, D. M., & Wallace, L. M. (2015). The frictional, hydrologic, metamorphic and thermal habitat of shallow slow earthquakes. *Nature Geoscience*, 8(8), 594–600. <https://doi.org/10.1038/ngeo2490>
- Sanchez, J., Mann, P., & Emmet, P. A. (2016). Late cretaceous-cenozoic tectonic transition from collision to transtension, honduran borderlands and Nicaraguan rise, NW Caribbean plate boundary. *Geological Society Special Publication*, 431(1), 273–297. <https://doi.org/10.1144/SP431.3>
- Schlaphorst, D., Kendall, J. M., Collier, J. S., Verdon, J. P., Blundy, J., Baptie, B., Latchman, J. L., Massin, F., & Bouin, M. P. (2016). Water, oceanic fracture zones and the lubrication of subducting plate boundaries-insights from seismicity. *Geophysical Journal International*, 204(3), 1405–1420. <https://doi.org/10.1093/gji/ggv509>
- Scholz, C. H., ed. (2002).” The seismic cycle, *The Mechanics of Earthquakes and Faulting* (2 ed.), Cambridge: Cambridge University Press, pp. 244–299, ISBN 978-0-511-81851-6
- Scholz, C. H. (1998). Earthquakes and friction laws. *Nature*, 391(6662), 37–42. <https://doi.org/10.1038/34097>
- Scholz, C. H., & Campos, J. (2012). The seismic coupling of subduction zones revisited. *Journal of Geophysical Research: Solid Earth*, 117(5), 1–22. <https://doi.org/10.1029/2011JB009003>
- Seely, D. R., Vail, P. R., & Walton, G. G. (1974). *Trench Slope Model*. <https://doi.org/10.29118/ipa.2054.333.351>
- Smith, D. K., Cann, J. R., & Escartín, J. (2006). Widespread active detachment faulting and core complex formation near 13°N on the Mid-Atlantic Ridge. *Nature*, 442(7101), 440–443. <https://doi.org/10.1038/nature04950>
- Stein, S., Engeln, J. F., Wiens, D. A., Fujita, K., & Speed, R. C. (1982). Subduction seismicity and tectonics in the Lesser Antilles arc. *Journal of Geophysical Research*, 87, 8642–8664.
- Stern, C. R. (2011). Subduction erosion: Rates, mechanisms, and its role in arc magmatism and the evolution of the continental crust and mantle. *Gondwana Research*, 20(2–3), 284–308. <https://doi.org/10.1016/j.gr.2011.03.006>
- Stern, R. J. (2002). Subduction zones. *Reviews of Geophysics*, 40(4), 3-1-3–38. <https://doi.org/10.1029/2001RG000108>
- Stern, R. J. (2010). The anatomy and ontogeny of modern intra-oceanic arc systems. *Geological Society, London, Special Publications*, 338(1), 7–34. <https://doi.org/10.1144/SP338.2>
- Symithe, S., Calais, E., De Chabalier, J. B., Robertson, R., & Higgins, M. (2015). Current block motions and strain accumulation on active faults in the Caribbean. *Journal of Geophysical Research: Solid Earth*, 120(5), 3748–3774. <https://doi.org/10.1002/2014JB011779>



- Szitkar, F., Dymant, J., Petersen, S., Bialas, J., Klischies, M., Graber, S., Klaeschen, D., Yeo, I., & Murton, B. J. (2019). Detachment tectonics at Mid-Atlantic Ridge 26°N. *Scientific Reports*, 9(1), 0–8. <https://doi.org/10.1038/s41598-019-47974-z>
- Ten Brink, U. S., Bakun, W. H., & Flores, C. H. (2011). Historical perspective on seismic hazard to Hispaniola and the northeast Caribbean region. *Journal of Geophysical Research: Solid Earth*, 116(12), 1–15. <https://doi.org/10.1029/2011JB008497>
- Thatcher, W. (1989). Earthquake recurrence and risk assessment in circum-Pacific seismic gap. *Letters to Nature*, 341(August), 3–5.
- Tse, S. T., & Rice, J. R. (1986). Crustal earthquake instability in relation to the depth variation of frictional slip properties. *Journal of Geophysical Research*, 91(B9), 9452. <https://doi.org/10.1029/jb091ib09p09452>
- Tsuru, T., Park, J.-O., Miura, S., Kodaira, S., Kido, Y., & Hayashi, T. (2002). Along-arc structural variation of the plate boundary at the Japan Trench margin: Implication of interplate coupling. *Journal of Geophysical Research: Solid Earth*, 107(B12), ESE 11-1-ESE 11-15. <https://doi.org/10.1029/2001jb001664>
- Ulmer, P., & Trommsdorff, V. (1995). Serpentine stability to mantle depths and subduction-related magmatism. *Science*, 268(5212), 858–861. <https://doi.org/10.1126/science.268.5212.858>
- Van Fossen, M.C., Channell, J.E., Schellekens, J.H. (1989). Paleomagnetic evidence for Tertiary anticlockwise rotation in southwest Puerto Rico. *Geophys. Res. Lett.* 16 (8), 819–822
- van Rijsingen, E., Lallemand, S., Peyret, M., Arcay, D., Heuret, A., Funiciello, F., & Corbi, F. (2018). How subduction interface roughness influences the occurrence of large interplate earthquakes. *Geochemistry, Geophysics, Geosystems*, 19(8), 2342–2370. <http://doi.org/10.1029/2018GC007618>
- van Rijsingen, E. M., Calais, E., Jolivet, R., de Chabaliere, J. B., Jara, J., Symithe, S., Robertson, R., & Ryan, G. A. (2021). Inferring Interseismic Coupling Along the Lesser Antilles Arc: A Bayesian Approach. *Journal of Geophysical Research: Solid Earth*, 126(2), 1–21. <https://doi.org/10.1029/2020JB020677>
- van Rijsingen, E. M., Calais, E., Jolivet, R., de Chabaliere, J.-B., Robertson, R., Ryan, G. A., & Symithe, S. (2022). Ongoing tectonic subsidence in the Lesser Antilles subduction zone. *Geophysical Journal International*, 319–326. <https://doi.org/10.1093/gji/ggac192>
- Von Huene, R., Culotta, R. (1989). Tectonic erosion at the front of the Japan Trench convergent margin. *Tectonophysics*, 160, pp. 75-90
- Von Huene, R., Lallemand, S. (1990). Tectonic erosion along the Japan and Peru convergent margins. *Geological Society of America Bulletin*, 102 (1990), pp. 704-720
- Von Huene, R., Bialas, J., Flueh, E., Cropp, B., Csernok, T., Fabel, E., Hoffmann, J., Emeis, K., Holler, P., Jeschke, G., Leandro M., C., Fernández, I. P., Chavarria S., J., Florez H., A., Escobedo Z., D., León, R., & Barrios L., O. (1995). Morphotectonics of the Pacific

- convergent margin of Costa Rica. *Special Paper of the Geological Society of America*, 295, 291–307. <https://doi.org/10.1130/SPE295-p291>
- von Huene, R., Ranero, C. R., & Vannucchi, P. (2004). Generic model of subduction erosion. *Geology*, 32(10), 913–916. <https://doi.org/10.1130/G20563.1>
- Vrolijk, P. (1990). On the mechanical role of smectite in subduction zones. *Geology*, 18(8), 703–707. <https://doi.org/10.1130/0091-7613>
- Wang, K., & Bilek, S. L. (2011). Do subducting seamounts generate or stop large earthquakes? *Geology*, 39(9), 819–822. <https://doi.org/10.1130/G31856.1>
- Westbrook, G. K. (1982). The Barbados Ridge Complex: Tectonics of a mature forearc system. *Geological Society Special Publication*, 10(Saunders 1979), 275–290. <https://doi.org/10.1144/GSL.SP.1982.010.01.18>
- Westbrook, G. K., Ladd, J. W., Buhl, P., Bangs, N., & Tiley, G. J. (1988). Cross section of an accretionary wedge: Barbados Ridge complex. *Geology*, 16, 631–635. <https://doi.org/10.1130/0091-7613>
- Westbrook, G. K., & Smith, M. J. (1983). Long décollements and mud volcanoes: Evidence from the Barbados Ridge Complex for the role of high pore-fluid pressure in the development of an accretionary complex. *Geology*, 11(5), 279–283. <https://doi.org/10.1130/0091-7613>
- White, R. S., McKenzie, D., & O’Nions, R. K. (1992). Oceanic crustal thickness from seismic measurements and rare earth element inversions. *Journal of Geophysical Research*, 97(B13). <https://doi.org/10.1029/92jb01749>
- Wright, A. (1984). Sediment Distribution and Depositional Processes Operating in The Lesser Antilles Intraoceanic Island Arc, Eastern Caribbean. Biju-Duval B., Moore J.C., *et al.* (Eds.), Initial Reports of the Deep-Sea Drilling Project, Vol. 78 A, U.S. Gov. Print. Off, Washington, DC, pp. 301-324
- Wright, Tim. J. (2013). Terrain Motion 1: The Earthquake deformation cycle. *4th Advanced Training Course in Land Remote Sensing*.
- Wunder, B., & Schreyer, W. (1997). Antigorite: High-pressure stability in the system MgO-SiO<sub>2</sub>-H<sub>2</sub>O (MSH). *Lithos*, 41(1–3), 213–227. [https://doi.org/10.1016/s0024-4937\(97\)82013-0](https://doi.org/10.1016/s0024-4937(97)82013-0)
- Xie, X., Mann, P., & Escalona, A. (2010). Regional provenance study of Eocene clastic sedimentary rocks within the South America – Caribbean plate boundary zone using detrital zircon geochronology. *Earth and Planetary Science Letters*, 291(1–4), 159–171. <https://doi.org/10.1016/j.epsl.2010.01.009>
- Zellmer, K. E., & Taylor, B. (2001). A three-plate kinematic model for Lau Basin opening. *Geochemistry, Geophysics, Geosystems*, 2, Paper number 2000GC000106

# Chapter 2

## Methods of data acquisition and analysis

### 2.1 Dataset

The dataset used in this work includes Multichannel seismic (MCS), bathymetric data, heat-flow data, and seismicity recordings. These data were acquired during the Antithesis 1 & 3 (Marcaillou & Klingelhoefer, 2013, 2013b, 2016), Sismantilles 2 (Laigle et al., 2007), and Manta-Ray (Klingelhoefer & Marcaillou, 2022) oceanographic campaigns. The MCS data consist of 105 lines, with 18 lines acquired during the Antithesis 1, 36 lines acquired during the Antithesis 3, and 51 lines acquired during the Manta-Ray campaign. They include both strike and dip lines that extends from the oceanic domain to the inner forearc in the Northern Lesser Antilles subduction margin (Figure 2.1.1). The heat-flow data consist of 39 measurements. 11 of them were acquired in the Northern Lesser Antilles at the latitude of Saint Martin, while 28 were acquired in the central Lesser Antilles offshore Martinique. The seismicity recordings are from a 5.5-year-long OBS deployments in the Central Lesser Antilles from South of Guadeloupe to Martinique, during the Sismantilles project (Laigle et al., 2013), while the bathymetric data were acquired during all the surveys.

In this chapter, we will focus on discussing the processing and interpretation methods that we applied to the MCS lines used in this study. We will then discuss the acquisition method of the heat-flow data, and the methods used in modelling the thermal structure of the margin.

### 2.2 MCS data processing

The MCS data that I processed and used during my PhD were acquired during the Antithesis 3 and Manta-Ray missions. They consist of six low frequency dip lines (Ant 47, 43, 54, 45, 52, and 49), one strike line (Ant 48), and three trench-normal high-resolution (HR) seismic lines (MTYHR 38, 39, 40) (Figure 2.1.1). The acquisition parameters and the processing workflow for these lines are presented in Table 2.2.1 and Figure 2.2.1 respectively. The data processing was done using the CGG-Geovation software, and was used to produce the final processed images of the subsurface.

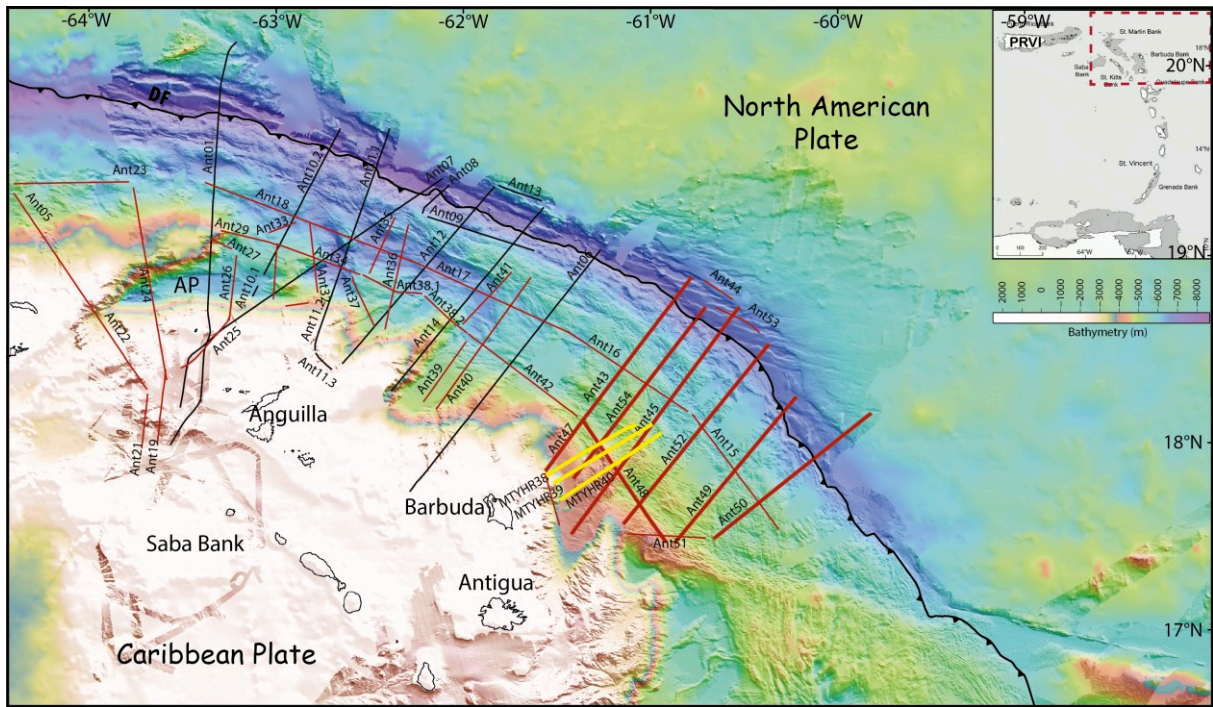


Figure 2.1.1: Survey area covered during Antithesis 1 & 3 oceanographic cruises showing the MCS lines. The black lines are MCS data acquired during Antithesis 1, while the red lines are MCS data acquired during Antithesis 3 cruise. The Yellow line are three Manta-Ray HR line integrated in this work. AP – Aneгада Passage, DF – Deformation front. The heat-flow acquisition locations are shown in a separate figure in section 2.4

| Survey                           | Antithesis 1 | Antithesis 3 | Manta-Ray (HR) |
|----------------------------------|--------------|--------------|----------------|
| Source volume (in <sup>3</sup> ) | 7699         | 6500         | 320            |
| Shot spacing                     | 154 m        | 150 m        | 10 s           |
| Rate of shot (s)                 | 1 shot/min   | 1 shot/min   | 6 shots/min    |
| Acquisition speed (Kn)           | 5            | 5            | 5              |
| Traces number                    | 300/288      | 720          | 480            |
| Traces spacing (m)               | 12.5         | 6.25         | 6.25           |
| Record time (s)                  | 25           | 20           | 9-13           |
| Data sampling (ms)               | 2            | 2            | 2              |

Table 2.2.1: Acquisition parameters of the seismic reflection during the Antithesis 1 & 3, and Mantay-Ray cruises

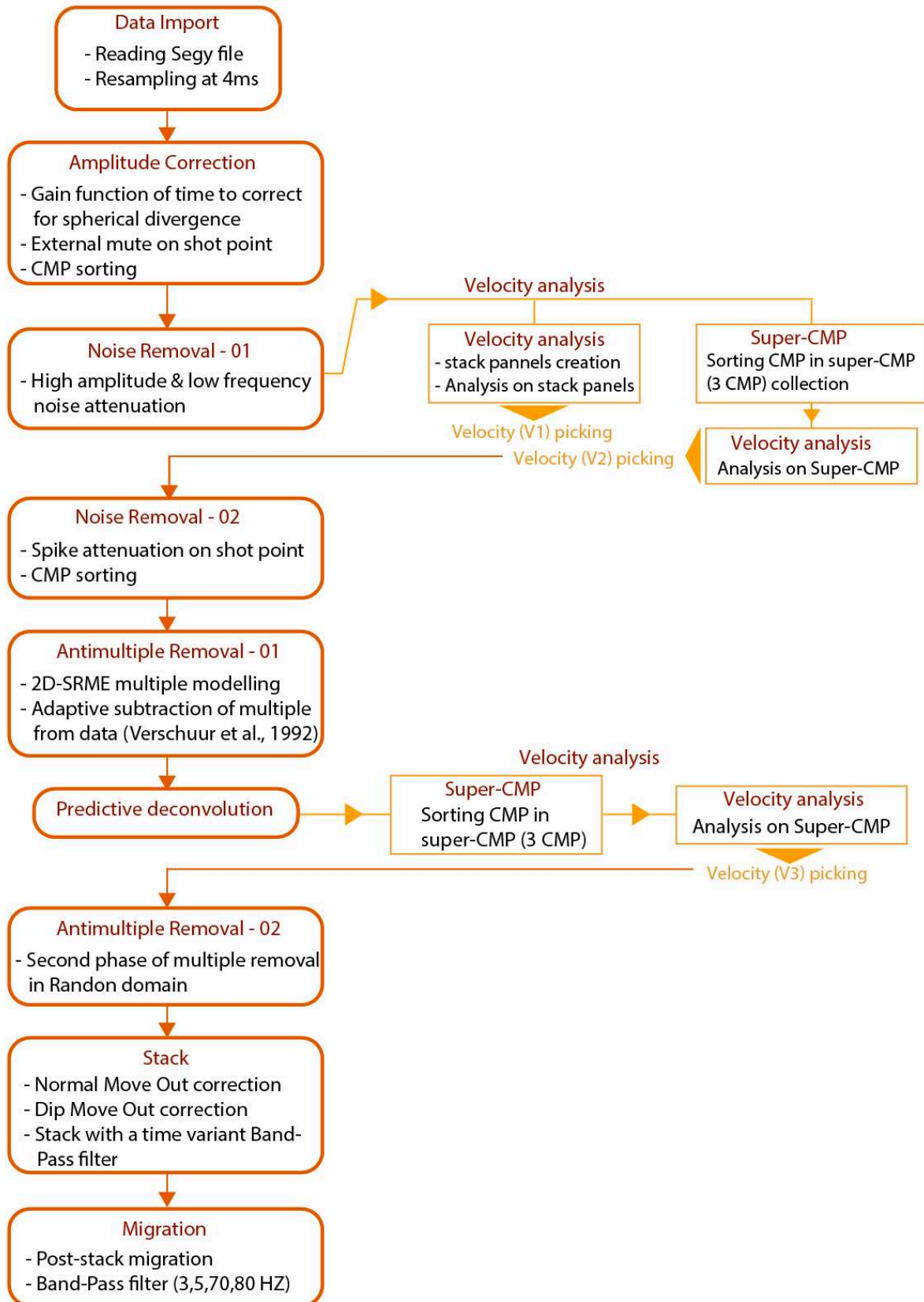


Figure 2.2.1: The workflow adopted in the image processing of the multichannel seismic data.

### 2.2.1 Resampling

We began the processing by resampling the seismic data that was acquired at a 2 ms sampling rate to a 4 ms sampling rate. This increase in the sampling rate of the seismic data reduced the data size by half, and the maximum signal frequency from 250 Hz to 125 Hz (Figure 2.2.2) in line with the Nyquist frequency criterion (e.g. Yilmaz, 1987). Our dataset is designed to image deep crustal structures, with an airgun source dedicated to generate a low-frequency content (5-30 Hz) for efficient intracrustal propagation, higher frequencies being absorbed rapidly at shallow depths; hence, this frequency range is acceptable since the usable part of the signal is below 60 Hz. Resampling of the data decreased the storage space and shortened the processing time without degrading the processing result.

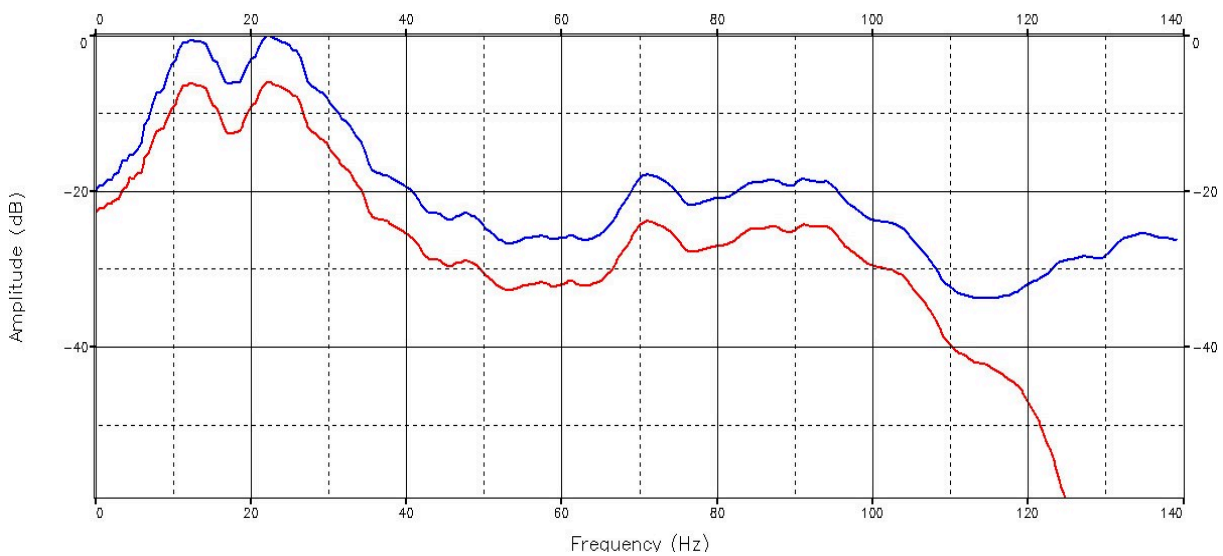


Figure 2.2.2: Amplitude spectrum of shot gather with 2 ms sampling rate (blue) before resampling, and 4 ms sampling rate (red) after resampling. The usable part of the recorded signal is in the frequency range of 3 to 60 Hz.

### 2.2.2 Spherical divergence correction

To compensate for amplitude loss with increasing depth due to spherical divergence of the wavefront, we applied an additional gain function of time. Seismic energy emitted by an acoustic source will diverge on a spherical wavefront as it propagates through the subsurface. As the sphere continually spreads out, the energy density decreases. In a homogenous and isotropic medium, the energy density of the wavefront decreases proportionally with the inverse of the square of the radius, and the amplitude is proportional to the square root of the energy density and decays with an inverse of the radius. Since the subsurface is not homogenous and seismic velocities increases with depth, there is an increase in divergence of the wavefront, which causes a rapid decay in amplitude with depth.

In the first phase of the processing, we do not have an accurate subsurface velocity information, thus, we applied a standard exponential, offset-dependent function to account for the amplitude loss using the SDICO module. However, this module was re-applied after the velocity analysis, and the correction for the spherical divergence was done using the stacking velocity. This correction increased the amplitude of the reflectors at depth. An example of a shot gather with and without spherical divergence correction is shown in Figure 2.2.3.

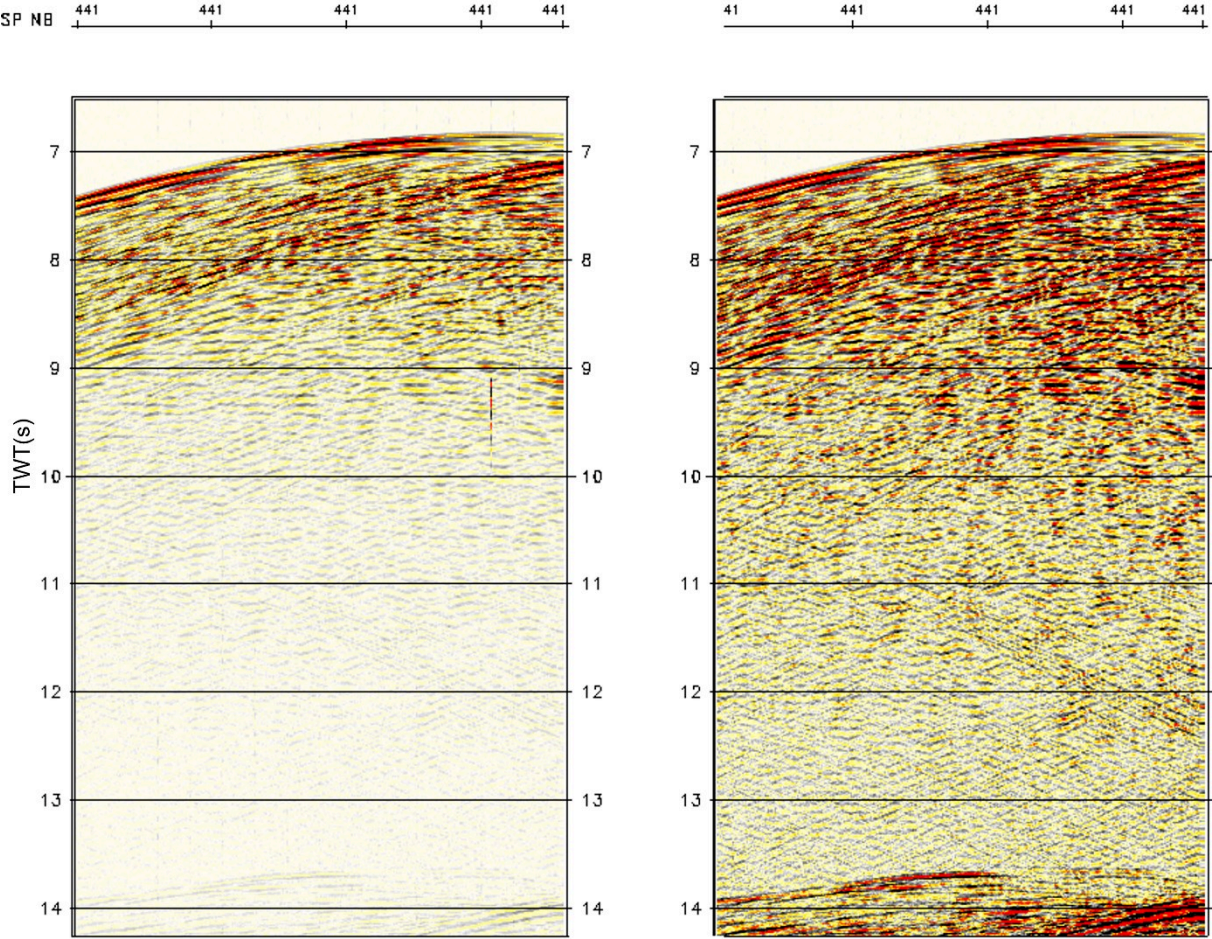
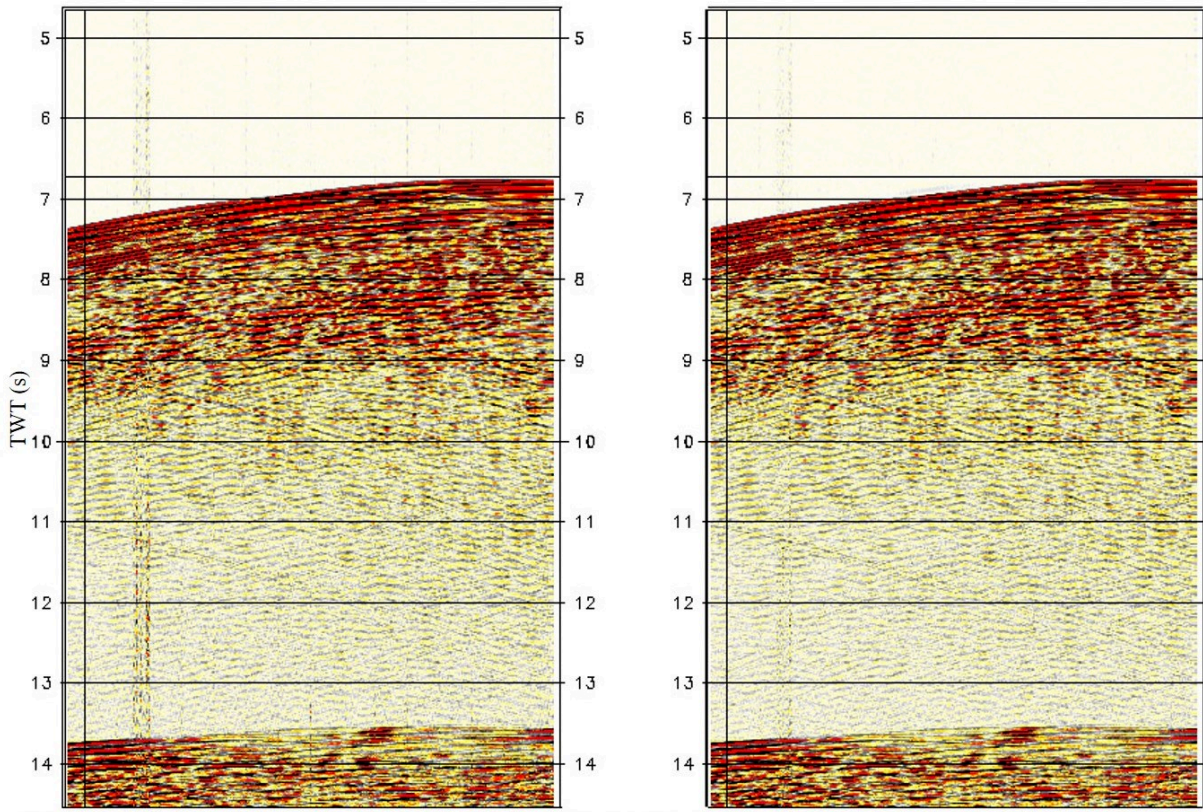


Figure 2.2.3: Shot gather (SP 441) of Ant 54 without gain correction (left) and after applying spherical divergence correction (right). There is an increase in the amplitude of the deep reflectors after applying the corrections. For instance the reflector at 10.5s which represents the interplate.

**2.2.3 Noise Attenuation**

In order to remove noise on the seismic data and increase the signal to noise ratio, we applied high amplitude and low frequency noise attenuation. The high amplitude noise blasts were scaled down using the Geovation module BLAST. By obtaining the average amplitude in noisy traces using the median absolute value of all the trace samples, the excessively high amplitude

envelope on each trace is detected. The noisy zones are then scaled down to match the amplitude of the other traces. To filter out the very low frequency noise, we apply a band-pass filter (high-pass) using the module FILTR. A shot gather before and after noise attenuation is shown in Figure 2.2.4.



*Figure 2.2.4: Shot point 211 from Ant 45 before (left) and after (right) noise attenuations. High amplitude noise blasts were scaled down, and very low frequencies noise were filtered using a band-pass filter.*

#### **2.2.4 Surface related multiple and adaptive model subtraction**

This processing involves the modelling of the surface related multiples, and adaptive subtraction of the multiple from the data as described in Verschuur et al., (1992). The surface related multiple elimination (SRME) process predicts the multiple without any prior knowledge of the subsurface, and does not require the input of the source and the surface reflectivity properties. The multiples were predicted using the SMMOD module on geovation, and subtracted adaptively by estimating an adaptation filter using the ADAPT module to attenuate the multiples. For improved performance, the SRME was applied twice during the processing. An example of a shot gather before and after SRME application is shown in figure 2.2.5.



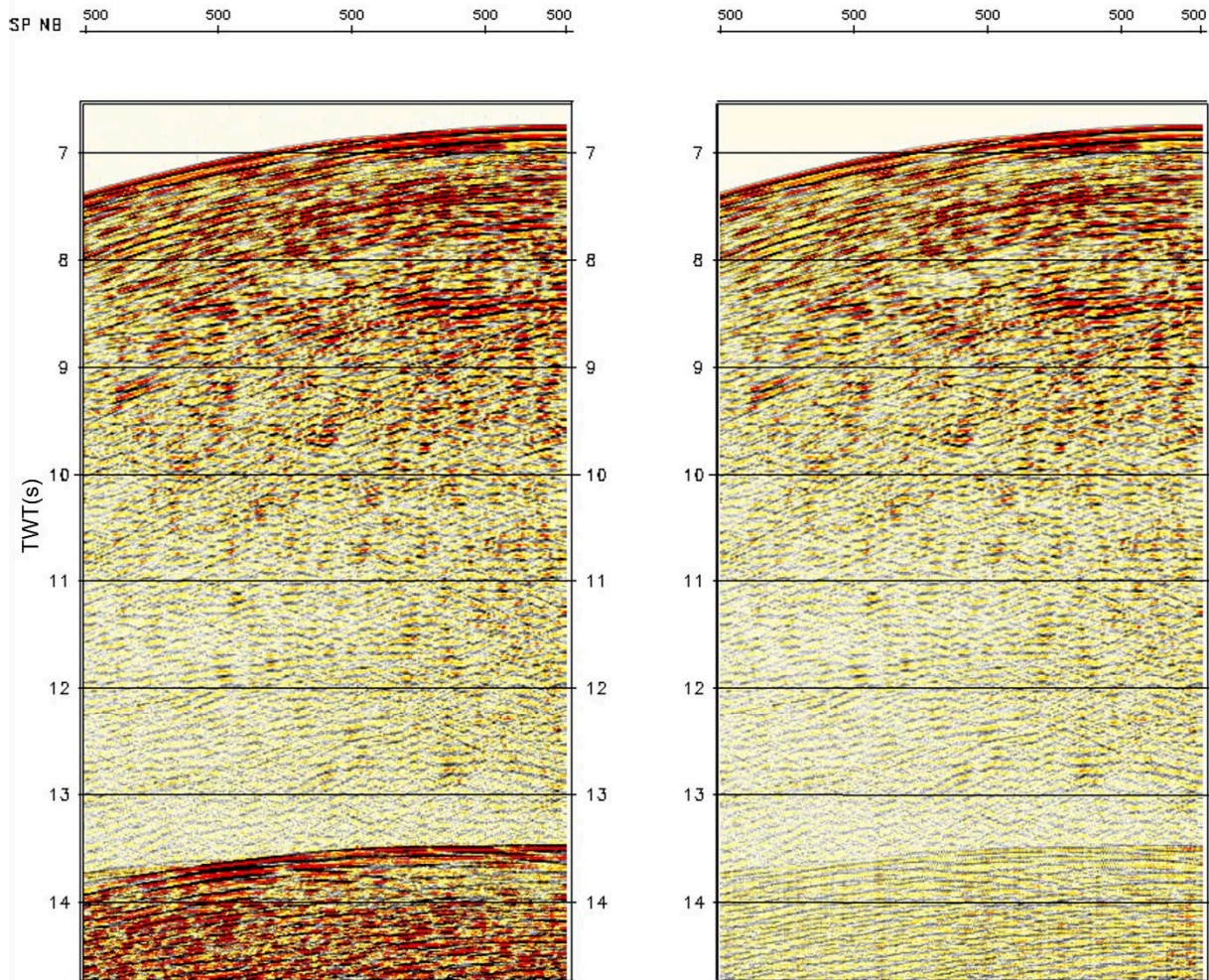


Figure 2.2.5: Shot gathers (Shot point 500) from Ant 54 showing before (left) and after (right) the application of surface related multiple elimination, and adaptive subtraction. Observe the surface multiples in the left image beyond 13 stwt that has been eliminated in the right image.

### 2.2.5 Deconvolution

To remove repeating signals such as reverberation from the seismic trace, we applied deconvolution. This process is an inverse filtering method that helps to improve the vertical resolution of the seismic data. Predictive deconvolution was applied using the module MCDEC in Geovation. In order to identify the signature of the wavelet and choose the accurate operators for the deconvolution, autocorrelation of the seismic trace was done. For the operator calculation, 2 windows were defined from a mute library (water bottom reflection picked on CMP gather): from 0s – 2s with a lag of 32-ms, and 8s – 10s with a lag of 54-ms. An operator length of 252- ms gives the best result. The autocorrelation of the seismic trace before and after the deconvolution process shows good reduction of the wavelet (Figure 2.2.6). The result of the deconvolution produced thinning of the reflectors and better vertical resolution (Figure 2.2.7).

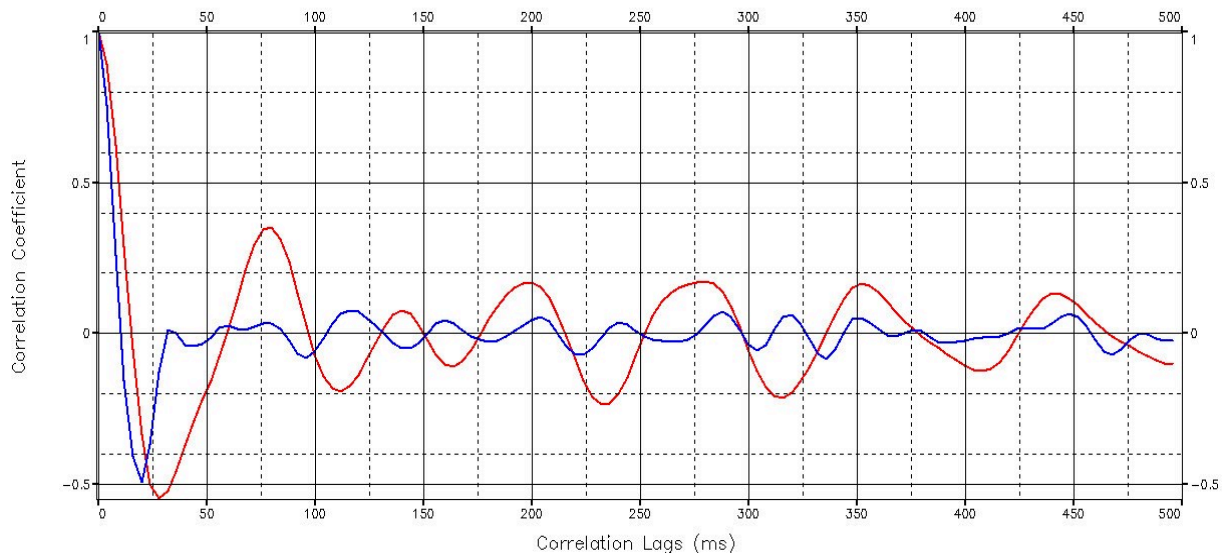


Figure 2.2.6: Autocorrelogram of the seismic trace before (red) and after (blue) deconvolution. The autocorrelogram after applying deconvolution shows a good reduction of the wavelet.

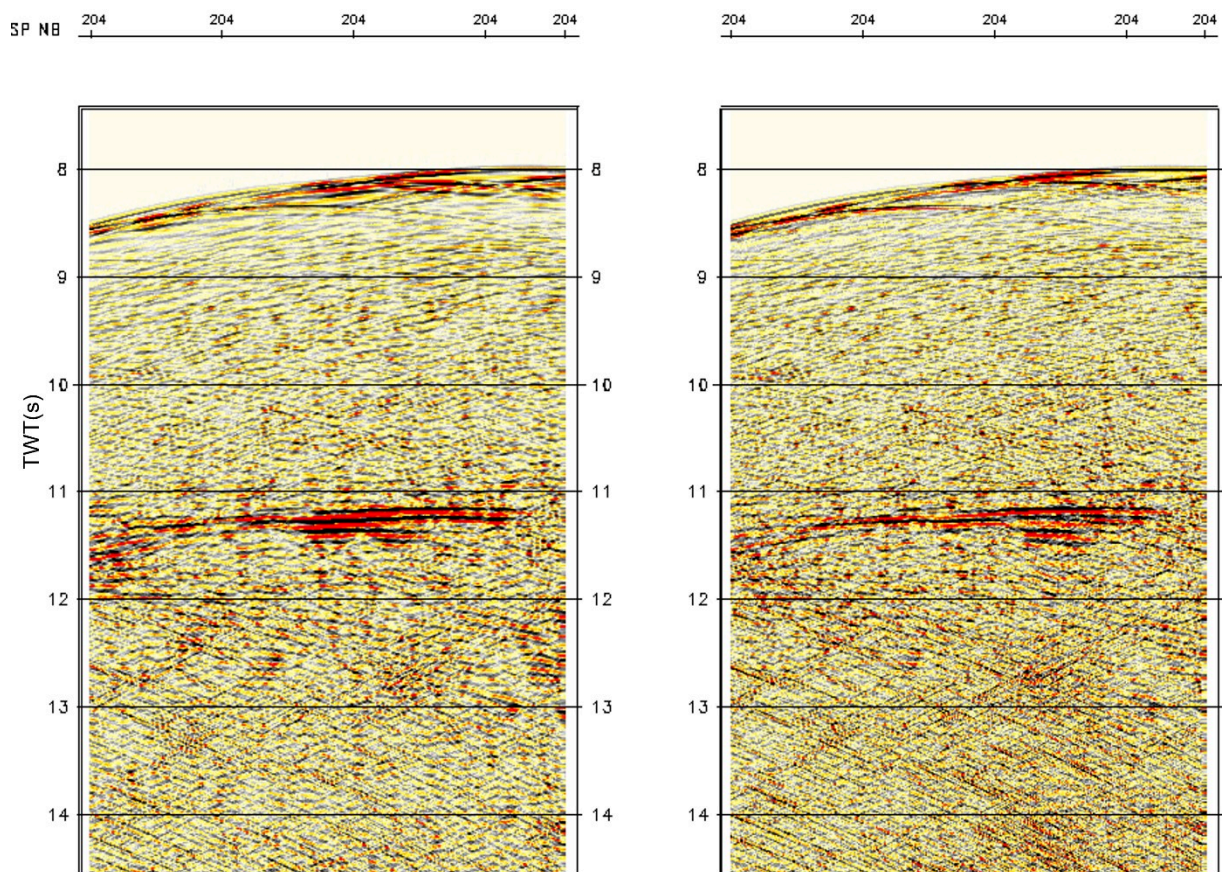


Figure 2.2.7: Shot point gather (SP 204) from Ant 54 showing before (left) and after (right) deconvolution. The deconvolution resulted to the thinning of the reflectors and improved vertical resolution.

## 2.2.6 Velocity Analysis

The purpose of the velocity analysis was to estimate CDP stacking velocities at regular spacing along each seismic line. This is in order to perform Normal Move Out (NMO) correction which flattens each reflection within each CMP gather before stacking the seismic traces to produce a seismic section (see following sub-section). The velocity spectra analysis was performed on super-CMP (3 CMP) collections, which produces better-resolved velocity spectra that facilitates the determination of the velocity functions. The real events that appear as high semblance values in the velocity spectrum (Figure 2.2.8) were manually picked in 3 phases to produce the final velocity function (Figure 2.2.9) by taking into consideration the geologic structures in the study area. The last of the velocity analysis was done after the elimination of surface related multiples. High semblance values that occur at unrealistic low velocities in the velocity spectrum before the sea-bottom multiple, represent internal multiples or ringing, and were avoided during the manual picking (Figure 2.2.8).

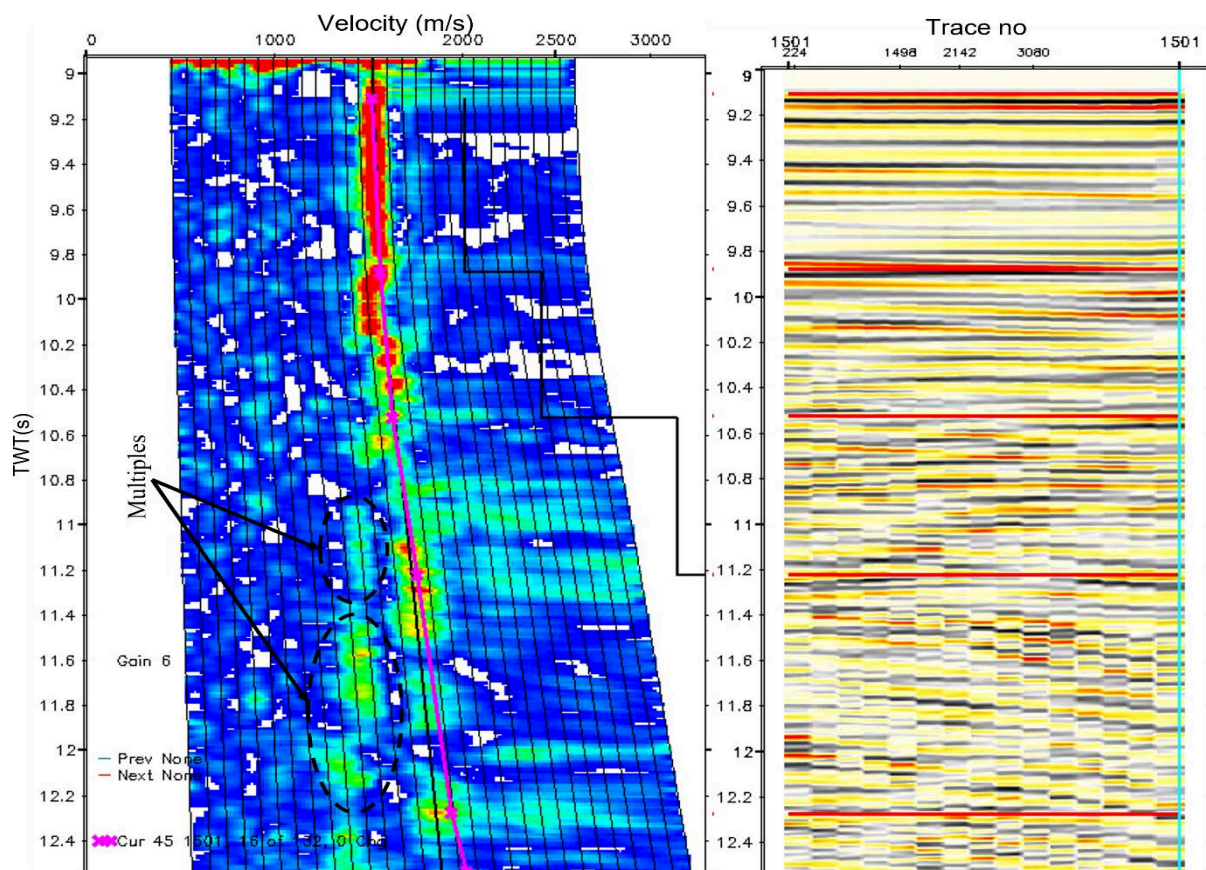


Figure 2.2.8: Example of velocity spectrum of a CDP gather (CDP 1501) from Ant45 line showing the picked velocities. High semblance corresponds to real events on the data. The dotted spheres are high semblance with unrealistic velocity values that occur as internal multiples (sea-bottom multiple expected at 18s).

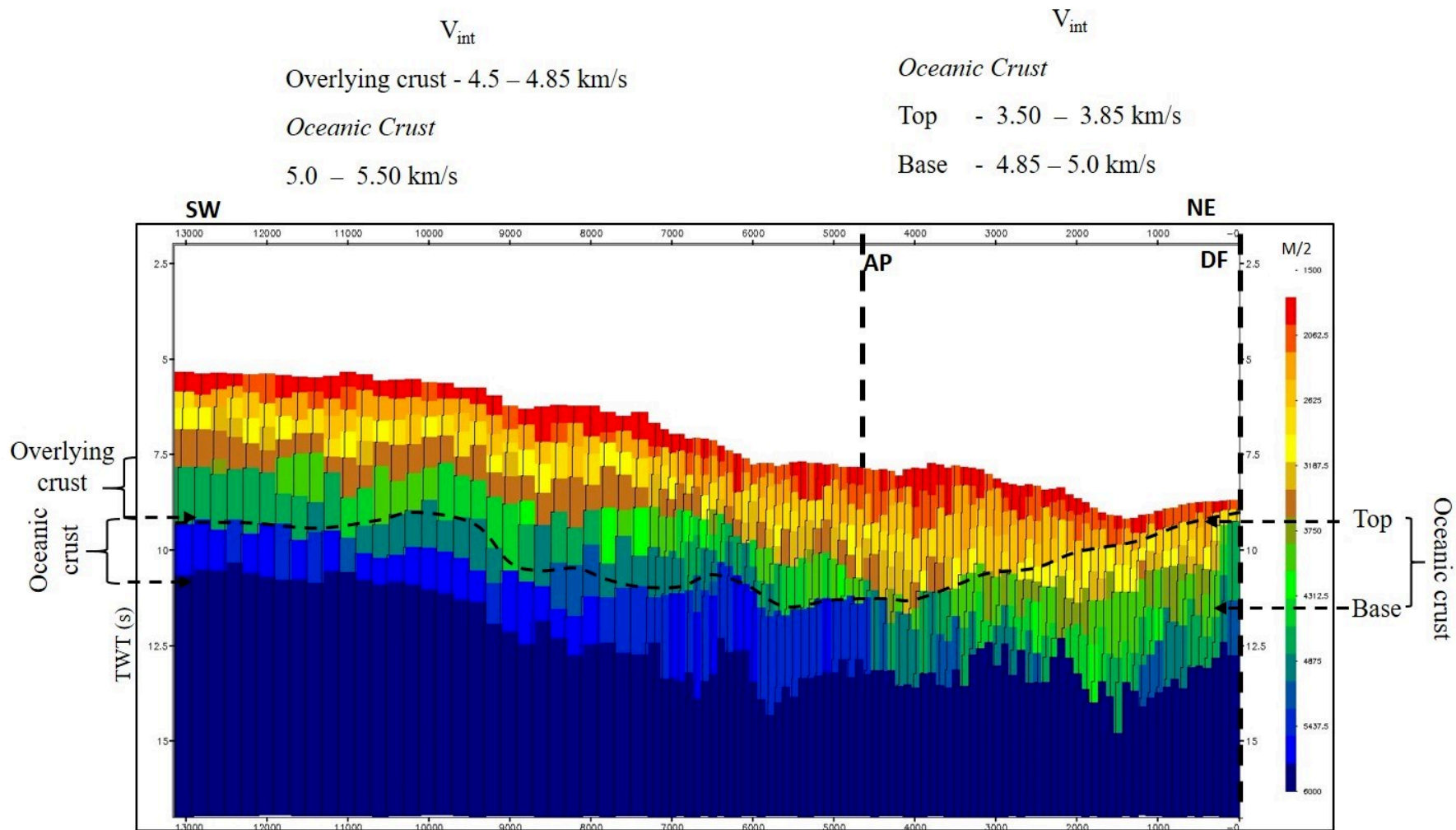


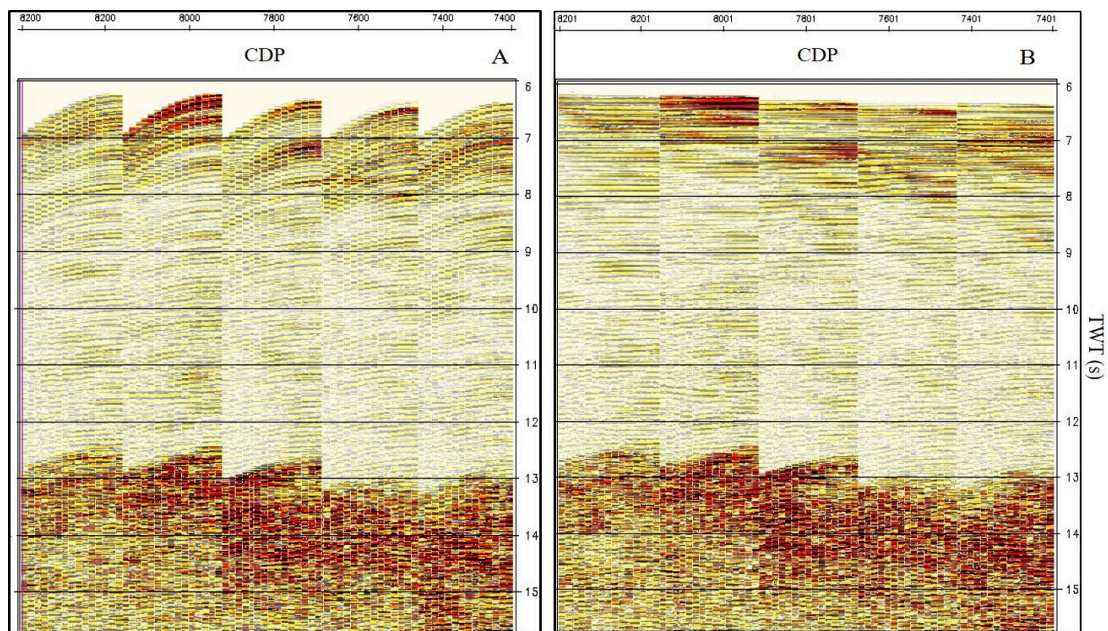
Figure 2.2.9: Velocity model developed from the final picked velocities in the velocity spectrum. The geologic structures of the study area were taken into consideration to arrive at the final velocities. Note the low velocities measured within the oceanic crust of the seaward portion (CDP 0-4700).  $V_{int}$  – Interval velocity, AP – Accretionary prism, DF – Deformation front.

### 2.2.7 Normal Move Out correction (NMO)

To flatten each recorded reflection hyperbola of each CMP gather before stacking the traces, we apply NMO correction by using the picked stacking velocities obtained from the velocity analysis (Figure 2.2.10). The procedure helps to increase the signal to noise ratio; thus, the quality of the final seismic section depends on the precision of this correction, which depends on the accuracy of the picked stacking velocities. For CMP gathers located in areas of shallow sea-bottom, we manually picked an external mute to remove the low-frequency stretched signals, when necessary, on the far offset traces.

### 2.2.8 Dip Move Out correction (DMO) and Stacking

After the NMO correction, we apply DMO correction to account for the effect of dipping reflection events. Since seismic layers are usually not horizontal, source-receiver pairs imaging the same mid-point do not occur at the same position, but vary depending on the dip of the layer, and the source-receiver distance. The DMO correction was performed on NMO corrected unstacked traces using KIDMO module in geovation, and sums traces belonging to a particular bin. This correction attempts to position the conflicting dips in the correct zero offset location such that after CMP stacking, the crossing events are preserved and not attenuated. A portion of the stacked section with improved reflector amplitudes after DMO correction is shown in Figure 2.2.11. After the DMO correction, all the traces were stacked to produce the seismic section for a given MCS line (Figure 2.2.12).



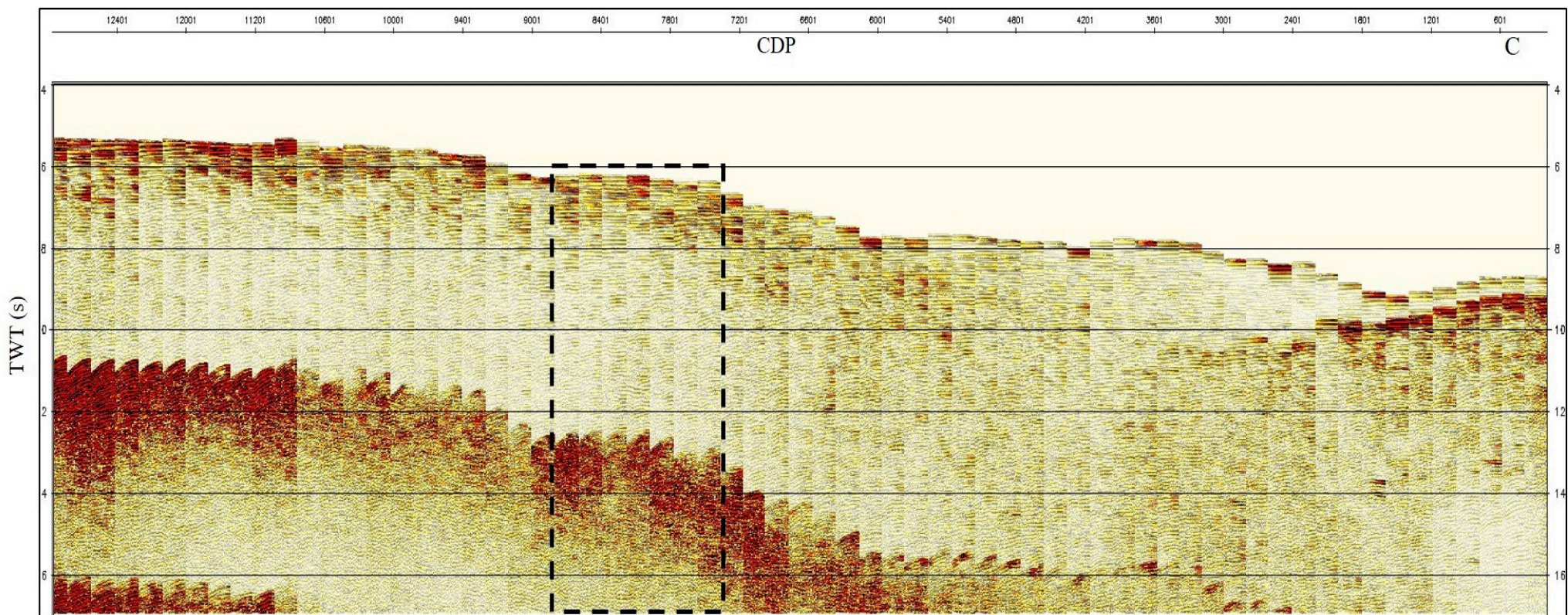


Figure 2.2.10: CMP gather before and after NMO correction. (A) Selected CMP gathers from Ant45 line before NMO correction. (B) Selected CMP gathers after NMO correction. (C) NMO correction for all the CMP gathers for MCS line Ant45. The dotted rectangle represents the region enlarged in A and B. The corrected CMPs has horizontally flattened reflectors where velocities were picked. The unflattened reflections at 11 to 17 stwt are sea bottom multiples.

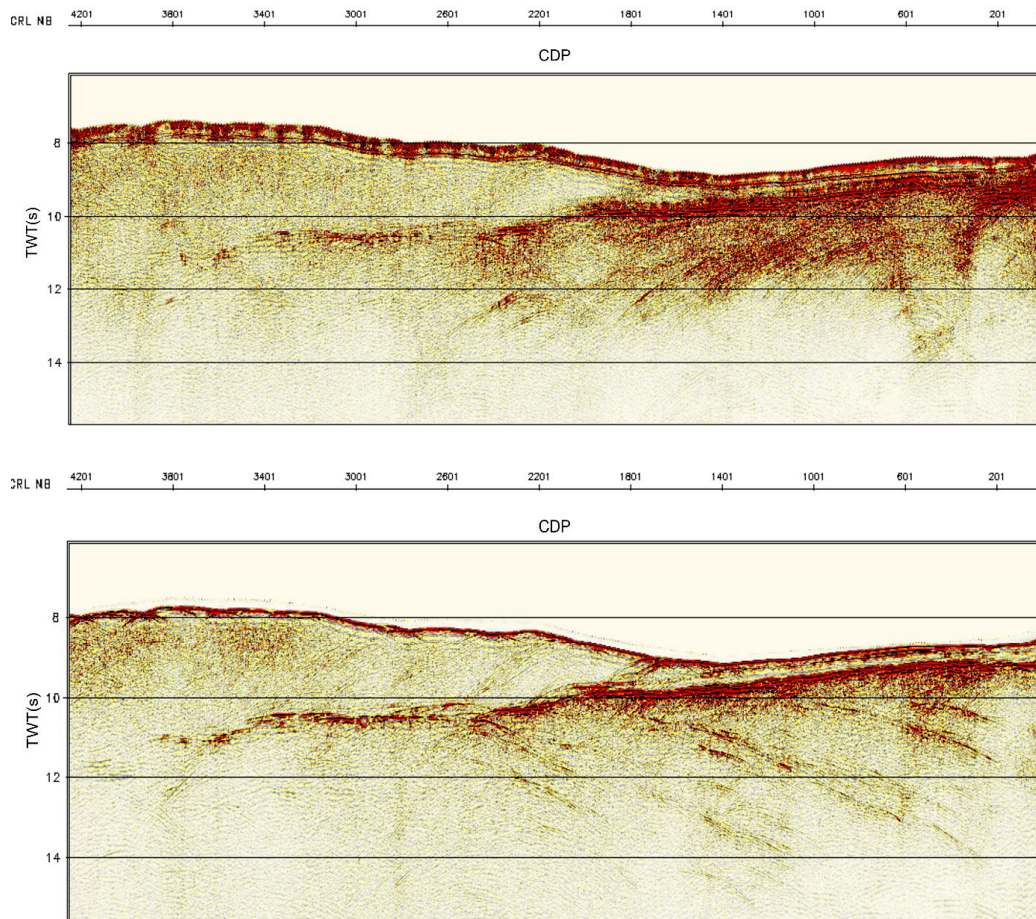


Figure 2.2.11: A portion of the stacked section of Ant45 before (above) and after (below) DMO correction. The complete section is shown in Figure 2.2.12

### 2.2.9 Post-stack (f,k) time migration

The final phase of the seismic processing involved migrating the stacked section in order to reposition the reflections in the seismic data to their true subsurface geologic positions, correct for the dip and length of the reflectors, and increase both the continuity of the reflectors and the sharpness of their lateral termination. In the processing, we used the time migration in f,k field at constant water velocity (1500 ms) at early stages, and with the velocity derived from structural velocity analysis at the late stages of the workflow. The impact of the used migration velocities is shown in Figure 2.2.13. Constant water velocities migration is very easy to set up and remove all the strong diffractions from rough sea-bottom topography, without prerequisite knowledge of the medium velocity. However, migration with structural velocity model produced a much better result especially with dipping reflectors and the reflectors at depths. This requires however, an accurate velocity model since any error in the velocity used for this kind of migration (especially over estimated values) results to migration artefact, e.g. smiles and loss of reflectors.

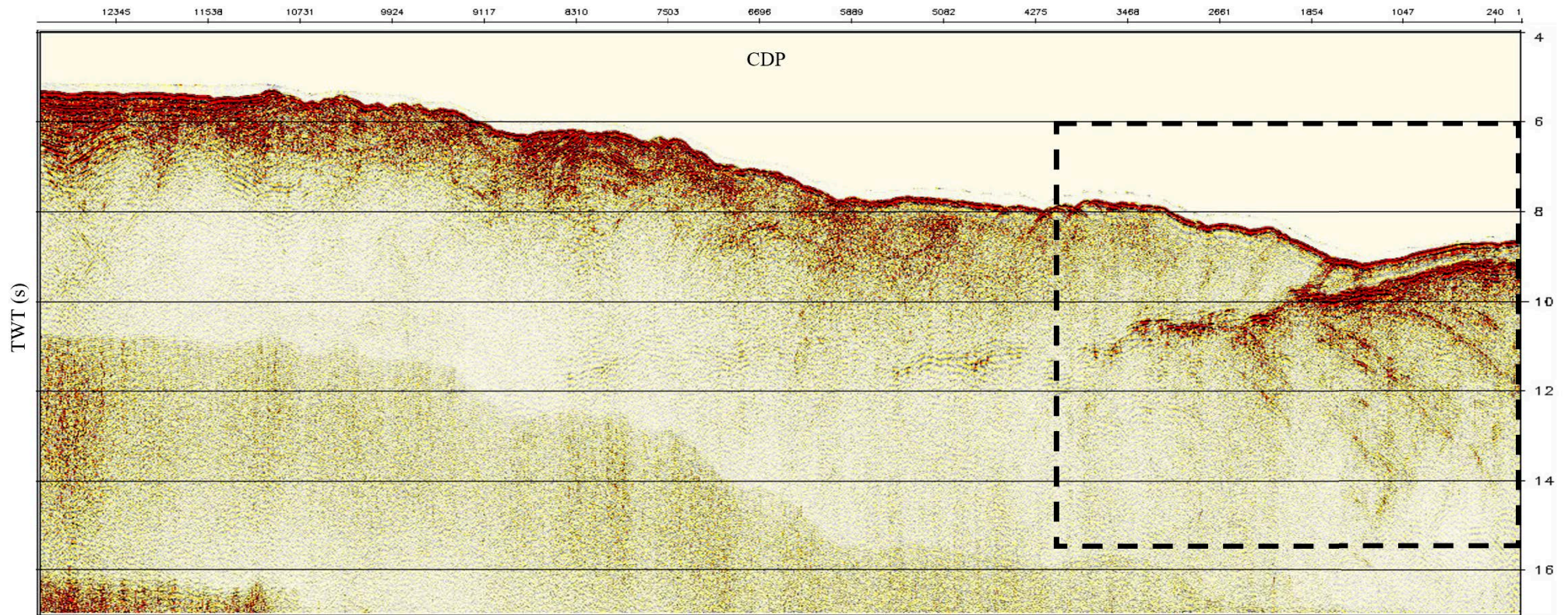
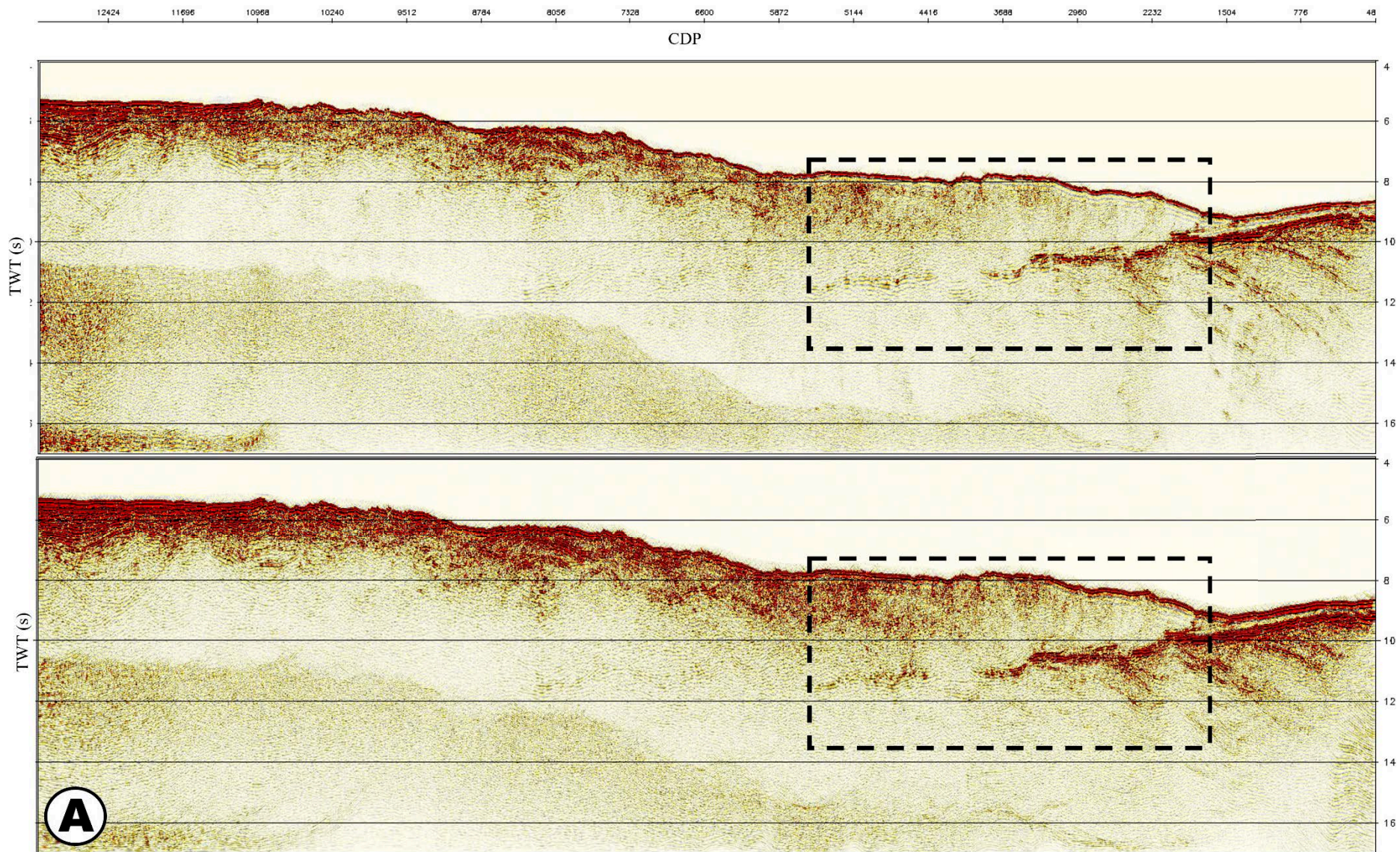


Figure 2.2.12: Stacked section of MCS line Ant45. The dotted box indicates the section shown in Figure 2.2.11 above





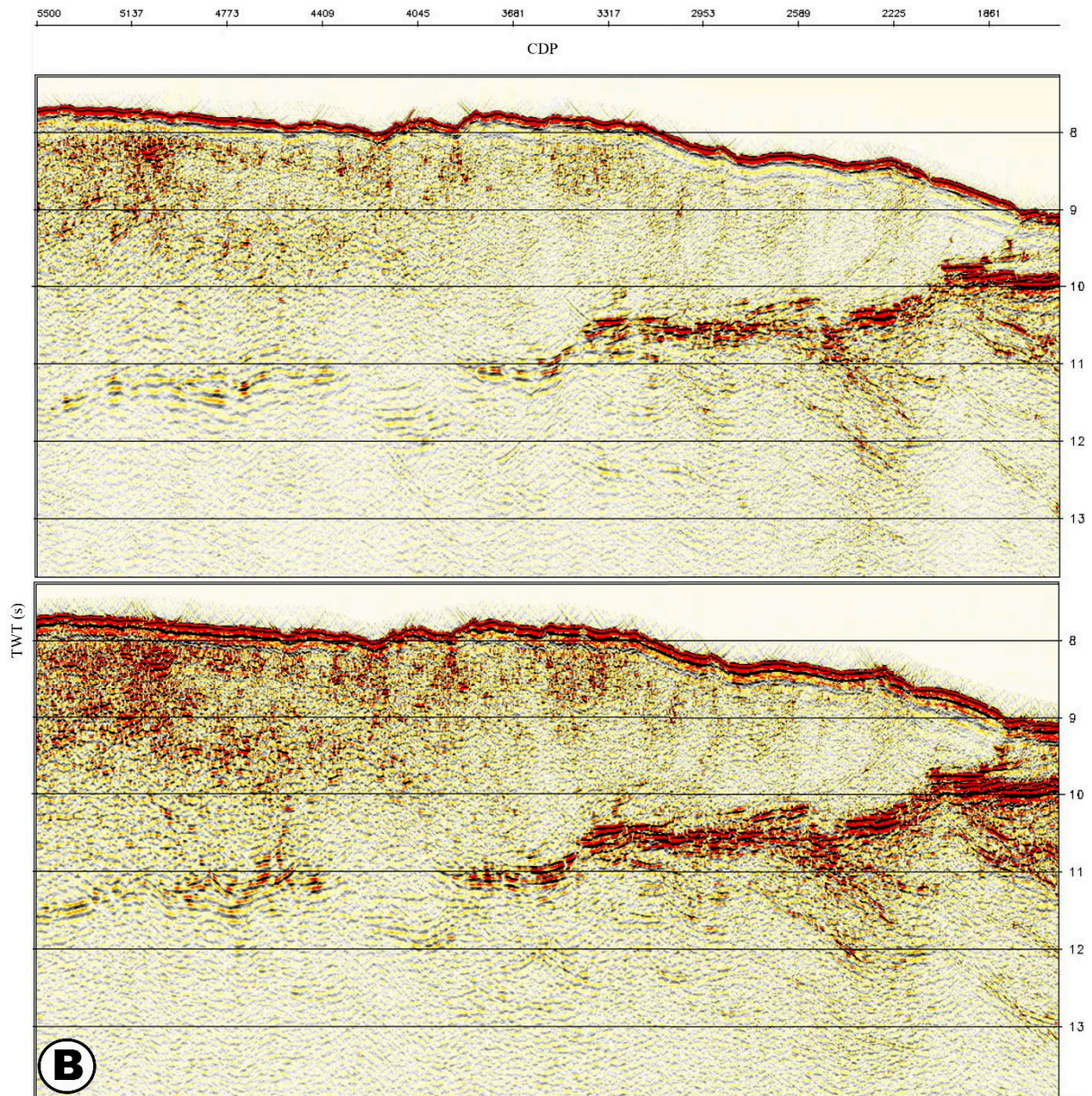


Figure 2.2.13: MCS line Ant45 after the post-stack migration. In (A), the section on top was migrated using a constant velocity at 1500 ms, while the section under was migrated using velocities derived from NMO velocity analysis. The dotted box shows the location of the blow-up in B. Both the interplate and sediment reflectors appear better and well migrated using the velocities from NMO velocity analysis.

## **2.3 Seismic interpretation methods**

The seismic reflection data was interpreted to infer subsurface geologic and tectonic features. Our methods of interpretations include both structural and stratigraphic seismic interpretations, and was geared towards providing a model of the subsurface.

### **2.3.1 Structural Interpretations**

The structural interpretations involve the identification of faults, lineament, antiforms and synforms. The faults were identified as breaks in reflection events or abrupt termination of reflectors represented on the seismic data as discontinuous lines along a preferred orientation of reflectors. We follow these identified faults to the seafloor and correlate them to the bathymetric data where they occur either as displacements or lineaments. The antiforms and synforms were identified on the seismic data as upwelling and depression features on the seafloor respectively.

### **2.3.2 Stratigraphic Interpretations**

To interpret the seismic stratigraphy, we determine the seismic facies based on criteria described by Roksandic, (1978) and Mitchum & Vail, (1977). The criteria include reflection geometries, amplitude, frequency, polarity, and the continuity of reflections (Figure 2.3.1). Each of the parameters used in describing the facies provides considerable information on the geology of the subsurface. The reflection geometric configuration reveals the gross stratigraphic pattern to interpret depositional processes, erosion and paleotopography (Mitchum & Vail, 1977). Continuity of the reflections highlight widespread, uniformly stratified deposits, while the reflection amplitude contains information on the velocity and density contrast of individual interface and their spacing. The frequency of the reflection shows the nature of the seismic pulse, and is also related to geologic factors such as reflector thickness or lateral changes in interval velocities (Vail et al., 1977), while the reflection continuity reveals the continuity of the strata. Hence, the seismic facies are linked to stratigraphic bodies, which can be used to make qualitative interpretation of environmental settings.

Using this approach for our seismic dataset, we distinguished between the basement reflectors and sedimentary reflectors. We identify different boundaries in the sedimentary units and separated them into seismic layers based on their different seismic characteristics.

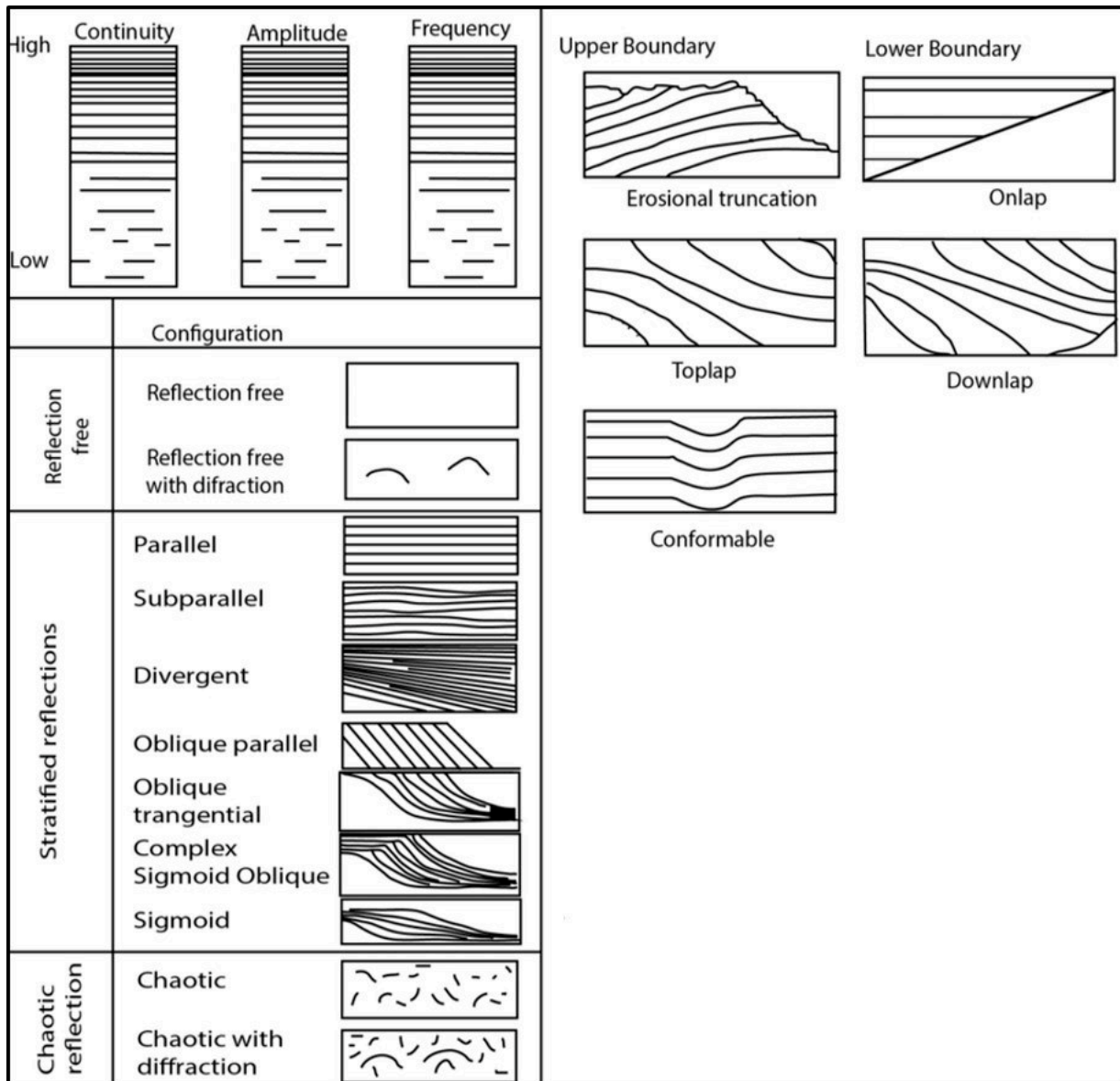


Figure 2.3.1: Seismic reflection configurations, relationships, and termination boundaries used in defining the seismic facies (Mitchum & Vail, 1977).

### 2.3.3 Seismic Attribute Analysis

Seismic attribute analysis involves analysis of subtle changes in proportion of particular reflections to determine rock properties, including fluid content (Taner, 2001). They present the possibility of creating different geological models in a faster and reliable way. Attribute analysis provides added values for identifying and delineating textural, structural and stratigraphic features associated with fluid-rich areas especially within the oil and gas industry (Taner, 2001; Barnes, 2001; Chopra & Marfurt, 2005).

For our dataset, we applied the Root Mean Square (RMS) amplitude seismic attribute. The amplitude content within the seismic data effectively provides physical parameters about the

subsurface such as acoustic impedance, reflection coefficient, velocities, and absorption effect (Taner, 2001; Barnes, 2001). Thus, the RMS amplitude attribute which is related to the variations in acoustic impedance is well suited for fluid identifications. The RMS is calculated as the square root of the sum of squared amplitude values divided by the number of samples over a selected time window. We performed the RMS attribute analysis on the datasets as a volume attribute on the 2D lines using the Schlumberger-Petrel software. The results were used in identifying acoustic anomalies relating to fluid contents in the dataset (see chapter 4).

## **2.4 Heat-flow data acquisition and thermal modelling**

This section is presented as the supplementary material of the article ‘*Thermally-constrained fluid circulation and seismicity in the Lesser Antilles Subduction zone*’ published in EPSL in October 2022, that constitute a chapter in this manuscript. It describes in detail the methods of acquisition of the heat-flow data, and the locations of the acquired data. It further explains the 2D finite element method that was used in modelling the thermal structure of the margin.

## Supplementary material:

# Thermally-constrained hydrothermal circulation and seismicity in the Lesser Antilles Subduction Zone

Ezenwaka, K., Marcaillou, B., Laigle, M., Klingelhoefer, F., Lebrun, J.-F., Paulatto, M., Biari, Y., Rolandone, F., Lucazeau, F., Heuret, A., Pichot, T., Bouquerel H.

## 1 Methods

### *1.1 Data acquisition and processing*

We acquired 39 heat-flow data (Figure 1 & Table 1). 35 using a microprocessor-controlled heat-flow (MCHF) instrument (ANQ XX\_XX) and 4, using autonomous thermal probes attached to a 5 m long sediment corer (ANQC XX\_XX). The MCHF includes a 5-meter pogo stick, which penetrates the sediment at the seafloor. In the pogo stick, seven sensors (thermistors) extrapolate stationary temperatures at various depth, from the thermal decay that follows the frictional heating. This temperature measurements result in a thermal gradient ( $\nabla T$ ). Penetration of sensor in the sediment is adjusted so that the extrapolation of the gradient at the surface is equal to the water temperature. The MCHF also includes a heating wire to measure in situ the thermal conductivity (Von Herzen & Maxwell, 1959). The wire generates a 3-min-long heat pulse in the sediment and the thermistors measure the temperature decay, which depends on the thermal conductivity ( $\lambda$ ). The thermal conductivity is thus determined by the slope of the linear regression in temperature variation / logarithm of time. With the sediment corer, we use five high-precision probes (THP from NKE<sup>®</sup>) that measure temperature with a precision of 0.005 °C. Then we measured thermal conductivity onboard the ship on recovered sediment cores using a needle probe instrument (THERMCON95). The heat flow ( $Q$ ) is then determined using Fourier's law with steady state condition as the product of the temperature gradient and the average thermal conductivity.

$$Q = -\lambda \cdot \nabla T \quad (1)$$

The locations of the heat flow measurements are consistent with the locations of seismic lines Ant06 published in Laurencin et al., (2019), for the Saint Martin profile, and line D of Laigle et al., (2013) for the margin in the Martinique profile. A close seismic profile to the Martinique measurements seaward of the trench is published in Pichot et al., (2012). The shallowest heat



Numerous multichannel seismic lines, wide-angle seismic and tomography models provide solid constraints for the structure and the geometry of the mesh (Figure 2) as detailed in section §2.1 in the text. The grid consists in six units including the sediment, the upper and lower crust, the mantle wedge, the subduction channel, and the oceanic lithosphere. Table 2 synthesizes the layers thermal parameters, which are consistent with numerous previous studies (Harris et al., 2010 & 2020, Gutscher et al., 2013, Marcaillou et al., 2008 & 2012). Offshore of Saint Martin, the slab geometry is constrained using wide angle and seismic reflection lines at shallow depth (Laurencin et al., 2019; Boucard et al., 2021), and wide angle data at greater depth (Klingelhoefer et al., 2018). The 2D model offshore of Martinique is based on seismic reflection and wide angle data at shallow depths (Laigle et al., 2013; Kopp et al., 2011), and 3D tomography model at greater depths (Paulatto et al., 2017).

The slab dip angle at depth shallower than 40 km is slightly steeper in the northern model than in the southern (Laurencin et al., 2019, Kopp et al., 2011) and is similar along both lines at greater depth (Paulatto et al., 2017). The along-strike variation in slab dip angle at shallow depth, when observed as a function of the distance from the trench (Figure 2), is only apparent and related to the reduced size of the accretionary prism offshore of Saint-Martin compared to that offshore of Martinique.

The modelled relative plate convergence is 2cm/yr (DeMets et al., 2000) and the subducting plate is set to 80 Myr-old (Roest & Collette, 1986).

The geotherm at the seaward boundary is calculated using a model of a conductive half space cooling lithosphere based on an originally 1-D approach (Hutchison, 1985) and detailed by (Marcaillou et al., 2008) (see section 3.3). The temperature at the upper boundary - the seafloor, is set to 0°C, consistently with in situ temperature measurements. At the lower boundary - the base of the lithosphere, the temperature is set to 1450°C. The arc-ward calculated backarc geotherm is located sufficiently far from the seismogenic zone to avoid edge effects, and to have negligible influence on the modeled thermal structure in the area of interest.



| Station ANQ                 | Longitude | Latitude | Penetration (m) | Tilt (°) | Te (°C) | nT | gradient G (mK.m <sup>-1</sup> ) | σG   | nλ | Conductivity λ (W.m <sup>-1</sup> .k <sup>-1</sup> ) | σλ    | Heat Flow Q (mw.m <sup>-2</sup> ) | σQ   |
|-----------------------------|-----------|----------|-----------------|----------|---------|----|----------------------------------|------|----|--|-------|-----------------------------------|------|
| <b>Saint Martin Profile</b> |           |          |                 |          |         |    |                                  |      |    |  |       |                                   |      |
| C03-01                      | -61.0900  | 19.2224  | 5.00            | 0.0      | 1.94    | 5  | 43.7                             | 0.9  | 10 | 0.937  | 0.043 | <b>40.9</b>                       | 5.3  |
| 03-02                       | -60.8625  | 19.2846  | 4.36            | 1.8      | 2.00    | 6  | 58.7                             | 1.7  | 5  | 0.940  | 0.012 | <b>55.2</b>                       | 1.8  |
| 02-08                       | -61.5186  | 18.8660  | 4.32            | 2.4      | 2.01    | 5  | 36.4                             | 1.1  | 4  | 0.964  | 0.024 | <b>35.0</b>                       | 1.4  |
| 02-07                       | -61.5760  | 18.8360  | 4.34            | 5.6      | 2.03    | 5  | 33.1                             | 4.7  | 4  | 0.878  | 0.039 | <b>29.1</b>                       | 4.4  |
| 02-06                       | -61.4942  | 18.7362  | 4.36            | 2.0      | 2.00    | 5  | 36.2                             | 1.2  | 4  | 0.939  | 0.038 | <b>34.0</b>                       | 1.8  |
| 02-05                       | -61.7025  | 18.4781  | 4.36            | 1.7      | 2.01    | 6  | 38.7                             | 66.8 | 5  | 0.892  | 0.022 | <b>34.5</b>                       | 59.6 |
| 02-04                       | -61.8766  | 18.2568  | 4.35            | 5.4      | 2.26    | 6  | 43.4                             | 3.4  | 5  | 0.929  | 0.023 | <b>40.3</b>                       | 3.3  |
| 02-03                       | -61.8899  | 18.2391  | 4.36            | 2.6      | 2.59    | 6  | 34.3                             | 3.8  | 5  | 1.051  | 0.018 | <b>36.0</b>                       | 4.1  |
| 02-02                       | -61.9038  | 18.2204  | 4.36            | 3.0      | 2.29    | 6  | 30.3                             | 3.9  | 5  | 0.977  | 0.019 | <b>29.6</b>                       | 3.8  |
| 02-01                       | -61.9141  | 18.2093  | 4.36            | 2.9      | 2.30    | 6  | 32.7                             |      | 5  | 0.976  | 0.019 | <b>32.0</b>                       | 3.6  |
| 01-04                       | -62.0111  | 18.0823  | 3.69            | 5.1      |         | 5  | 23.7                             | 7.7  | 4  | 0.949  | 0.036 | <b>22.5</b>                       | 7.3  |
| <b>Martinique Profile</b>   |           |          |                 |          |         |    |                                  |      |    |  |       |                                   |      |
| 03-04                       | -58.6265  | 16.7633  | 3.59            | 3.3      |         | 4  | 85.1                             | 3.0  | 3  | 0.877  | 0.019 | <b>74.4</b>                       | 3.1  |
| 03-05                       | -58.6019  | 16.7553  | 3.51            | 2.0      |         | 4  | 76.5                             | 4.5  | 3  | 0.896  | 0.020 | <b>68.5</b>                       | 4.3  |
| 04-01                       | -58.5815  | 16.4414  | 0.93            | 0.8      |         | 2  | 100.1                            | 10.2 | 1  | 0.815  | 0.008 | <b>81.6</b>                       | 8.3  |
| 04-02                       | -58.5796  | 16.3732  | 3.71            | 1.0      |         | 5  | 57.7                             | 8.0  | 4  | 0.806  | 0.008 | <b>46.5</b>                       | 6.5  |
| C04-04                      | -57.9488  | 16.0729  | 5.00            | 1.9      | 1.88    | 5  | 68.7                             | 0.2  | 7  | 0.810  | 0.027 | <b>55.6</b>                       | 2.0  |
| 04-05                       | -58.3030  | 15.8422  | 3.71            | 0.2      |         | 5  | 77.7                             | 18.9 | 4  | 0.813  | 0.037 | <b>63.1</b>                       | 15.7 |
| 04-06                       | -58.4832  | 15.9404  | 3.71            | 0.9      |         | 5  | 117.8                            | 1.5  | 4  | 1.018  | 0.027 | <b>119.9</b>                      | 3.5  |
| C04-09                      | -58.6683  | 15.4155  | 5.00            | 2.0      | 2.24    | 5  | 111.0                            | 0.2  | 5  | 0.84   | 0.010 | <b>93.2</b>                       | 1.2  |

|        |          |         |      |     |      |   |       |      |   |       |       |             |      |
|--------|----------|---------|------|-----|------|---|-------|------|---|-------|-------|-------------|------|
| 04-08  | -58.4993 | 15.3221 | 3.55 | 2.2 |      | 5 | 84.3  | 4.2  | 4 | 0.89  | 0.019 | <b>75.0</b> | 4.1  |
| C04-10 | -58.6814 | 15.7299 | 5.00 | 1.3 | 1.94 | 5 | 103.9 | 0.3  | 6 | 0.747 | 0.019 | <b>77.6</b> | 2.2  |
| 05-01  | -58.8524 | 15.6882 | 3.42 | 1.4 |      | 5 | 80.2  | 3.4  | 4 | 0.792 | 0.038 | <b>63.5</b> | 4.1  |
| 05-02  | -58.8958 | 15.6710 | 3.39 | 1.7 |      | 5 | 78.3  | 5.4  | 4 | 0.85  | 0.024 | <b>66.6</b> | 5.0  |
| 05-04  | -58.9668 | 15.6359 | 3.69 | 3.0 |      | 5 | 54.7  | 12.8 | 4 | 0.879 | 0.018 | <b>48.1</b> | 11.3 |
| 05-03  | -58.9931 | 15.6318 | 2.83 | 0.5 | 2.21 | 5 | 59.5  | 1.5  | 4 | 0.956 | 0.025 | <b>56.9</b> | 2.1  |
| 05-06  | -59.1022 | 15.5979 | 2.64 | 1.2 | 2.58 | 5 | 50.7  | 2.2  | 4 | 0.896 | 0.016 | <b>45.4</b> | 2.2  |
| 05-05  | -59.2257 | 15.5544 | 3.70 | 2.0 |      | 5 | 44.7  | 7.5  | 4 | 0.945 | 0.027 | <b>42.2</b> | 7.2  |
| 05-07  | -59.3454 | 15.5066 | 2.11 | 1.8 |      | 3 | 55.8  | 3.7  | 2 | 0.967 | 0.008 | <b>54.0</b> | 3.6  |
| 05-08  | -59.4971 | 15.4456 | 3.70 | 5.8 | 4.82 | 4 | 53.5  | 2.7  | 3 | 0.863 | 0.046 | <b>46.2</b> | 3.4  |
| 05-09  | -59.6188 | 15.4311 | 3.70 | 2.3 | 2.33 | 4 | 49.6  | 1.6  | 3 | 0.924 | 0.024 | <b>45.8</b> | 1.9  |
| 06-01  | -59.9823 | 15.4100 | 4.04 | 2.2 | 2.39 | 5 | 33.5  | 5.0  | 4 | 0.944 | 0.059 | <b>31.6</b> | 5.1  |
|        |          |         |      |     |      |   |       |      |   |       |       |             |      |
| 06-13  | -59.9940 | 15.2933 | 4.34 | 2.4 | 2.32 | 5 | 36.2  | 1.5  | 5 | 0.902 | 0.031 | <b>32.7</b> | 1.8  |
| 06-12  | -60.0244 | 15.1419 | 1.43 | 2.7 | 2.33 | 3 | 60.1  | 37.9 | 3 | 0.916 | 0.193 | <b>55.0</b> | 36.6 |
| 06-05  | -60.2200 | 15.0523 | 1.31 | 3.9 | 2.51 | 3 | 57.0  | 3.0  | 3 | 1.04  | 0.422 | <b>59.3</b> | 24.3 |
| 06-11  | -60.2611 | 15.0420 | 3.29 | 5.3 | 2.63 | 5 | 47.3  | 4.9  | 4 | 1.126 | 0.136 | <b>53.3</b> | 8.5  |
| 06-07  | -60.3511 | 15.0072 | 4.36 | 3.0 | 2.79 | 5 | 41.2  | 2.6  | 5 | 1.249 | 0.204 | <b>51.4</b> | 9.0  |
| 06-08  | -60.4372 | 14.9797 | 3.27 | 7.1 |      | 5 | 52.6  | 9.1  | 5 | 1.103 | 0.075 | <b>58.0</b> | 10.8 |

Table 1: Heat flow measured with “microprocessor-controlled heat-flow instrument” (ANQ XX\_XX) and autonomous thermal probes on sediment corer (ANQC XX\_XX) at every station with location (longitude and latitude), depth of penetration (in m), tilt recorded by the instrument (in degree from the vertical),  $T_e$ : temperature at the seafloor,  $nT$ : number of temperature determinations,  $G$  and  $\sigma G$ : thermal gradient and associated standard error (in  $mK.m^{-1}$ ),  $n\lambda$ : number of thermal conductivity determinations,  $\lambda$  and  $\sigma\lambda$ : thermal conductivity and associated standard error (in  $W.m^{-1}.K^{-1}$ ),  $Q$  and  $\sigma Q$ : estimated heat flow and associated standard error (in  $mW.m^{-2}$ ).

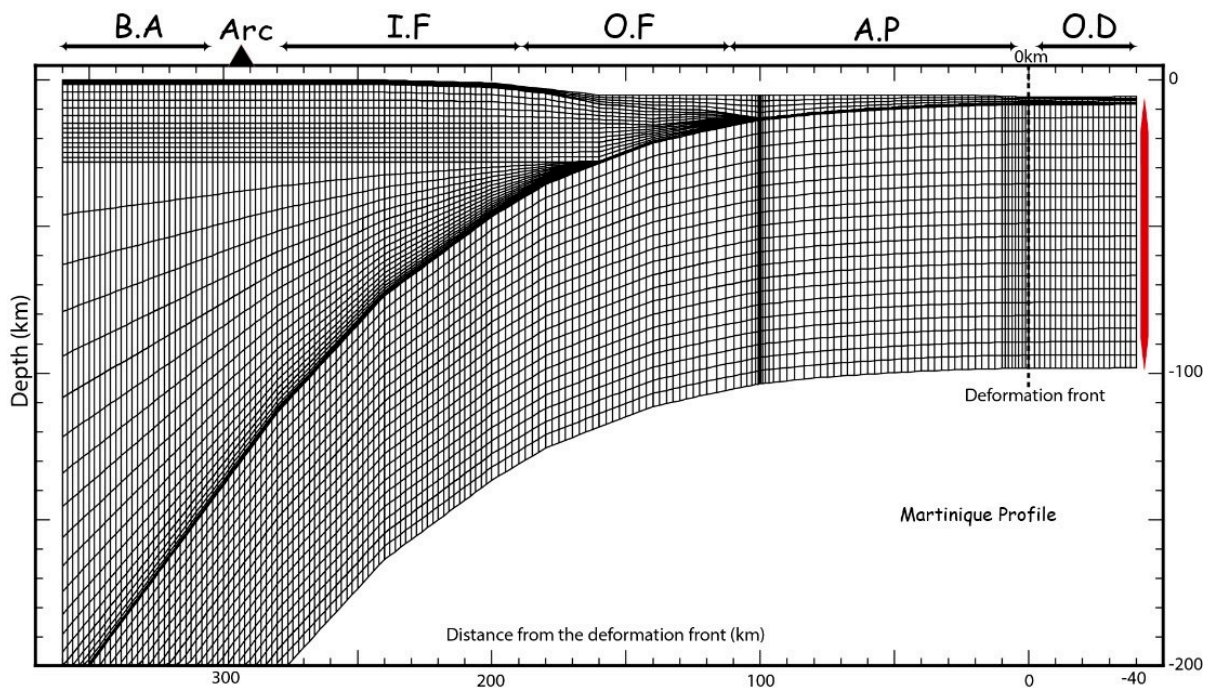
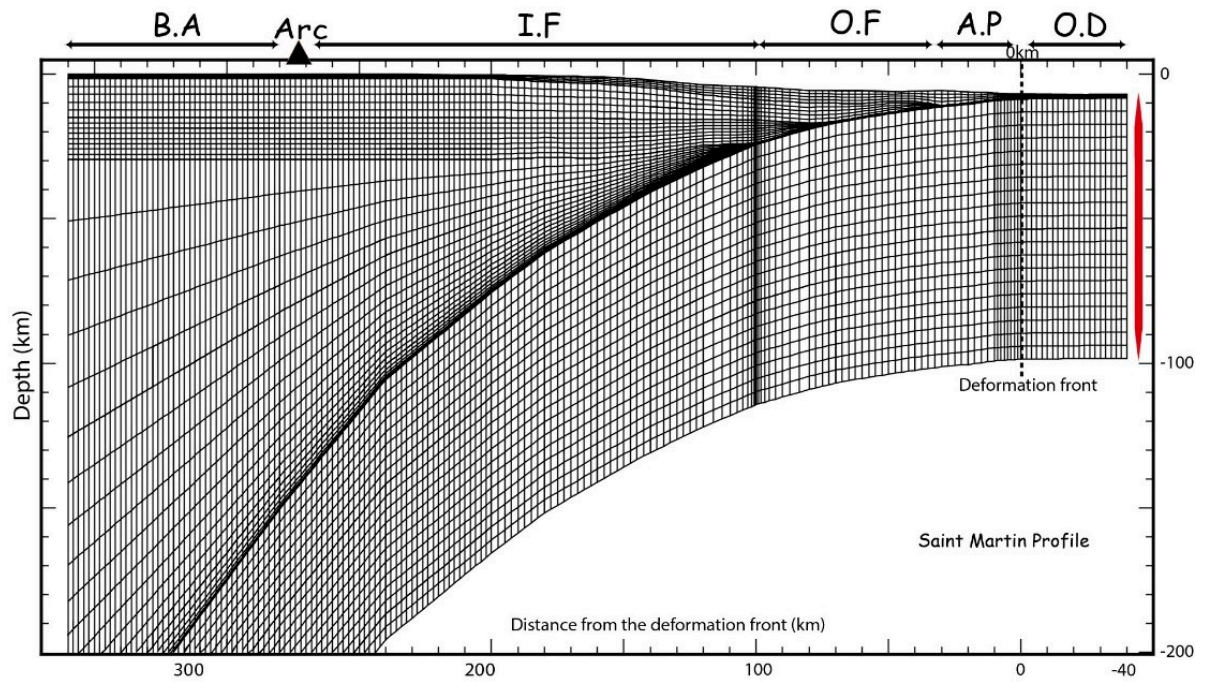


Figure 2 : Geometry of the finite element mesh used for the 2D Steady-state thermal modelling. 1D geotherm was calculated for an ~ 80 Ma old incoming oceanic plate in the trench (Red line). [O.D – Oceanic domain, A.P – Accretionary prism, O.F – Outer forearc, I.N – Inner forearc, B.A – Backarc]

| Layer (Units)           | Thermal conductivity<br>( $\text{W.m}^{-1}.\text{K}^{-1}$ ) | Heat generation<br>( $\mu\text{W.m}^{-3}$ ) | Thermal capacity<br>( $\text{MJ.K}^{-1}.\text{m}^{-3}$ ) |
|-------------------------|---|---|--|
| Sediments               | $1.8 \pm 0.2$   | $0.8 \pm 0.2$                               | 2.5  |
| Upper continental crust | $3.0 \pm 0.5$   | $0.05 \pm 0.05$                             | 2.75   |
| Lower continental crust | $3.5 \pm 0.5$   | $0.05 \pm 0.05$                             | 2.75   |
| Continental mantle      | 3.1   | 0.02  | 3.3  |
| Subduction channel      | 3.0   | 1.0   | 3.3  |
| Oceanic lithosphere     | 2.9   | 0.02  | 3.3  |

Table 2: Thermal parameters of the various units used in the modelling

### 1.3 Fluid-driven heat advective thermal modelling

Within a subducting crust, fluid flow is usually confined in the upper 600m of the oceanic lithosphere known as the crustal aquifer (Spinelli et al., 2018). This upper unit of the crust have high permeability relative to the underlying lower crust with very low permeability (Fisher et al., 1998), and an overlying seafloor sediments with permeabilities of  $\sim 3 - 10$  order of magnitudes lower (Spinelli et al., 2018). Moreover, high permeability sand bodies and fault zones within the sediment compared to the entire seafloor sediment body can also focus fluid flow (Saffer & Sreaton, 2003, and Saffer, 2010).

Since subduction zone temperatures are influenced by the thermal state of the incoming lithosphere entering the subduction zone (Dumitru, 1991 and Harris et al., 2010), we vary the initial geotherm of the incoming plates. For the oceanic geotherm in the insulated model, we assume an equal thermal gradient for the crustal aquifer and the base of the sediment layer. Below the aquifer, we allow a conductive cooling model with a net reduction in heat that reflects an increased heat transfer into the aquifer (Figure 3). In the ventilated fluid circulation system, we impose a low thermal gradient ( $10\text{ }^{\circ}\text{C/km}$ ) through the sediment and the subduction channel, but allows a conductive half space cooling model appropriate for the age of the crust for the lower slab.

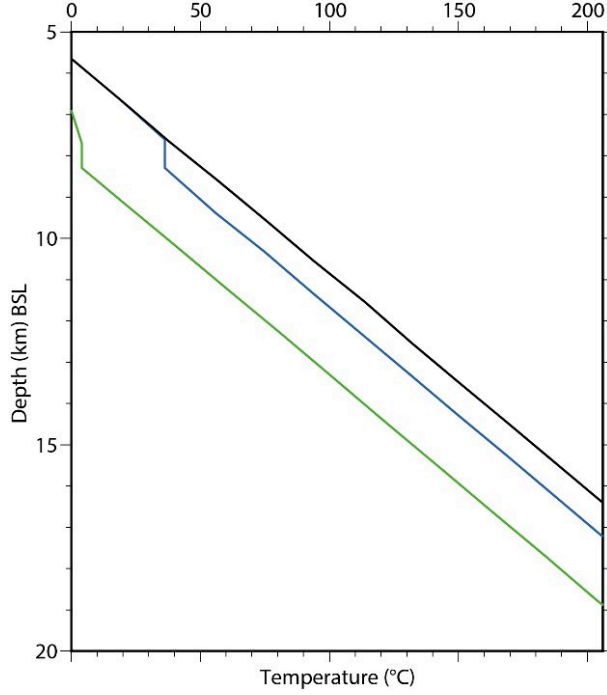


Figure 3: Seaward boundary temperatures showing incoming plate geotherm. Black line is the conductive model for a half space cooling lithosphere. Blue line represent an insulated model having the same gradient through the base of the sediment and the crustal aquifer. Green line represents initial geotherm for a ventilated model with an imposed low thermal gradient ( $10^{\circ}\text{C}/\text{km}$ ) through the sediment.

To model vigorous fluid circulation along the subduction system we use a high thermal conductivity proxy (e.g., (Davis et al., 1997)). The vigorous circulation is described by the Nusselt number (Nu) as discussed by several authors (Spinelli & Wang, 2008, 2018, Harris et al., 2017 & 2020). The Nusselt No represents the ratio of the total heat that is transported in a convecting layer to the amount that would be transported by conduction alone (Spinelli et al., 2018). Nu quantifies the effect of vigourous circulation (Davis et al., 1997), and is given as;

$$Nu = \frac{q}{\lambda\Gamma} \quad (2)$$

Where  $q$  is the total heat transport,  $\lambda\Gamma$  are thermal conductivity and thermal gradient respectively. In order to simulate the effect of very vigorous circulation, a high thermal conductivity proxy is used. This relationship between the thermal conductivity and vigor of hydrothermal circulation is expressed using the Rayleigh number, Ra.

$$Ra = \frac{\alpha g k L^2 \rho f q}{\lambda \mu \kappa} \quad (3)$$

Where  $\alpha$  represents thermal expansivity,  $g$  is the acceleration due to gravity,  $k$  is depth dependent permeability, and follows the trend as in (Spinelli & Wang, (2008),  $L$  is the layer thickness,  $\rho f$  is temperature dependent values of the fluid density, and  $\lambda\mu\kappa$  represents thermal conductivity, viscosity, and thermal diffusivity.

The Nusselt No is then calculated from an empirical relationship that relates it to the Rayleigh no as;

$$Nu = 0.08Ra^{0.89} \quad (4)$$

To simulate heat transport by vigorous fluid circulation, we then multiply the intrinsic thermal conductivity of the layer by the Nusselt No.

## References

- Barnes, A. E. (2001). Seismic Attribute in Your Facies. *CSEG Recorder*, 41–47.
- Boucard, M., Marcaillou, B., Lebrun, J. F., Laurencin, M., Klingelhoefer, F., Laigle, M., Lallemand, S., Schenini, L., Graindorge, D., Cornée, J. J., Münch, P., Philippon, M., & the, A. (2021). Paleogene V-Shaped Basins and Neogene Subsidence of the Northern Lesser Antilles Forearc. *Tectonics*, 40(3), 1–18. <https://doi.org/10.1029/2020TC006524>
- Chopra, S., & Marfurt, K. J. (2005). Seismic attributes - A historical perspective. *Geophysics*, 70(5). <https://doi.org/10.1190/1.2098670>
- Davis, E. E., Wang, K., He, J., Chapman, D. S., Villinger, H., & Rosenberger, A. (1997). An unequivocal case for high Nusselt number hydrothermal convection in sediment-buried igneous oceanic crust. *Earth and Planetary Science Letters*, 146(1–2), 137–150. [https://doi.org/10.1016/s0012-821x\(96\)00212-9](https://doi.org/10.1016/s0012-821x(96)00212-9)
- DeMets, C., Jansma, P. E., Mattioli, G. S., Dixon, T. H., Farina, F., Bilham, R., Calais, E., & Mann, P. (2000). GPS geodetic constraints on Caribbean-North America Plate Motion. *Geophysical Research Letters*, 27(3), 437–440. <https://doi.org/10.1029/1999gl005436>
- Dumitru, T. A. (1991). Effects of subduction parameters on geothermal gradients in forearcs, with an application to Franciscan Subduction in California. *Journal of Geophysical Research*, 96(B1), 621. <https://doi.org/10.1029/90jb01913>
- Fisher, D. M., Gardner, T. W., Marshall, J. S., Sak, P. B., & Protti, M. (1998). Effect of subducting sea-floor roughness on fore-arc kinematics, Pacific coast, Costa Rica. *Geology*, 26(5), 467–470. <https://doi.org/10.1130/0091-7613>
- Gutscher, M. A., Westbrook, G. K., Marcaillou, B., Graindorge, D., Gailler, A., Pichot, T., & Maury, R. C. (2013). How wide is the seismogenic zone of the Lesser Antilles forearc? *Bulletin de La Societe Geologique de France*, 184(1–2), 47–59. <https://doi.org/10.2113/gssgfbull.184.1-2.47>
- Harris, R. N., Spinelli, G. A., & Fisher, A. T. (2017). Hydrothermal circulation and the thermal structure of shallow subduction zones. *Geosphere*, 13(5), 1425–1444. <https://doi.org/10.1130/GES01498.1>
- Harris, R. N., Spinelli, G. A., & Hutnak, M. (2020). Heat Flow Evidence for Hydrothermal Circulation in Oceanic Crust Offshore Grays Harbor, Washington. *Geochemistry*,

*Geophysics, Geosystems*, 21(6), 0–2. <https://doi.org/10.1029/2019GC008879>

Harris, R. N., Spinelli, G., Ranero, C. R., Grevenmeyer, I., Villinger, H., & Barckhausen, U. (2010). Thermal regime of the Costa Rican convergent margin: 2. Thermal models of the shallow Middle America subduction zone offshore Costa Rica. *Geochemistry, Geophysics, Geosystems*, 11(12), 1–22. <https://doi.org/10.1029/2010GC003273>

Hutchison, I. (1985). The effects of sedimentation and compaction on oceanic heat flow. *Development*, 82, 439–459.

Klingelhofer, F., & Marcaillou, B. (2022). *MANTA-RAY* cruise, *RV L'Atalante*. <https://doi.org/https://doi.org/10.17600/18002498>

Klingelhofer, F., Marcaillou, B., Laurencin, M., Biari, Y., Laigle, M., Graindorge, D., Evain, M., Lebrun, J.-F., & Paulatto, M. (2018). Relation Between the Nature of the Subducting Plate, Heat Flow and Fluid Escape Structures at the Lesser Antilles Island arc. *American Geophysical Union Fall Meeting, Washington, DC, USA, T22B-04*, 10–14.

Kopp, H., Weinzierl, W., Becel, A., Charvis, P., Evain, M., Flueh, E. R., Gailler, A., Galve, A., Hirn, A., Kandilarov, A., Klaeschen, D., Laigle, M., Papenberg, C., Planert, L., & Roux, E. (2011). Deep structure of the central Lesser Antilles Island Arc: Relevance for the formation of continental crust. *Earth and Planetary Science Letters*, 304(1–2), 121–134. <https://doi.org/10.1016/j.epsl.2011.01.024>

Laigle, M., Becel, A., de Voogd, B., Sachpazi, M., Bayrakci, G., Lebrun, J. F., & Evain, M. (2013). Along-arc segmentation and interaction of subducting ridges with the Lesser Antilles Subduction forearc crust revealed by MCS imaging. *Tectonophysics*, 603, 32–54. <https://doi.org/10.1016/j.tecto.2013.05.028>

Laigle, M., Hirn, A., Sapin, M., Bécél, A., Charvis, P., Flueh, E., Diaz, J., Lebrun, J. F., Gesret, A., Raffaele, R., Galvé, A., Evain, M., Ruiz, M., Kopp, H., Bayrakci, G., Weinzierl, W., Hello, Y., Lépine, J. C., Viodé, J. P., ... Nicolich, R. (2013). Seismic structure and activity of the north-central Lesser Antilles subduction zone from an integrated approach: Similarities with the Tohoku forearc. *Tectonophysics*, 603, 1–20. <https://doi.org/10.1016/j.tecto.2013.05.043>

Laigle, M., Lebrun, J.-F., & Hirn, A. (2007). *SISMANTILLES 2* cruise, *RV L'Atalante*. <https://doi.org/https://doi.org/10.17600/7010020>



- Laurencin, M., Marcaillou, B., Graindorge, D., Lebrun, J. F., Klingelhoefer, F., Boucard, M., Laigle, M., Lallemand, S., & Schenini, L. (2019). The Bunce Fault and Strain Partitioning in the Northern Lesser Antilles. *Geophysical Research Letters*, *46*(16), 9573–9582. <https://doi.org/10.1029/2019GL083490>
- Marcaillou, B., Henry, P., Kinoshita, M., Kanamatsu, T., Screatton, E., Daigle, H., Harcouët-Menou, V., Lee, Y., Matsubayashi, O., Kyaw Thu, M., Kodaira, S., & Yamano, M. (2012). Seismogenic zone temperatures and heat-flow anomalies in the To-nankai margin segment based on temperature data from IODP expedition 333 and thermal model. *Earth and Planetary Science Letters*, *349–350*, 171–185. <https://doi.org/10.1016/j.epsl.2012.06.048>
- Marcaillou, B., & Klingelhoefer, F. (2013a). *ANTITHESIS-1-Leg1 Cruise, RV L'Atalante*. <https://doi.org/doi:10.17600/13010070>
- Marcaillou, B., & Klingelhoefer, F. (2013b). *ANTITHESIS-1-Leg2 Cruise, RV Pourquoi Pas?* <https://doi.org/doi:10.17600/13030100>
- Marcaillou, B., & Klingelhoefer, F. (2016). *ANTITHESIS-3 Cruise, RV Pourquoi Pas?* <https://doi.org/doi:10.17600/16001700>
- Marcaillou, B., Spence, G., Wang, K., Collot, J. Y., & Ribodetti, A. (2008). Thermal segmentation along the N. Ecuador-S. Colombia margin (1–4°N): Prominent influence of sedimentation rate in the trench. *Earth and Planetary Science Letters*, *272*(1–2), 296–308. <https://doi.org/10.1016/j.epsl.2008.04.049>
- Mitchum Jr., R. M., & Vail, P. R. (1977). Seismic Stratigraphy and Global Changes of Sea Level, Part 7: Seismic Stratigraphic Interpretation Procedure1. In C. E. Payton (Ed.), *Seismic Stratigraphy — Applications to Hydrocarbon Exploration* (Vol. 26, p. 0). American Association of Petroleum Geologists. <https://doi.org/10.1306/M26490C9>
- Paulatto, M., Laigle, M., Galve, A., Charvis, P., Sapin, M., Bayrakci, G., Evain, M., & Kopp, H. (2017). Dehydration of subducting slow-spread oceanic lithosphere in the Lesser Antilles. *Nature Communications*, *8*, 240. <https://doi.org/10.1038/ncomms15980>
- Pichot, T., Patriat, M., Westbrook, G. K., Nalpas, T., Gutscher, M. A., Roest, W. R., Deville, E., Moulin, M., Aslanian, D., & Rabineau, M. (2012). The Cenozoic tectonostratigraphic evolution of the Barracuda Ridge and Tiburon Rise, at the western end of the North America-South America plate boundary zone. *Marine Geology*, *303–306*, 154–171. <https://doi.org/10.1016/j.margeo.2012.02.001>

- Roest, W. R., & Collette, B. J. (1986). The Fifteen Twenty Fracture Zone and the North American-South American plate boundary. *Journal of the Geological Society*, *143*(5), 833–843. <https://doi.org/10.1144/gsjgs.143.5.0833>
- Roksandic, M. M. (1978). Seismic facies analysis. *Geophysical Prospecting*, *26*, 383–398.
- Saffer, D. M. (2010). Hydrostratigraphy as a control on subduction zone mechanics through its effects on drainage: An example from the Nankai Margin, SW Japan. *Geofluids*, *10*(1–2), 114–131. <https://doi.org/10.1111/j.1468-8123.2009.00276.x>
- Saffer, D. M., & Screaton, E. J. (2003). Fluid flow at the toe of convergent margins: Interpretation of sharp pore-water geochemical gradients. *Earth and Planetary Science Letters*, *213*(3–4), 261–270. [https://doi.org/10.1016/S0012-821X\(03\)00343-1](https://doi.org/10.1016/S0012-821X(03)00343-1)
- Spinelli, G. A., & Wang, K. (2008). Effects of fluid circulation in subducting crust on Nankai margin seismogenic zone temperatures. *Geology*, *36*(11), 887–890. <https://doi.org/10.1130/G25145A.1>
- Spinelli, G., Wada, I., Wang, K., He, J., Harris, R., & Underwood, M. (2018). Diagenetic, metamorphic, and hydrogeologic consequences of hydrothermal circulation in subducting crust. *Geosphere*, *14*(6), 2337–2354. <https://doi.org/10.1130/GES01653.1>
- Taner, M. T. (2001). Seismic Attributes. *CSEG Recorder*, 49–56.
- Vail, P. R., Mitchum, R., & Thompson, S. (1977). *Seismic Stratigraphy and Global Changes of Sea Level: Part 3. Relative Changes of Sea Level from Coastal Onlap: Section 2. Application of Seismic Reflection Configuration to Stratigraphic Interpretation.*
- Verschuur, D. J., Berkhout, A. J., & Wapenaar, C. P. A. (1992). Adaptive surface-related multiple elimination. *Geophysics*, *57*(9), 1166–1177. <https://doi.org/10.1190/1.1443330>
- Von Herzen, R. P., & Maxwell, A. E. (1959). The measurement of thermal conductivity of deep-sea sediments by a needle-probe method. *Journal of Geophysical Research*, *64*(5), 1557–1563. [https://doi.org/10.1016/s0016-0032\(23\)90620-4](https://doi.org/10.1016/s0016-0032(23)90620-4)
- Wang, K., Hyndman, R. D., & Yamano, M. (1995). Thermal regime of the Southwest Japan subduction zone: effects of age history of the subducting plate. *Tectonophysics*, *248*(1–2), 53–69. [https://doi.org/10.1016/0040-1951\(95\)00028-L](https://doi.org/10.1016/0040-1951(95)00028-L)

Yilmaz, Ö., & Doherty, S. M. (1987). *Seismic Data Processing*. Society of Exploration Geophysicists. <https://books.google.fr/books?id=ecspwgEACAAJ>

## Chapter 3

### **Nature of the Oceanic crust, Fluid circulation, and thermal structure of the Margin**

Amongst the features that impact subduction zone dynamics, the nature of the subducting plate, fluids and temperature contribute significantly to its seismogenic potentials. Therefore in this chapter, we investigate these parameters in order to understand their relationships, and seismogenic impacts in the Lesser Antilles subduction zone, where seismological heterogeneities and low seismic activities has been recorded over a long period of time.

#### **3.1 The nature of the subducting oceanic crust**

In this section of the thesis, we discuss the complex nature of the subducting oceanic crust below the Northern Lesser Antilles margin, and its implication on seismicity. This study is published in *Communications Earth and Environment* in 2021 titled “Pervasive detachment faults within the slow spreading oceanic crust at the poorly coupled Antilles subduction zone”. I participated to this publication by processing seismic data and discussing the results with co-authors.







The study presents a newly detected along-strike variations in the subducting oceanic fabric, that constitute patches of highly-hydrated mantle rocks hosted along deep and pervasive detachment faults, which were formed in the basement during its formation. MCS and bathymetric data image seafloor features and deep crustal structures within the Jacksonville Patch that differ significantly from that of the oceanic plate in neighbouring zones. These features were described as Ridgeward-Dipping oceanic-basement Reflectors (RDRs) due to their angle and direction of dips. They are closely spaced, and root from the top of the oceanic basement, although most of them do not fracture the oceanic basement and the sediment.

Based on the analysis of these reflectors and the velocity field, we proposed that the oceanic basement in the Jacksonville Patch consists of hydrated and serpentized mantle rocks, possibly including gabbroic bodies, exhumed along detachment faults. We conclude that the RDRs represent wide-spread detachment faults that formed at the slow-spreading Mid-Atlantic Ridge. Close to the trench, these faults are reactivated due to plate bending, and favour fluid percolation, as well as rock alteration.


Lastly, we discussed the implications of the subduction of these patches of hydrated, serpentized mantle rocks on the interplate seismicity, and conclude that based on their nature,

they will contribute to the megathrust weakness and reduced seismicity recorded in the Saint-Martin margin segment, located between Barbuda and the Virgin Islands.

## Pervasive detachment faults within the slow spreading oceanic crust at the poorly coupled Antilles subduction zone

Boris Marcaillou <sup>1</sup>, Frauke Klingelhofer <sup>2</sup>, Muriel Laurencin <sup>3</sup>, Jean-Frédéric Lebrun<sup>4</sup>, Mireille Laigle <sup>1</sup>, Serge Lallemand<sup>5</sup>, Laure Schenini<sup>1</sup>, Aurélien Gay<sup>5</sup>, Milton Boucard <sup>4</sup>, Kingsley Ezenwaka<sup>1</sup> & David Graindorge<sup>6</sup>

Oceanic crust formed at slow-spreading ridges is currently subducted in only a few places on Earth and the tectonic and seismogenic imprint of the slow-spreading process is poorly understood. Here we present seismic and bathymetric data from the Northeastern Lesser Antilles Subduction Zone where thick sediments enable seismic imaging to greater depths than in the ocean basins. This dataset highlights a pervasive tectonic fabric characterized by closely spaced sequences of convex-up Ridgeward-Dipping Reflectors, which extend down to about 15 km depth with a 15-to-40° angle. We interpret these reflectors as discrete shear planes formed during the early stages of exhumation of magma-poor mantle rocks at an inside corner of a Mid-Atlantic Ridge fracture zone. Closer to the trench, plate bending could have reactivated this tectonic fabric and enabled deep fluid circulation and serpentinization of the basement rocks. This weak serpentinized basement likely explains the very low interplate seismic activity associated with the Barbuda-Anegada margin segment above.

<sup>1</sup> Université Côte d'Azur, CNRS, Observatoire de la Côte d'Azur, IRD, Géoazur, Valbonne, France. <sup>2</sup> IFREMER, Dpt. of Marine Geosciences, Plouzané, France. <sup>3</sup> Université de Lille, CNRS, Univ. Littoral Côte d'Opale, UMR 8187, LOG, Laboratoire d'Océanologie et de Géosciences, Lille, France. <sup>4</sup> Géosciences Montpellier, Université de Montpellier, CNRS, Université des Antilles, Pointe à Pitre, Guadeloupe(FWI). <sup>5</sup> Geosciences Montpellier, Université de Montpellier, CNRS, Université des Antilles, Montpellier, France. <sup>6</sup> Geosciences Océan, UMR 6538, Université Bretagne Occidentale, Institut Universitaire Européen de la Mer, Plouzané, France. email: [boris.marcaillou@geoazur.unice.fr](mailto:boris.marcaillou@geoazur.unice.fr)

Oceanic basement formed at slow-spreading mid-ocean ridges (MORs), exhibits remarkable variations in crustal thickness, seismic velocity and tectonic fabric, as previously inferred from bathymetric data<sup>1–3</sup>, paleomagnetic studies<sup>4,5</sup> sampling and drilling of outcrops of deep-seated rocks<sup>6,7</sup> and numerical modelling<sup>8,9</sup>. In contrast, few seismic data image this fabric variability at depth<sup>10–13</sup>. Poorly sedimented seafloor near MORs causes severe scattering of seismic waves during mapping expeditions, which impedes accurate intra-crustal imaging at depth<sup>14</sup>. As a result, deciphering the complex variability of oceanic tectonic fabric in seismic images remains challenging.

This variability, from magmatically robust to tectonically dominated segments, depends on the spreading rate and the relative contribution of tectonic extension and magmatic dike to oceanic spreading<sup>8,9</sup>. At magmatically robust segments, oceanic spreading is mainly taken up by vigorous melt delivery, which leads to typical velocity-depth “Penrose” structure of extrusive basalts overlying intrusive gabbros<sup>15</sup>. In contrast, tectonically dominated spreading favors stretched and thinned crust possibly hosting widely spaced, long-lived, low-angle, rideward-dipping detachment faults<sup>16</sup>, exhuming serpentinized peridotites with a varying amount of gabbro bodies. This heterogeneous crustal composition is referred to as the “plum-pudding model”<sup>17,18</sup>. The velocity-depth structure then usually consists of one layer with a rather constant velocity gradient<sup>19–21</sup> depending on a decreasing serpentinization degree with depth<sup>22</sup>. Reston et al.<sup>11</sup> argue that more closely spaced faulting may result from a tectonic sequence where a detachment fault forms, slips, flexes and becomes inactive when a new detachment fault develops nearby. However, in the absence of convincing deep seismic images for such tectonic sequences, the model of widely spaced detachment faults frequently prevails.

New bathymetric and multichannel seismic (MCS) data, collected in the NLA trench during cruises ANTITHESIS 1 and 3<sup>23,24</sup> call into question this generic model for the first time. The sedimentary layer reduces the scattering, allowing up-to-6-s-two-way-traveltime (stwt) deep seismic imaging, which is unprecedented for slow-spreading oceanic basement. These data reveal impressive along-strike variations in oceanic fabric, showing an unexpected deep and pervasive tectonic pattern within the basement created at a segment end of the Mid-Atlantic Ridge. These images challenge the long-lived detachment model, highlight that the tectonic imprint of slow-spreading onto the oceanic basement has possibly been underestimated, and raise questions about the seismic consequences of subduction of tectonically dominated, hydrated, serpentinized, and weak oceanic basement patches.

## Results and discussion

### Oceanic tectonic pattern near the Jacksonville Fracture zone.

The ~N120°-trending Jacksonville Fracture Zone extends from the Northwestern Atlantic to the NLA Subduction Zone<sup>25</sup> (Fig. 1). To the south, the 15–20 Fracture Zone subducts beneath the margin at a convergence rate of 20 mm/yr in the N254°E direction<sup>26</sup>. Between these fracture zones, the Cretaceous oceanic basement in the trench (Fig. 1A) ages westward<sup>27</sup>. Based on the 300–330 km distance between chron C34 (83 Ma) and C32 (71.6 Ma)<sup>28</sup>, the mean half-spreading rate was low, 26–29 mm/yr, at the spreading center.

The Jacksonville Patch, originated from the ridge segment end close to the Jacksonville Fracture Zone, is currently located in the trench between 18 and 19°N. The bathymetry and deep structure within this patch drastically differs from that of the incoming oceanic plate in neighboring zones.

To the southeast and the northwest of this patch, the oceanic fabric of the incoming plate corresponds to ~N20°-trending

elongated topographic highs sub-parallel to the magnetic anomalies (Fig. 1B, Supplementary Fig. 1). In addition, in every seismic line perpendicular to the trench (Ant01 07, 10, 11, 12, 14, and 50) reflectors of the seafloor, oceanic sediments, and the basement top step down westward along steep fault planes that dominantly dip toward the margin (Fig. 2A). These normal faults penetrate the basement down to gently southwestward-dipping discontinuous reflections *M*, 1.9 to 2.2 stwt beneath the top of the basement, interpreted as the Moho. These faults crop out at bathymetric scarps, directed N100–120°E, sub-parallel or slightly oblique to the deformation front.

This margin sub-parallel faulting in the outer trench wall has long been described as the result of the incoming plate bending into the subduction zone<sup>29,30</sup>. According to these studies, plate bending mainly reactivates inherited tectonic structures of the oceanic fabric when favorably oriented (sub-parallel to the trench) and produces new faults when the fabric is highly oblique with respect to the trench. Offshore of the NLA, the oceanic fabric trends at more than 70° angle to the trench. The southwestward-dipping faults, sub-parallel to the deformation front, are thus likely to be newly formed plate bending faults.

Within the Jacksonville Patch, the bathymetric map and associated dip and strike seismic lines (Ant06, 43, 44, 45, 52, 53, and 54) show a drastically different tectonic pattern in the trench (Fig. 1B, Supplementary Fig. 1B). The smoother seafloor is neither spiked with the N20°-trending ridges of the oceanic fabric, nor deformed by the margin-subparallel scarps of plate-bending normal faults. In contrast, short, shallow and steep faults dipping toward east and west bound ~4–6 km wide grabens in the oceanic basement. These grabens define ~N100–110°-directed seafloor undulations trending at 40° angle to the margin front. The seismic lines do not show organized reflections at typical Moho depths. The most striking features are 5–10-km-spaced, convex-up, high-amplitude reflector sequences, which dip from the top of the oceanic basement down to 5 stwt below the seafloor (Fig. 2B). The sequences are 0.1–0.2-stwt-thick (200 to 500 m) and locally up-to-0.5-stwt-thick (1 to 1.5 km).

### Rideward-Dipping oceanic-basement Reflectors (RDRs).

In order to estimate the true dip direction and geometry of these reflector sequences, we performed depth-conversion of MCS lines Ant45 and 53 interpretations (Fig. 3) as well as a pre-stack depth migration of line Ant45. We used a combined MCS / wide-angle seismic (WAS) velocity model based on nearby WAS line Ant06<sup>31</sup> (Supplementary Fig. 3). In this model, the basement corresponds to a 5.6–6.5-km-thick single layer with a 5.5–7.4 km/s velocity range from top to bottom and a constant velocity gradient of 0.27 s<sup>-1</sup>. Moreover, we used seismic attributes derived from seismic data in order to confirm the reflector sequences geometry. Computing RMS amplitude provides information about reflection physical properties and particularly fluid content<sup>32</sup>. This analysis suggests that the reflector sequences, compared to other intra-crustal reflections, show physical properties consistent with fluid-rich and/or serpentinized rocks within the upper 6 km of the oceanic basement. At greater depths, the dimming of reflections suggests a decreasing fluid content and/or serpentinization degree (Supplementary Fig. 4). The mean apparent dip angle increases from 17° to 25° in N125°E-trending line Ant53 and from 15° to 35° in N40°E-trending line Ant45 (Fig. 3A, Supplementary Fig. 5). These lines intersect each other (Fig. 3B) and reveal that the reflectors dip in a N60–90°E direction, towards the Mid-Atlantic Ridge, with a dip angle that increases from 20–30° in the upper 3 km, up to 45° between 3 and 8 km depth (Fig. 3C). We refer to these sequences as Rideward-Dipping oceanic-basement Reflectors (RDRs) (Fig. 4).

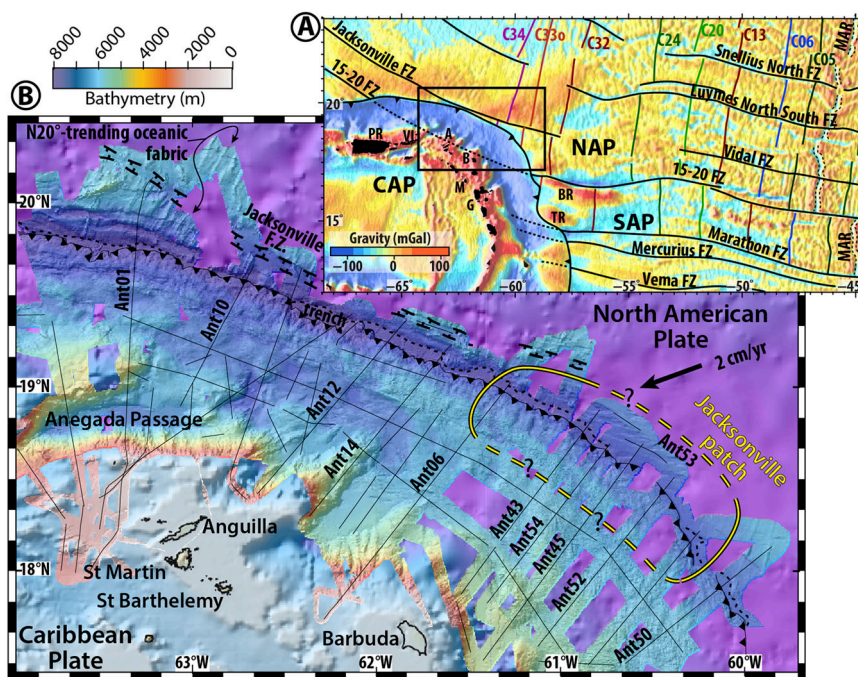


**Fig. 1** Maps of the study area. **A** Satellite free-air gravity map<sup>62</sup> showing fracture zones (solid lines), synthetic flow lines (colored lines), and the Mid-Atlantic Ridge (dotted lines) in the Central Atlantic for chrons 5 (8.9 Ma), 6 (19.4 Ma), 13 (35.3 Ma), 20 (44.7 Ma), 24 (55 Ma), 32 (71.6 Ma), 330 (80.2 Ma), and 34 (84 Ma)<sup>63</sup>. A stands for Anegada, B for Barbuda, BR for Barracuda Ridge, CAP for Caribbean Plate, FZ for Fracture Zone, G for Guadeloupe, M for Montserrat, MAR for Mid-Atlantic Ridge, NAP for North American Plate, TR for Tiburon Ridge, PR for Puerto-Rico, SAP South American Plate, and VI for Virgin Island. The black frame refers to Fig. 1B. **B** Bathymetric map showing location for multichannel seismic lines labeled AntXX and the Jacksonville Fracture Zone (dashed black lines). Close-up on target zones are in Supplementary Fig. 1.

Previous seismic data depicted distant convex-up ridgeward-dipping reflectors with similar dipping angle at segment ends of slow-spreading ridges, interpreted as large-offset long-lived detachment faults, for instance in the Cretaceous-aged Eastern Central Atlantic<sup>11,13</sup> and at the South West Indian Ridge (SWIR)<sup>10</sup>. At the SWIR, the faults are associated with similar ~0.5-stwt-thick sub-parallel bright discontinuous reflectors interpreted as damage zones. The RDRs are also partly consistent with closely spaced, ~1-km-thick sequences of convex-up LCRs (Lower-Crust ridgeward-dipping Reflectors) in the Northwestern Atlantic<sup>12,33</sup> as well as in lower crust generated at the faster Mid-Pacific spreading ridge offshore of the Middle America Trench<sup>34</sup>, Japan<sup>35–37</sup>, Alaska<sup>38</sup>, and Hawaii<sup>39</sup>. These LCRs have been interpreted as lithological layering resulting from magma flow in the Atlantic<sup>33</sup> and the Pacific<sup>40,41</sup>. However, discrete spacing of reflectors rather than pervasive layering more readily supports ductile shear zones<sup>37,42</sup> due to spreading-related deep tectonic events<sup>12</sup> and/or anomaly in melt delivery at the mid-ocean ridge<sup>42</sup>.

The RDRs size and geometry partly differ from these analogues. These reflectors extend from the top of the oceanic basement to, at least, 6 km below (Fig. 3, Supplementary Fig. 5) while the LCRs are restricted to the lower crust and sole out downward onto the Moho. Discretely spaced thin sequences of subparallel RDRs are poorly consistent with pervasive and massive fan-shaped layering at Seaward Dipping Reflectors (SDRs) and lava flows. At last, the RDRs are closely spaced and most of them do not deform or fracture the top of the oceanic basement and the sediment layer, contrasting with the classical image of distant detachment faults<sup>11</sup> with topographic expressions<sup>3</sup>, in the Northeastern Atlantic. However, this fault spacing at a slow to intermediate spreading axis depends on the fraction of the plate separation rate that is accommodated by magmatic ridge-axis dyke intrusion<sup>8</sup>. According to these authors,

a tectonically dominated slow-spreading ridge segment with moderate magmatic activity can generate closely spaced detachment-type deformation zones during early stages of basement exhumation.

Based on this discussion, we propose that the Jacksonville Patch lithosphere consists of serpentinized mantle rocks, possibly hosting gabbro bodies exhumed along low-angle detachment systems<sup>16</sup> or by serpentine diapirism up high-angle faults<sup>43</sup>. Although we cannot rule out serpentine diapirism, inside corners of fracture zones are known to be prone to detachment faulting<sup>44</sup>, the RDRs more readily image pervasive proto-detachment shear zones related to early tectonic extension at a magma-poor inside corner of the segmented MAR. In this interpretation, the RDRs more readily image pervasive proto-detachment shear zones related to early tectonic extension at a magma-poor inside corner of the segmented MAR. Approaching the trench, the plate bending, reactivates extensional strain along the RDRs, favoring fluid percolation, rock alteration and serpentinization, increasing acoustic impedance contrast and reflection amplitude. The RMS analysis supports this interpretation showing high RMS amplitude along the RDRs within the upper 6 km and at the top of the oceanic crust above the RDRs (Supplementary Fig. 4).

### Seismogenic behavior of subducting serpentine-bearing rocks.

The NLA Subduction Zone has hosted only 39 thrust-faulting earthquakes, detected teleseismically ( $M_w > 5$ ), with focal mechanisms compatible with interplate co-seismic slips since 1973 (Fig. 5). Most of these subduction-type events occurred to the North of Guadeloupe where they are aggregated in two seismicity clusters: from Montserrat to Barbuda and from the Anegada Passage to Virgin Island<sup>45</sup>. Very few of them occurred along the ~110-km-wide margin segment in between and to the South of Guadeloupe.



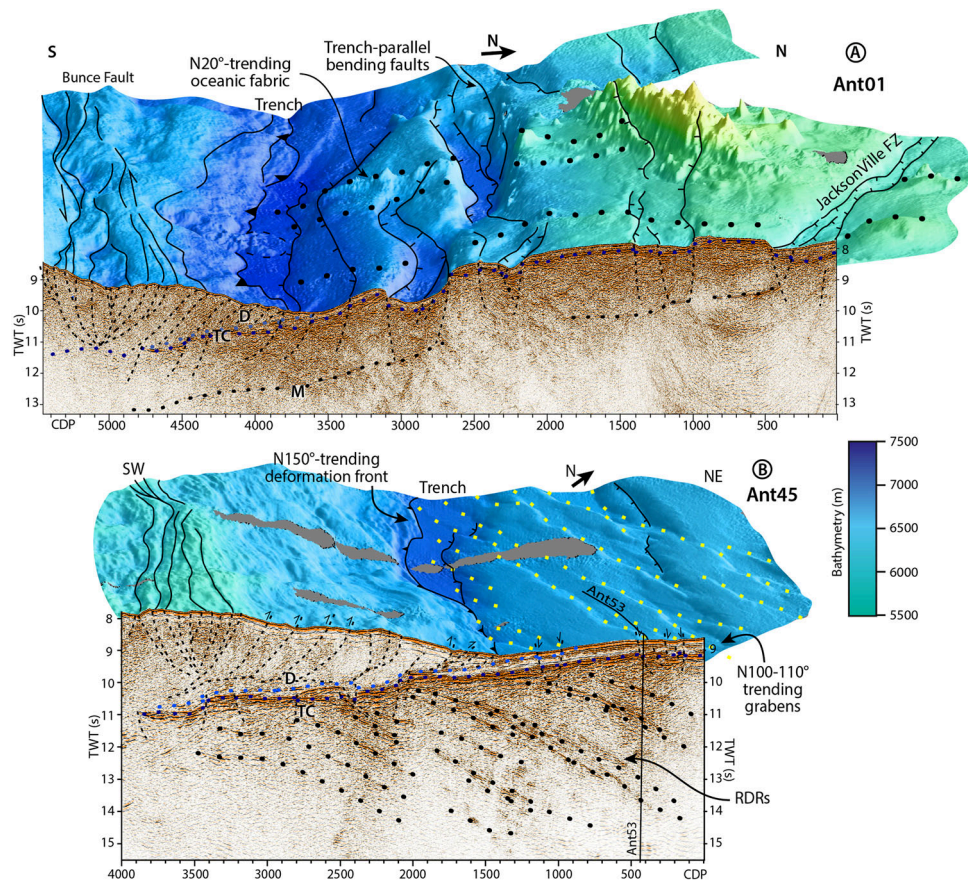


**Fig. 2 3D seismic-bathymetry blocks at magmatically robust and tectonically dominated segments.** Three-dimensional seismic-bathymetry views illustrating typical oceanic basement (**A** line Ant01) and the spectacular, tectonically dominated, exhumed oceanic basement (**B** line Ant45) located outside and inside the Jacksonville Patch, respectively. D, TC, and M stand for Decollement, Top of the oceanic Crust, and Moho, respectively. Black and yellow dotted lines underline the Ridgeward-Dipping oceanic-basement Reflectors (RDRs) and the oceanic grabens direction, respectively. Vertical Exaggeration 1:3.5. Additional 3D blocks are in Supplementary Fig. 2.

In the Southern and Central Lesser Antilles, numerous fracture zones in the subducting South American Plate (Fig. 1A) likely trigger deep crustal hydration and mantle serpentinization<sup>46–48</sup>. This high water budget is prone to impede large interplate coseismic rupture, rather favoring alternate slip behavior (SSE, VLFE, EETS)<sup>49</sup> and/or numerous low-magnitude events<sup>46,48</sup>. In contrast, in the NLA, the only fracture zone (the 15–20 FZ) of the subducting North American Plate to interact with the subduction zone (Fig. 1) has not subducted deep enough to favor dehydration of the subducting serpentinized mantle<sup>47</sup>. This fracture zone, located at less than 30 km depth beneath the forearc<sup>31</sup>, could trigger shallow dewatering and margin tectonic deformation, weakening the interplate contact, reducing the seismic coupling and affecting the megathrust seismogenic behavior. However, the fracture zone underthrusts similarly the two clusters of subduction-type teleseisms ( $M_w > 5$ ), and the gap in between (Fig. 5) suggesting a low influence onto the interplate seismicity in the NLA.

We propose that the reduced strength of the subducting plate basement at least partly made of serpentinized mantle rocks strongly contributes to the megathrust weakness and the interplate seismicity reduction. Low-temperature species of serpentine minerals, chrysotile, and lizardite have a low coefficient of internal friction, low fracture strength, and a nominally non-dilatant mode of brittle deformation, which favor localized slip on discrete surfaces, cataclastic flow by shear microcracking<sup>50–52</sup>, and plastic flow within individual grains<sup>53</sup>. This substantial weakening of serpentine-

bearing rocks is not a linear function of the degree of serpentinization but is similar in slightly hydrated peridotites and pure serpentinites<sup>22</sup>. The subduction of an heterogeneously faulted, hydrated and serpentinized basement is likely to generate an interplate patchiness of contrasting frictional properties, which may impede full interplate coupling<sup>53</sup>, instead favoring a mix of stable and unstable behaviors prone to triggering small- $M_w$ , slow-slip, and/or very-low frequency earthquakes<sup>54</sup>. Similar conditions are suspected in anomalous non-seismic regions in locally hydrated forearc mantle within Northeast Japan<sup>53</sup>.

The Lesser Antilles is an end-member subduction zone, which undergoes the subduction of highly hydrated fracture zones and unsuspected large-scale tectonically dominated oceanic patches. Our data depict for the first time pervasive and closely spaced proto-detachment shear planes, reactivated by the plate bending in the trench within the oceanic basement, at least partly made of serpentinized mantle rocks exhumed at a former inside corner of the MAR. The landward extent of this patch is unclear beyond 40 km from the deformation front, because of seismic amplitude loss at great depth. However, downdip, tectonic interaction and fluid circulation between the patch and the 15–20 Fracture Zone possibly alter the forearc strength. Thus, the reduced strength and fluid circulation related to the Jacksonville serpentinized basement, its pervasive tectonic fabric, and the proximity of the hydrated 15–20 Fracture Zone are likely to account for the heterogeneous distribution of subduction earthquakes in the NLA.

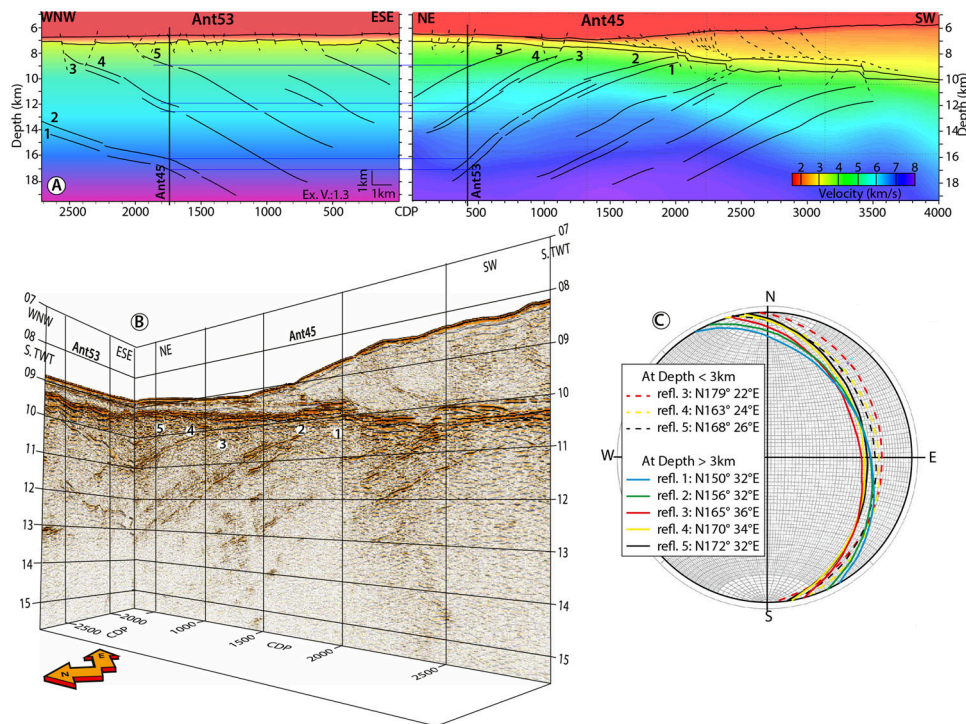


**Fig. 3 Geometry and direction of Ridgeward Dipping Reflectors.** Depth-converted interpretation for lines Ant45 and Ant53 (A), 3D view in time section (B), and Schmidt diagram (C) reveal that the convex-up sequences of RDRs in the oceanic basement dip toward the Mid Atlantic Ridge. Lines location is in Figs. 1B and 3D bathymetry-seismic view for lines Ant45 and Ant53 are in Fig. 2B and Supplementary Fig. 2, respectively. Figure 4 shows an interpreted perspective view of the RDRs.

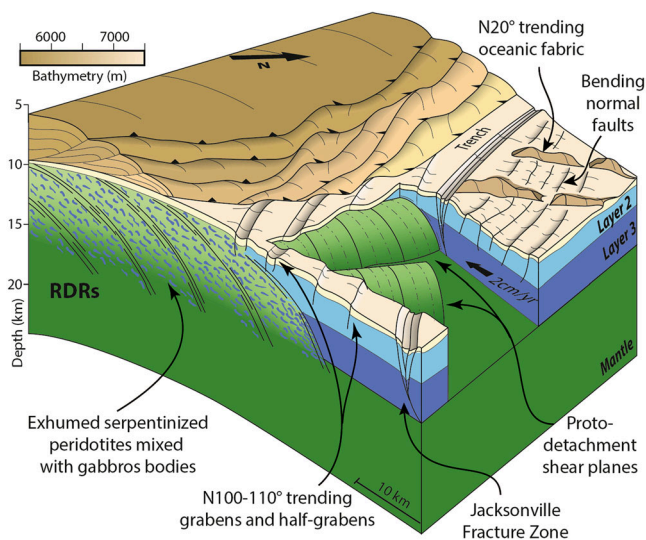


**Fig. 4 Interpreted 3D view of the tectonically dominated slow-spreading basement subducting beneath the Northern Lesser Antilles Subduction Zone.** Perspective view showing the structural transition of the Atlantic basement from the inside to the outside corner of the Jacksonville Fracture Zone. The Jacksonville patch at the inside corner consists of serpentinized mantle rock possibly mixed with gabbro bodies exhumed along proto-detachment shear planes which formed at a tectonically dominated magma poor ridge segment end. These detachments, reactivated while subducting beneath the NLA draw Ridgeward Dipping Reflectors (RDRs) in along-dip vertical sections.

**Methods**

**Data acquisition.** Our results are based on recent multichannel seismic (MCS) wide-angle (WAS) seismic and bathymetric data collected during cruises ANTITHESIS 1<sup>23</sup> and ANTITHESIS 3<sup>24</sup>. Multibeam swath bathymetry data were

recorded using a Kongsberg EM122 and a RESON Seabat7150 (432 – 880 beams echosounders) during ANTITHESIS 1 and 3, respectively. We recorded MCS lines Ant01, 10.2 and 12 during Antithesis 1<sup>23</sup>, using a 7699 cu in 18-elements airgun seismic source towed at 17-m-depth and a 3-km-long streamer composed of 288 channels spaced at 12.5 m and towed at 20-m-depth. We acquired lines Ant45, 50, 53, and 54 during Antithesis 3<sup>24</sup>, using a 6500 cu in, 16-elements airgun seismic source towed at 14-m-depth and a 4.5-km-long streamer composed of 720 channels spaced at 6.25 m and towed at 15-m-depth. Shots were fired every 75 m providing a 30-fold coverage.

**Data processing.** Swath processing consists in spikes and excessive slopes removal by automatic procedure and manual ping editing using *Caribes*<sup>®</sup> and *Globe*<sup>®</sup> softwares (IFREMER). Digital terrain models were produced with a grid spacing of 75 m. Vertical accuracy is between a few meters and tens of meters depending on depth. Bathymetric and slope maps were calculated and processed using *QGis*. Maps reveal reliefs in the order of tens of meters high and few hundred meters apart.

MCS data processing includes quality control, binning, band-pass filtering, fK filtering, external and internal mutes, noise attenuation, predictive deconvolution, multiple suppression, velocity analysis, normal move out and dip move out corrections, stacking and pre-stack time migration, using *Solid-QC*<sup>®</sup> (Ifremer) and *Geovation*<sup>®</sup> (CGG-Veritas) Softwares<sup>55</sup>. We performed iterative Prestack Kirchhoff time migration (PSTM) to yield optimal migration velocities and form the final prestack migrated images. PSTM results in focusing correctly seismic energy from genuine basement reflections but not from out-of-planes arrivals from seafloor or basement propagating through regions of lower root-mean-square velocity. Thus, any intra-basement event observed on presented PSTM images can be interpreted as true reflection.

**Depth-converted interpretation and depth-migrated seismic data.** Converting and/or migrating to depth the seismic images is a mandatory condition to address the questions of the geometry, dipping angle, and orientation of the RDRs. The depth of investigation (11 to 18 km) is much larger than the streamer length (4 and 4.5 km for Antithesis 1 and 3, respectively). At great depth, this relative shortness of the streamers results in high uncertainties in interval velocity model strictly inferred from Normal-Move-Out (NMO) velocities. In order to reduce this uncertainty, we build composite velocity models based on MCS lines Ant45 and 53 and WAS line Ant06<sup>31</sup> (Supplementary Fig. 3), located within the Jacksonville Patch 70 km to the northwest. These models consists in: 1/ NMO velocities converted to interval velocities using the Dix formula at shallow depth (i.e., from the seafloor to the topmost hundreds of milliseconds in the subducting basement) and

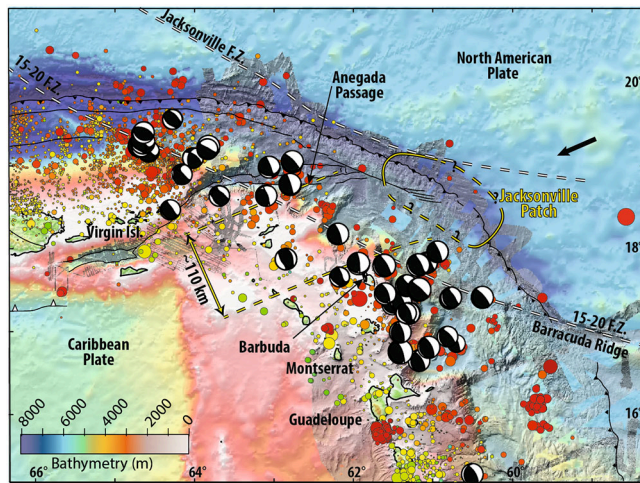


**Fig. 5 Seismicity map.** Map view of the seismic activity in the Northern Lesser Antilles. The circles represent the earthquakes from the EHB catalogue and the USGS PDE, sized by magnitude and colored by depth. Black focal mechanisms are thrust earthquakes from the gCMT catalogue, aggregated in two clusters separated by a 110-km large quiet zone (dashed yellow lines). Dashed white lines indicate the 15-20 and Jacksonville Fracture Zones.

2/ velocities inferred from first-arrival traveltimes tomography for line Ant06 at greater depth in the basement and the mantle. We then base our investigations on two complementary methodological approaches. We convert to depth the interpretation for seismic lines An45 and 53 (Fig. 3) using these combined MCS/WAS velocity models. In order to confirm this conversion, MCS line Ant45 is migrated to depth (Supplementary Fig. 5) with a preserved amplitude Pre-Stack Depth Migration (PSDM) approach<sup>56–60</sup> performed in the angle domain. The velocity macro-model is iteratively corrected during migration, using the “migration-velocity-analysis” approach<sup>61</sup> until Common Image Gathers (CIG) show flat reflections. When this condition is satisfied, the CIG are stacked, providing an increased accuracy for the migrated image. In this methodological approach, it is noteworthy that parallel lines Ant45 and 06 are located 70 km from each other. As a result, the PSDM of line Ant45 should be considered as an additional constraint for the RDRs geometry complementing the rougher depth conversion, more than as a robust image for the deep structure of the subduction zone. Despite this uncertainty, both methods result in similar location, depth, geometry, and dipping angles for the RDRs. These reflectors are slightly deeper and steeper in the depth-converted image than in the interpreted PSDM MCS line.

**RMS amplitude analysis.** Seismic amplitude attributes analysis is commonly used in basin and oil exploration in order to identify and delineate structural and stratigraphic features associated with fluid-rich intervals<sup>32</sup>. The Root Mean Square (RMS), based on reflection coefficient, independently from the reflection polarity, is particularly suited for fluid content analysis. The RMS amplitude  $A_{RMS}$  is calculated from original signal amplitudes  $a_i(t)$  over a time window of  $N$  samples indexed with  $i$ , using the « Petrel » software (Schlumberger):

$$A_{RMS} = \frac{1}{N} \sum_i (a_i(t))^2$$

As a result, this analysis estimates the signal overall amplitude and describes the signal average amplitude within a time window.

### Data availability

Every geophysical data of the ANTITHESIS cruises are available on the internet site of the French Oceanographic Fleet (<https://campagnes.flotteoceanographique.fr/search>). Interested readers write/select “Antithesis” in field “search campaign” and the desired data set in field “Data Managed by SISMER.” Once every needed data set is selected, the readers can download it from “My basket” page.

### Code availability

Seismic data processing used softwares *SolidQC* (Ifremer) and *Geovation* (CGG), bathymetric data were processed with softwares *Globe* and *Claritas* (Ifremer). We used *Kingdom Suite* for the RMS analysis. Maps and 3D bathymetric views were drafted using *GMT*, *Qgis*, and *Adobe Illustrator*. The ray-Born PSDM code derives from an original private version by P. Thierry and G. Lambaré (Mines School of Paris) and the Migration-

velocity analysis code, from the original version by W. Agudelo and A. Ribodetti (Geoazur).

Received: 28 January 2021; Accepted: 8 September 2021;  
Published online: 30 September 2021

### References

- Cann, J. R. et al. Corrugated slip surfaces formed at ridge–transform intersections on the Mid-Atlantic Ridge. *Nature* **385**, 329 (1997).
- Sauter, D. et al. Continuous exhumation of mantle-derived rocks at the Southwest Indian Ridge for 11 million years. *Nat. Geosci.* **6**, 314–320 (2013).
- Smith, D. K., Cann, J. R. & Escartin, J. Widespread active detachment faulting and core complex formation near 13 degrees N on the Mid-Atlantic Ridge. *Nature* **442**, 440–443 (2006).
- Garcés, M. & Gee, J. S. Paleomagnetic evidence of large footwall rotations associated with low-angle faults at the Mid-Atlantic Ridge. *Geology* **35**, 279 (2007).
- Morris, A. et al. Footwall rotation in an oceanic core complex quantified using reoriented Integrated Ocean Drilling Program core samples. *Earth Planet. Sci. Lett.* **287**, 217–228 (2009).
- MacLeod, C. J. et al. Direct geological evidence for oceanic detachment faulting: the Mid-Atlantic Ridge, 15°45'N. *Geology* **30**, 879–882 (2002).
- Schroeder, T. & John, B. E. Strain localization on an oceanic detachment fault system, Atlantis Massif, 30°N, Mid-Atlantic Ridge. *Geochem. Geophys. Geosyst.* **5**, Q11007 (2004).
- Buck, W. R., Lavier, L. L. & Poliakov, A. N. B. Modes of faulting at mid-ocean ridges. *Nature* **434**, 719–723 (2005).
- Tucholke, B. E., Behn, M. D., Buck, W. R. & Lin, J. Role of melt supply in oceanic detachment faulting and formation of megamullions. *Geology* **36**, 455 (2008).
- Momoh, E., Cannat, M., Watremez, L., Leroy, S. & Singh, S. C. Quasi-3-D seismic reflection imaging and wide-angle velocity structure of nearly amagmatic oceanic lithosphere at the ultraslow-spreading Southwest Indian Ridge. *J. Geophys. Res.* **122**, 9511–9533 (2017).
- Reston, T. J. & Ranero, C. R. The 3-D geometry of detachment faulting at mid-ocean ridges. *Geochem. Geophys. Geosyst.* **12**, <https://doi.org/10.1029/2011gc003666> (2011).
- Morris, E. et al. Seismic structure of oceanic crust in the western North Atlantic. *J. Geophys. Res.* **98**, 13, 879–813,903 (1993).
- Ranero, C. R. & Reston, T. J. Detachment faulting at ocean core complexes. *Geology* **27**, 983–986 (1999).
- Peirce, C., Sinha, M., Topping, S. & Gill, C. Morphology and genesis of slow-spreading ridges-seabed scattering and seismic imaging within the oceanic crust. *Geophys. J. Int.* **168**, 59–89 (2007).
- White, R. S., McKenzie, D. & O’Nions, R. K. Oceanic crustal thickness from seismic measurements and rare earth element inversions. *J. Geophys. Res.* **97**, 19683–19715 (1992).
- Smith, D. K. Tectonics: mantle spread across the sea floor. *Nat. Geosci.* **6**, 247–248 (2013).
- Cannat, M. How thick is the magmatic crust at slow spreading oceanic ridges? *J. Geophys. Res.* **101**, 2847–2857 (1996).
- Ildefonse, B. et al. Oceanic core complexes and crustal accretion at slow-spreading ridges. *Geology* **35**, 623 (2007).
- Dean, S. M., Minshull, T. A., Whitmarsh, R. B. & Loudon, K. E. Deep structure of the ocean-continent transition in the southern Iberia Abyssal Plain from seismic refraction profiles: the IAM-9 transect at 40°20'N. *J. Geophys. Res.* **105**, 5859–5885 (2000).
- Grevemeyer, I. et al. Episodic magmatism and serpentinized mantle exhumation at an ultraslow-spreading centre. *Nat. Geosci.* **11**, 444–448 (2018).
- Van Avendonk, H. J. A. et al. Seismic velocity structure of the rifted margin of the eastern Grand Banks of Newfoundland, Canada. *J. Geophys. Res.* **111**, 1–26 (2006).
- Escartin, J., Hirth, G. & Evans, B. Strength of slightly serpentinized peridotites: implications for the tectonics of oceanic lithosphere. *Geology* **29**, 1023–1026 (2001).
- Marcaillou, B. & Klingelhoefer, F. ANTITHESIS-1-Leg1 Cruise, RV L’Atalante, <https://doi.org/10.17600/13010070> (2013).
- Marcaillou, B. & Klingelhoefer, F. ANTITHESIS-3 Cruise, RV Pourquoi Pas? <https://doi.org/10.17600/16001700> (2016).
- Bouysse, P., Garcia-Reyes, A., Mercier de Lépinay, B. & Pubellier, M. (CCGM/CGMW, 2020).
- DeMets, C., Gordon, R. G. & Argus, D. F. Geologically current plate motions. *Geophys. J. Int.* **181**, 1–80 (2010).

27. Müller, R. D., Royer, J.-Y., Cande, S. C., Roest, W. R. & Maschenkov, S. *Caribbean Basins. Sedimentary Basins of the World 4* (ed Mann, P.) (Elsevier Science B.V. 1999).
28. Cande, S. C. & Kent, D. V. Revised calibration of geomagnetic polarity timescale for the late Cretaceous and Cenozoic. *J. Geophys. Res.* **100**, 6093–6095 (1995).
29. Masson, D. G. Fault patterns at outer trench walls. *Marine Geophys. Res.* **13**, 209–225 (1991).
30. Ranero, C. R., Phipps Morgan, J., McIntosh, K. D. & Reichert, C. Bending-related faulting and mantle serpentinization at the Middle America trench. *Nature* **425**, 367–373 (2003).
31. Laurencin, M., Graindorge, D., Klingelhoefer, F., Marcaillou, B. & Evain, M. Influence of increasing convergence obliquity and shallow slab geometry onto tectonic deformation and seismogenic behavior along the Northern Lesser Antilles zone. *Earth Planet. Sci. Lett.* **492**, 59–72 (2018).
32. Chopra, S. & Marfurt, K. J. Seismic attributes – a historical perspective. *Geophysics* **70**, 3SO–28SO (2005).
33. McCarthy, J., Mutter, J. C., Morton, J. L., Sleep, N. H. & Thompson, G. A. Relic magma chamber structures preserved within the Mesozoic North Atlantic crust? *GSA Bulletin* **100**, 1423–1436 (1988).
34. Hallenborg, E., Harding, A. J. & Kent, G. M. Seismic structure of 15 Ma oceanic crust formed at an ultrafast spreading East Pacific rise: evidence for kilometer-scale fracturing from dipping reflectors. *J. Geophys. Res.* **108**, <https://doi.org/10.1029/2003jb002400> (2003).
35. Kodaira, S. et al. Seismological evidence of mantle flow driving plate motions at a palaeo-spreading centre. *Nat. Geosci.* **7**, 371–375 (2014).
36. Ranero, C. R., Reston, T. J., Belykh, I. & Gribidenko, H. Reflective oceanic crust formed at a fast spreading center in the Pacific. *Geology* **25**, 499–502 (1997).
37. Reston, T. J., Ranero, C. R. & Belykh, I. The structure of Cretaceous oceanic crust of the NW Pacific: constraints on processes at fast spreading centers. *J. Geophys. Res.* **104**, 629–644 (1999).
38. Bécel, A., Shillington, D. J., Nedimović, M. R., Webb, S. C. & Kuehn, H. Origin of dipping structures in fast-spreading oceanic lower crust offshore Alaska imaged by multichannel seismic data. *Earth Planet. Sci. Lett.* **424**, 26–37 (2015).
39. Eittrheim, S. L. et al. Oceanic crustal thickness and seismic character along a central Pacific transect. *J. Geophys. Res.* **99**, 3139–3145 (1994).
40. Henstock, T. J., Woods, A. W. & White, R. S. The accretion of oceanic crust by episodic sill intrusion. *J. Geophys. Res.* **98**, 4143–4161 (1993).
41. Phipps Morgan, J. & Chen, Y. J. The genesis of oceanic crust: magma injection, hydrothermal circulation, and crustal flow. *J. Geophys. Res.* **98**, 6283–6297 (1993).
42. Han, S. et al. Seismic reflection imaging of the Juan de Fuca plate from ridge to trench: new constraints on the distribution of faulting and evolution of the crust prior to subduction. *J. Geophys. Res.* **121**, 2015JB012416 (2016).
43. Zhou, H. & Dick, H. J. B. Thin crust as evidence for depleted mantle supporting the Marion rise. *Nature* **494**, 195–200 (2013).
44. Reston, T. J. et al. A rifted inside corner massif on the Mid-Atlantic Ridge at 5°S. *Earth Planet. Sci. Lett.* **200**, 255–269 (2002).
45. Hayes, G. P., McNamara, D. E., Seidman, L. & Roger, J. Quantifying potential earthquake and tsunami hazard in the lesser Antilles subduction zone of the Caribbean region. *Geophys. J. Int.* **196**, 510–521 (2013).
46. Paulatto, M. et al. Dehydration of subducting slow-spread oceanic lithosphere in the Lesser Antilles. *Nat. Commun.* **8**, (2017).
47. Cooper, G. F. et al. Variable water input controls evolution of the Lesser Antilles volcanic arc. *Nature* **582**, 525–529 (2020).
48. Schlaphorst, D. et al. Water, oceanic fracture zones and the lubrication of subducting plate boundaries—insights from seismicity. *Geophys. J. Int.* **204**, 1405–1420 (2016).
49. Saffer, D. M. & Tobin, H. J. Hydrogeology and mechanics of subduction zone forearcs: fluid flow and pore pressure. *Annu. Rev. Earth Planet. Sci.* **39**, 157–186 (2011).
50. Escartín, J., Hirth, G. & Evans, B. Nondilatant brittle deformation of serpentinites: implications for Mohr-Coulomb theory and the strength of faults. *J. Geophys. Res.* **102**, 2897–2913 (1997).
51. Moore, D. E., Lockner, D. A., Shengi, M., Summers, R. & Byerlee, J. D. Strengths of serpentinite gouges at elevated temperature. *J. Geophys. Res.* **102**, 14714–787801 (1997).
52. Reinen, L. A. Seismic and aseismic slip indicators in serpentinite gouge. *Geology* **28**, 135–138 (2000).
53. Hirauchi, K.-I., Katayama, I., Uehara, S., Miyahara, M. & Takai, Y. Inhibition of subduction thrust earthquakes by low-temperature plastic flow in serpentine. *Earth Planet. Sci. Lett.* **295**, 349–357 (2010).
54. Saffer, D. M. & Wallace, L. M. The frictional, hydrologic, metamorphic and thermal habitat of shallow slow earthquakes. *Nat. Geosci.* **8**, 594–600 (2015).
55. Laurencin, M. et al. The polyphased tectonic evolution of the Anegada Passage in the northern Lesser Antilles subduction zone. *Tectonics* **36**, <https://doi.org/10.1002/2017TC004511> (2017).
56. Lambaré, G., Operto, S., Podvin, P. & Thierry, P. 3D ray+born migration/inversion - part 1: theory. *Geophysics* **68**, 1348–1356 (2003).
57. Lambaré, G., Virieux, J., Madariaga, R. & Jin, S. Iterative asymptotic inversion in the acoustic approximation. *Geophysics* **57**, 1138–1154 (1992).
58. Operto, S., Xu, S. & Lambaré, G. Can we quantitatively image complex structures with rays. *Geophysics* **65**, 1223–1238 (2000).
59. Thierry, P., Lambaré, G., Podvin, P. & Noble, M. 3D preserved amplitude prestack depth migration on a workstation. *Geophysics* **64**, 222–229 (1999).
60. Ribodetti, A., Operto, S., Agudelo, W. S., Collot, J.-Y. & Virieux, J. Joint ray +born least-squares migration and simulated annealing optimization for high-resolution target-oriented quantitative seismic imaging. *Geophysics* **76**, <https://doi.org/10.1190/1.3554330> (2011).
61. Al-Yahya, K. M. Velocity analysis by iterative profile migration. *Geophysics* **54**, 718–729 (1989).
62. Sandwell, D. T. & Smith, W. H. F. Slope correction for ocean radar altimetry. *J. Geodesy* **88**, 765–771 (2014).
63. Müller, R. D. & Roest, W. R. Fracture zones in the North Atlantic from combined Geosat and Seasat data. *J. Geophys. Res.* **97**, 3337–3350 (1992).

### Acknowledgements

We thank the captain and crew of the R/Vs “*L’Atalante*” and “*Pourquoi Pas?*” for the data acquisition during marine surveys ANTITHESIS 1 and 3. M.B.’s PhD Thesis was funded by the Regional Council of Guadeloupe. M.Lau.’s PhD thesis was funded by The Regional Council of Bretagne. We gratefully acknowledge S. Sambolian, S. Operto, and A. Ribodetti for providing the optimized version of the PSDM code, and A. Ribodetti for adapting the codes to the MCS data of this study. Special thanks to Marc-Andre Gutscher for revising the English and providing us with insightful comments.

### Author contributions

B.M. supervised the data processing and wrote the manuscript. B.M., F.K., and J.-F.L. conceived the ANTITHESIS project and were Principal Investigators onboard RVs “*L’Atalante*” and “*Pourquoi Pas?*”. L.S. and J.-F.L. supervised the seismic and multibeam onboard processing, respectively. M.Lau., M.B., and K.E. performed the post-cruise seismic processing during their PhD, supervised by B.M., D.G., J.-F.L., F.K., M.Lai., and S.L. A.G. performed RMS analyses. All authors participated in the Antithesis cruises, discussed the scientific issues, and commented on the manuscript.

### Competing interests

The authors declare no competing interests.

### Additional information

**Supplementary information** The online version contains supplementary material available at <https://doi.org/10.1038/s43247-021-00269-6>.

**Correspondence** and requests for materials should be addressed to Boris Marcaillou.

**Peer review information** *Communications Earth & Environment* thanks Harm Van Avendonk and the other, anonymous, reviewer(s) for their contribution to the peer review of this work. Primary Handling Editors: Luca Dal Zilio, Joe Aslin. Peer reviewer reports are available.

**Reprints and permission information** is available at <http://www.nature.com/reprints>

**Publisher’s note** Springer Nature remains neutral with regard to jurisdictional claims in published maps and institutional affiliations.



**Open Access** This article is licensed under a Creative Commons Attribution 4.0 International License, which permits use, sharing, adaptation, distribution and reproduction in any medium or format, as long as you give appropriate credit to the original author(s) and the source, provide a link to the Creative Commons license, and indicate if changes were made. The images or other third party material in this article are included in the article’s Creative Commons license, unless indicated otherwise in a credit line to the material. If material is not included in the article’s Creative Commons license and your intended use is not permitted by statutory regulation or exceeds the permitted use, you will need to obtain permission directly from the copyright holder. To view a copy of this license, visit <http://creativecommons.org/licenses/by/4.0/>.

© The Author(s) 2021

## Supplementary Material for

# Pervasive detachment faults within the slow spreading oceanic crust at the poorly-coupled Antilles Subduction Zone

**Boris Marcaillou<sup>1</sup>, Frauke Klingelhofer<sup>2</sup>, Muriel Laurencin<sup>3</sup>, Jean-Frédéric Lebrun<sup>4</sup>, Mireille Laigle<sup>1</sup>, Serge Lallemand<sup>5</sup>, Laure Schenin<sup>1</sup>, Aurélien Gay<sup>5</sup>, Milton Boucard<sup>4</sup>, Kingsley Ezenwaka<sup>1</sup>, David Graindorge<sup>6</sup>**

<sup>1</sup> Université Côte d'Azur, CNRS, Observatoire de la Côte d'Azur, IRD, Géoazur, Valbonne, France

<sup>2</sup> IFREMER, Dpt. of Marine Geosciences, Plouzané, France

<sup>3</sup> Université de Lille, CNRS, Univ. Littoral Côte d'Opale, UMR 8187, LOG, Laboratoire d'Océanologie et de Géosciences, Lille, France

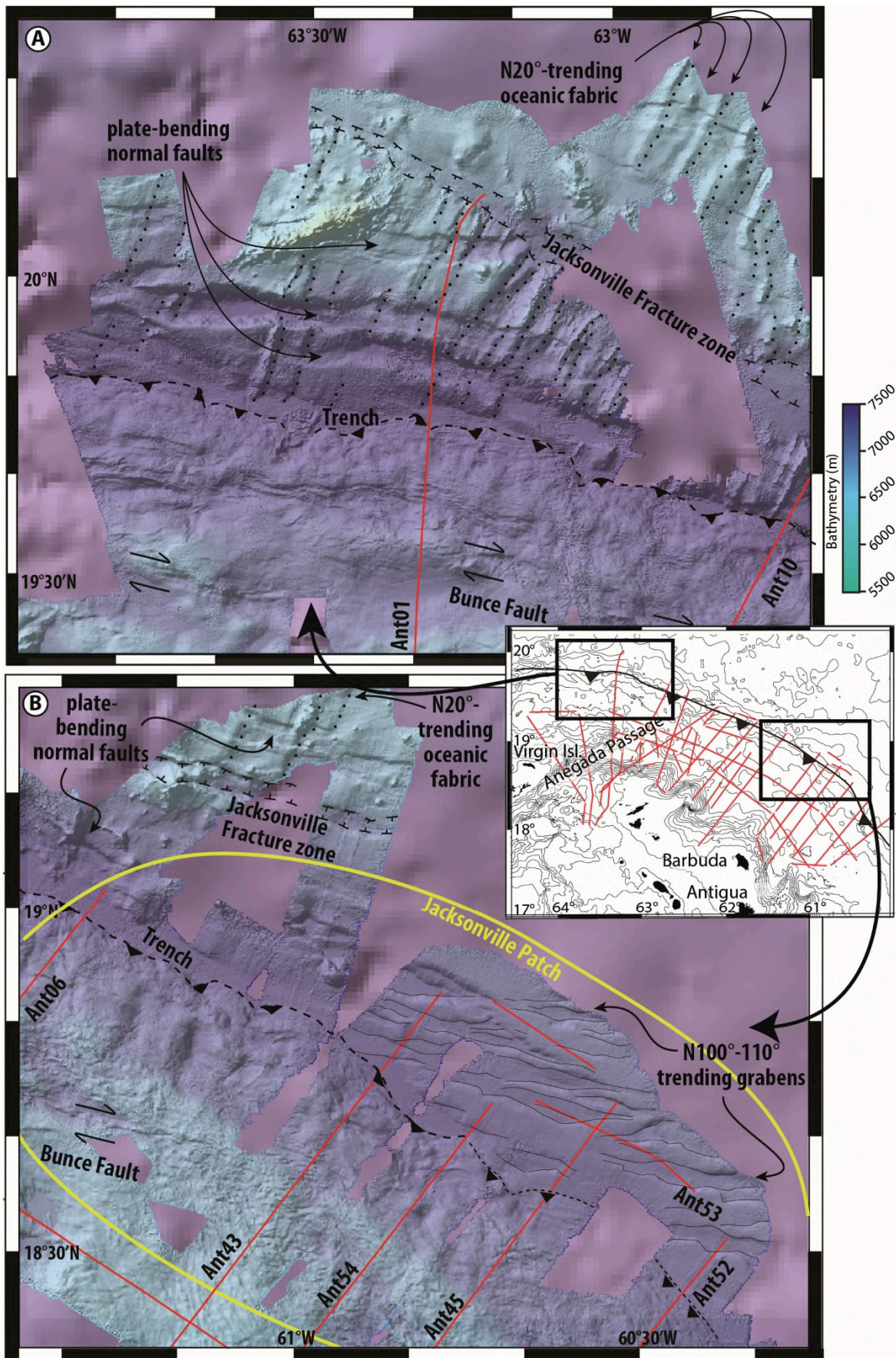
<sup>4</sup> Géosciences Montpellier, Université de Montpellier, CNRS, Université des Antilles, Pointe à Pitre, Guadeloupe (FWI)

<sup>5</sup> Géosciences Montpellier, Université de Montpellier, CNRS, Université des Antilles, Montpellier, France

<sup>6</sup> Géosciences Océan, UMR 6538, Université Bretagne Occidentale, Institut Universitaire Européen de la Mer, Plouzané, France

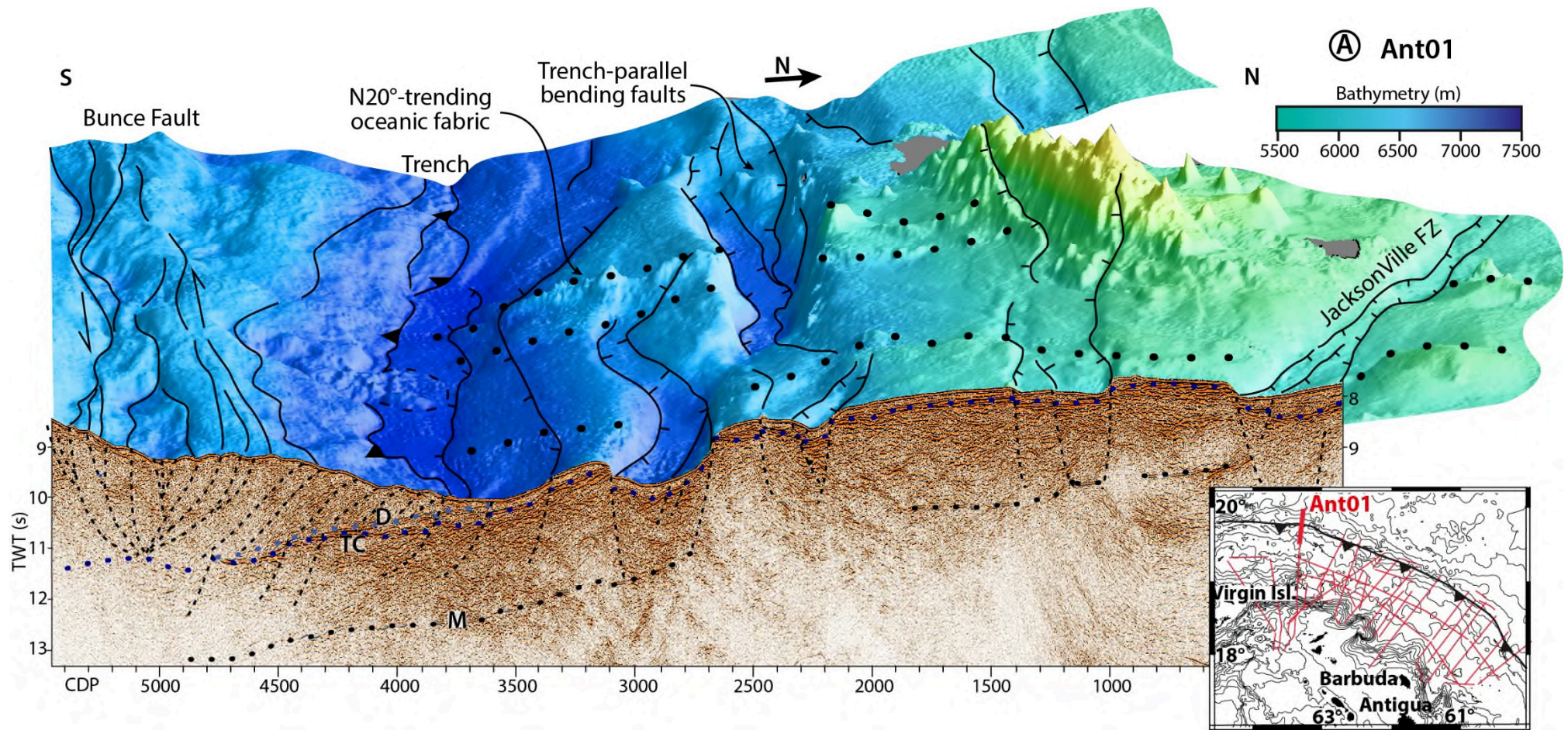
Corresponding author: [boris.marcaillou@geoazur.unice.fr](mailto:boris.marcaillou@geoazur.unice.fr)

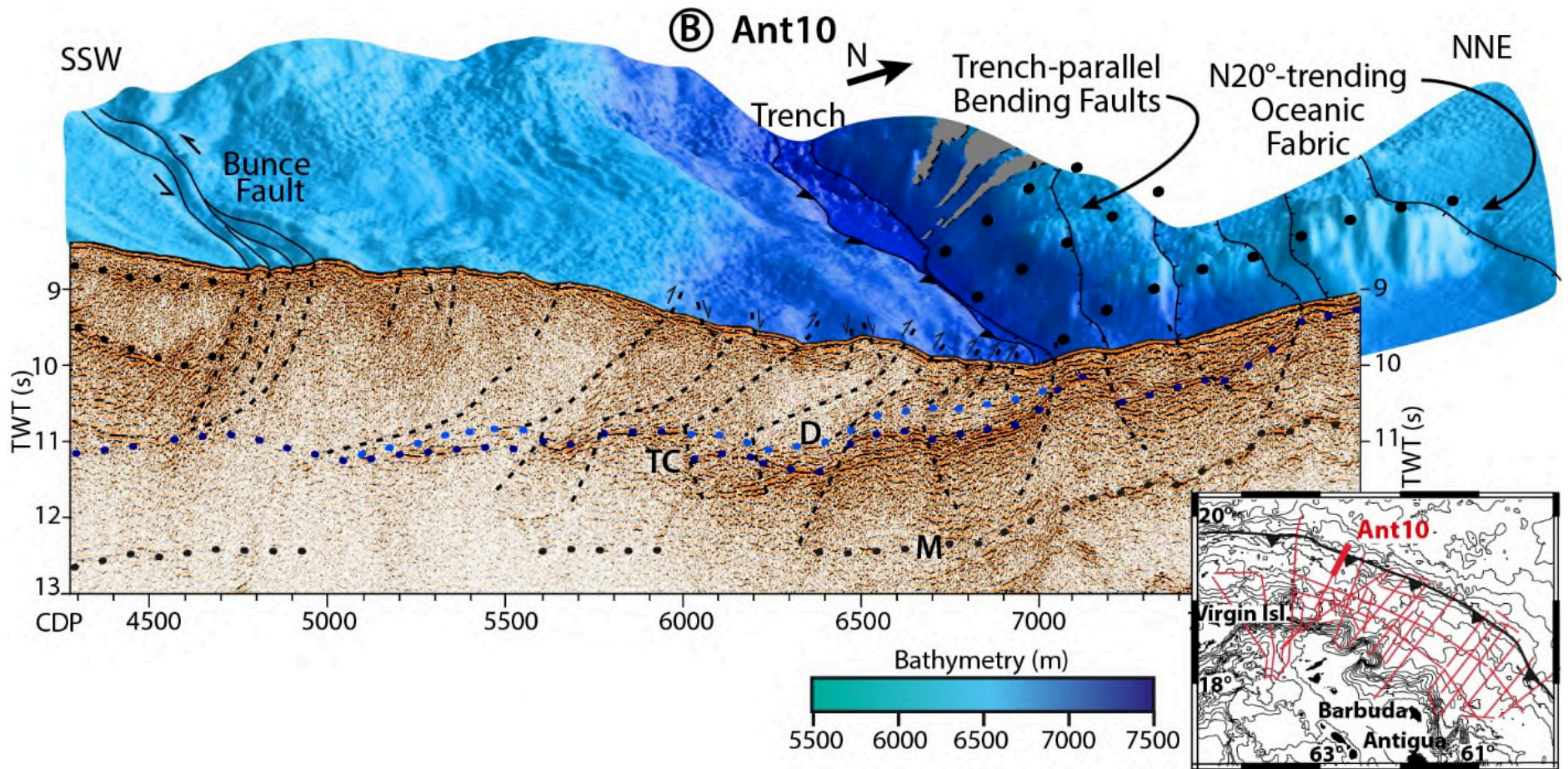
Supplementary Figure 1: Close-up on the bathymetric map.



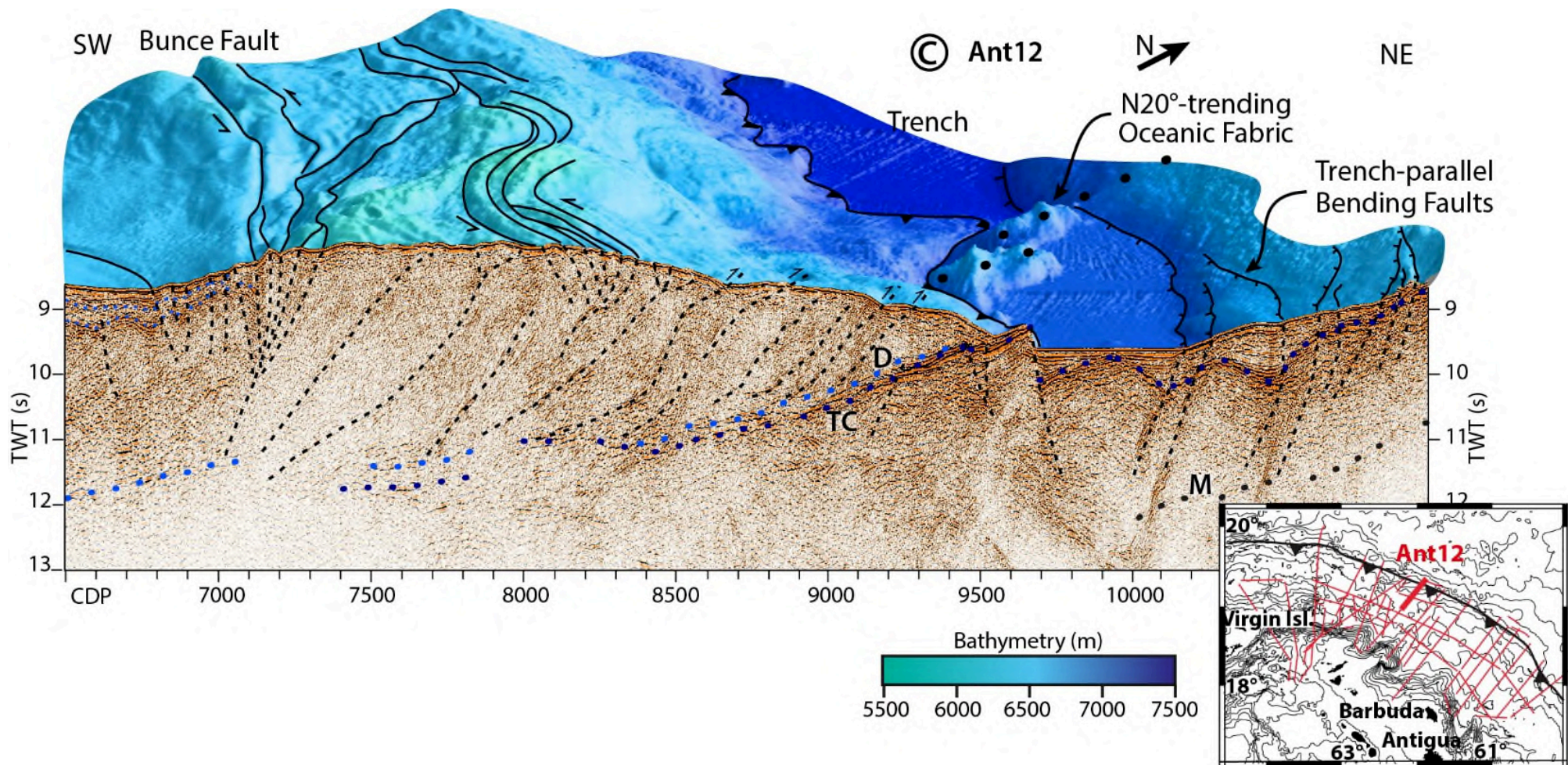
The bathymetry shows the key-features of the oceanic seafloor at the Northern Lesser Antilles Subduction Zone, outside (A) and inside (B) the Jacksonville Patch.

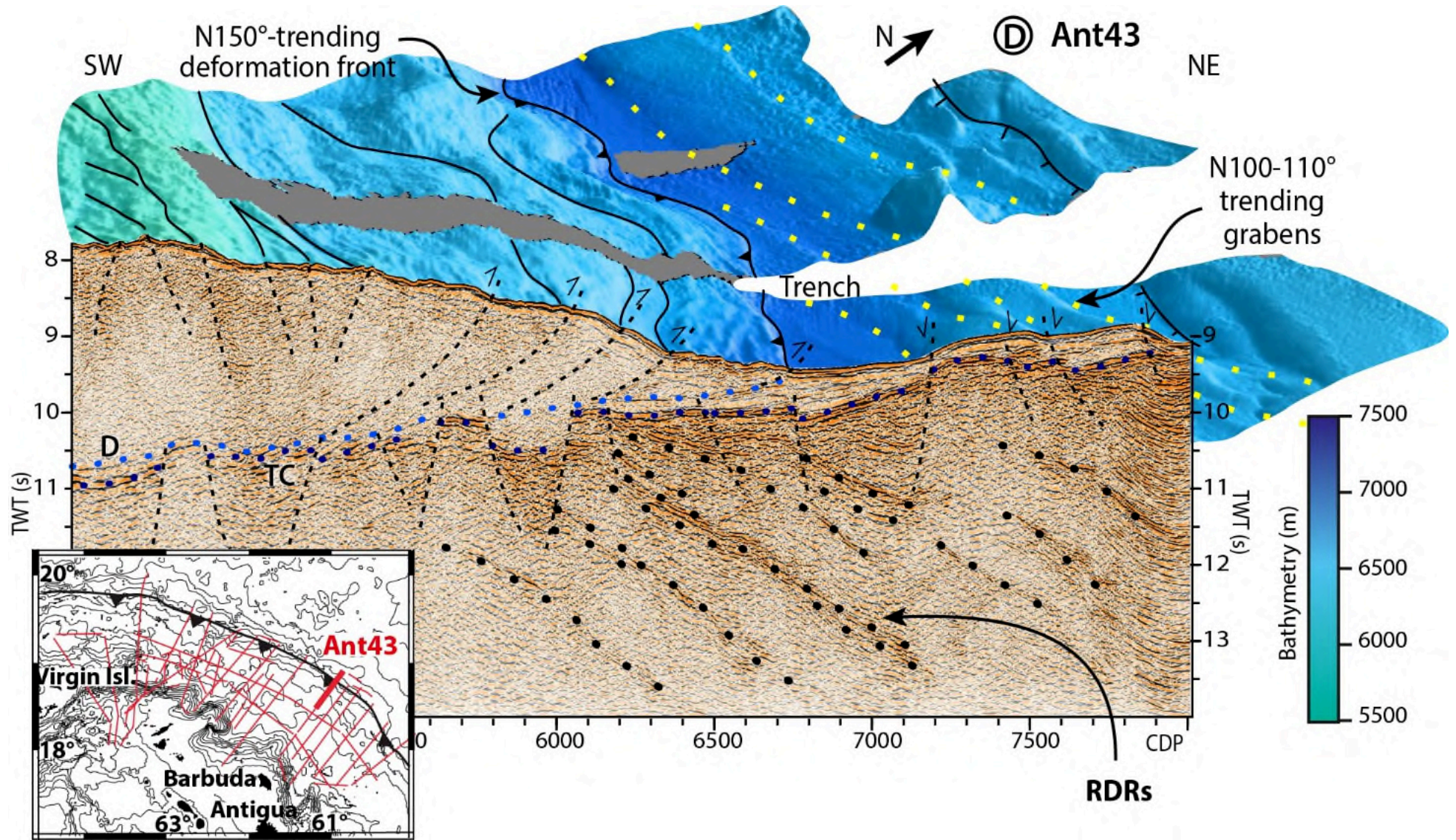
Supplementary Figure 2: Three-dimensional seismic-bathymetry views.

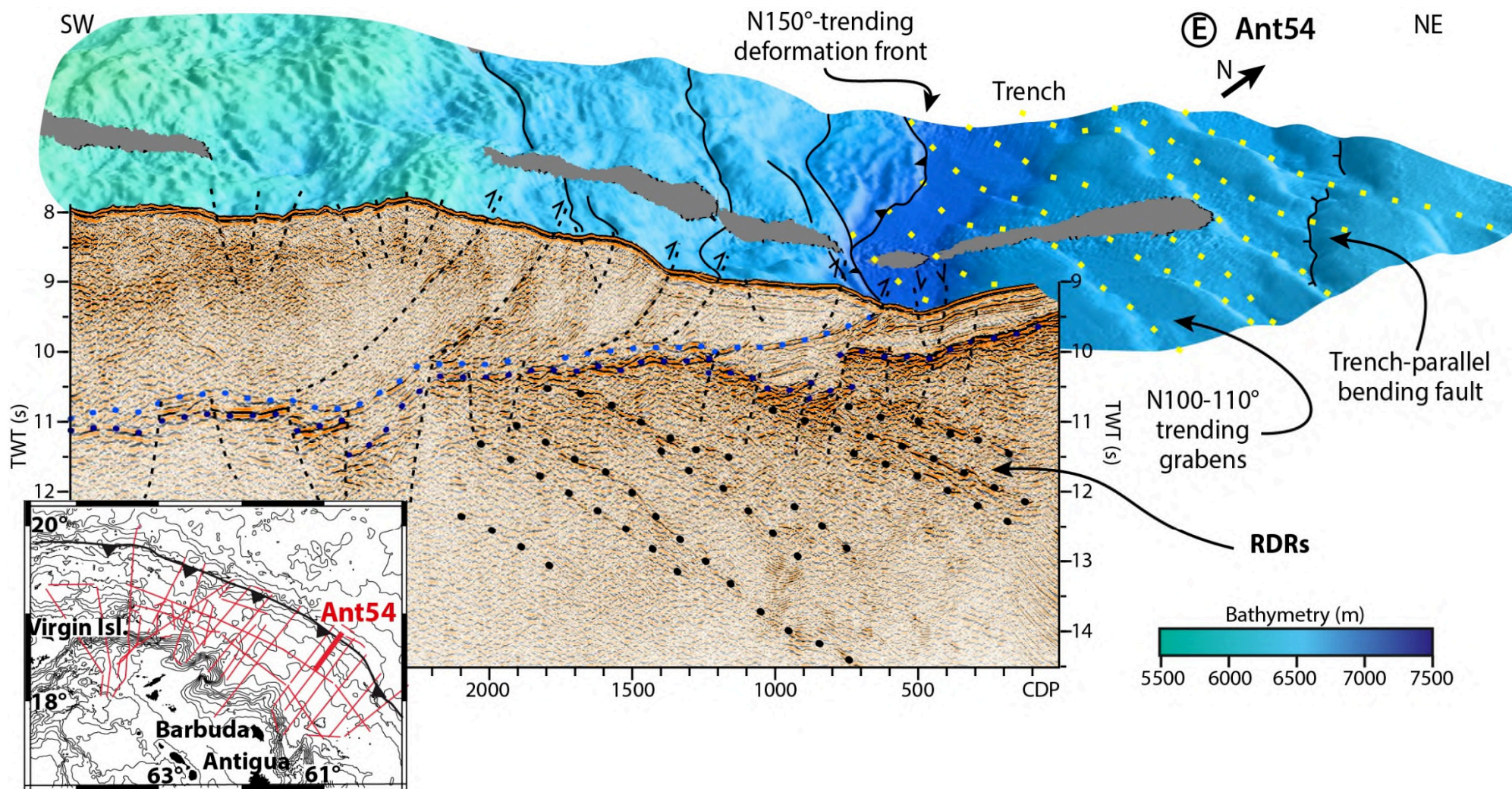


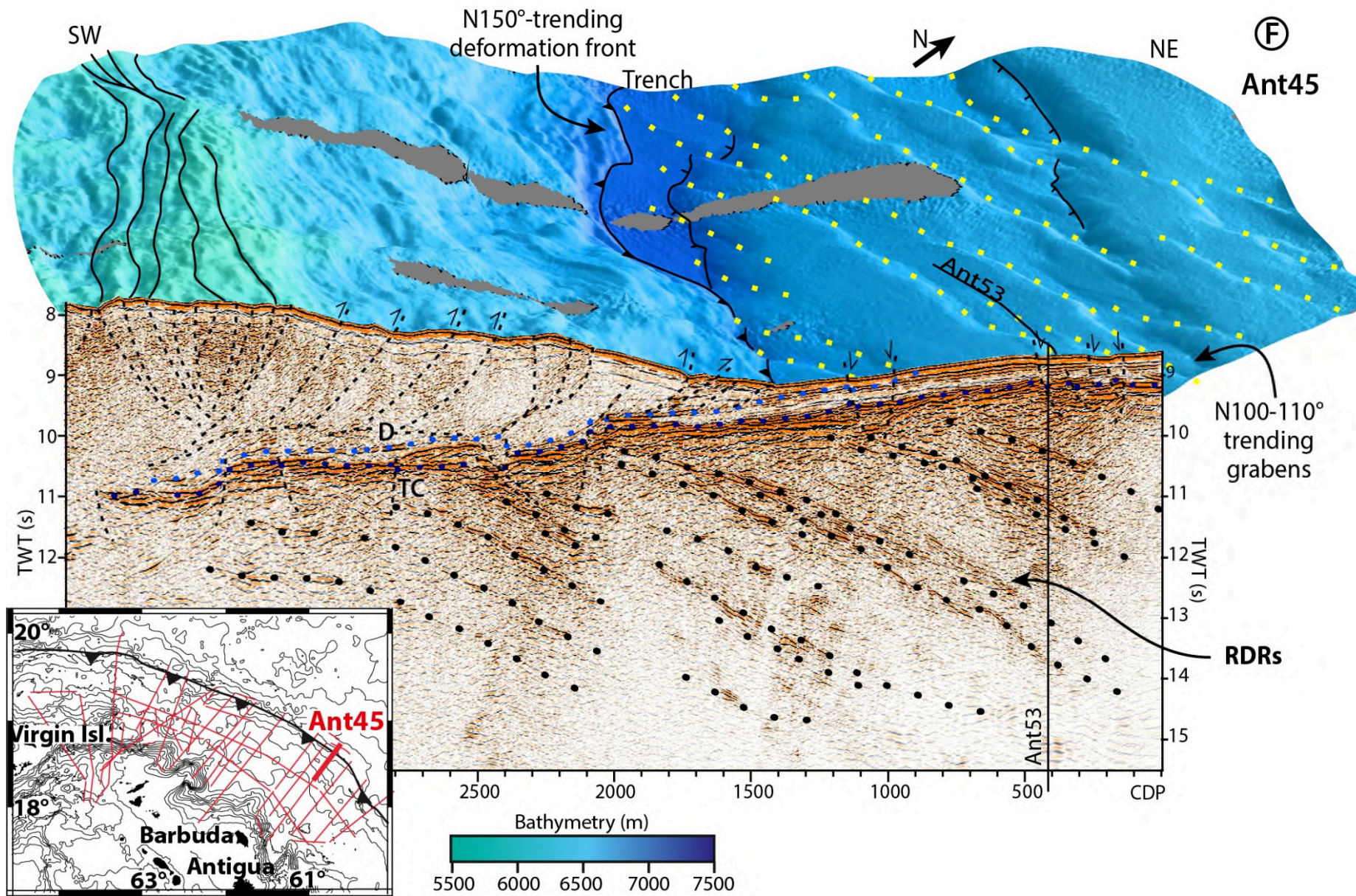


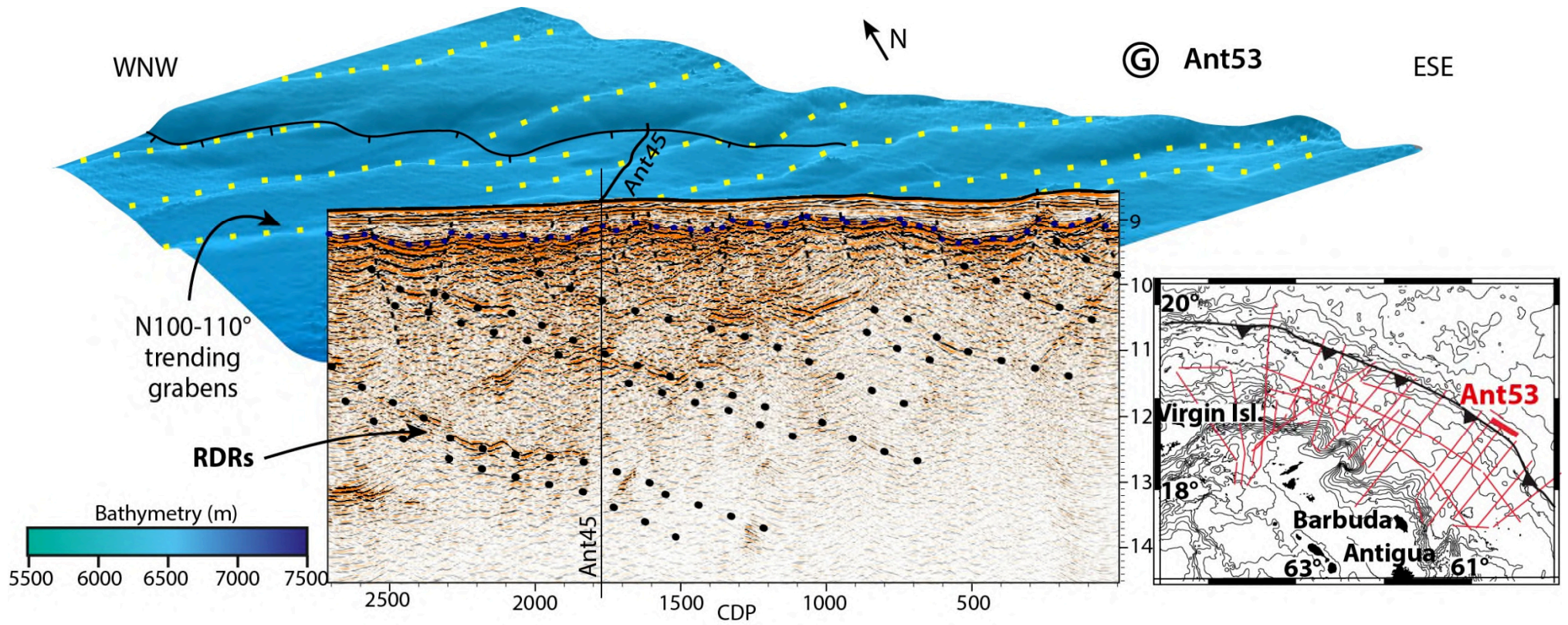


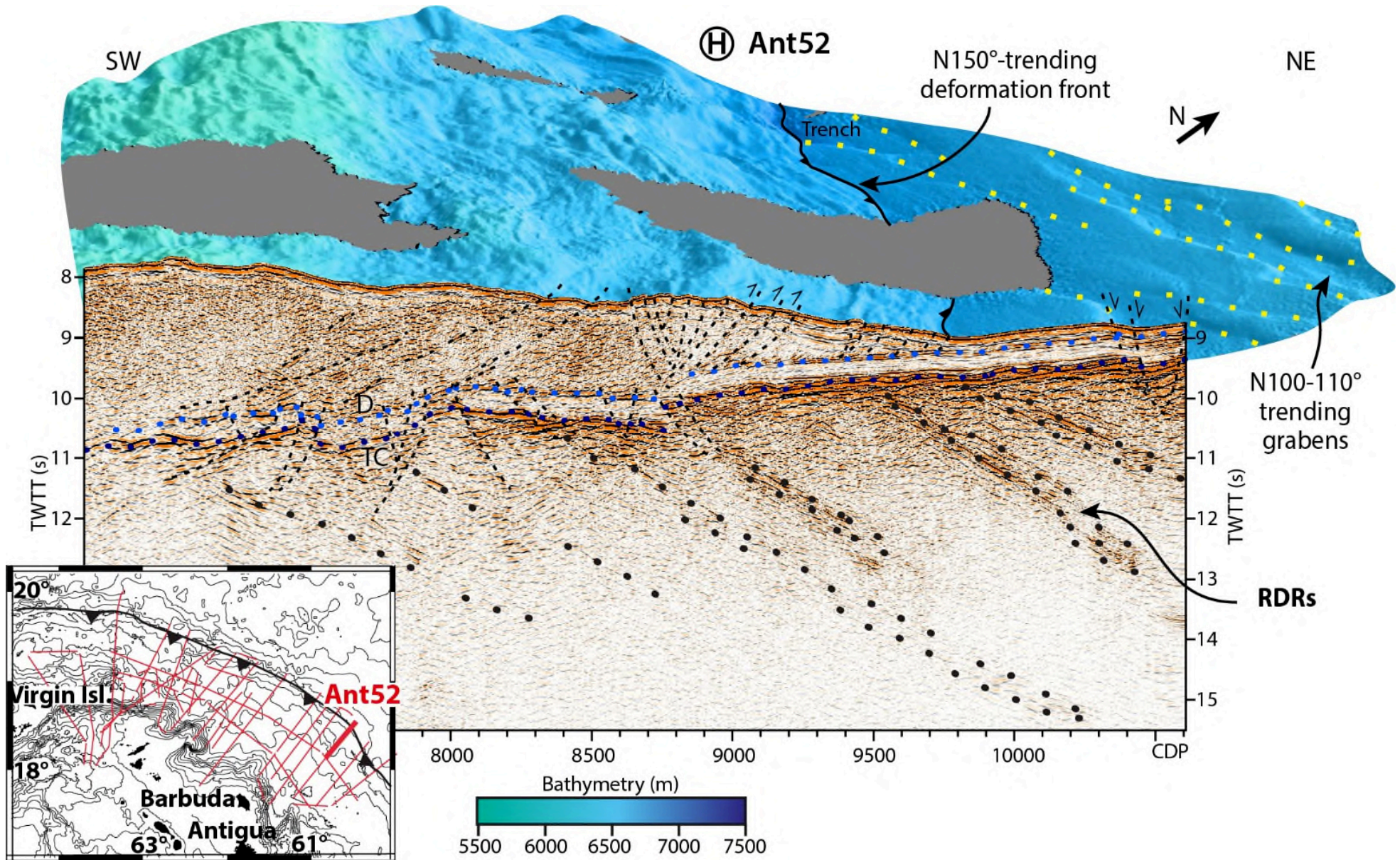


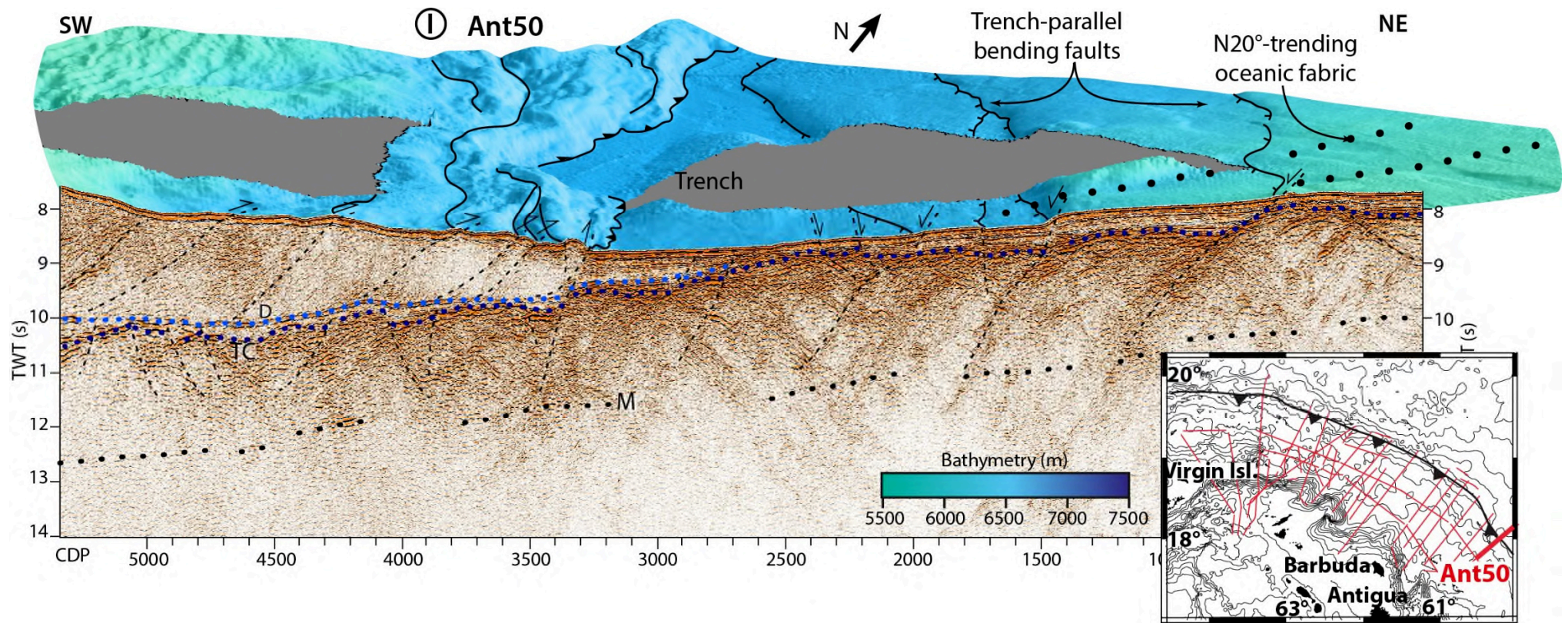






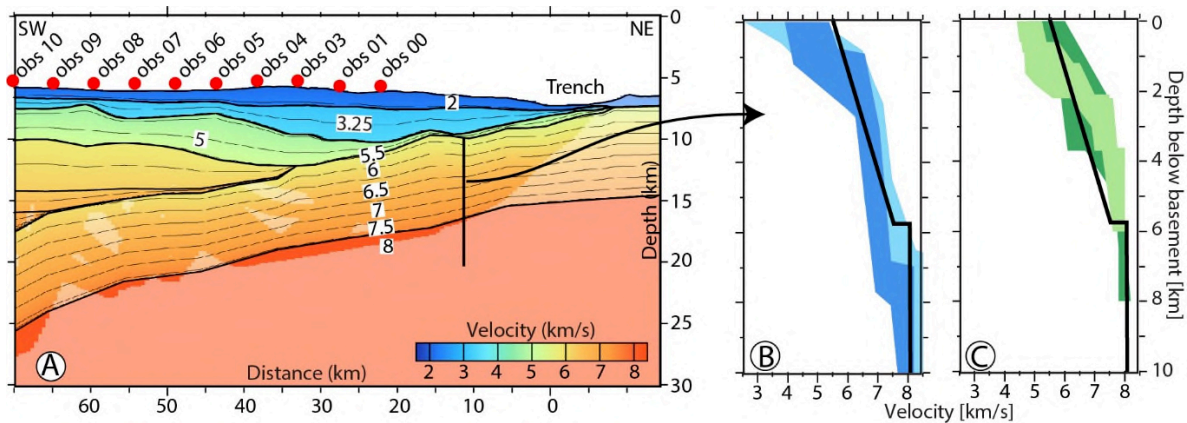






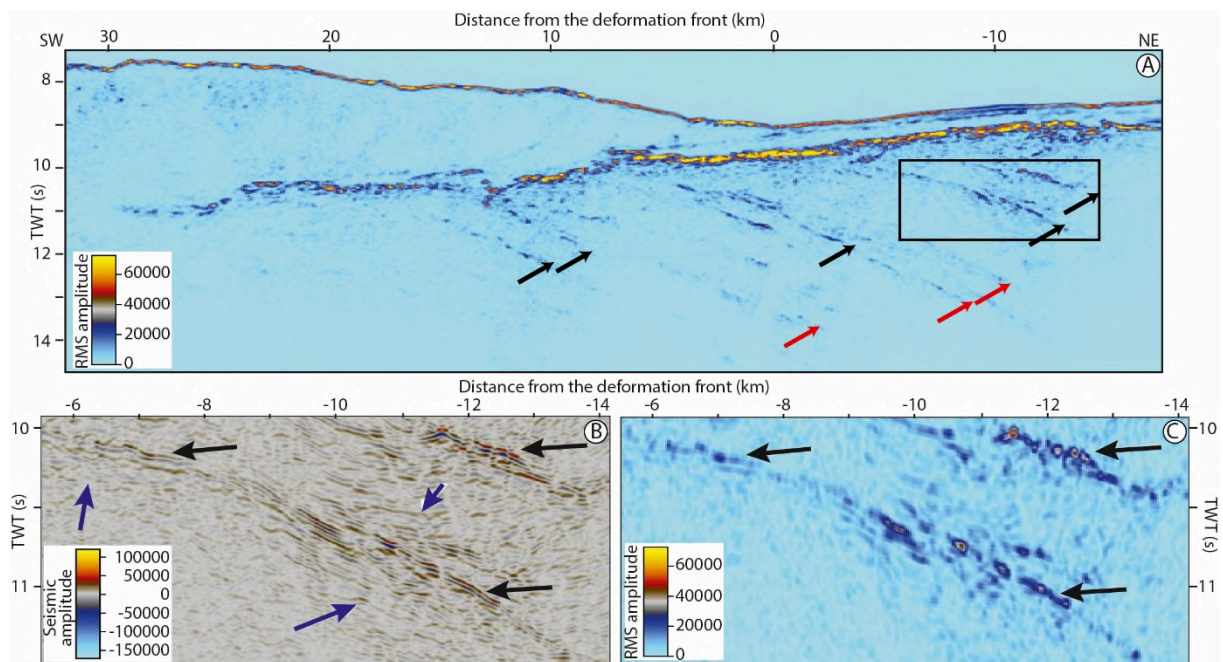
The 3D views illustrate typical oceanic basement in line Ant01 (A), Ant10 (B), Ant12 (C) and Ant50 (I) and the spectacular, tectonically-dominated, exhumed oceanic basement in line Ant43 (D), Ant54 (E), Ant45 (F), Ant53 (G) and Ant52 (H) located outside and inside the Jacksonville Patch respectively. D, TC and M stand for Decollement, Top of the oceanic Crust and Moho respectively. Vertical Exaggeration 1:3.5.

**Supplementary Figure 3: Velocity model of wide-angle data along line Ant06.**



(A): Velocity model derived from forward modelling of wide-angle data along line Ant06 <sup>1</sup>. Velocity contours are shown every 0.25 km/s and shaded areas are constrained by rays. Red dots indicate the location of the seafloor instruments along the model. (B) and (C): Velocity-depth profiles (black lines) extracted beneath the basement top at km 10 and compared to typical Atlantic and Pacific crust blue polygons from white et al. (1992) <sup>2</sup> and to exhumed upper mantle basement light and dark green polygons from Dean et al. (2000) <sup>3</sup> and Van Avendonk et al. (2006) <sup>4</sup>.

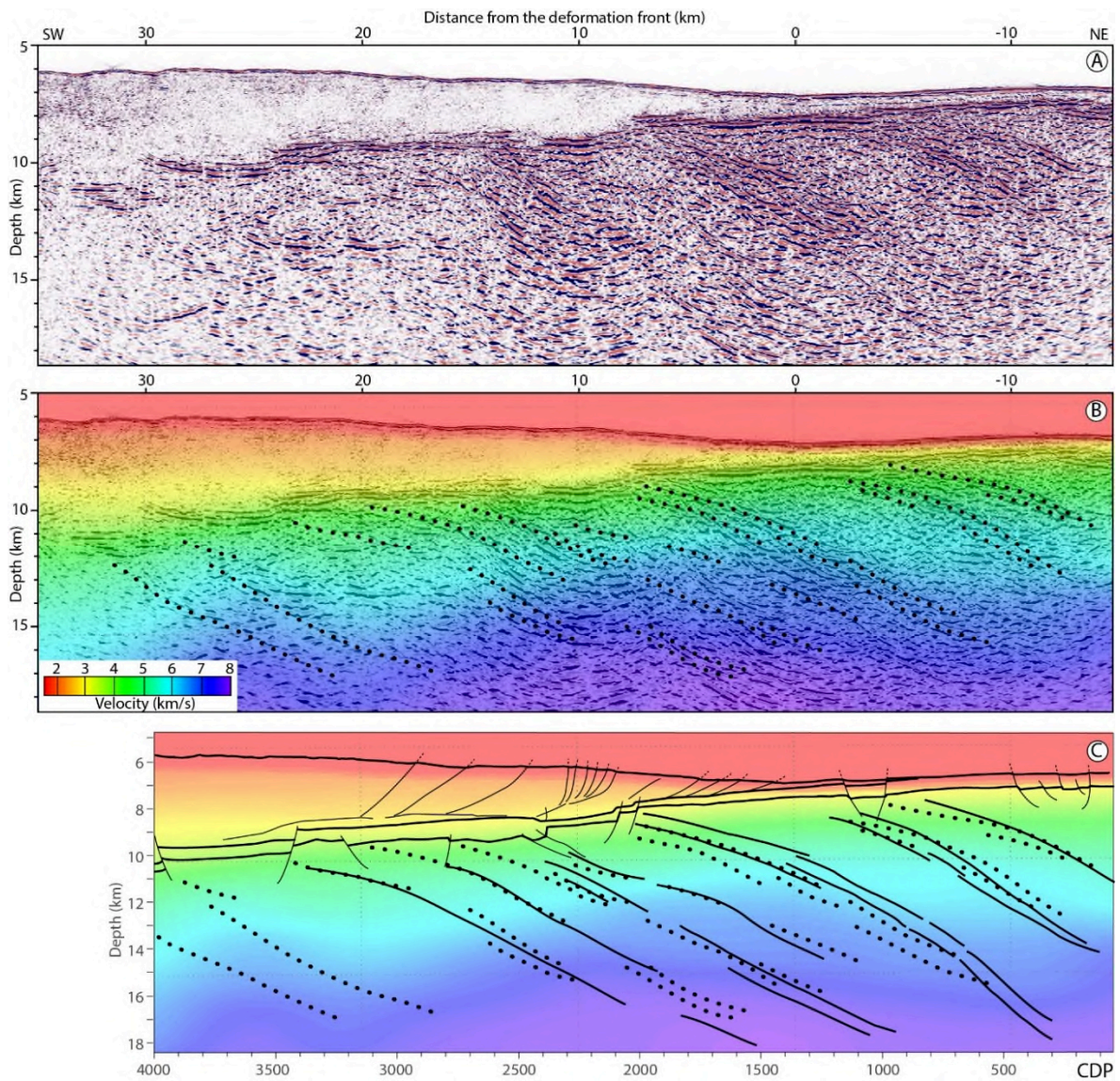
**Supplementary Figure 4: RMS amplitude analysis for line Ant45.**



(A) RMS amplitude analysis for line Ant45, (B) close-up views on seismic amplitude and (C) RMS amplitude for sequences of Ridgeward Dipping Reflectors (RDRs). The RDRs show high RMS amplitudes (>20000) from the top of the oceanic basement down to 2.4 stwt (6 km) below (black arrows in Supplementary Figure 3A) and dimmed RMS amplitudes at greater depths (red arrows in Supplementary Figure 3B). Moreover, RDRs high seismic amplitudes correspond to high RMS amplitudes (black arrows in Supplementary Figure 3B, C) which contrast with other intra-basement reflections (blue arrows in Supplementary Figure 3B). This RMS amplitude analysis thus suggests that the RDRs show physical properties consistent with fluid-rich and/or serpentinized rocks within the upper 6 km of the oceanic basement. At greater depths, the dimming of reflections suggests a decreasing fluid content and/or serpentinization degree.



**Supplementary Figure 5: Pre-Stack Depth Migration of line Ant45.**



(A) Pre-Stack Depth Migration (PSDM) of MCS line Ant45 with (B) the color-coded velocity model and the interpreted RDRs in the oceanic basement (dotted lines). (C) Comparison between Depth-converted interpretation of line Ant45 (plain lines) and interpreted RDRs from PSDM line Ant45 (dotted lines) overlying the color-coded velocity model.

### *Supplementary References*

- 1 Laurencin, M., Graindorge, D., Klingelhoefer, F., Marcaillou, B. & Evain, M. Influence of increasing convergence obliquity and shallow slab geometry onto tectonic deformation and seismogenic behavior along the Northern Lesser Antilles zone. *Earth and Planetary Science Letters* **492**, 59-72, doi:10.1016/j.epsl.2018.03.048 (2018).
- 2 White, R. S., McKenzie, D. & O'Nions, R. K. Oceanic crustal thickness from seismic measurements and rare earth element inversions. *J. geophys. Res.* **97**, 19683-19715, doi:10.1029/92JB01749 (1992).
- 3 Dean, S. M., Minshull, T. A., Whitmarsh, R. B. & Loudon, K. E. Deep structure of the ocean-continent transition in the southern Iberia Abyssal Plain from seismic refraction profiles: The IAM-9 transect at 40°20N. *J. geophys. Res.* **105**, 5859-5885, doi:10.1029/1999jb900301 (2000).
- 4 Van Avendonk, H. J. A. *et al.* Seismic velocity structure of the rifted margin of the eastern Grand Banks of Newfoundland, Canada. *J. geophys. Res.* **111**, 1-26, doi:10.1029/2005jb004156 (2006).

### **3.2 Thermal structure and fluid circulation in the Lesser Antilles subduction zone**

This part of the thesis is presented in the form of a paper which is published in *Earth and Planetary Science Letters* in October 2022 titled “Thermally-constrained fluid circulation and seismicity in the Lesser Antilles subduction zone”. In the paper, we highlight for the first time the thermal state and fluid circulation in the Lesser Antilles subduction margin using a recently acquired robust heat-flow data.

The Lesser Antilles is an end-member subduction zone which undergoes the subduction of a highly hydrated slow-spreading oceanic lithosphere (cf 3.1). Our work aims at using heat-flow variations in order to investigate fluid circulation at depth. The drastic mismatch between measurements and calculated values from conductive cooling modelling highlights the strong influence of fluid-driven heat advection on the heat-flow at the surface. In the Lesser Antilles, this variation relates to a ventilated and insulated hydrothermal circulation in the Northern and Central Lesser Antilles respectively. Hence, to produce an accurate thermal model of the margin, we incorporated heat advection due to circulating fluids. Using our final results, we predict depths of crustal dehydrations, fluid generations and migration pathways within the margin. We also predict temperatures along the plate interface and show the thermally-defined seismogenic zone for the Lesser Antilles.

Based on our results, we highlight the variation in fluid circulation pattern between the North and Central Lesser Antilles, and discuss its effect in the width and depth of the seismogenic zone. We postulate that the constant fluid circulation along the plate interface may reduce the interplate coupling, thus, favor aseismic slip, and increase return time of large seismic events. This result is in agreement with existing work that highlights low coupling in the Lesser Antilles. Finally, we showed that seismicity distribution has a close relationship to temperature-related dehydration reactions. All these results and discussions are presented in more details in the paper attached below.

# 1 Thermally-constrained fluid circulation and seismicity in the 2 Lesser Antilles Subduction Zone

3 Ezenwaka, K.<sup>a</sup>, Marcaillou, B.<sup>a</sup>, Laigle, M.<sup>a</sup>, Klingelhoefer, F.<sup>b</sup>, Lebrun, J.-F.<sup>c</sup>, Paulatto, M.<sup>d</sup>, Biari,  
4 Y.<sup>a,e</sup>, Rolandone, F.<sup>f</sup>, Lucazeau, F.<sup>g</sup>, Heuret, A.<sup>h</sup>, Pichot, T.<sup>b,i</sup>, Bouquerel H.<sup>g</sup>

5 <sup>a</sup> Université Côte d'Azur, CNRS, Observatoire de la Côte d'Azur, IRD, Géoazur, Valbonne, France.

6 <sup>b</sup> Geo-Ocean, Univ Brest, CNRS, Ifremer, UMR6538, F-29280 Plouzane, France.

7 <sup>c</sup> Géosciences Montpellier, Université de Montpellier, CNRS, Université des Antilles, Pointe à Pitre,  
8 Guadeloupe (FWI), France.

9 <sup>d</sup> Imperial College London, Department of Earth Science and Engineering, Prince Consort Road, UK.

10 <sup>e</sup> Capgemini – Oil & Gas Centre of Excellence, Technopole Hélioparc Bâtiment Newton, 4 Rue Jules Ferry,  
11 64000, Pau, France.

12 <sup>f</sup> Sorbonne Université, CNRS, Institut des Sciences de la Terre de Paris, IStEP UMR 7193, Paris, France.

13 <sup>g</sup> Université de Paris, Institut de physique du globe de Paris, CNRS, Paris, France.

14 <sup>h</sup> Université de Guyane, Géosciences Montpellier (UMR 5243), Cayenne, 97300, France.

15 <sup>i</sup> Beicip-Franlab, 232 avenue Napoleon Bonaparte Rueil-Malmaison, Paris 92500, France.

## 16 **Abstract**

17 At subduction zones, fluid circulation and elevated pore pressure are key factors controlling the  
18 seismogenic behavior along the plate interface by reducing absolute fault strength, increasing the time  
19 return of high magnitude co-seismic rupture and favoring aseismic slip. The Lesser Antilles is an end-  
20 member subduction zone where the slow subduction of numerous trans-oceanic fracture zones and  
21 patches of pervasively fractured, hydrated and serpentized exhumed mantle rocks increase the water  
22 input. Heat-flow variations measured in the trench and the forearc during the Antithesis 1 cruise reveal  
23 heat advection by fluid circulation and shed a new light onto the thermal control of seismicity location  
24 in the subduction zone.

25 In the Northern Lesser Antilles, heat-flow anomalies, negative in the trench and positive in the  
26 forearc, reveal a ventilated fluid circulation with downward percolation of cold fluids at the sediment-  
27 starved, pervasively fractured trench and upward discharge of warm fluids through the Tintamarre Fault  
28 Zone in the forearc. In contrast, in the Central Lesser Antilles, a positive heat-flow anomaly at the trench  
29 and the accretionary wedge is typical of an insulated fluid circulation where warm fluids invade the plate  
30 interface flowing updip from the subduction depths up to the trench.

31 The investigated margin segments correspond with a very low number of interplate thrust  
32 earthquakes, illustrating the frequent statement that fluids in subduction zones tend to reduce the  
33 interplate coupling, favor slow to aseismic slip behavior, and increase the time return of large seismic  
34 events. Moreover, the location of intraslab, and supraslab earthquakes at depth beneath the Central  
35 Lesser Antilles suggest a close relation to temperature-related dehydration reactions.

36

37       **Keywords**

38       Thermal modelling, Heat-flow, Lesser Antilles, Subduction zone, Seismogenic zone, Serpentinite  
39       dehydration reaction

40       **1. Introduction**

41       In subduction zones, complex temperature–fluid interactions control predominantly the seismogenic  
42       behavior of the megathrust, which hosts most of the large ( $M_w > 7$ ) to great ( $M_w > 8$ ) subduction  
43       earthquakes in the world. The temperature increases with depth and the transition from shallow stable  
44       (aseismic) to deeper stick-slip (seismogenic) behavior along the interplate contact depends on  
45       mechanical and chemical processes promoting gouge consolidation at temperature of 60–150°C (Moore  
46       & Saffer, 2001, Vrolijk, 1990). At greater depth, the onset of deep stable sliding for a “normal type”  
47       oceanic crust is generally associated with temperatures of 350–450°C (Tse & Rice, 1986) and/or the  
48       interaction of the interplate with the serpentinized mantle wedge of the upper plate (Hyndman et al.,  
49       1997). However, subduction of exhumed ultramafic rocks of slow-spreading oceanic crust and deep  
50       fluid circulation may affect thermally and mechanically this evolution of the interplate sliding behavior.  
51       Pore fluid overpressure possibly correlates with patches of low interseismic coupling (e.g. Moreno et  
52       al., 2014) and promotes aseismic creep, slow-slip and very-low frequency earthquakes (SSE and VLFE)  
53       rather than large co-seismic ruptures (Saffer & Wallace, 2015, and Kodaira et al., 2004). Moreover, fluid  
54       circulation at depth partly controls earthquake recurrence (Byerlee, 1993, Sibson, 2013, Saffer & Tobin,  
55       2011).

56       Fluids enter subduction zones through different processes at work before the trench. These processes  
57       includes fluids trapped in the subduction channel sediments (e.g. Calahorrano et al., 2008), or  
58       hydrothermal flow in the oceanic upper crustal aquifer (e.g. Fisher & Becker, 2000), or trapped at greater  
59       depth in hydrous minerals down to the lithospheric mantle through different types of structure such as  
60       trans-oceanic fracture zones (Cooper et al., 2020), large-scale detachments at slow-spread oceanic ridges  
61       (Marcaillou et al., 2021), crustal-scale folded ridge (Kodaira et al., 2004), or outer rise slab-bending  
62       faults (e.g. Ranero et al., 2003). Circulating fluids advect heat which may drastically change the oceanic  
63       plate geotherm prior to subduction, modulate temperatures along the plate interface and change the heat  
64       flow at the surface and the margin thermal structure with respect to that estimated from the model of a  
65       conductively cooling plate (Kummer & Spinelli, 2008; Harris et al., 2010; Harris et al., 2017; Harris et  
66       al., 2020; Spinelli et al., 2018). The effect of hydrothermal fluids on thermal structure depends on the  
67       mode of circulation. Thick, continuous and undeformed sediments in the trench prevent fluid exchange  
68       between the ocean and the crust and favor insulated hydrothermal circulation (Harris et al., 2017). In  
69       this context, warm fluids flowing from subduction depth updip along the basement aquifer may generate  
70       heat-flow values higher than that predicted by conductive heat transfer models in the accretionary wedge  
71       and at the trench (e.g., Nankai ; Spinelli & Wang, 2008). In contrast, fractured oceanic crust with a thin

72 sediment cover in the trench, and/or a deeply fractured forearc crust favor fluid-driven heat advection to  
73 and/or from the ocean, generating the so-called ventilated hydrothermal circulation (Harris et al., 2017).  
74 As a result, downward percolation of cold fluids in the trench may generate significantly lower heat-  
75 flow values than that predicted by conductive heat transfer models (e.g., Costa Rica; Harris & Wang,  
76 2002). Moreover, in a deeply and pervasively fractured forearc, fluid upward migration along fault  
77 planes and expulsion at the seafloor can generate elevated heat flow (Pecher et al., 2017). Hence,  
78 measured heat-flow values significantly different from those expected for conductive heat transfer  
79 provide indirect constraint on fluids circulation at depth.

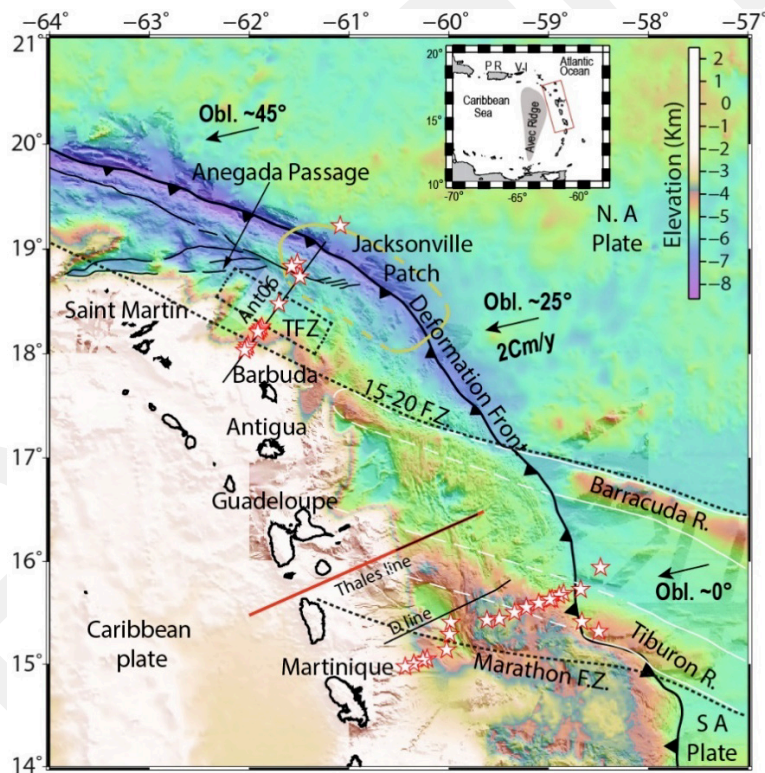
80 The Lesser Antilles is an end-member subduction zone, which undergoes the subduction of a slow-  
81 spreading oceanic lithosphere, partly made of exhumed, hydrated, serpentinized peridotite patches  
82 within the slab crust (Paulatto et al., 2017), fractured with pervasive detachment faults (Marcaillou et  
83 al., 2021) and/or highly hydrated trans-oceanic fracture zones (Cooper et al., 2020). Moreover, the  
84 Lesser Antilles seismicity is heterogeneous, with along-strike variations in b-value (Schlaphorst et al.,  
85 2016) and isolated nests of thrust-faulting earthquakes (Hayes et al., 2013). This subduction zone is thus  
86 a promising study area to investigate the influence of along-strike variations in deep hydrothermal  
87 circulation onto the interplate seismic activity. During cruises Antithesis 1 and 3, we acquired a grid of  
88 multichannel seismic (MCS), four trench-normal Wide-Angle Seismic (WAS) profiles, and heat-flow  
89 measurements along two trench-normal profiles at the Lesser Antilles Subduction zone (Marcaillou &  
90 Klingelhoefer, 2013a, 2013b, 2016). These measurements offshore of Martinique and Saint Martin  
91 islands respectively (Figure 1) aim at investigating heat-flow variations related to fluid circulation at  
92 depth. Drastic mismatches between measurements of heat flow and predictions assuming conductive  
93 cooling highlight the strong influence of fluid-driven heat advection on the heat-flow at the surface. We  
94 analyze pathways for fluid charge and discharge, the impact of this hydrothermal circulation on the  
95 regional heat-flow and the temperature along the interplate contact, and discuss the relation to the  
96 seismicity location in the Lesser Antilles Subduction Zone (LASZ).

## 97 **2. Regional setting**

### 98 ***2.1 Geodynamical and structural background***

99 The Caribbean plate overthrusts the North and South American Plates in a N76° direction with a 2  
100 cm/yr convergence rate (DeMets et al, 2000). In the study area, the calculated age of the subducting  
101 oceanic plate at the trench from the nearby magnetic anomaly C34 of the North American Plate ranges  
102 from 83 Ma east of Barbuda island to 98 Ma east of southern Martinique island (Carpentier et al., 2008).  
103 A dense geophysical dataset - including bathymetric, multichannel seismic and wide-angle seismic data  
104 - constrain the along-strike variations in structure of the LASZ (Kopp et al., 2011, Pichot et al., 2012,  
105 Laigle et al., 2013b, Evain et al., 2013, Paulatto et al., 2017, Laurencin et al., 2017, 2018, 2019, and  
106 Boucard et al., 2021).

107 The nature and structure of the Atlantic subducting crust is expected to vary both in the north-south  
 108 and east-west directions. At slow-spreading mid-ocean ridges, magmatically-robust segments promote  
 109 typical layer 2/3 “Penrose” structure (e.g. White et al., 1992), while tectonically-dominated segments  
 110 generate stretched and thinned crust frequently hosting large bodies of exhumed, hydrated and  
 111 serpentinized upper mantle peridotites (e.g. Cannat et al., 2006, Escartín et al., 2008). Numerous  
 112 occurrences of tectonically-dominated basement have been observed near the Mid-Atlantic Ridge,  
 113 where Oceanic Core-Complexes and Megamullions outcrop (e.g. Tucholke et al., 1998, Ildefonse et al.,  
 114 2007, Sztikar et al., 2019), between the Mid-Atlantic Ridge and the Lesser Antilles Subduction Zone  
 115 about 300 km from the trench (Davy et al., 2020), and at the Jacksonville Patch in the trench offshore  
 116 of Barbuda island (Marcaillou et al., 2021). Moreover, numerous trans-oceanic fracture zones deeply  
 117 hydrate the oceanic crust and mantle. The subducting Vema, Marathon, Mercurius and Doldrums  
 118 Fracture zones of the South American Plate generate vigorous dewatering beneath the Central Lesser  
 119 Antilles Arc (Cooper et al., 2020). The 15-20 Fracture Zone in the North American Plate (Braszus et al.,  
 120 2021) located beneath the Northern Lesser Antilles forearc is likely to favor fluids circulation at depth  
 121 (Marcaillou et al., 2021).



122  
 123 *Figure 1: Bathymetric map of the Northern Lesser Antilles based on data recorded during cruises Antithesis*  
 124 *I, III (Marcaillou & Klingelhoefer, 2013a, 2013b, 2016), Sismantilles II (Laigle et al., 2013a, b). The map shows*  
 125 *the location for heat-flow measurements recorded during Antithesis cruise (plain stars), Multichannel and Wide-*  
 126 *Angle seismic lines (black and red lines respectively) Ant06 (Laurencin et al., 2017, Boucard et al., 2021), Thales*  
 127 *line (Kopp et al., 2011), D line (Laigle et al., 2013a, b). The black dotted line shows the projection onto the seafloor*  
 128 *of the 15-20 and Marathon Fracture Zones, which deeply incise the subducting oceanic plate, and the dotted frame*  
 129 *shows the 60-km-wide Tintamarre Fault Zone (TFZ) in the forearc. N A – North American, S A – South American,*  
 130 *PR – Puerto Rico, VI – Virgin Islands.*

131 The sediment thickness in the trench decreases northward from approximately ~3 km south of  
132 Tiburon Rise (Pichot et al., 2012) offshore of Martinique, to ~0.5 km north of Barracuda Ridge offshore  
133 of Saint Martin (Laurencin et al., 2019). The width of the accretionary prism also decreases from 110 to  
134 30 km (Laurencin et al., 2019, Laigle et al., 2013b). Seismic lines in the Northern Lesser Antilles  
135 (Laurencin et al., 2017, Boucard et al., 2021) and in the Central Lesser Antilles (De Min et al., 2015,  
136 Laigle et al., 2013a, 2013b) show that the overall thickness of the forearc sedimentary layer and the  
137 margin basement is similar along-strike. In the forearc domain offshore of Antigua-Barbuda, the >100-  
138 km-long and 60-km-wide N120° trending Tintamarre Fault Zone deeply and pervasively fractures the  
139 margin (Figure 1) (Boucard et al., 2021). The slab dip angle shows apparent along-strike variation at the  
140 shallower part, when observed as a function of the distance from the trench. For instance, the slab dip is  
141 ~10° at 30 km and 110 km distance offshore of Saint Martin and Martinique islands respectively  
142 (Laurencin et al., 2019, Boucard et al., 2021, Kopp et al., 2011, Laigle et al., 2013b). This difference  
143 corresponds to the along-strike variation in accretionary wedge size. In contrast, the landward increase  
144 in slab dip angle is similar on the two profiles when observed as a function of interplate depth. At large  
145 depth, the slab dip angle is up to 51° at 280 km distance from the trench and shows no significant along-  
146 strike variation up to Guadeloupe (Paulatto et al., 2017), and Saint Martin when projected from Wide  
147 angle model of Klingelhoefer et al., (2018). The mantle wedge of the upper plate intersects the slab at  
148 24 km and 28 km depth (~100 km and ~160 km from the deformation front) offshore of Saint Martin  
149 and Martinique islands respectively (Laurencin et al., 2018, Kopp et al., 2011).

## 150 ***2.2 Seismicity and seismogenic zone***

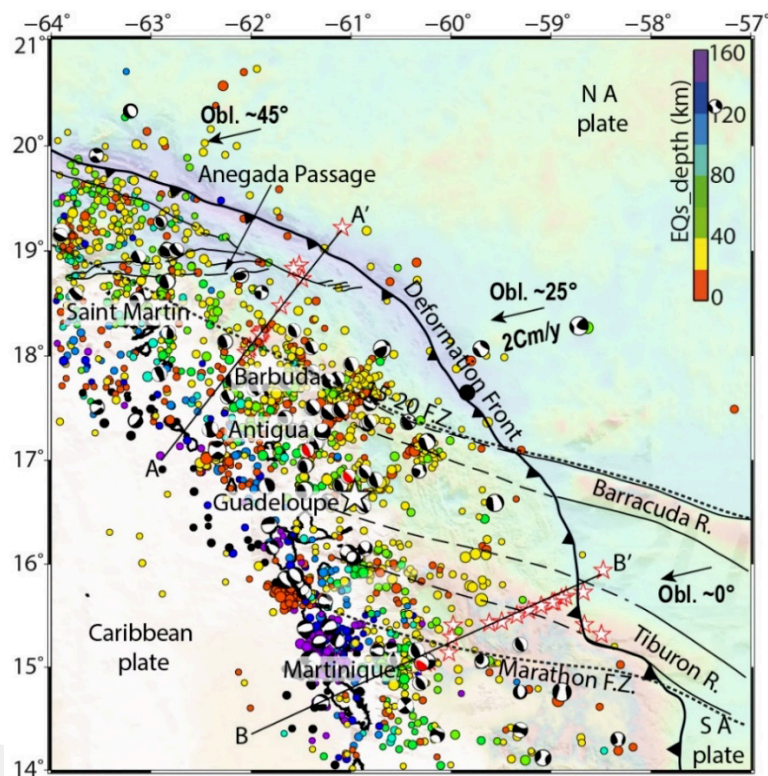
151 A recent re-interpretation of the available campaign and continuous GPS measurements in the  
152 Caribbean resulted in a re-evaluated plate velocity field (van Rijsingen et al., 2021). These authors  
153 propose that the plate coupling along the Puerto-Rico and Lesser Antilles subduction interface is very  
154 low. Consistently, the seismicity catalogue record only a few hundred earthquakes per year in the Lesser  
155 Antilles (Figure 2). However, investigations on some coral micro-atolls suggest that vertical  
156 deformation are possibly related to a local increase in interseismic coupling at great depth (Philibosian  
157 et al., 2022). A more recent study (van Rijsingen et al., 2022) has however, presented vertical velocities  
158 for the Lesser Antilles Islands and examine the link between the short and long-term vertical motions  
159 and their underlying processes. Based on their elastic dislocation models, they show that a locked or  
160 partially locked interplate up to 60 km depth would produce uplift of the island arcs, which is opposite  
161 to the observations of microatolls and GNSS data. Thus, suggesting low coupling for this subduction  
162 zone.

163 During the historical period, only few earthquakes among damaging events occurred on the plate  
164 interface, including the largest 1843 event with an intensity-based magnitude possibly ranging between  
165 7.0 (Bernard & Lambert, 1988) and 8.4 (Feuillet et al., 2011; Hough, 2013). The CMT catalog  
166 (Dziewonski et al., 1981; Ekström et al., 2012) indicate that only about 46 earthquakes along ~800-km-



167 long segment, with  $M_w > 5$  and focal mechanisms consistent with a co-seismic rupture along the  
 168 subduction interface, have been recorded teleseismically since 1973 (Figure 2). This scarce interplate  
 169 seismicity is mainly aggregated in two clusters: one from Montserrat to Barbuda and the other from the  
 170 Anegada Passage to the Virgin Islands. Between these regions and to the south of Guadeloupe,  
 171 subduction earthquakes are very rare in the instrumental period, and small earthquakes ( $M_w < 5$ )  
 172 dominate (Schlaphorst et al., 2016). The scarcity of subduction earthquakes raises the question of  
 173 seismic gaps in the Lesser Antilles, particularly between Barbuda and the Anegada Passage (Marcaillou  
 174 et al., 2021).

175



176

177 *Figure 2: Seismicity distribution along the Lesser Antilles margin. The colored circles are the earthquakes*  
 178 *from the USGS catalogue ( $M_w > 3.5$  from 1900 to 2022), with size and color representing magnitude and*  
 179 *epicentral depth, respectively. The black star represents the epicenter of the 1843 earthquakes. Black focal*  
 180 *mechanisms are thrust-type earthquakes recorded teleseismically (from the gCMT catalogue 1976 – 2021). Red*  
 181 *focal mechanisms are relocated flat thrust earthquakes based on OBS deployment (Laigle et al., 2013a). Black*  
 182 *lines AA' and BB' show the location of the thermal models and the earthquake profiles shown in Figure 8.*

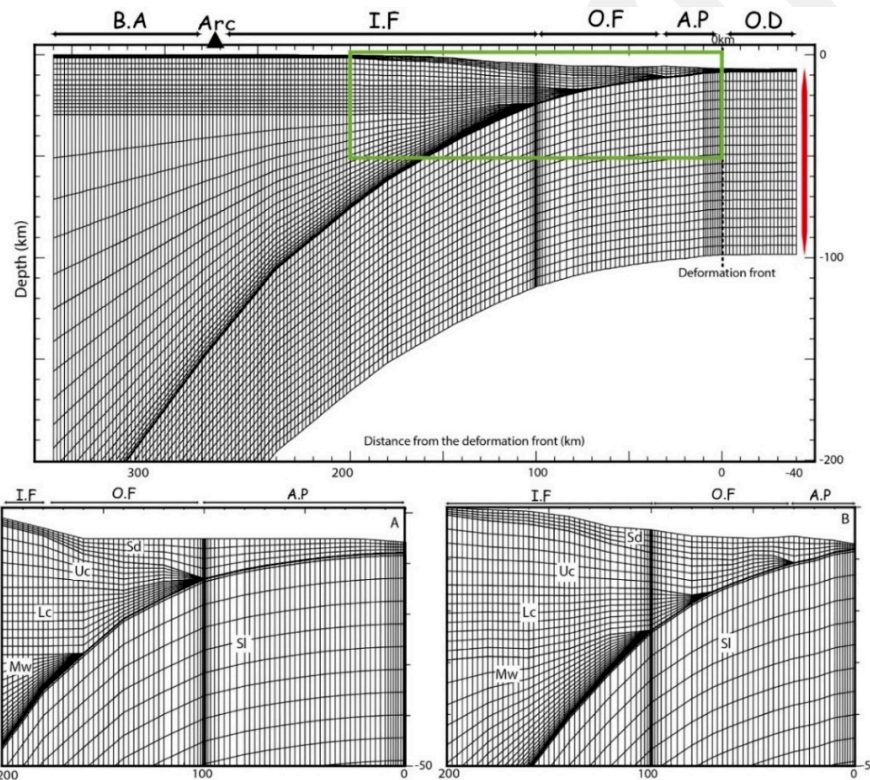
### 183 **2.3 Thermal regime**

184 Prior to the Antithesis cruises, old, scarce and highly scattered heat-flow measurements existed in  
 185 the Lesser Antilles forearc and the trench. More recent data were acquired in the Grenada backarc basin  
 186 and Island arcs (Manga et al., 2012). Gutscher et al. (2013) proposed first thermal models at various  
 187 latitudes along the Lesser Antilles. In their study, lines AA' and CC' approximately correspond to the  
 188 Saint Martin and Martinique heat-flow profiles in the current study. However, along these two lines, the  
 189 modelling resulted in a poorly constrained thermal structure. Offshore of Antigua, only one heat-flow

190 measurement (82 mW/m<sup>2</sup>) in the forearc constrain the model, and offshore of Martinique, old heat flow  
 191 measurements scattered between 30 and 90 mW/m<sup>2</sup>. Thus, the margin thermal structure needs to be re-  
 192 evaluated in the Northern and Central Lesser Antilles.

### 193 3 Methods

194 During the Antithesis 1 cruise (Dec 2013 - Jan 2014), we acquired 39 heat-flow measurements using  
 195 a microprocessor-controlled heat-flow (MCHF) instrument (see the Supplementary Material for  
 196 description). We model the thermal structure of the subduction zone along two trench-normal profiles,  
 197 one located between Barbuda and Saint Martin islands and crossing the volcanic arc at St Kitts island  
 198 (hereafter named ‘Saint Martin’ profile), and the other crossing Martinique island forearc and active  
 199 volcanic arc (hereafter named ‘Martinique’ profile) (Figure 1). The 2-D finite-element steady-state  
 200 modelling method (Wang et al., 1997), the mesh geometry (Figure 3), the input parameters and the  
 201 thermal boundary conditions are described in details in the supplementary material.  
 202



203  
 204 *Figure 3 : Geometry of the finite element mesh used for the 2D steady-state thermal modelling. The green*  
 205 *frame indicates projected regions for (A) Martinique profile and (B) Saint Martin profile. The red line indicates*  
 206 *the location of the calculated oceanic geotherm. [O.D – Oceanic domain, A.P – Accretionary prism, O.F – Outer*  
 207 *forearc, I.N – Inner forearc, B.A – Backarc, Sd – Sediment, Sl – Slab, Uc – Upper crust, Lc – Lower crust, Mw –*  
 208 *Mantle wedge]*

209 For conductive models, the geotherm at the oceanic boundary is calculated using a model of a  
 210 conductive half-space cooling lithosphere based on a 1-D approach (Hutchison, 1985) and detailed by  
 211 Marcaillou et al., (2008). However, fluid circulation within the incoming oceanic crust can cause

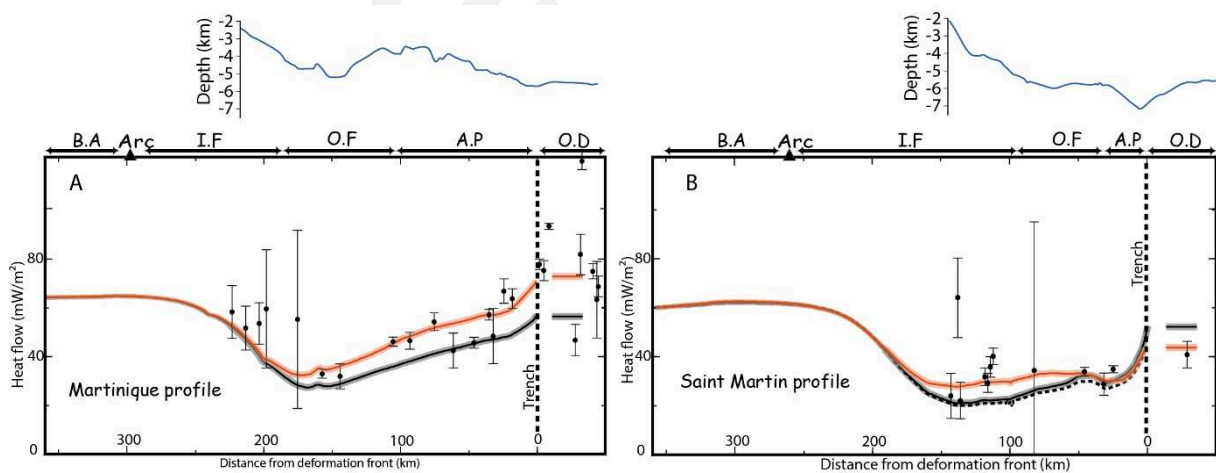
212 hydrothermal warming (e.g. Spinelli & Wang, 2008) or cooling (e.g. Harris & Wang, 2002) in the trench,  
 213 and modify the heat flow at the surface, the oceanic geotherm and the temperature along the subduction  
 214 interface. We use the methods by (Spinelli & Wang, 2008, Harris & Wang, 2002) to calculate the oceanic  
 215 geotherm where anomalous heat flow (i.e. heat-flow different from conductive value) indicate  
 216 significant heat advection. This approach requires the use of Nusselt number (Nu) as a proxy to model  
 217 heat advection due to hydrothermal circulation (See the Supplementary material).

## 218 4 Regional heat-flow and fluid-driven heat advection

219 In the following, we describe the measured and calculated heat-flow values based on conductively  
 220 cooling modelling and heat advection in order to discuss the influence of fluid circulation.

### 221 4.1 Measurements

222 We recorded 13 and 26 heat-flow measurements, at depth greater than 2400m, from 30-50 km before  
 223 the trench up to the inner forearc, at the latitude of Saint Martin and Martinique respectively (Figure 1).  
 224 Water depths for heat-flow measurements are indicated in Figure 4. Along the Martinique profile, the  
 225 heat flow decreases progressively from  $\sim 78\text{mW/m}^2$  in the trench to  $35\text{-}45\text{mW/m}^2$  at 100-150 km from  
 226 the deformation front in the outer forearc and increases to  $\sim 60\text{mW/m}^2$  towards the arc (Figure 4A). In  
 227 contrast, along the Saint Martin profile, the heat flow does not significantly vary from the trench,  
 228  $\sim 42\text{mW/m}^2$ , to the forearc, where values range from 30 to  $42\text{mW/m}^2$  between 45 and 120 km from the  
 229 deformation front (Figure 4B). The two profiles differ in two key ways. First, the heat flow is 53%  
 230 higher in the trench offshore of Martinique than of Saint Martin. Moreover, the heat flow decreases from  
 231 the trench to the outer forearc along the former but remains constant along the latter.



233 *Figure 4: Measured and calculated heat-flow along Martinique profile (A) and Saint Martin profile (B). The*  
 234 *figures show the heat-flow measurements (black dots), the calculated heat-flow for conductive models (black line)*  
 235 *and for models including fluid thermal convection (red line) with 10% uncertainty (shaded area). In the oceanic*  
 236 *domain, the horizontal lines are 1D calculated values. The dash line represent model without fluid expulsion*  
 237 *in the forearc. The blue lines are the shapes of the bathymetry along the collected heat-flow data for the both profiles.*  
 238 *[O.D – Oceanic domain, A.P – Accretionary prism, O.F – Outer forearc, I.N – Inner forearc, B.A – Backarc]*

239 **4.2 Calculated conductive heat flow**

240 Conductive thermal modelling predicts a heat flow profile which decreases from the oceanic domain  
241 to the forearc, from 56 to 26 mW/m<sup>2</sup> along the Martinique Profile and from 52 to 22 mW/m<sup>2</sup> along the  
242 Saint Martin Profile (black lines in Figure 4A and Figure 4B). The calculated heat flow at the trench is  
243 consistent with the expected value for an 80-Myr-old oceanic plate (Stein & Stein, 1994; Lucazeau,  
244 2019). Along both profiles, the calculated conductive heat flow poorly fits the measurements. Offshore  
245 of Martinique, the calculated heat flow is ~30% lower than the measurements in the trench and decreases  
246 westward similarly as the measurements, thus remaining significantly lower along the outer forearc. In  
247 other words, the heat-flow mismatch at the trench and the accretionary prism indicates a positive thermal  
248 anomaly compared to the conductive model at the margin front. In contrast, on Saint Martin profile, the  
249 calculated conductive heat-flow is ~23% higher than the measurement in the oceanic Jacksonville Patch  
250 (Figure 1). Moreover, the calculated heat-flow decreases westward, along the forearc and is lower than  
251 the measurements between 60 and 140 km from the deformation front. Thus, compared to the conductive  
252 model, this result indicates contrasting thermal anomalies: one negative near the trench and at the  
253 accretionary prism, the other positive at the forearc.

254 **4.3 Sensitivity tests for the calculated conductive heat-flow**

255 We performed sensitivity tests for the key-parameters of the conductively cooling model to check  
256 whether heat conduction can possibly account for the measured heat-flow variations, or if these  
257 variations are necessarily related to fluid-driven thermal advection.

258 In the frame of a conductively cooling oceanic lithosphere, the northward decrease in measured heat-  
259 flow from 78 to 42mW/m<sup>2</sup> in the trench is possibly related to two parameters: the incoming plate age  
260 and the oceanic sedimentation rate (Hyndman & Wang, 1993; Marcaillou et al., 2008). However, this  
261 decrease would require an increase in the oceanic plate age from 40 Myr to >120 Myr, which is highly  
262 unreasonable at the Lesser Antilles, where the age of the ~80-Myr-old American Plate does not vary  
263 significantly along-strike (Müller et al., 2019). Moreover, a sedimentation rate in the trench, offshore of  
264 Saint Martin, high enough to reduce the heat-flow by 23% is inconsistent with the <500-m-thick trench  
265 fill (Laurencin et al., 2019). Offshore of Martinique, the trench fill is up to 3 km thick (Pichot et al.,  
266 2012), but even a theoretical model with zero sedimentation rate results in calculated heat-flow that  
267 remains ~30% lower than the measurements. As a result, in the trench, heat conduction cannot generate  
268 the high heat-flow along the Martinique profile and low heat-flow along the Saint Martin profile without  
269 a key-contribution by heat advection.

270 Along the Saint Martin profile, measurements indicate an intriguingly stable heat-flow from the  
271 trench to the inner forearc, while typically at subduction zone, the heat-flow decreases as the oceanic  
272 plate deepens beneath the margin (Wang et al., 1995). In the conductively cooling model, the slab-  
273 dipping angle and the upper plate thermal conductivity are the key parameters that control the landward

274 decrease of the calculated heat-flow (Figure 4). Fitting the measurements by varying the slab-dipping  
275 angle is obtained when involving flat slabs geometries in the models (slab dip angle  $< 2^\circ$ ). However,  
276 offshore of Saint Martin, wide-angle models (Laurencin et al., 2018) and MCS data (Laurencin et al.,  
277 2019) show that the slab dip is up to  $\sim 25^\circ$  beneath the forearc. In addition, fitting the measurements by  
278 varying the thermal conductivity in the upper-plate and the sediments would require values greater than  
279  $10 \text{ W}\cdot\text{m}^{-1}\cdot\text{K}^{-1}$ , which is unrealistic for these lithologies (Beardsmore & Cull, 2010).

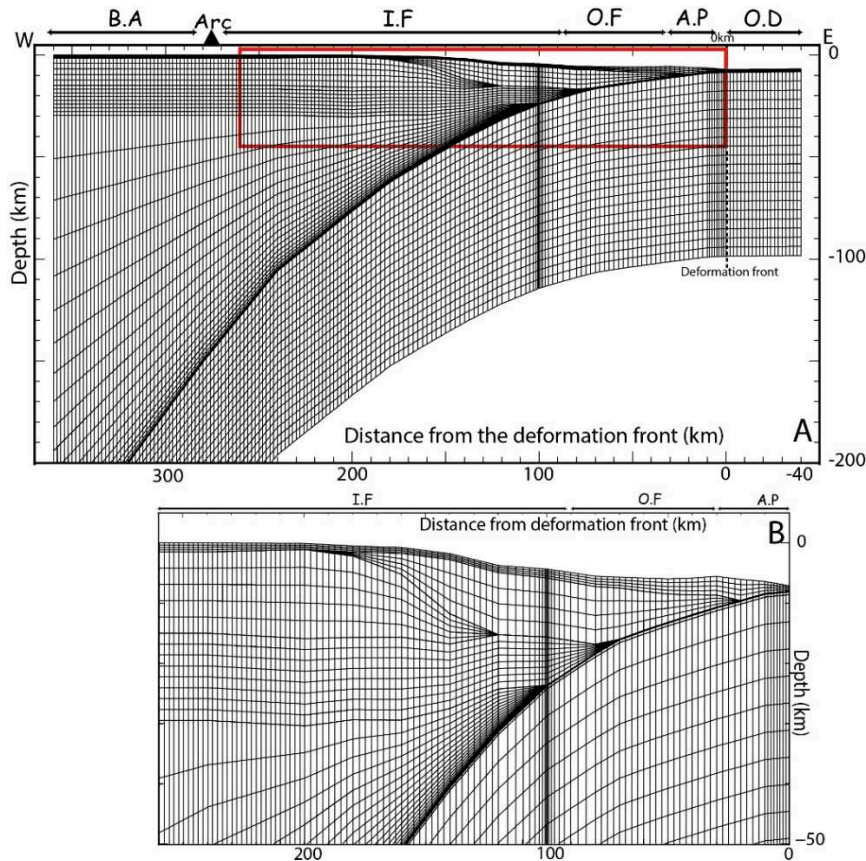
280 These tests thus indicate that conductively cooling models cannot satisfactorily account for 1) the  
281 heat-flow in the trench, which is too high offshore of Martinique and too low offshore of Saint Martin  
282 and 2) the high heat-flow at 60-140 km from the deformation front at the forearc of Saint Martin.

#### 283 *4.4 Calculated heat advection*

284 Offshore of Martinique, anomalously high heat flow in the trench and at the deformation front is  
285 typical of the hydrothermal warming related to insulated circulation: warm fluids flow updip along the  
286 oceanic basement aquifer to the trench, where thick and poorly faulted sedimentary fill reduces  
287 exchanges with seawater (Spinelli & Wang, 2008, Harris et al., 2010). A similar insulated system has  
288 been observed and modelled in the Nankai subduction zone (Spinelli & Wang, 2008). We applied the  
289 methodological approach used by these authors to model heat advection (See the Supplementary  
290 material). In this approach, increasing the Nusselt Number (Nu) in a mesh layer that represent the crustal  
291 aquifer simulates fluid flow along this region. Using Nu of 1000, consistent with previous modelling in  
292 other subduction zones (e.g. Harris et al., 2020), results in higher calculated heat-flow of  $76 \text{ mW}/\text{m}^2$  in  
293 the trench and at the deformation front, which is consistent with the measurements. The addition of fluid  
294 advection results in a landward decreasing calculated heat-flow that fits the measurements from the  
295 trench to the inner forearc (red line in Figure 4A).

296 Offshore of Saint Martin, anomalously low heat-flow in the poorly sedimented and pervasively  
297 fractured trench is typical of ventilated hydrothermal systems where cold seawater percolates through  
298 oceanic basement faults (e.g. Harris & Wang, 2002). In Costa-Rica, these authors successfully modelled  
299 hydrothermal cooling by reducing the oceanic geotherm of the incoming plate. In our model, reducing  
300 the oceanic geotherm at the seaward boundary results in lowering the calculated heat-flow to  $45 \text{ mW}/\text{m}^2$ ,  
301 in the trench and at the margin deformation front (black dotted line in Figure 4B) which is consistent  
302 with the measurements. Hydrothermal cooling in the trench reduces the calculated heat-flow along the  
303 accretionary wedge where it fits the measurements, but does not significantly change the calculated  
304 value beneath the forearc (60-140 km from the deformation front) where it remains much lower than the  
305 measurements. This positive thermal anomaly in the forearc corresponds to the location of the  
306 Tintamarre Fault Zone suggesting warm fluid upward migration to the seafloor as consistently proposed  
307 by previous studies based on tectonic observations (Boucard et al., 2021), wide-angle derived velocity  
308 anomaly (Klingelhoefer et al., 2018) and discussion from geochemical data (Cooper et al., 2020). We  
309 model this heat migration, using a Nusselt Number of 3.5 at the forearc area where the Tintamarre Fault

310 Zone (TFZ) deeply fracture the margin (Figure 5). The TFZ covers ~100 km wide and ~6km depth  
 311 (second layer in the close up in Figure 5B), and is in line with the extent of the faults zone as  
 312 imaged in seismic and bathymetric data (Boucard et al., 2021). This value of Nu accounts for the  
 313 thermal effects of heat transfer by fluid circulation in this unit. This modelling generates heat-flow of  
 314 34 mW/m<sup>2</sup> at the surface, which fits the measurements (Figure 4b) and thus approximate the upward  
 315 heat migration in the Tintamarre Fault Zone.

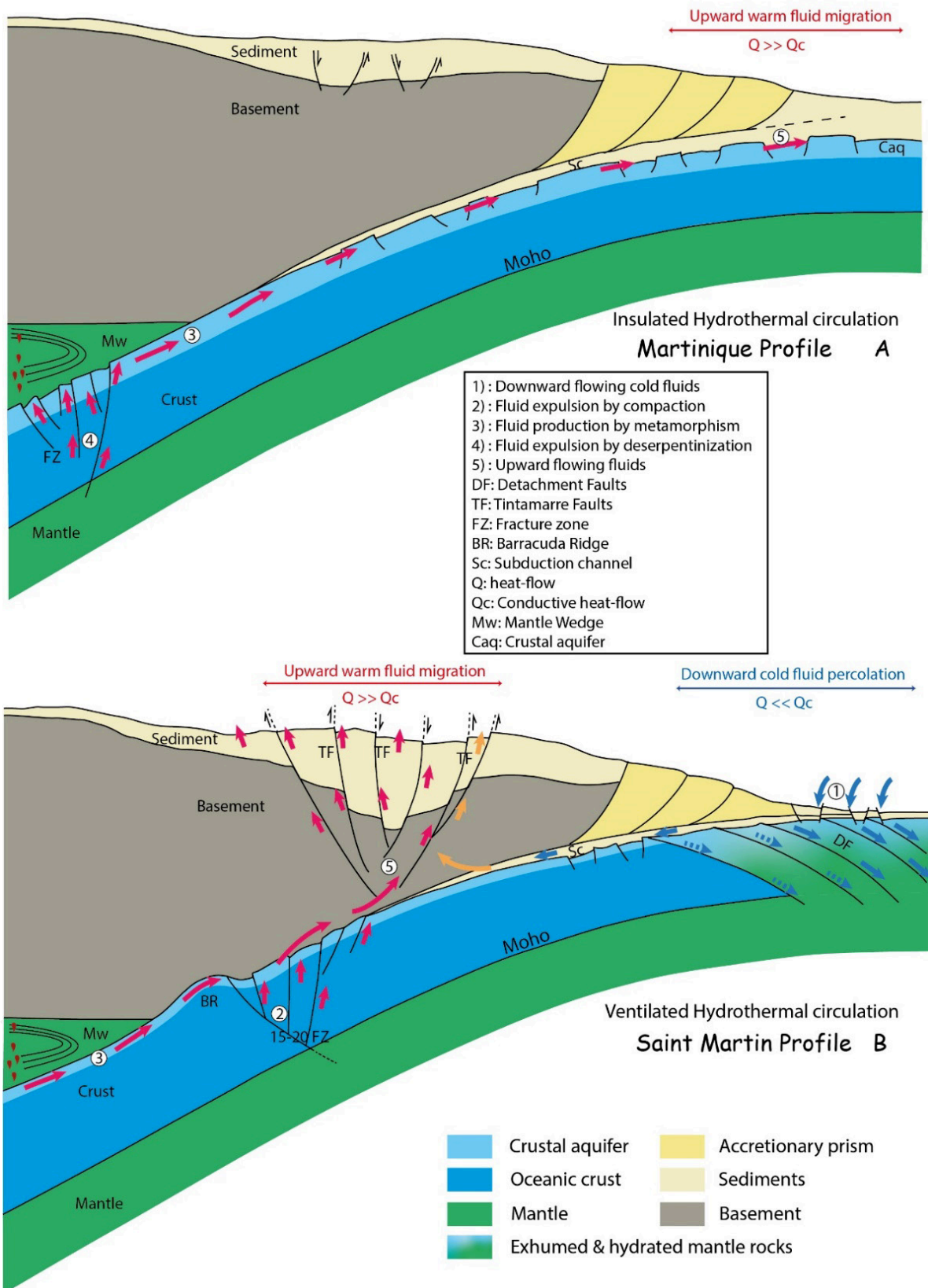


316

317 *Figure 5: Global view (A) and close up (B) of the modified 2D mesh grid for the Saint Martin. The mesh*  
 318 *includes a theoretical layer, which corresponds with the forearc area where the Tintamarre Fault Zone deeply*  
 319 *and pervasively fractures the margin. Increasing the Nusselt Number in this layer (see supplementary material)*  
 320 *accounts for the high heat-flow measured in surface, inconsistent with conductive modelling and thus likely related*  
 321 *with upward fluid-driven heat-flow along the Tintamarre Fault planes.*

## 322 5 Hydrothermal circulation within the Lesser Antilles subduction zone

323 Measurements provide unexpected heat-flow values in the trench, at the deformation front and in the  
 324 forearc of the Lesser Antilles Subduction Zone. Conductively cooling modelling cannot predict heat-  
 325 flow values which satisfactorily fit the measurements indicating that fluid-driven heat advection strongly  
 326 influences the heat transfer in the margin segments. This result is consistent with an increasing number  
 327 of recent studies, which conclude that the LASZ is extremely hydrated (e.g. Schlaphorst et al., 2016,  
 328 Paulatto et al., 2017, Cooper et al., 2020, Marcaillou et al., 2021). Moreover, the measurements and  
 329 models indicate that the fluid circulation varies along-strike, as discussed below.



330

331 *Figure 6: Interpretative sketches of the fluid circulation in the subduction for (A) an insulated hydrothermal*  
 332 *system in the Central Lesser Antilles, offshore of Martinique and (B) a ventilated hydrothermal system in the*  
 333 *Northern Lesser Antilles, offshore of Saint Martin. The structures are based on MCS profiles and Wide Angle*  
 334 *interpretations of (Laigle et al., 2013b, Kopp et al., 2011) for the Martinique profile, and (Boucard et al., 2021,*  
 335 *Marcaillou et al., 2021, Laurencin et al., 2018) for the Saint Martin profile (See section 2 for details).*

336 **5.1 Central Lesser Antilles, offshore of Martinique**

337 Along the Martinique profile, the heat flow is significantly higher than the conductive value in the  
338 trench, decreasing regularly landward beneath the forearc. This behavior is typical of shallow  
339 hydrothermal warming related to insulated circulation, as described for instance in Nankai (Spinelli &  
340 Wang, 2008, Harris et al., 2017). In the Central Lesser Antilles, Boron isotope ratio indicates excess  
341 dehydration, i.e. high rate of water released from the slab, at great depth beneath the volcanic arc (Cooper  
342 et al., 2020). These authors thus confirm previous geophysical studies, which highlighted the strong  
343 hydration of this subduction segment (Schlaphorst et al., 2016, Paulatto et al., 2017). They indicate that  
344 the subduction of numerous deep large-scale oceanic transform fault zones and potentially exhumed  
345 mantle rocks related to the slow-spreading Mid-Atlantic Ridge have the potential to supply substantial  
346 volumes of fluid to the subduction. We propose that warm fluids, released at shallow depths by sediment  
347 compaction and at greater depths by metamorphic dehydration and/or deserpentinization of exhumed  
348 mantle rocks along major fracture zones (e.g. Marathon F.Z.), collected within the oceanic basement  
349 aquifer and the interplate fault zone, migrate updip along the subduction interface and the shallow crustal  
350 aquifer toward the trench, as exemplified in Chile by Moreno et al. (2014) and in Nankai by Spinelli &  
351 Wang, (2008). The 2-to-3-km thick poorly-faulted sedimentary trench fill to the South of the Barracuda  
352 Ridge, impedes cold seawater downward percolation into the trench, insulating the downgoing oceanic  
353 plate. As a result, fluids updip migration warms up the subduction interface beneath the shallow portion  
354 of the accretionary prism, the deformation front and the trench, increasing the heat-flow at the seafloor  
355 (Figure 6A).

356 **5.2 Northern Lesser Antilles, offshore of Saint Martin**

357 Along the Saint Martin profile, the measured heat flow is significantly lower than the conductive  
358 value in the trench and at the accretionary wedge. This behavior is typical in the presence of shallow  
359 hydrothermal cooling and ventilated circulation, as described for instance in Costa-Rica (Harris &  
360 Wang, 2002, Harris et al., 2010). In the trench, the subducting oceanic basement within the Jacksonville  
361 patch consists of exhumed and hydrated mantle rocks deeply and pervasively fractured by widespread  
362 detachment faults overlain with a fractured <500-m-thin sedimentary layers (Marcaillou et al., 2021).  
363 These detachment faults, likely reactivated by plate bending, and the thin fractured sedimentary layers  
364 favor downward cold seawater percolation and hydrothermal cooling in the trench. Outside the  
365 Jacksonville patch, within the oceanic domain, a second heat-flow measurement (55mW/m<sup>2</sup>) is  
366 consistent with an expected conductive heat-flow value. However, this region shows no evidence of  
367 highly faulted sediment and oceanic basement as observed in the patch (Marcaillou et al., 2021). Thus,  
368 it is likely that hydrothermal cooling maybe restricted to the extent of the Jacksonville patch in the  
369 oceanic domain. However, this is based only on the 2 heat-flow values acquired inside and outside of  
370 the patch respectively. In the forearc, the Tintamarre Fault deeply fractures the basement, while the 15-  
371 20 Fracture Zone deeply fractures the subducting oceanic plate at greater depth beneath the forearc. The



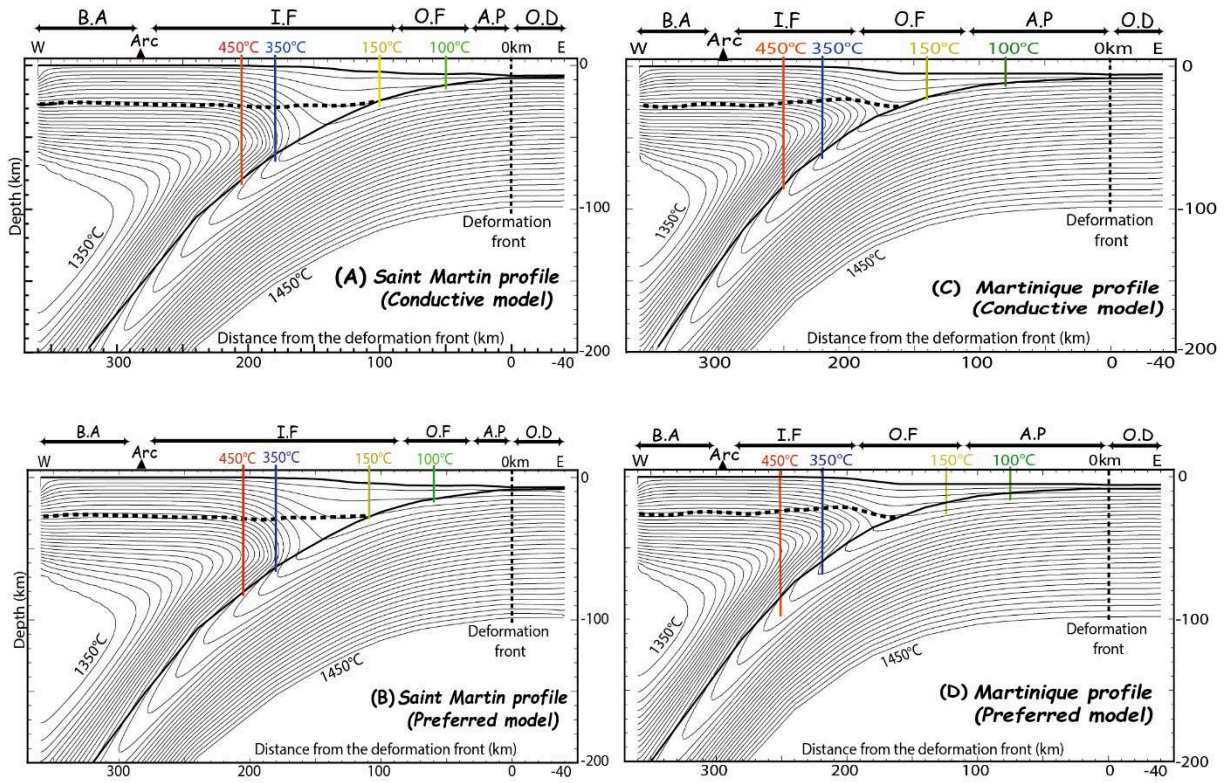
372 slab dehydration at depth, by sediment compaction, metamorphic reactions and deserpentinization of  
373 basement and/or mantle rocks probably releases large amount of fluids into the interplate fault damaged  
374 zone. We propose that the >100-km-long and 60-km-wide Tintamarre Fault Zone associated to intense  
375 basal erosion (Boucard et al., 2021) offers efficient pathways for fluid upward migration up to the  
376 seafloor where they create numerous possible pockmarks (Klingelhoefer et al., 2018). As a result,  
377 downward percolation of cold seawater through reactivated detachment faults in the trench, and warm  
378 fluid upward migration through major fault zones in the forearc are consistent with heat-flow  
379 measurements respectively lower and higher than conductive value in this ventilated hydrothermal  
380 system (Figure 6B).

## 381 **6 Thermal structure and potential seismogenesis**

382 The thermal structures for the Saint Martin and Martinique profile models, with and without heat  
383 advection, show small variations in the location of the 100, 150, 350 and 450°C isotherms often  
384 interpreted to be associated with the updip and downdip limit of seismogenic zones when located at  
385 shallower depth than hydrated mantle wedge (e.g. Hyndman et al., 1995) (Table 1 and Figure 7).

386 When comparing the effect of advection vs conduction, offshore of Martinique, fluid updip migration  
387 warms up a shallow section of the interplate contact, from 190 km to the trench, shifting the 150°C  
388 isotherms seaward by 15 km. In contrast, this heat advection has no effect on the thermal structure of  
389 the deepest part of the interplate contact, which is mostly controlled by the mantle wedge. Along the  
390 Saint Martin profile, cold fluid downward percolation in the Jacksonville Patch cools down the  
391 temperature of the frontal segment of the interplate contact and this cooling effect rapidly decreases  
392 landward. As a result, the 100 and 150°C isotherms are shifted by 10 km by this hydrothermal cooling,  
393 which has no impact on the location of the 350 and 450°C isotherms. The moderate effect of this  
394 hydrothermal circulation onto the thermal structure is likely related to the old age of the oceanic plate  
395 and the slow convergence rate. The age and convergence rate of the oceanic plate in the LA typically  
396 generate cold subduction zone and thus reduce the influence of hydrothermal circulation onto the  
397 thermal structure.

398 What is noteworthy are the significant distances from the trench of the 150°C and 350°C  
399 temperatures on the interplate fault : they are both located beneath the inner forearc for the Saint Martin  
400 profile and beneath the outer forearc for the Martinique profile. The distance between the 150°C and  
401 350°C, often referred to as the minimum width of the thermally defined seismogenic zone, varies from  
402 80 to 94 km for the Martinique profile, and from 80 to 72 km for the Saint Martin profile from the  
403 conductive to the advective models.



404

405 *Figure 7: Thermal structure of the Lesser Antilles Margin at the latitude of Saint Martin (A, B) and Martinique*  
 406 *(C, D) predicted by the conductive models and the advective models (preferred models). The location of the 100,*  
 407 *150, 350 and 450°C isotherms are marked with vertical lines.*

408

| (A) Martinique model   | Conductive Model                     |            | Insulated Model                      |            |
|------------------------|--------------------------------------|------------|--------------------------------------|------------|
|                        | Distance from deformation front (km) | Depth (km) | Distance from deformation front (km) | Depth (km) |
| 100°C                  | 80                                   | 12         | 75                                   | 10         |
| 150°C                  | 140                                  | 22         | 124                                  | 20         |
| 350°C                  | 220                                  | 60         | 220                                  | 60         |
| 450°C                  | 250                                  | 85         | 250                                  | 85         |
| (B) Saint Martin model | Conductive Model                     |            | Insulated Model                      |            |
|                        | Distance from deformation front (km) | Depth (km) | Distance from deformation front (km) | Depth (km) |
| 100°C                  | 50                                   | 12         | 60                                   | 15         |
| 150°C                  | 100                                  | 23         | 110                                  | 25         |
| 350°C                  | 180                                  | 62         | 180                                  | 65         |
| 450°C                  | 205                                  | 80         | 205                                  | 80         |

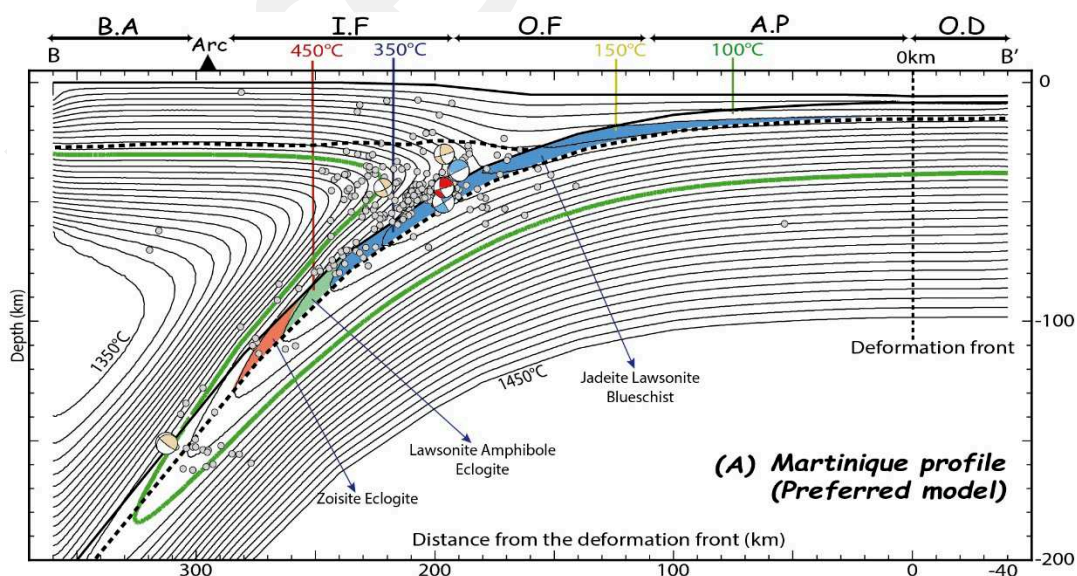
409 *Table 1: Calculated depth and distance from the deformation front for isotherms 100°C, 150°C, 350°C and*  
 410 *450°C for the Martinique (A) and Saint Martin (B) models. These isotherms are commonly associated with the*  
 411 *updip and downdip limits for the thermally-defined seismogenic zone.*

412 Along the Martinique profile, temperatures of 150°C and 350°C reach depths of 20 km and 60 km  
 413 respectively on the interplate fault. The forearc Moho located at a shallower depth (28 km) than 350°C  
 414 would thus become the downdip limit of the potential seismogenic portion (Hyndman et al., 1997), with  
 415 a sharp reduction of the width to 36 km. On the Saint Martin Profile, a greater depth of 25 km for the  
 416 150°C marking the updip limit, and a shallower moho (25 km) appear to further reduce the potential  
 417 width of the seismogenic portion, making it potentially almost non-existent. In case of subducting  
 418 exhumed mantle patches within the slab's crust outcropping along the plate interface, seismogenic width  
 419 will be even more reduced due to their expected serpentinization at those low temperatures. However,  
 420 we can still not quantify the degree of serpentinization of these mantle materials (wedge and slab's crust)  
 421 along the interplate contact, and these new measurements and models of thermal structure provide up-  
 422 to-date estimations of temperatures along the megathrust fault. Moreover, up to Mw ~5 flat-thrust events  
 423 have been recorded at the depth of 40-45 km (Laigle et al., 2013), and up to 51 km (Bie et al., 2019) in  
 424 the Central Lesser Antilles, offshore Martinique. These events highlight a deep seismogenic zone which  
 425 appears to extend (or resume) beyond the intersection between the forearc moho and the interplate, but  
 426 raises question as to the nature of the subducting crust and/or the forearc mantle materials.

## 427 7 Relationship between temperature, fluids, and seismicity

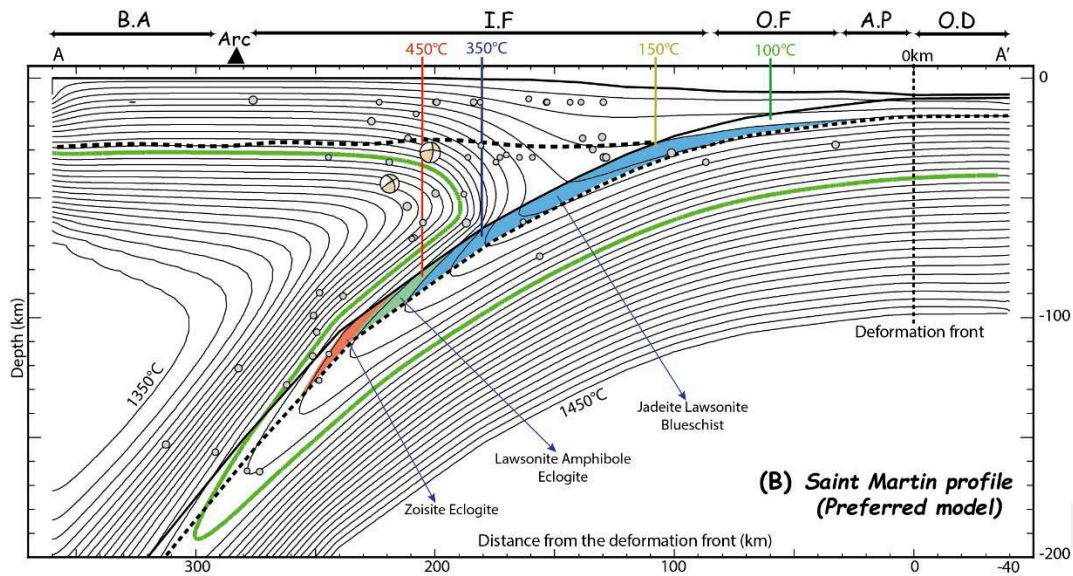
428 We investigate the relationship between the thermal structure of the margin, fluid release, and the  
 429 location of intraslab, supraslab, and interplate seismicity (Figure 8). We put a particular emphasis on the  
 430 Martinique profile (Figure 8A) where 5.5-years-long OBS deployments provide us with numerous and  
 431 accurately relocated earthquakes (Laigle et al., 2013a). In contrast, the seismicity in the vicinity of the  
 432 Saint Martin profile is sparse and poorly located (Figure 8B).

433



434

435



436

437

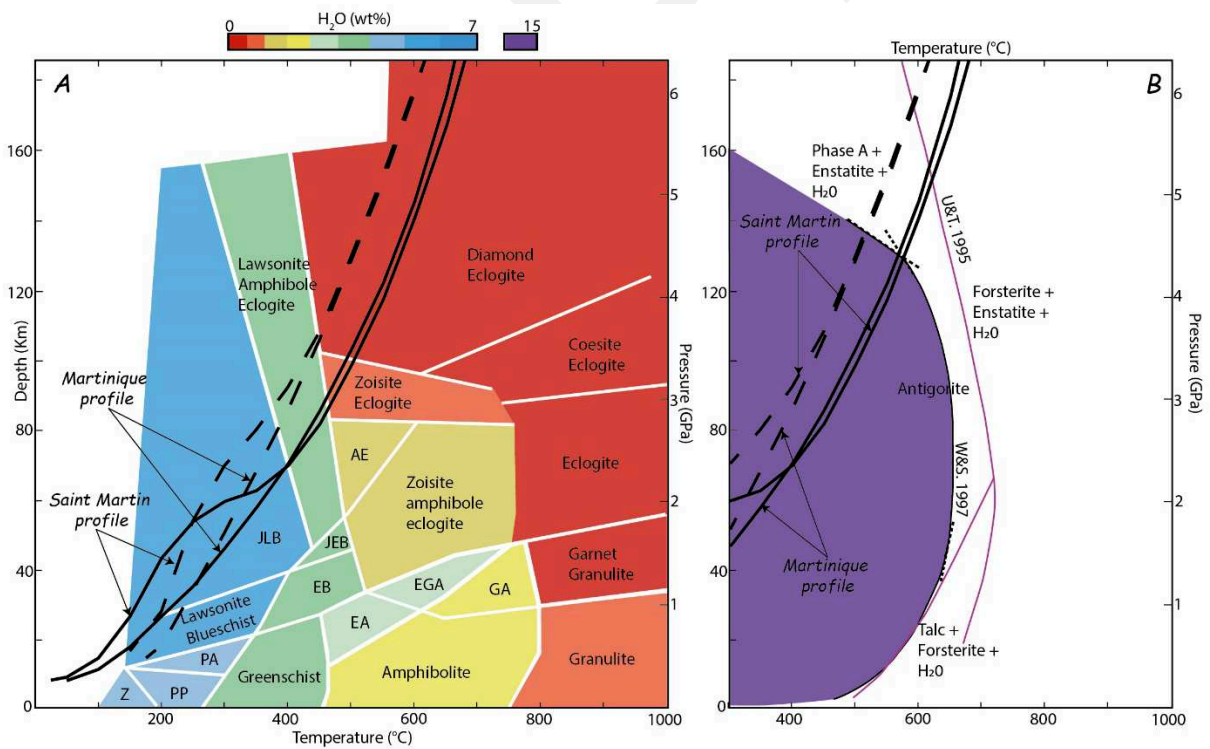
Figure 8: Thermal structure of the LASZ with cross-sections of the hypocenters for earthquakes located within 25 km on each side of the Martinique (A) and Saint Martin (B) profiles (see figure 2). The gray circles are relocated earthquakes from OBS deployment (Laigle et al., 2013a) for the Martinique profile, and earthquakes from USGS catalogue for Saint Martin profile. The blue focal mechanisms are thrust faults, and the red is a relocated flat thrust event, while the yellow represents other focal mechanism from CMT catalogue. The black thick line represent the top of the subducting slab, while the black dotted lines represent the Moho. The green contour line marks the 600 °C isotherm usually considered as an averaged temperature for antigorite dehydration.

440

441

442

443



444

445

Figure 9: Phase diagram and maximum H<sub>2</sub>O content for (A) metamorphosed MORB modified from Hacker, et al., (2003) and (B) hydrated mantle modified from (Wunder & Schreyer, 1997 and Ulmer & Trommsdorff, 1995), showing the Pressure-Temperature (PT) path for the slab tops (thick black lines), and moho (dash lines) offshore of Martinique and Saint Martin in the LASZ. (Z – Zeolite, PP – Prehnite pumpellyite, PA – Prehnite actinolite, JLB – Jadeite lawsonite blueschist, EB – Epidote blueschist, EA – Epidote amphibolite, JEB – Jadeite epidote blueschist, AE – Amphibole eclogite, EGA – Epidote garnet amphibolite, GA – Garnet amphibolite).

449

450

## 451 **7.1 Intraslab seismicity**

452 At depth in subduction zones, the location of intraslab seismicity is mainly controlled by the  
453 combined influence of pressure, temperature, slab bending stresses, and fluid release related to  
454 dehydration reactions, in particular, crust eclogitisation and mantle deserpentinization (Kirby et al.,  
455 1996; Hacker et al., 2003; Ferrand, 2019). Intraslab seismicity in the LASZ is distributed both within  
456 the crust and the mantle of the slab. At the LASZ, numerous fracture zones and detachment faults deeply  
457 incise the basement of the incoming oceanic plate, down to the mantle, likely favoring deep hydration  
458 and serpentinization of mantle rocks before the trench (Cooper et al., 2020; Marcaillou et al., 2021).  
459 These hydrated rocks are more stable at shallow depths and transport volatiles to dehydrate at greater  
460 depths during deserpentinization reaction at temperatures greater than 450°C (Ulmer & Trommsdorff,  
461 1995 and Van Keken et al., 2011; Ferrand, 2019; Bie et al., 2022). Since the composition of the  
462 subducting oceanic crust of the slow-spreading mid-Atlantic ridge can vary from mid-oceanic basalt up  
463 to serpentinized exhumed mantle, we report the slab's top and moho on a phase diagram for  
464 metamorphosed mid-oceanic ridge basalt (MORB) (e.g. Hacker, et al., 2003) and for hydrated mantle  
465 materials (e.g. Wunder & Schreyer, 1997; Ulmer & Trommsdorff, 1995) (Figure 9A & B). We also  
466 report on the thermal structure and seismicity cross-section (Figure 8A) the main metamorphic facies of  
467 the MORB phase diagram, as well as the 600 °C isotherm which could be used as a proxy of the  
468 maximum temperature for antigorite stability (650°C).

469 Slab's intracrustal seismicity in the LASZ is distributed between 35 and 165 km depth, which  
470 corresponds to calculated temperature's range of 240-625°C (Figure 8A). According to the *PT* path of  
471 the slab's top and moho, slab's intracrustal seismicity at 70-80 km depth at 400-450°C could result from  
472 dehydration reaction at the Blueschist-Eclogite transition. This depth is consistent with the downdip  
473 extent of the low-Vp anomaly in the slab crust and the transition towards higher Vp interpreted to be the  
474 result of crustal eclogitization (Paulatto et al., 2017). Fluids generated by dehydration reactions could  
475 migrate upward into the mantle wedge and updip through the slab, driven by gradients in tectonic  
476 stresses related to slab bending/unbending and densification (Faccenda et al., 2012; Paulatto et al.,  
477 2017), induce hydrofracturing, and trigger earthquakes within the shallow slab crust at 35-70 km depth.  
478 The oceanic crustal portions made of exhumed serpentinized peridotites is expected to dehydrate at  
479 depths >130 km above 550°C, and also be responsible for fluids upward migration and associated  
480 seismicity by dehydration embrittlement at these depths.

481 Within the slab mantle, the seismicity is aggregated in two main zones within a ~25-km-thick band  
482 beneath the slab top, at 35-80 km and 140–165 km depths, which correspond to calculated intraslab  
483 temperature's range of 250-450°C and 550-800°C respectively (Figure 8A). According to *PT* path of  
484 the slab's moho reported on the hydrated mantle phase diagram (Figure 9B), antigorite is expected to be  
485 unstable from 140 km at 520°C and up to ~620°C within the slab mantle along the depth of 160 km.  
486 Thus, we propose that the deeper intraslab seismicity zone located at 140–165 km depth, within the

487 antigorite destabilization zone, is related to dehydration of serpentinized peridotite. This is consistent  
488 with elevated  $V_p/V_s$  ratio observed at similar depth which is interpreted to correspond to peak water  
489 release (Bie et al., 2022). For the shallower active zone within the slab mantle at 35-80 km depth, the  
490 deepest events below the slab top close to the isotherms of  $>450-520^\circ\text{C}$  could be associated to antigorite  
491 destabilization process-related temperatures as proposed by Laigle et al., (2013a). The shallower events  
492 within the 20 km thick mantle band below the slab top may be linked to other processes similar to the  
493 reactivated faults of this slow-spreading oceanic lithosphere. The origin of the seismic activity located  
494 in the footwall of the deep-rooted detachments faults at the Mid-Atlantic ridge down to  $\sim 10$  km depth  
495 (e.g. Parnell-Turner et al., 2017) is not yet really understood. However, their seismogenic potential might  
496 persist even at those depths of 50 km, thanks to the still preserved thermal structure of the lithospheric  
497 mantle.

## 498 **7.2 Supraslab seismicity**

499 Supraslab earthquakes, offshore of Martinique are aggregated in a cluster located at 30-60 km depth  
500 in the mantle wedge, and extending up to 80 km arcward of the contact between the interplate and the  
501 upper plate moho (Figure 1Figure 8A). The seismicity occurring above the slab at depths greater than  
502 100 km may be interplate or slab crust/mantle events, and could be related to uncertainties of seismicity  
503 location/ or slab geometry. The supraslab seismicity zone is distributed over isotherms between  $200^\circ\text{C}$   
504 and  $800^\circ\text{C}$ . At temperature below  $450^\circ\text{C}$ , antigorite is expected to be stable, and mantle rocks to undergo  
505 serpentinization in the presence of fluid. Existing hypothesis for supraslab seismicity in the LASZ  
506 suggests heterogeneous mantle wedge and upward fluid migration (Laigle et al., 2013a; Paulatto et al.,  
507 2017). Our predicted temperature and depth of crustal eclogitization and fluid production at 70-80 km  
508 supports this hypothesis for the earthquakes occurring at least  $\sim 50$  km arcward of the mantle wedge  
509 corner, at temperatures lower than  $500^\circ\text{C}$ . Beyond the 50 km distance, and between  $500-800^\circ\text{C}$ , we  
510 propose that supraslab seismicity in this subduction zone could be related to dehydration embrittlement  
511 due to deserpentinization reaction in the serpentinized mantle wedge, as invoked beneath northeast New  
512 Zealand (e.g. Davey & Ristau, 2011).

## 513 **7.3 Interplate seismicity**

514 Interplate seismicity is located at depth greater than 25 km, and distance greater than 160 km from  
515 the deformation front (Figure 8A), and includes deep moderate size flat-thrust earthquakes between 40-  
516 50 km depth and 190-200 km distance from the deformation front. This seismicity corresponds to  
517 calculated temperatures ranging from  $200^\circ\text{C}$  and  $450^\circ\text{C}$  at the slab top, while the upper-plate Moho  
518 intersects the subduction interface at  $\sim 28$  km depth and temperature of  $\sim 210^\circ\text{C}$ . The interplate  
519 seismogenic zone thus extends downdip of the upper-plate Moho, consistently with other cold  
520 subduction zones, e.g. Tohoku, where flat-thrust earthquakes are observed at similar depth in the Mantle  
521 (Uchida & Matsuzawa, 2011). Thermal models predict a cold forearc mantle above the location of the

522 Mw 5 flat-thrust event (Figure 8A), and downdip slab dehydration, with updip fluid migration into the  
523 mantle wedge, favourable for serpentinization reaction to occur. This result suggests that dry peridotite  
524 in the mantle is unlikely, rather, tilts towards existing hypothesis of chemical heterogeneity of the mantle  
525 corner (Laigle et al., 2013a) as mechanism for this “deep flat-thrust” earthquakes. The interplate contact  
526 beneath the forearc, from the trench to 110-125 km distance westward (Table 1), corresponds to  
527 temperatures lower than 150°C, frequently considered as poorly, or conditionally favorable to stick-slip  
528 behavior. Hence, temperatures lower than 100°C below the accretionary prism make seismic rupture up  
529 to the trench very unlikely. Thus, the thermal models highlight a deep “thermally-defined seismogenic  
530 zone” (i.e. 150° - 350°C temperature range), typical of cold subduction zones, associated with intense  
531 fluid circulation from the subduction depth to the trench.

532 These features shed light on the mechanical conditions and the sliding behavior along the interplate  
533 contact at the Lesser Antilles. Geodetic modelling predict very low interplate coupling (van Rijnsingen  
534 et al., 2021) consistent with scarce interplate thrust earthquakes mostly aggregated in two local clusters  
535 (Hayes et al., 2013) (see details in §2.2). Intense fluid circulation, as suggested by the thermal models,  
536 is able to increase the pore-fluid pressure, reducing the effective stress along the interplate contact  
537 (Moreno et al., 2014). A heterogeneous reduction of this effective stress may generate an interplate  
538 patchiness of contrasting frictional properties. Moreover, the rheology of low-temperature species of  
539 serpentine minerals results in substantial weakening of serpentine-bearing faults and crustal rocks  
540 formed and altered at tectonically-dominated slow-spreading segments ridges (eg. Escartin et al., 1997).  
541 The ongoing subduction of tectonically-dominated oceanic patches, such as the Jacksonville patch  
542 identified at the trench (Marcaillou et al., 2021), may also favor this heterogeneity in interplate frictional  
543 properties. In subduction zones, the patchiness of contrasting frictional properties may impede large-  
544 scale zones of full interplate coupling (Hirauchi et al., 2010), instead favoring a mix of stable and  
545 unstable behaviors prone to triggering moderate-sized-Mw, slow-slip and/or very-low frequency  
546 earthquakes (Saffer & Wallace, 2015), and increasing time return of large co-seismic rupture.

## 547 **Conclusion**

548 Thermal models of the Lesser Antilles Subduction Zone, based on heat-flow data recorded during  
549 Antithesis 1 cruise (2013), show that fluid-driven heat advection strongly influences the heat transfer  
550 across the margin. Moreover, variations in heat-flow anomalies, compared to the regional conductive  
551 heat-flow, highlight the varying fluid flow pattern from ventilated to insulated circulation systems.

552 In the Central Lesser Antilles, offshore of Martinique, warm fluids released at depths in the  
553 subduction zone migrate updip along the subduction interface generating hydrothermal warming in the  
554 trench and at the margin front. The low level of fluid exchange with the water column is typical of  
555 insulated systems. Contrastingly, in the Northern Lesser Antilles, offshore of Saint Martin, downward  
556 percolation of cold fluids through crustal detachment faults in the trench triggers hydrothermal cooling  
557 at the margin front, while warm fluid upward migration through major fault zones in the forearc

558 generates hydrothermal warming in the margin. These interpreted vigorous fluid exchanges with the  
559 water column are typical of ventilated systems.

560 Based on the model offshore Martinique, we show that intraslab, supraslab, and interplate seismicity  
561 distribution has a close relationship with temperature-related dehydration reactions at depth in the  
562 subduction. It is noteworthy that typical temperature and depth of eclogitisation and deserpentinisation  
563 reactions correspond to intraslab and supraslab seismicity clusters. Consistently with previous tectonic  
564 investigations, these thermal models confirm that the Northern Lesser Antilles is an end member  
565 subduction zone where the subduction of oceanic transform fault zones and oceanic patches partly made  
566 of exhumed and serpentinised mantle rocks deeply hydrate the subduction zone at depth. This “hyper-  
567 hydration” likely explains the very low interplate coupling and the scarce large co-seismic ruptures,  
568 possibly favoring alternate mode of sliding behavior, such as low velocity earthquakes, which are yet to  
569 be investigated.

#### 570 **CRedit authorship contribution statement**

571 **K.E.** wrote the manuscript. **K.E.**, and **Y.B.** performed the thermal modelling supervised by **B.M.** and  
572 **M.L. B.M., F.K., J.-F.L., F.R., A.H., T.P., F.L., M.P., M.L.** and **B.H.** were onboard RVs “l’Atalante”  
573 and “Pourquoi Pas?” during the ANTITHESIS cruise and acquired the heat-flow data. All authors  
574 discussed the scientific issues and commented on the manuscript.

#### 575 **Declaration of Competing Interest**

576 The authors declare that they have no known competing financial interests or personal relationships  
577 that could have appeared to influence the work reported in this paper.

#### 578 **Acknowledgments**

579 We thank the crew and the scientific party of the R/V “*Pourquoi Pas?*” for the heat-flow acquisition  
580 during marine surveys ANTITHESIS 1, leg 2. The thesis of Kingsley Ezenwaka is funded by the  
581 Petroleum Technology Development Fund (PTDF). We gratefully acknowledge Kelin Wang for  
582 providing the optimized version of the thermal modelling code.

#### 583 **References**

- 584 Beardmore, G. R., & Cull, J. P. (2010). Heat Flow. *Crustal Heat Flow*, 207–236.  
585 <https://doi.org/10.1017/cbo9780511606021.007>
- 586 Bernard, P., & Lambert, J. (1988). Subduction and seismic hazard in the northern Lesser Antilles:  
587 revision of the historical seismicity. *Bulletin - Seismological Society of America*, 78(6), 1965–  
588 1983.
- 589 Bie, L., Hicks, S., Rietbrock, A., Goes, S., Collier, J., Rychert, C., Harmon, N., & Maunder, B. (2022).  
590 Imaging slab-transported fluids and their deep dehydration from seismic velocity tomography in  
591 the Lesser Antilles subduction zone. *Earth and Planetary Science Letters*, 586, 117535.  
592 <https://doi.org/10.1016/j.epsl.2022.117535>



- 593 Bie, L., Rietbrock, A., Hicks, S., Allen, R., Blundy, J., Clouard, V., Collier, J., Davidson, J., Garth, T.,  
594 Goes, S., Harmon, N., Henstock, T., Van Hunen, J., Kendall, M., Krüger, F., Lynch, L.,  
595 Macpherson, C., Robertson, R., Rychert, K., ... Wilson, M. (2019). Along-arc heterogeneity in  
596 local seismicity across the Lesser Antilles subduction zone from a dense ocean-bottom  
597 seismometer network. *Seismological Research Letters*, *91*(1), 237–247.  
598 <https://doi.org/10.1785/0220190147>
- 599 Boucard, M., Marcaillou, B., Lebrun, J. F., Laurencin, M., Klingelhoefer, F., Laigle, M., Lallemand, S.,  
600 Schenini, L., Graindorge, D., Cornée, J. J., Münch, P., Philippon, M., & the, A. (2021). Paleogene  
601 V-Shaped Basins and Neogene Subsidence of the Northern Lesser Antilles Forearc. *Tectonics*,  
602 *40*(3), 1–18. <https://doi.org/10.1029/2020TC006524>
- 603 Braszus, B., Goes, S., Allen, R., Rietbrock, A., Collier, J., Harmon, N., Henstock, T., Hicks, S., Rychert,  
604 C. A., Maunder, B., van Hunen, J., Bie, L., Blundy, J., Cooper, G., Davy, R., Kendall, J. M.,  
605 Macpherson, C., Wilkinson, J., & Wilson, M. (2021). Subduction history of the Caribbean from  
606 upper-mantle seismic imaging and plate reconstruction. *Nature Communications*, *12*(1).  
607 <https://doi.org/10.1038/s41467-021-24413-0>
- 608 Byerlee, J. (1993). Model for episodic flow of high-pressure water in fault zones before earthquakes.  
609 *Geology*, *21*(4), 303–306. [https://doi.org/10.1130/0091-](https://doi.org/10.1130/0091-7613(1993)021<0303:MFEFOH>2.3.CO;2)  
610 [7613\(1993\)021<0303:MFEFOH>2.3.CO;2](https://doi.org/10.1130/0091-7613(1993)021<0303:MFEFOH>2.3.CO;2)
- 611 Calahorrano B., A., Sallarès, V., Collot, J. Y., Sage, F., & Ranero, C. R. (2008). Nonlinear variations of  
612 the physical properties along the southern Ecuador subduction channel: Results from depth-  
613 migrated seismic data. *Earth and Planetary Science Letters*, *267*(3–4), 453–467.  
614 <https://doi.org/10.1016/j.epsl.2007.11.061>
- 615 Cannat, M., Sauter, D., Mendel, V., Ruellan, E., Okino, K., Escartin, J., Combier, V., & Baala, M.  
616 (2006). Modes of seafloor generation at a melt-poor ultraslow-spreading ridge. *Geology*, *34*(7),  
617 605–608. <https://doi.org/10.1130/G22486.1>
- 618 Carpentier, M., Chauvel, C., & Mattielli, N. (2008). Pb-Nd isotopic constraints on sedimentary input  
619 into the Lesser Antilles arc system. *Earth and Planetary Science Letters*, *272*(1–2), 199–211.  
620 <https://doi.org/10.1016/j.epsl.2008.04.036>
- 621 Cooper, G. F., Macpherson, C. G., Blundy, J. D., Maunder, B., Allen, R. W., Goes, S., Collier, J. S.,  
622 Bie, L., Harmon, N., Hicks, S. P., Iveson, A. A., Prytulak, J., Rietbrock, A., Rychert, C. A.,  
623 Davidson, J. P., Cooper, G. F., Macpherson, C. G., Blundy, J. D., Maunder, B., ... Wilson, M.  
624 (2020). Variable water input controls evolution of the Lesser Antilles volcanic arc. *Nature*,  
625 *582*(7813), 525–529. <https://doi.org/10.1038/s41586-020-2407-5>
- 626 Davey, F. J., & Ristau, J. (2011). Fore-arc mantle wedge seismicity under northeast New Zealand.  
627 *Tectonophysics*, *509*(3–4), 272–279. <https://doi.org/10.1016/j.tecto.2011.06.017>

- 628 Davy, R. G., Collier, J. S., Henstock, T. J., Rietbrock, A., Goes, S., Blundy, J., Harmon, N., Rychert,  
629 C., Macpherson, C. G., Van Hunen, J., Kendall, M., Wilkinson, J., Davidson, J., Wilson, M.,  
630 Cooper, G., Maunder, B., Bie, L., Hicks, S., Allen, R., ... Labahn, E. (2020). Wide-Angle Seismic  
631 Imaging of Two Modes of Crustal Accretion in Mature Atlantic Ocean Crust. *Journal of*  
632 *Geophysical Research: Solid Earth*, 125(6), 1–21. <https://doi.org/10.1029/2019JB019100>
- 633 De Min, L., Lebrun, J. F., Cornée, J. J., Münch, P., Léticée, J. L., Quillévére, F., Melinte-Dobrinescu,  
634 M., Randrianasolo, A., Marcaillou, B., & Zami, F. (2015). Tectonic and sedimentary architecture  
635 of the Karukéra spur: A record of the Lesser Antilles fore-arc deformations since the Neogene.  
636 *Marine Geology*, 363, 15–37. <https://doi.org/10.1016/j.margeo.2015.02.007>
- 637 DeMets, C., Jansma, P. E., Mattioli, G. S., Dixon, T. H., Farina, F., Bilham, R., Calais, E., & Mann, P.  
638 (2000). GPS geodetic constraints on Caribbean-North America Plate Motion. *Geophysical*  
639 *Research Letters*, 27(3), 437–440. <https://doi.org/10.1029/1999gl005436>
- 640 Dziewonski, A. M., Chou, T. A., & Woodhouse, J. H. (1981). Determination of earthquake source  
641 parameters from waveform data for studies of global and regional seismicity. *Journal of*  
642 *Geophysical Research*, 86(B4), 2825–2852. <https://doi.org/10.1029/JB086iB04p02825>
- 643 Ekström, G., Nettles, M., & Dziewoński, A. M. (2012). The global CMT project 2004–2010: Centroid-  
644 moment tensors for 13,017 earthquakes. *Physics of the Earth and Planetary Interiors*, 200–201,  
645 1–9. <https://doi.org/10.1016/j.pepi.2012.04.002>
- 646 Escartin, J., Hirth, J. G., & Evans, B. (1997). Effects of serpentization on the lithospheric strength  
647 and the style of normal faulting at slow-spreading ridges. *Earth and Planetary Science Letters*,  
648 151, 181–189.
- 649 Escartín, J., Smith, D. K., Cann, J., Schouten, H., Langmuir, C. H., & Escrig, S. (2008). Central role of  
650 detachment faults in accretion of slow-spreading oceanic lithosphere. *Nature*, 455(7214), 790–  
651 794. <https://doi.org/10.1038/nature07333>
- 652 Evain, M., Galve, A., Charvis, P., Laigle, M., Kopp, H., Bécel, A., Weinzierl, W., Hirn, A., Flueh, E.  
653 R., & Gallart, J. (2013). Structure of the Lesser Antilles subduction forearc and backstop from 3D  
654 seismic refraction tomography. *Tectonophysics*, 603, 55–67.  
655 <https://doi.org/10.1016/j.tecto.2011.09.021>
- 656 Faccenda, M., Gerya, T. V., Mancktelow, N. S., & Moresi, L. (2012). Fluid flow during slab unbending  
657 and dehydration: Implications for intermediate-depth seismicity, slab weakening and deep water  
658 recycling. *Geochemistry, Geophysics, Geosystems*, 13(1). <https://doi.org/10.1029/2011GC003860>
- 659 Ferrand, T. P. (2019). Seismicity and mineral destabilizations in the subducting mantle up to 6 GPa,  
660 200 km depth. *Lithos*, 334–335, 205–230. <https://doi.org/10.1016/j.lithos.2019.03.014>
- 661 Feuillet, N., Beauducel, F., & Tapponnier, P. (2011). Tectonic context of moderate to large historical  
662 earthquakes in the Lesser Antilles and mechanical coupling with volcanoes. *Journal of*

663 *Geophysical Research: Solid Earth*, 116(10), 1–26. <https://doi.org/10.1029/2011JB008443>

664 Fisher, A. T., & Becker, K. (2000). Channelized fluid flow in oceanic crest reconciles heat-flow and  
665 permeability data. *Nature*, 403(6765), 71–74. <https://doi.org/10.1038/47463>

666 Gutscher, M. A., Westbrook, G. K., Marcaillou, B., Graindorge, D., Gailler, A., Pichot, T., & Maury,  
667 R. C. (2013). How wide is the seismogenic zone of the Lesser Antilles forearc? *Bulletin de La*  
668 *Societe Geologique de France*, 184(1–2), 47–59. <https://doi.org/10.2113/gssgfbull.184.1-2.47>

669 Hacker, B. R., Abers, G. A., & Peacock, S. M. (2003). Subduction factory 1. Theoretical mineralogy,  
670 densities, seismic wave speeds, and H<sub>2</sub>O contents. *Journal of Geophysical Research: Solid*  
671 *Earth*, 108(B1), 1–26. <https://doi.org/10.1029/2001jb001127>

672 Hacker, B. R., Peacock, S. M., Abers, G. A., & Holloway, S. D. (2003). Subduction factory 2. Are  
673 intermediate-depth earthquakes in subducting slabs linked to metamorphic dehydration reactions?  
674 *Journal of Geophysical Research: Solid Earth*, 108(B1). <https://doi.org/10.1029/2001jb001129>

675 Harris, R. N., Spinelli, G. A., & Fisher, A. T. (2017). Hydrothermal circulation and the thermal structure  
676 of shallow subduction zones. *Geosphere*, 13(5), 1425–1444. <https://doi.org/10.1130/GES01498.1>

677 Harris, R. N., Spinelli, G. A., & Hutnak, M. (2020). Heat Flow Evidence for Hydrothermal Circulation  
678 in Oceanic Crust Offshore Grays Harbor, Washington. *Geochemistry, Geophysics, Geosystems*,  
679 21(6), 0–2. <https://doi.org/10.1029/2019GC008879>

680 Harris, R. N., Spinelli, G., Ranero, C. R., Grevemeyer, I., Villinger, H., & Barckhausen, U. (2010).  
681 Thermal regime of the Costa Rican convergent margin: 2. Thermal models of the shallow Middle  
682 America subduction zone offshore Costa Rica. *Geochemistry, Geophysics, Geosystems*, 11(12), 1–  
683 22. <https://doi.org/10.1029/2010GC003273>

684 Harris, R. N., & Wang, K. (2002). Thermal models of the Middle America Trench at the Nicoya  
685 Peninsula, Costa Rica. *Geophysical Research Letters*, 29(21), 6-1-6-4.  
686 <https://doi.org/10.1029/2002GL015406>

687 Hayes, G. P., McNamara, D. E., Seidman, L., & Roger, J. (2013). Quantifying potential earthquake and  
688 tsunami hazard in the Lesser Antilles subduction zone of the Caribbean region. *Geophysical*  
689 *Journal International*, 196(1), 510–521. <https://doi.org/10.1093/gji/ggt385>

690 Hirauchi, K. I., Katayama, I., Uehara, S., Miyahara, M., & Takai, Y. (2010). Inhibition of subduction  
691 thrust earthquakes by low-temperature plastic flow in serpentine. *Earth and Planetary Science*  
692 *Letters*, 295(3–4), 349–357. <https://doi.org/10.1016/j.epsl.2010.04.007>

693 Hough, S. E. (2013). Missing great earthquakes. *Journal of Geophysical Research: Solid Earth*, 118(3),  
694 1098–1108. <https://doi.org/10.1002/jgrb.50083>

695 Hutchison, I. (1985). The effects of sedimentation and compaction on oceanic heat flow. *Development*,  
696 82, 439–459.

697 Hyndman, R. D., & Wang, K. (1993). Thermal constraints on the zone of major thrust earthquake failure:

698 the Cascadia Subduction Zone. *Journal of Geophysical Research*, 98(B2), 2039–2060.  
699 <https://doi.org/10.1029/92JB02279>

700 Hyndman, R. D., Wang, K., & Yamano, M. (1995). Thermal constraints on the seismogenic portion of  
701 the southwestern Japan subduction thrust. *Journal of Geophysical Research*, 100(15), 373–392.

702 Hyndman, R. D., Yamano, M., & Oleskevich, D. A. (1997). The seismogenic zone of subduction thrust  
703 faults. *Island Arc*, 6(3), 244–260. <https://doi.org/10.1111/j.1440-1738.1997.tb00175.x>

704 Ildefonse, B., Blackman, D. K., John, B. E., Ohara, Y., Miller, D. J., MacLeod, C. J., Abe, N., Abratis,  
705 M., Andal, E. S., Andréani, M., Awaji, S., Beard, J. S., Brunelli, D., Charney, A. B., Christie, D.  
706 M., Delacour, A. G., Delius, H., Drouin, M., Einaudi, F., ... Zhao, X. (2007). Oceanic core  
707 complexes and crustal accretion at slow-spreading ridges. *Geology*, 35(7), 623–626.  
708 <https://doi.org/10.1130/G23531A.1>

709 Kirby, S., Engdahl, E. R., & Denlinger, R. (1996). Intermediate-depth intraslab earthquakes and arc  
710 volcanism as physical expressions of crustal and uppermost mantle metamorphism in subducting  
711 slabs. *Geophysical Monograph Series*, 96, 195–214. <https://doi.org/10.1029/GM096p0195>

712 Klingelhoefer, F., Marcaillou, B., Laurencin, M., Biari, Y., Laigle, M., Graindorge, D., Evain, M.,  
713 Lebrun, J.-F., & Paulatto, M. (2018). Relation Between the Nature of the Subducting Plate, Heat  
714 Flow and Fluid Escape Structures at the Lesser Antilles Island arc. *American Geophysical Union*  
715 *Fall Meeting, Wahsington, DC, USA, T22B-04*, 10–14.

716 Kodaira, S., Iidaka, T., Kato, A., Park, J. O., Iwasaki, T., & Kaneda, Y. (2004). High pore fluid pressure  
717 may cause silent slip in the Nankai Trough. *Science*, 304(5675), 1295–1298.  
718 <https://doi.org/10.1126/science.1096535>

719 Kopp, H., Weinzierl, W., Becel, A., Charvis, P., Evain, M., Flueh, E. R., Gailler, A., Galve, A., Hirn,  
720 A., Kandilarov, A., Klaeschen, D., Laigle, M., Papenberg, C., Planert, L., & Roux, E. (2011). Deep  
721 structure of the central Lesser Antilles Island Arc: Relevance for the formation of continental crust.  
722 *Earth and Planetary Science Letters*, 304(1–2), 121–134.  
723 <https://doi.org/10.1016/j.epsl.2011.01.024>

724 Kummer, T., & Spinelli, G. A. (2008). Hydrothermal circulation in subducting crust reduces subduction  
725 zone temperatures. *Geology*, 36(1), 91–94. <https://doi.org/10.1130/G24128A.1>

726 Laigle, M., Hirn, A., Sapin, M., Bécel, A., Charvis, P., Flueh, E., Diaz, J., Lebrun, J. F., Gesret, A.,  
727 Raffaele, R., Galvé, A., Evain, M., Ruiz, M., Kopp, H., Bayrakci, G., Weinzierl, W., Hello, Y.,  
728 Lépine, J. C., Viodé, J. P., ... Nicolich, R. (2013b). Seismic structure and activity of the north-  
729 central Lesser Antilles subduction zone from an integrated approach: Similarities with the Tohoku  
730 forearc. *Tectonophysics*, 603, 1–20. <https://doi.org/10.1016/j.tecto.2013.05.043>

731 Laigle, M, Becel, A., de Voogd, B., Sachpazi, M., Bayrakci, G., Lebrun, J. F., & Evain, M. (2013a).  
732 Along-arc segmentation and interaction of subducting ridges with the Lesser Antilles Subduction

733 forearc crust revealed by MCS imaging. *Tectonophysics*, 603, 32–54.  
734 <https://doi.org/10.1016/j.tecto.2013.05.028>

735 Laurencin, M., Graindorge, D., Klingelhofer, F., Marcaillou, B., & Evain, M. (2018). Influence of  
736 increasing convergence obliquity and shallow slab geometry onto tectonic deformation and  
737 seismogenic behavior along the Northern Lesser Antilles zone. *Earth and Planetary Science  
738 Letters*, 492, 59–72. <https://doi.org/10.1016/j.epsl.2018.03.048>

739 Laurencin, M., Marcaillou, B., Graindorge, D., Klingelhofer, F., Lallemand, S., Laigle, M., & Lebrun,  
740 J. F. (2017). The polyphased tectonic evolution of the Anegada Passage in the northern Lesser  
741 Antilles subduction zone. *Tectonics*, 36(5), 945–961. <https://doi.org/10.1002/2017TC004511>

742 Laurencin, M., Marcaillou, B., Graindorge, D., Lebrun, J. F., Klingelhofer, F., Boucard, M., Laigle,  
743 M., Lallemand, S., & Schenini, L. (2019). The Bunce Fault and Strain Partitioning in the Northern  
744 Lesser Antilles. *Geophysical Research Letters*, 46(16), 9573–9582.  
745 <https://doi.org/10.1029/2019GL083490>

746 Lucazeau, F. (2019). Analysis and Mapping of an Updated Terrestrial Heat Flow Data Set.  
747 *Geochemistry, Geophysics, Geosystems*, 20(8), 4001–4024.  
748 <https://doi.org/10.1029/2019GC008389>

749 Manga, M., Hornbach, M. J., Le Friant, A., Ishizuka, O., Stroncik, N., Adachi, T., Aljhdali, M.,  
750 Boudon, G., Breitzkreuz, C., Fraass, A., Fujinawa, A., Hatfield, R., Jutzeler, M., Kataoka, K.,  
751 Lafuerza, S., Maeno, F., Martinez-Colon, M., McCanta, M., Morgan, S., ... Wang, F. (2012). Heat  
752 flow in the Lesser Antilles island arc and adjacent back arc Grenada basin. *Geochemistry,  
753 Geophysics, Geosystems*, 13(8), 1–19. <https://doi.org/10.1029/2012GC004260>

754 Marcaillou, B., & Klingelhofer, F. (2013a). *ANTITHESIS-1-Leg1 Cruise, RV L'Atalante*.  
755 <https://doi.org/doi:10.17600/13010070>

756 Marcaillou, B., & Klingelhofer, F. (2013b). *ANTITHESIS-1-Leg2 Cruise, RV Pourquoi Pas?*  
757 <https://doi.org/doi:10.17600/13030100>

758 Marcaillou, B., & Klingelhofer, F. (2016). *ANTITHESIS-3 Cruise, RV Pourquoi Pas?*  
759 <https://doi.org/doi:10.17600/16001700>

760 Marcaillou, B., Klingelhofer, F., Laurencin, M., Lebrun, J.-F., Laigle, M., Lallemand, S., Schenini, L.,  
761 Gay, A., Boucard, M., Ezenwaka, K., & Graindorge, D. (2021). Pervasive detachment faults within  
762 the slow spreading oceanic crust at the poorly coupled Antilles subduction zone. *Communications  
763 Earth & Environment*, 2(1). <https://doi.org/10.1038/s43247-021-00269-6>

764 Marcaillou, B., Spence, G., Wang, K., Collot, J. Y., & Ribodetti, A. (2008). Thermal segmentation along  
765 the N. Ecuador-S. Colombia margin (1–4°N): Prominent influence of sedimentation rate in the  
766 trench. *Earth and Planetary Science Letters*, 272(1–2), 296–308.  
767 <https://doi.org/10.1016/j.epsl.2008.04.049>

768 Moore, J. C., & Saffer, D. (2001). Updip limit of the seismogenic zone beneath the accretionary prism  
769 of Southwest Japan: An effect of diagenetic to low-grade metamorphic processes and increasing  
770 effective stress. *Geology*, 29(2), 183–186. [https://doi.org/10.1130/0091-](https://doi.org/10.1130/0091-7613(2001)029<0183:ULOTSZ>2.0.CO;2)  
771 [7613\(2001\)029<0183:ULOTSZ>2.0.CO;2](https://doi.org/10.1130/0091-7613(2001)029<0183:ULOTSZ>2.0.CO;2)

772 Moreno, M., Haberland, C., Oncken, O., Rietbrock, A., Angiboust, S., & Heidbach, O. (2014). Locking  
773 of the Chile subduction zone controlled by fluid pressure before the 2010 earthquake. *Nature*  
774 *Geoscience*, 7(4), 292–296. <https://doi.org/10.1038/ngeo2102>

775 Müller, R. D., Zahirovic, S., Williams, S. E., Cannon, J., Seton, M., Bower, D. J., Tetley, M. G., Heine,  
776 C., Le Breton, E., Liu, S., Russell, S. H. J., Yang, T., Leonard, J., & Gurnis, M. (2019). A Global  
777 Plate Model Including Lithospheric Deformation Along Major Rifts and Orogens Since the  
778 Triassic. *Tectonics*, 38(6), 1884–1907. <https://doi.org/10.1029/2018TC005462>

779 Parnell-Turner, R., Sohn, R. A., Peirce, C., Reston, T. J., MacLeod, C. J., Searle, R. C., & Simão, N. M.  
780 (2017). Oceanic detachment faults generate compression in extension. *Geology*, 45(10), 923–926.  
781 <https://doi.org/10.1130/G39232.1>

782 Paulatto, M., Laigle, M., Galve, A., Charvis, P., Sapin, M., Bayrakci, G., Evain, M., & Kopp, H. (2017).  
783 Dehydration of subducting slow-spread oceanic lithosphere in the Lesser Antilles. *Nature*  
784 *Communications*, 8, 240. <https://doi.org/10.1038/ncomms15980>

785 Pecher, I. A., Villinger, H., Kaul, N., Crutchley, G. J., Mountjoy, J. J., Huhn, K., Kukowski, N., Henrys,  
786 S. A., Rose, P. S., & Coffin, R. B. (2017). A Fluid Pulse on the Hikurangi Subduction Margin:  
787 Evidence From a Heat Flux Transect Across the Upper Limit of Gas Hydrate Stability.  
788 *Geophysical Research Letters*, 44(24), 12,385–12,395. <https://doi.org/10.1002/2017GL076368>

789 Philibosian, B., Feuillet, N., Weil-Accardo, J., Jacques, E., Guihou, A., Mériaux, A. S., Anglade, A.,  
790 Saurel, J. M., & Deroussi, S. (2022). 20th-century strain accumulation on the Lesser Antilles  
791 megathrust based on coral microatolls. *Earth and Planetary Science Letters*, 579, 117343.  
792 <https://doi.org/10.1016/j.epsl.2021.117343>

793 Pichot, T., Patriat, M., Westbrook, G. K., Nalpas, T., Gutscher, M. A., Roest, W. R., Deville, E., Moulin,  
794 M., Aslanian, D., & Rabineau, M. (2012). The Cenozoic tectonostratigraphic evolution of the  
795 Barracuda Ridge and Tiburon Rise, at the western end of the North America-South America plate  
796 boundary zone. *Marine Geology*, 303–306, 154–171.  
797 <https://doi.org/10.1016/j.margeo.2012.02.001>

798 Ranero, C. R., Morgan, J. P., McIntosh, K. D., & Reichert, C. (2003). Bending-related faulting and  
799 mantle serpentinization at the Middle America trench. *Nature*, 425, 367–373.

800 Saffer, D. M., & Tobin, H. J. (2011). Hydrogeology and mechanics of subduction zone forearcs: Fluid  
801 flow and pore pressure. *Annual Review of Earth and Planetary Sciences*, 39, 157–186.  
802 <https://doi.org/10.1146/annurev-earth-040610-133408>

- 803 Saffer, D. M., & Wallace, L. M. (2015). The frictional, hydrologic, metamorphic and thermal habitat of  
804 shallow slow earthquakes. *Nature Geoscience*, 8(8), 594–600. <https://doi.org/10.1038/ngeo2490>
- 805 Schlaphorst, D., Kendall, J. M., Collier, J. S., Verdon, J. P., Blundy, J., Baptie, B., Latchman, J. L.,  
806 Massin, F., & Bouin, M. P. (2016). Water, oceanic fracture zones and the lubrication of subducting  
807 plate boundaries-insights from seismicity. *Geophysical Journal International*, 204(3), 1405–1420.  
808 <https://doi.org/10.1093/gji/ggv509>
- 809 Sibson, R. H. (2013). Stress switching in subduction forearcs: Implications for overpressure containment  
810 and strength cycling on megathrusts. *Tectonophysics*, 600, 142–152.  
811 <https://doi.org/10.1016/j.tecto.2013.02.035>
- 812 Spinelli, G. A., & Wang, K. (2008). Effects of fluid circulation in subducting crust on Nankai margin  
813 seismogenic zone temperatures. *Geology*, 36(11), 887–890. <https://doi.org/10.1130/G25145A.1>
- 814 Spinelli, G., Wada, I., Wang, K., He, J., Harris, R., & Underwood, M. (2018). Diagenetic, metamorphic,  
815 and hydrogeologic consequences of hydrothermal circulation in subducting crust. *Geosphere*,  
816 14(6), 2337–2354. <https://doi.org/10.1130/GES01653.1>
- 817 Stein, C. A., & Stein, S. (1994). Constraints on hydrothermal heat flux through the oceanic lithosphere  
818 from global heat flow. *Journal of Geophysical Research*, 99(B2), 3081–3095.  
819 <https://doi.org/10.1029/93JB02222>
- 820 Szitkar, F., Dymant, J., Petersen, S., Bialas, J., Klischies, M., Graber, S., Klaeschen, D., Yeo, I., &  
821 Murton, B. J. (2019). Detachment tectonics at Mid-Atlantic Ridge 26°N. *Scientific Reports*, 9(1),  
822 0–8. <https://doi.org/10.1038/s41598-019-47974-z>
- 823 Tse, S. T., & Rice, J. R. (1986). Crustal earthquake instability in relation to the depth variation of  
824 frictional slip properties. *Journal of Geophysical Research*, 91(B9), 9452.  
825 <https://doi.org/10.1029/jb091ib09p09452>
- 826 Tucholke, B. E., Lin, J., & Kleinrock, M. C. (1998). Megamullions and mullion structure defining  
827 oceanic metamorphic core complexes on the Mid-Atlantic Ridge. *Journal of Geophysical*  
828 *Research: Solid Earth*, 103(5), 9857–9866. <https://doi.org/10.1029/98jb00167>
- 829 Uchida, N., & Matsuzawa, T. (2011). Coupling coefficient, hierarchical structure, and earthquake cycle  
830 for the source area of the 2011 off the Pacific coast of Tohoku earthquake inferred from small  
831 repeating earthquake data. *Earth, Planets and Space*, 63(7), 675–679.  
832 <https://doi.org/10.5047/eps.2011.07.006>
- 833 Ulmer, P., & Trommsdorff, V. (1995). Serpentine stability to mantle depths and subduction-related  
834 magmatism. *Science*, 268(5212), 858–861. <https://doi.org/10.1126/science.268.5212.858>
- 835 Van Keken, P. E., Hacker, B. R., Syracuse, E. M., & Abers, G. A. (2011). Subduction factory: 4. Depth-  
836 dependent flux of H<sub>2</sub>O from subducting slabs worldwide. *Journal of Geophysical Research: Solid*  
837 *Earth*, 116(1). <https://doi.org/10.1029/2010JB007922>

- 838 van Rijnsingen, E. M., Calais, E., Jolivet, R., de Chabalier, J.-B., Robertson, R., Ryan, G. A., & Smithe,  
839 S. (2022). Ongoing tectonic subsidence in the Lesser Antilles subduction zone. *Geophysical*  
840 *Journal International*, 319–326. <https://doi.org/10.1093/gji/ggac192>
- 841 van Rijnsingen, E. M., Calais, E., Jolivet, R., de Chabalier, J. B., Jara, J., Smithe, S., Robertson, R., &  
842 Ryan, G. A. (2021). Inferring Interseismic Coupling Along the Lesser Antilles Arc: A Bayesian  
843 Approach. *Journal of Geophysical Research: Solid Earth*, 126(2), 1–21.  
844 <https://doi.org/10.1029/2020JB020677>
- 845 Vrolijk, P. (1990). On the mechanical role of smectite in subduction zones. *Geology*, 18(8), 703–707.  
846 [https://doi.org/10.1130/0091-7613\(1990\)018<0703:OTMROS>2.3.CO;2](https://doi.org/10.1130/0091-7613(1990)018<0703:OTMROS>2.3.CO;2)
- 847 Wang, K., He, J., & Davis, E. E. (1997). Influence of basement topography on hydrothermal circulation  
848 in sediment-buried igneous oceanic crust. *Earth and Planetary Science Letters*, 146(1–2), 151–  
849 164. [https://doi.org/10.1016/s0012-821x\(96\)00213-0](https://doi.org/10.1016/s0012-821x(96)00213-0)
- 850 Wang, K., Hyndman, R. D., & Yamano, M. (1995). Thermal regime of the Southwest Japan subduction  
851 zone: effects of age history of the subducting plate. *Tectonophysics*, 248(1–2), 53–69.  
852 [https://doi.org/10.1016/0040-1951\(95\)00028-L](https://doi.org/10.1016/0040-1951(95)00028-L)
- 853 White, R. S., McKenzie, D., & Nions, K. O. (1992). Oceanic Crustal Thickness From Seismic  
854 Measurements and Rare Earth Element Inversions. *Journal of Geophysical Research*, 97(B13),  
855 19,683–19,715.
- 856 Wunder, B., & Schreyer, W. (1997). Antigorite: High-pressure stability in the system MgO-SiO<sub>2</sub>-H<sub>2</sub>O  
857 (MSH). *Lithos*, 41(1–3), 213–227. [https://doi.org/10.1016/s0024-4937\(97\)82013-0](https://doi.org/10.1016/s0024-4937(97)82013-0)
- 858



## Chapter 4

### **The tectonic impact of fluids and subducting ridges on the Northern Lesser Antilles margin**

In the previous chapter, we show the distinct nature of the oceanic crust that is entering the subduction zone especially within the Northern Lesser Antilles. The crust, formed at slow-spreading Mid-Atlantic Ridge likely possess patches of exhumed and hydrated mantle rocks. As we discussed, the highly pervasive fractured oceanic basement that we imaged in the Jacksonville Patch favours fluid percolation and serpentinization. Moreover, the 15-20 fracture zone, which deeply incise the oceanic crust and favour mantle rock serpentinisation before subduction, is located at depth beneath the inner forearc in this region. All these features are likely to introduce a high volume of fluid into the subduction system.

Consistently, measured heat-flow values in the forearc off St Martin segment are too high to be resolved with a thermal conductive model. These high values are most likely to be related to fluids that invade the forearc and migrates through deep-rooted faults up to the seafloor, where they percolate at numerous pockmarks and mud volcanoes. In addition, the topographic Barracuda Ridge has been interacting with the northern margin and sweeping south since its uplift.

Bearing all these tectonic features in mind for the northern Lesser Antilles margin, in this chapter, we investigate the respective impacts of fluid upward migration and Barracuda Ridge subduction onto the margin tectonic deformation. We use integrated MCS, high-resolution seismic data and bathymetric data to interpret the tectonic evolution of this margin segment. The results highlight a globally erosive margin segment, which has undergone minor and temporary accretion phases that decrease northwards.

In the forearc, normal faults subparallel to the ridge characterize the southward sweeping Barracuda Ridge, and highlights its possible initiation point beneath the forearc. Most of the faults are deeply-rooted and fracture the basement, forming pathways for fluid migration up-to the seafloor. Typical features in seismic lines, such as, deep penetrating fluid pipes and reverse polarities attest for fluid accumulation and circulation. The fluid pipes rise up to the seafloor where they coincide with locations of pockmarks and volcanoes observed on the bathymetry, highlighting again, massive fluid occurrence in the NLA forearc margin. In addition, the fluid-related features on the seafloor correspond with deeply fractured, eroded and subsiding forearc

area. At last, we record widespread margin subsidence and basement thinning, which cannot be accounted for by the displacements along the deeply-rooted faults. The rate of subsidence is consistent with previous estimate to the north of our study area.

Following these observations, we propose that the Northern Lesser Antilles margin has undergone long-term frontal and basal tectonic erosion dominated by the tectonic impact of circulating fluids and more recently increased by the southward sweeping of the subducting Barracuda Ridge.

Our results and the discussions in this chapter are presented in the form of a paper that is in preparation and which will be submitted for publication shortly.

ImP Prep

# Mechanism of tectonic erosion at the Northern Lesser Antilles margin

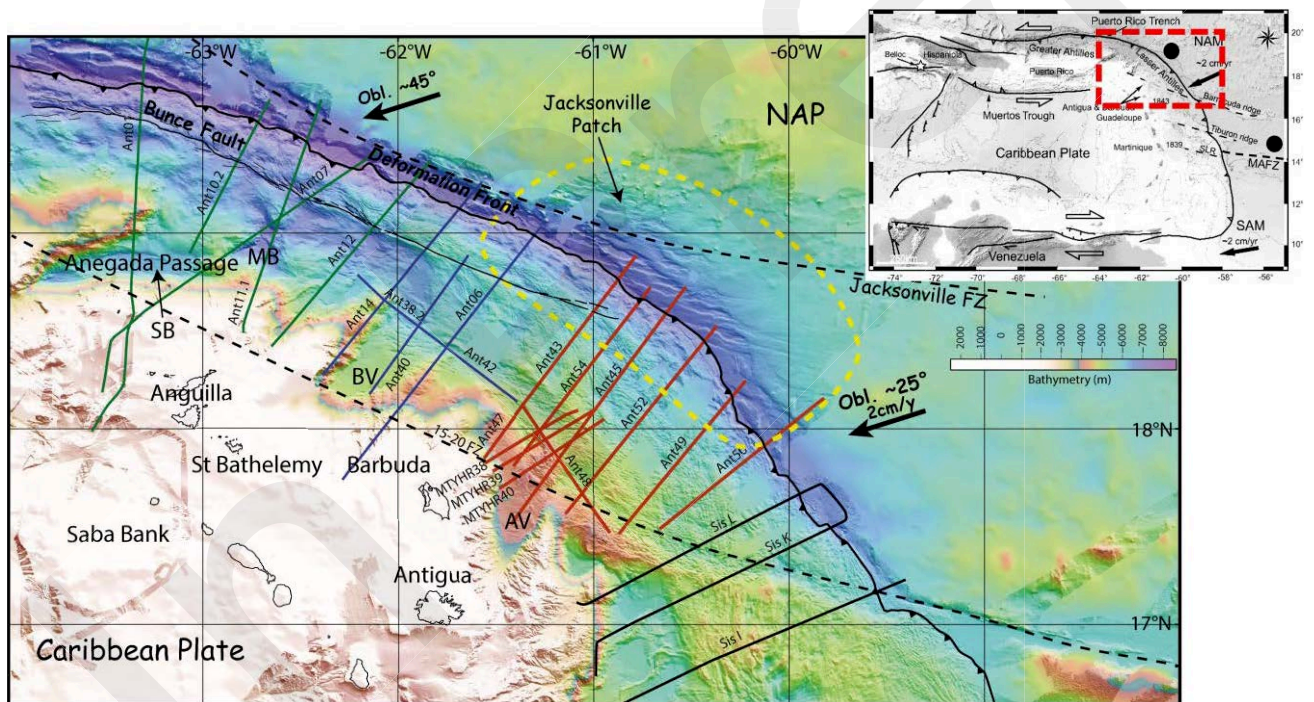
## 1.0 Introduction

Subduction erosion occur at varying degrees in more than 55% of subduction zones along active convergent margins worldwide (Stern, 2011; von Huene & Scholl, 1991; Clift & Vannucchi, 2004; Lallemand et al., 1994). This erosion could result from material removal at the margin front (e.g. Ranero & Von Huene, 2000) and/or abrasion and hydrofracturing at the base of the upper plate (e.g. Stern, 2011). The processes and rate of basal erosion cannot be observed directly but can be inferred from geophysical and geological observations such as large-scale forearc subsidence and associated basement thinning, and inland migration of the volcanic arc (von Huene & Scholl, 1991; Scholl & Von Huene, 2009; Stern, 2011; Stern & Scholl, 2010; Lallemand et al., 1994). At erosional margins, various features are likely to control the rate of subduction erosion; 1/ high plate convergence rate (Clift & Vannucchi, 2004), 2/ subducting plate rugosity, particularly when spiked with seamounts, ridges, and oceanic plateaus (Dominguez et al., 2000) and/or covered with very thin sediment layer (Ranero and VonHuene, 2000), and 3/ Hydrofracturing by overpressured fluids (von Huene et al., 2004). These overpressured fluids are present within the subduction interface. They penetrate the upper plate fractures, causes hydrofracturing of the upper plate and separates fragments, which are dislodged into the subduction channel (e.g. von Huene et al., 2004). This process leads to erosion, subsidence, and upper plate thinning and faulting in response to elastic strain. However, imaging the role of fluids in basal tectonic erosion remains challenging because of the depth of subduction channels below the seafloor; as a result, seismic images of this erosion remain scarce.

The Northern Lesser Antilles (NLA) forearc has undergone a complex tectonic history during Cenozoic times (e.g. Laurencin et al., 2017 and reference herein). This evolution includes a polyphased history of vertical motions (Philippon et al., 2020; Cornée et al., 2021), whose last phase is a long-term subsidence possibly related to subduction erosion at the margin toe (De Min et al., 2015; Boucard et al, 2021). Thus, the Northern Lesser Antilles Subduction Zone (Figure 1) is a relevant region to study the causes and processes for margin erosion. The subduction and southward sweeping of a sediment-starved and rough oceanic plate (Laurencin et al., 2017) spiked with topographic ridges (McCann & Sykes, 1984), incised with oceanic Fractures Zones, locally consisting in serpentized mantle rocks exhumed along detachment fault lately reactivated in the trench (Marcaillou et al., 2022; Davy et al., 2020) favour hydration

34 at subduction depths (Cooper et al., 2020), fluid upward circulation through the margin  
 35 (Ezenwaka et al., 2022) and basal hydrofracturing (Von Huene et al., 2004). Thus, the nature  
 36 and the pervasive fracturing of the subducting oceanic basement, the fluid circulations, the thin  
 37 sediment layer and the plate roughness provide favourable conditions for margin tectonic  
 38 erosion.

39 However, global compilations of subduction zones classified the entire Lesser Antilles margin  
 40 as accretionary (e.g. Clift & Vannucchi, 2004; Noda, 2016). These classifications were based  
 41 on geometry, tectonics and sedimentary features in the south of the Lesser Antilles margin  
 42 without considering the geodynamic processes that shape the margin from north to south. Here,  
 43 we use joint interpretation of recently collected high-resolution bathymetry and multi-channel  
 44 seismic profiles (MCS) north of the subducted Barracuda ridge to show that the Lesser Antilles  
 45 Margin is there erosive, and propose a mechanism for this tectonic erosion.



46  
 47 *Figure 1: Bathymetric map of the Northern Lesser Antilles subduction zone based on data*  
 48 *recorded during cruises Antithesis I, III (Marcaillou & Klingelhoefer, 2013a, 2013b, 2016),*  
 49 *Sismantilles II (Laigle et al., 2007), Manta-Ray (Klingelhoefer & Marcaillou, 2022), and*  
 50 *GEBCO 2014 dataset. The map shows the locations of the Multichannel Seismic as interpreted*  
 51 *in Laurencin et al., (2017) – Green lines, Boucard et al., (2021) – Blue lines, Laigle et al.,*  
 52 *(2013) – Black lines, and present study – Red lines. The locations of the Bunce Fault, the*  
 53 *Fifteen-Twenty and Jacksonville fracture zone (black dotted lines) are also shown on the map.*  
 54 *The yellow dotted ellipse is the location of the Jacksonville Patch. NAP: North American Plate;*  
 55 *SB: Sombrero Basin; MB: Malliwana Basin; BV: Barthelemy Valley; AV: Antigua Valley;*  
 56 *MAFZ: Marathon Fracture Zone. The black dots on the inset map are locations of identified*  
 57 *patches of tectonically-dominated oceanic fabrics (North - Marcaillou et al., (2021), Central –*  
 58 *Davy et al., 2020).*

## 59 **2.0 Geological Settings**

### 60 **2.1 Geodynamic context of the Northern Lesser Antilles Margin**

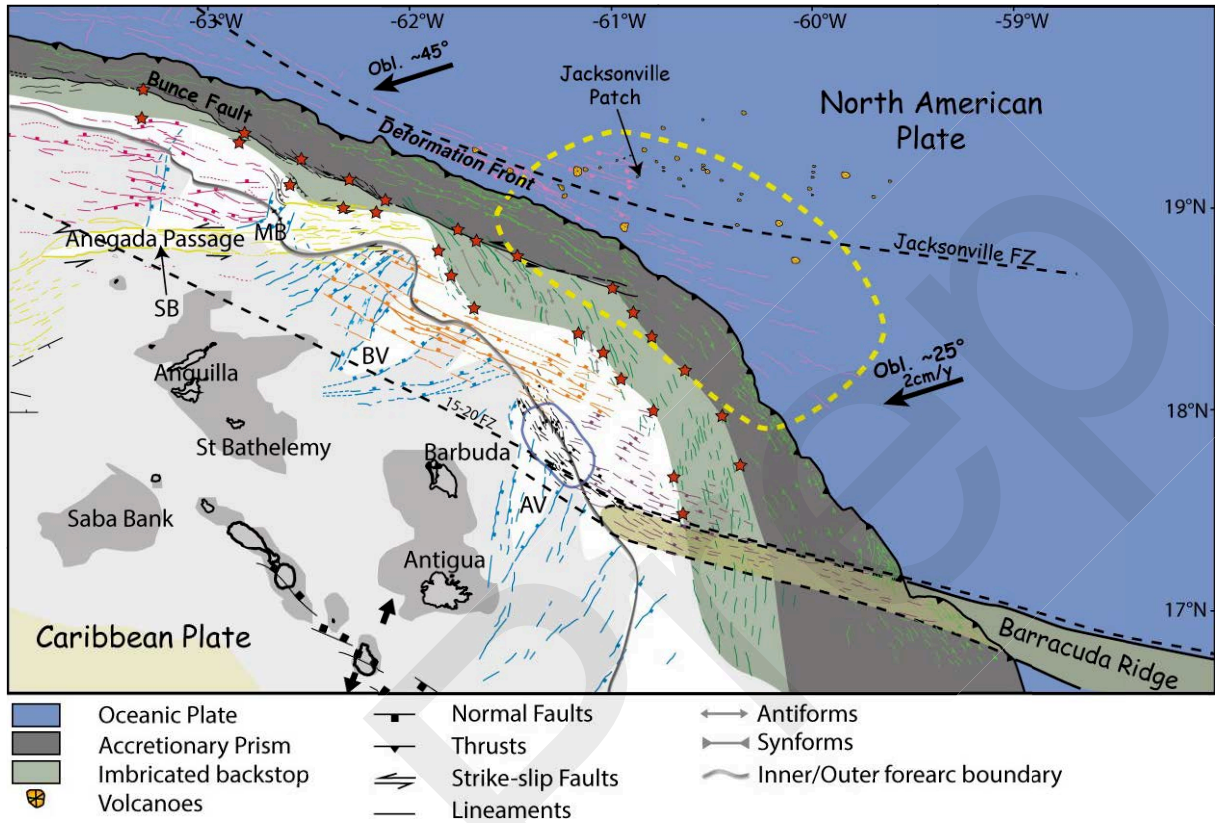
61 In the Lesser Antilles Subduction Zone (LASZ), the North and South American plates subduct  
62 beneath the Caribbean plate at ~20mm/year in a ~S74°W direction (DeMets et al., 2010). The  
63 margin has been bending in an eastward convex shape during the Bahamas Bank collision with  
64 the Puerto-Rico trench since the Paleocene (Mann, 1999) (Figure 1). Since the end of the  
65 Oligocene, the margin has recorded a counterclockwise rotation of 40° - 45° in the Puerto-Rico  
66 to Northern Lesser Antilles block (Calais et al., 2016; Mann et al., 2005; Reid et al., 1991; Van  
67 Fossen et al., 1989; Philippon et al., 2020 ; Montheil et al., 2023). This margin convex shape  
68 results in an increasing convergence obliquity ranging from 0° - subduction normal to the  
69 margin - offshore of Central Antilles to greater than 75° to the North of Virgin Islands. Farther  
70 westward, from Hispaniola to Cuba, the subduction turns to collision and strike-slip  
71 deformation (Mann & Burke, 1984). The convex shape result in a slab dip angle lower beneath  
72 the Virgin Island Platform than beneath the central Antilles at distance from the trench lower  
73 than 75 km (Laurencin et al., 2018), and likely impact tectonic deformation pattern and seismic  
74 activity.

75 The Atlantic basement consists in patches of magmatic robust and tectonically dominated  
76 oceanic crust related to the slow spreading Mid-Atlantic Ridge (Davy et al., 2020). The  
77 subducting tectonically dominated Jacksonville patch, for instance, is partly made of hydrated  
78 and serpentinised mantle rocks, exhumed along pervasive deep rooting detachment fault  
79 reactivated in the trench (Marcaillou et al., 2021). Moreover, the oceanic basement is deeply  
80 incised by numerous fracture zones, among which, the Fifteen-Twenty and Marathon Fracture  
81 zones have been subducting and sweeping south underneath the margin for up to 10 and 30 Myr  
82 respectively (Braszus et al., 2021, Mccann & Sykes, 1984), while the Jacksonville fracture zone  
83 is located in the trench offshore the latitude of Barbuda in the NLA.

84 Convergence between the North and South American Plates successively resulted in the uplifts  
85 of the Tiburon and the Barracuda Ridges (Muller & Smith, 1993; Muller et al., 1999). In the  
86 trench, these uplifts likely occurred during the middle-Late Miocene and the Pleistocene  
87 respectively (Pichot et al., 2012). Ongoing forearc crustal deformation imaged by MCS profiles  
88 and topographic deformation in the Central Lesser Antilles margin indicate that the ridges have  
89 subducted underneath the margin (Laigle et al., 2013b). These elongated topographic highs  
90 impede the northward transport of sediments from the South American River sources to the  
91 trench (Westbrook, 1982), resulting in a drastic decrease of oceanic sediment thickness

92 (Laurencin et al., 2017). As a result, north of Barracuda Ridge, a rough seafloor spiked with  
 93 seamounts and N20°-trending elongated ridges related to the oceanic fabric subducts beneath  
 94 the margin, except within parts of the Jacksonville patch (Figure 1).

95



96

97 *Figure 2: Structural map of the Northern Lesser Antilles margin generated from the combined*  
 98 *interpretations of Laurencin et al., (2017; 2019), Boucard et al., (2021), Laigle et al., (2013),*  
 99 *and the present study. The blue lines show the trench perpendicular normal faults that bound*  
 100 *the V-shaped basins. The yellow lines are the en-echelon fault system that bound the Sombrero*  
 101 *and Malliwana basins within the Anegada Passage. The pink and orange lines that runs from*  
 102 *the north to latitude 18°N in the forearc are the Tintamarre faults that trends at N100°E and*  
 103 *N120°E respectively. Black and Purple lines show the N160°E - N110°E trending faults*  
 104 *respectively that rotates with the trend of the Barracuda ridge. The red stars represent the*  
 105 *extent of the imbricated backstop constrained by the MCS data. The blue ellipse show area with*  
 106 *basement highs, and fluid escape features on the seafloor.*

107

108 The accretionary prism decreases from >150 km in the Central Antilles (Laigle et al., 2013b)  
 109 to ~30 km in the NLA (Laurencin et al., 2019). In the NLA, the landward extent of the prism  
 110 northwest of -61°W corresponds to the location of the Bunce Fault which extends over ~850  
 111 km from Puerto Rico up to north of the Anegada passage, highlighting the increase in plate  
 112 obliquity and strain partitioning (Laurencin et al., 2019). The outer forearc consists in ~4.5 km  
 113 deep flat Sombrero and Malliwana basins bounded by en-echelon fault systems in the Anegada

114 passage (Laurencin et al., 2017), and N140°E – N170°E trending lineaments in a more elevated  
115 seafloor southeast of the basins (Dark green lines in Fig 2) (Boucard et al., 2021). Further south,  
116 the outer forearc is a transition zone towards the accretionary prism made of imbricated and  
117 underplated materials or damaged upper plate igneous basement covered with thinner forearc  
118 sedimentary deposits (Bangs et al., 2003; Laigle et al., 2013; Evain et al., 2013). From the  
119 Anegada passage to the Karukera Spur, the inner forearc domain is dominated by V-shaped  
120 basins and spurs bounded by trench perpendicular linear faults (Boucard et al., 2021) (blue lines  
121 in Figure 2). The opening of these V-shaped basins and the Sombrero and Malliwana basins are  
122 interpreted to be due to an N-S to NW-SW extension at Oligocene to Mid-Miocene (Boucard  
123 et al., 2021; Laurencin et al., 2017; Legendre et al., 2018), related to the margin convex bending  
124 and counterclockwise block rotations (Jany et al., 1990; Masson & Scanlon, 1991; Philippon et  
125 al., 2020; Montheil et al., 2023). The V-shaped basins in the NLA forearc is fractured by trench-  
126 normal, deeply-rooted Tintamarre Faults associated with a major basement thinning and forearc  
127 extension and subsidence in the Mid-Miocene (Boucard et al., 2021).

## 128 ***2.2 Stratigraphic and faulting context of the NLA Margin***

129 Previous stratigraphic studies located to the northwest of the Antigua Valley (Figure 1) indicate  
130 that the forearc sedimentary layer consists of four main sedimentary units lying unconformably  
131 above the basement (Laurencin et al., 2017; Boucard et al., 2021). The complete series are best  
132 preserved within the forearc basins where they are the thickest. The deepest two units are faulted  
133 by the deeply rooted trench perpendicular faults that bound the V-shaped basins, and are  
134 separated from the overlying two shallow units (Boucard et al., 2021) by a regional late Eocene  
135 unconformity (Philippon et al., 2020; Cornée et al., 2021). Above the unconformity, the shallow  
136 units are less deformed by the trench perpendicular faults, and hence seal off these faults.  
137 However, the deep trench parallel Tintamarre Faults offset the seafloor and the trench  
138 perpendicular faults (Boucard et al., 2021). The stratigraphic succession in the NLA forearc has  
139 led to the interpretation of two tectonic extensional phases (Oligocene – earliest Middle  
140 Miocene and Middle Miocene – Recent respectively), separated by a regional emersion during  
141 the earliest middle Miocene (e.g. Cornée et al., 2021; Boucard et al., 2021).

## 142 **3.0 Data Acquisition and Analysis**

143 The multichannel seismic (MCS) includes low frequency and high-resolution reflection lines  
144 acquired during the ANTITHESIS 3, and MANTA-RAY oceanographic cruises. The MCS  
145 acquisition parameters are shown in the supplementary material. In this study, we present ten  
146 of the MCS lines acquired along the Antigua Valley to north of the Barracuda ridge, which

147 complete the uninterpreted portion of the forearc domain in the Northern Lesser Antilles. Six  
148 of the MCS lines are low frequency dip lines (Ant 43, 47, 54, 45, 52, 49), three are high-  
149 resolution dip lines (MTYHR38, 39, 40), while one is a strike line (Ant 48) that intersects six  
150 of the dip lines (Figure 1). The MCS data quality control and processing were performed on-  
151 board and post-cruise using the Ifremer SolidQC and CGG GEOVATION software  
152 respectively. The data processing workflow is shown in the supplementary material.

153 In addition, we combined other structural interpretations from low frequency MCS line (Laigle  
154 et al., 2013b – black lines in Figure 1, Laurencin et al., 2017; 2019 – green lines, and Boucard  
155 et al., 2021 – blue lines), acquired during the SISMANTILLES 2, and ANTITHESIS 1 & 3  
156 surveys respectively.

157 The multibeam bathymetric data were also acquired during the Antithesis and Sismantilles  
158 projects, and complemented with recent data from the Manta-Ray campaign. We calculate  
159 digital elevation models at 100 and 50-m grid, and process the data using Caraibes and Globe  
160 software. Further processing was done using QGIS software to produce high-resolution maps  
161 that aided the interpretation of seafloor outcropping structures, which we correlate to the  
162 seismic interpretations.

## 163 **4.0 Results**

164 Our descriptions are based on along-dip and along-strike seismic lines, and the newly completed  
165 bathymetric data that extends from the latitude of Antigua to the Barracuda ridge.

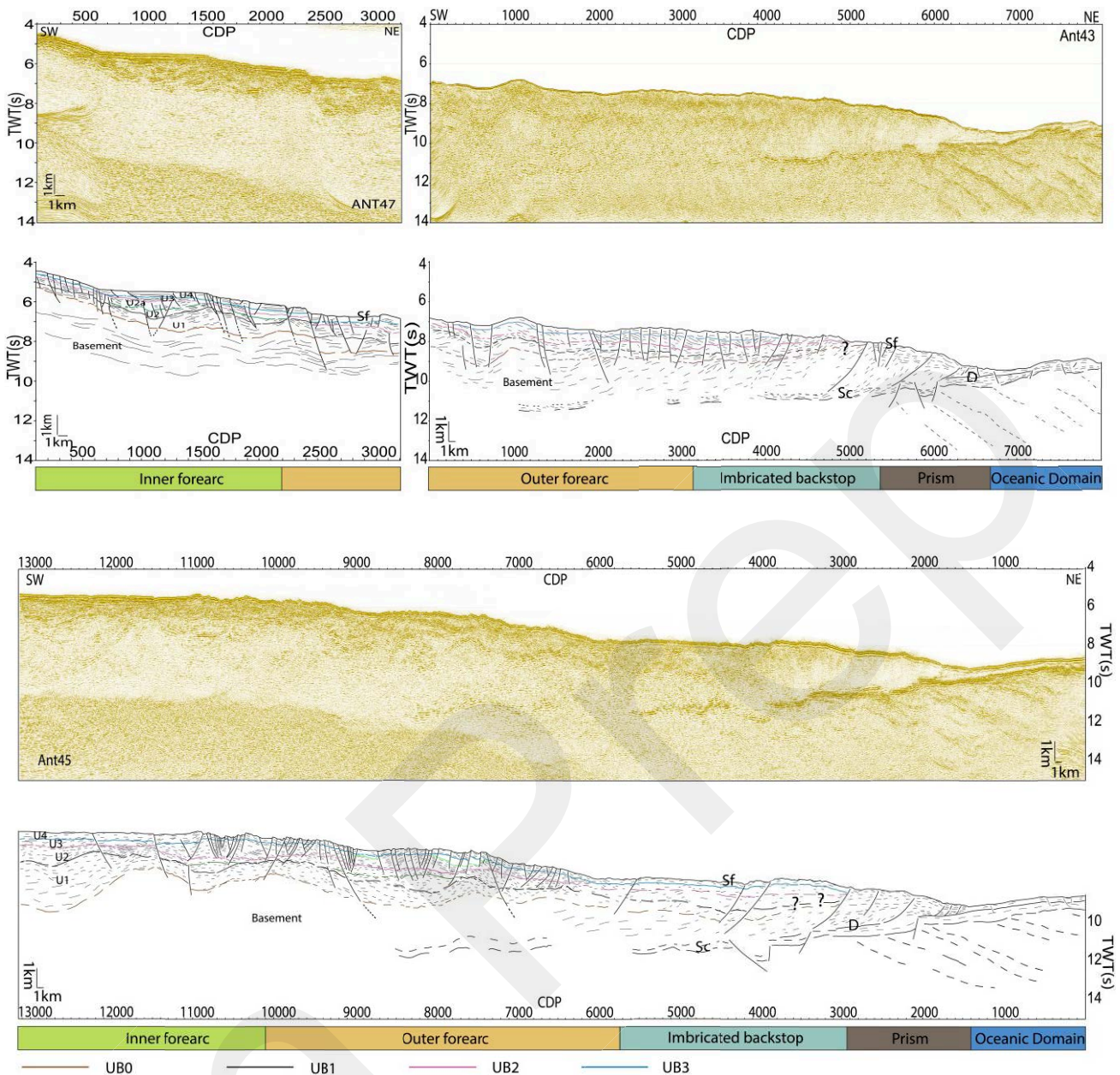
### 166 **4.1 Seismic stratigraphic units**

167 In the study area, four units U1 to U4, separated by three unconformities, UB1 to UB3 (Figure  
168 3 and supplementary material), show amplitude, frequency, continuity and geometric features  
169 closely consistent with those observed farther north along St Barthelemy Valley (see description  
170 in Boucard et al., 2021, § 4.3.3). In the following, we synthesize this description.

171 U1 lies unconformably above UB0, the top of the forearc basement, and covers the entire  
172 basement unit. Along strike, from the northern flank of the Barracuda Ridge to the north of  
173 Antigua valley, U1 thickness is ~ 0.9-1.1 stwt in the inner forearc and at least halfway through  
174 the outer forearc (MTYHR38 CDP 5500-7000 in Figure 6), and then decreases to ~ 0.5 stwt  
175 close to the accretionary prism (Ant43 CDP 2500-4000 in figure 3). However, U1 is thinner (~  
176 0.2 stwt) where upper plate basement highs are present (Ant54 CDP 7800-8500 in the  
177 supplementary material).

178

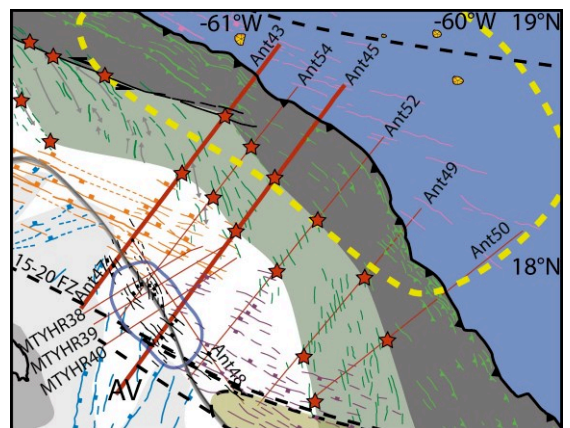




179

180 *Figure 3: Stratigraphic and structural interpretation*  
 181 *for dip lines Ant 43, 47, and 45. Other lines are shown*  
 182 *in the supplementary material. D – Decollement, Sf –*  
 183 *Seafloor, Sc – Subduction channel. U1 – U4 are*  
 184 *interpreted seismic stratigraphic layers. UB0 – UB3*  
 185 *represent seismic stratigraphic surfaces. Inset map*  
 186 *show the location of the MCS lines (thick red line).*  
 187 *See Fig 2 for map legends.*

188



189 U2 overlies U1 unconformably, both units being separated by the discontinuity UB1. At the top  
190 of Unit U2, discontinuity UB2 truncates the uppermost reflectors of U2. UB2 appears as a high  
191 amplitude reflector that occurs regionally through the study area. U2 has a subunit U2a and is  
192 thickest in the Antigua Valley with up to 0.8 stwt thickness (Ant 45 CDP 12600 – 13000). It  
193 decreases drastically to ~ 0.4 stwt elsewhere.

194 Unit U3 shows high frequency and average amplitude reflectors downlapping onto the UB2  
195 boundary. The youngest unit U4 conformably overlies this unit, with the UB3 boundary  
196 separating them. Reflectors of U4 units are rectilinear, sub-parallel and poorly deformed,  
197 especially within the Antigua valley where they are less faulted. In the forearc, unit U3 and U4  
198 show similar structural patterns where they are cut by normal faults and graben structures  
199 (Figure 3 and 5). The two units are consistent throughout the study zone, but vary slightly in  
200 thickness from one place to another.

#### 201 ***4.2 Tectonic features of NLA margin***

202 We describe the tectonic features of the NLA from the trench to the inner forearc based on MCS  
203 lines and bathymetric data acquired from the Jacksonville patch to the subducting Barracuda  
204 ridge. We correlate these descriptions to the published lines in Boucard et al., (2021) and  
205 (Laurencin et al., 2019) to discuss the mechanism of subduction erosion in the NLA.

##### 206 ***4.2.1 The Downgoing Plate***

207 The top of the downgoing oceanic crust show low frequency, and strong amplitude reflectors  
208 truncated by normal faults to form horst and graben structures (Figure 4). These reflectors are  
209 consistently visible beneath the prism and gradually fades away beneath the outer forearc.  
210 Within the oceanic Jacksonville patch, southeast of longitude – 61°E, seismic reflections on dip  
211 lines show high amplitude reflector sequences that dip from the top of the crust to ~5 stwt below  
212 the seafloor (Figure 4 and other lines in supplementary materials). These reflectors, described  
213 as widespread ridgeward dipping detachment faults, formed at the Mid Atlantic Ridge, and  
214 reactivated during the plate bending (Marcaillou et al., 2021) extend beneath the margin at least  
215 to ~10 km distance from the deformation front and likely farther. To the North and the South  
216 of the Jacksonville patch, the bathymetric map shows the oceanic fabric: elongated ~N20°-  
217 trending topographic ridges and broad topographic highs up-to ~1500m higher than  
218 surrounding seafloor bathymetry. Seafloor morphology west of longitude -61°E also reveals  
219 typical parallel margin plate bending faults that are locally associated to the Jacksonville  
220 fracture zone, that lie almost parallel to the trench at this location. In contrast, the oceanic fabric

221 disappears after the western boundary of the Jacksonville Patch where the seafloor is relatively  
222 smooth and even (Figure 1).

223 At the trench, the oceanic crust is covered by medium to high amplitude, sub parallel reflectors  
224 that represent thin sediment units, with a thickness that varies from ~0.3 km in Ant01  
225 (Laurencin et al., 2019) where they are thinnest, to ~0.5 km in Ant45 where they are thickest.  
226 They are cut across by east and west dipping faults that penetrate the basement. In the  
227 Jacksonville patch, these faults slightly offset the seafloor and the trench-sediment reflectors.  
228 However, northwest of the Jacksonville patch, the trench sediment-fill reflectors appear to be  
229 deformed and terminate against oceanic crust reliefs that correspond to graben structures,  
230 creating a rough seafloor (see Ant01 in Laurencin et al., 2019).

231 The high-amplitude reflectors for the Decollement level and the Top of the Oceanic Crust  
232 encompass deformed stratified reflector sequences of the subduction channel (Figure 3 and  
233 supplementary material). These reflectors extend from the trench to beneath the outer forearc  
234 and are poorly resolved at greater depth. Normal faults locally offset these decollement  
235 reflectors and form grabens. The reflector of the decollement level shows reversed polarity  
236 compared to seafloor reflector as described in section 4.3. At the deformation front, and beneath  
237 the prism, the separation between the reflector of the interplate thrust and the top of the oceanic  
238 crust (subduction channel) maintain an almost equal twt thickness except inside the grabens  
239 where they are thickest. However, northwest of longitude - 61°E, these reflectors appear  
240 variable and disorganized especially due to the topography of the subducting crust at this  
241 location.

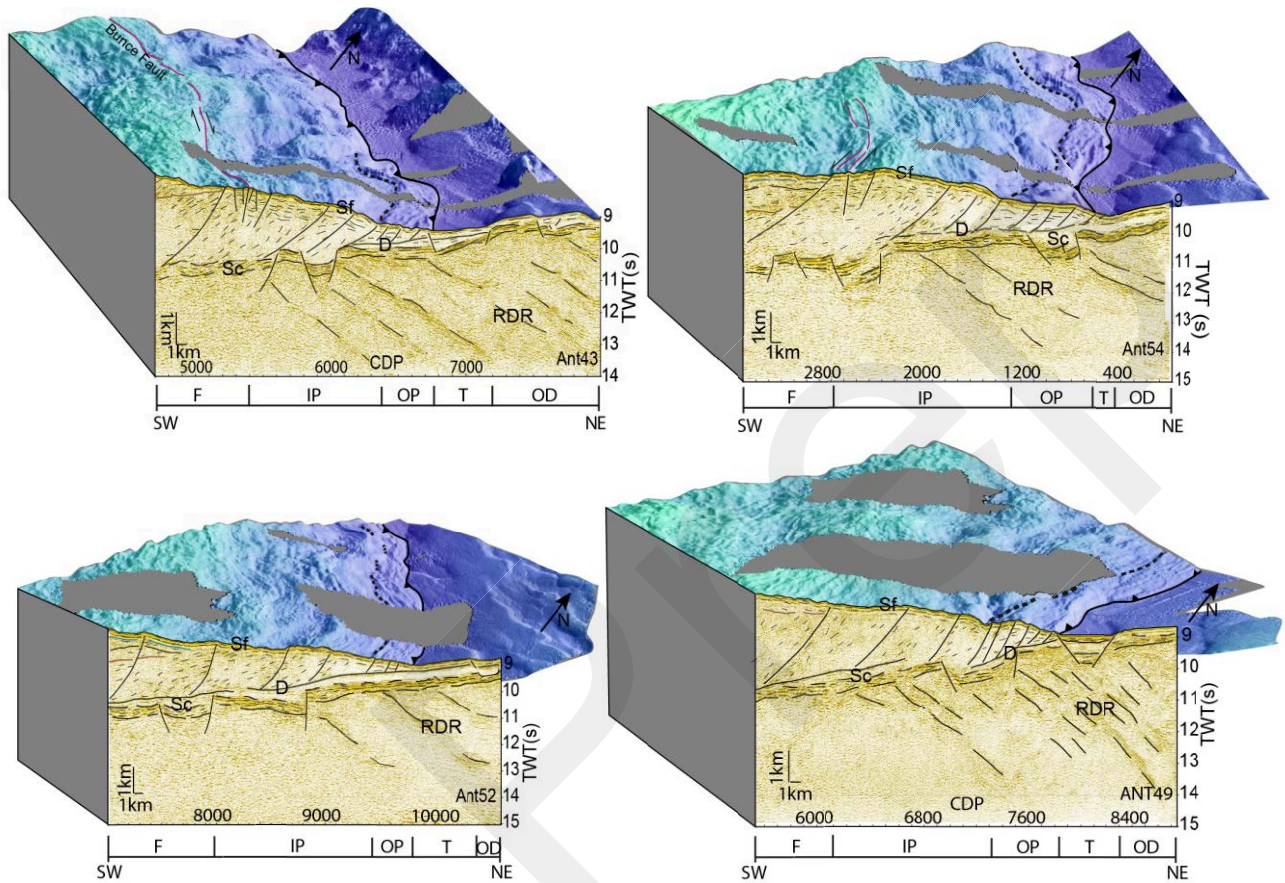
#### 242 **4.2.2 The Frontal prism**

243 In the prism, MCS lines show low amplitude landward-dipping reflectors that correspond with  
244 bathymetric lineaments sub-parallel to the trench (Light green lines in Figure 2), representing  
245 thrusts typical of frontal accretionary systems. Along every MCS line from Ant01 to Ant43, the  
246 prism extends from the trench to the Bunce fault (see lines in (Laurencin et al., (2019), Boucard  
247 et al., (2021) and Figure 04). To the South of line Ant43, the Bunce fault progressively  
248 anastomoses in a diffuse strike-slip fault zone in the prism (Ant54 in Figure 4). Further south,  
249 the margin backstop separates the frontal accretionary prism from the margin basement and  
250 forearc basin imaged by typical reflection, such as prominent unconformity UB0 for instance  
251 (Ant45, 52, and 49 in Figure 3 and 4, and other lines in the supplementary material).

252 The seismic and bathymetric data consistently image a southward growing prism from line  
253 Ant01 where it is the narrowest (17 km between CDP 3800 – 5400) to line Ant06 (~30 km

254 between CDP 700 – 3300) (See lines in Laurencin et al., 2019). Immediately north of the  
 255 Barracuda ridge, the prism is ~21 km at line Ant49 (CDP 6000 – 7800) (Figure 4), however,  
 256 south of the ridge, the width of the prism increases steadily to more than a factor of three.

257

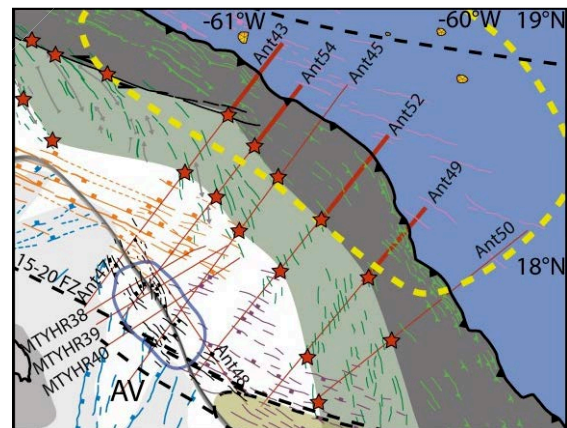


258

259 *Figure 4: Three-dimensional seismic bathymetry view of*  
 260 *the prism for lines Ant43, 54, 52 and 49 from North to*  
 261 *South of the study area. OD: Oceanic domain, T:*  
 262 *Trench, OP: Outer prism, IP: Inner prism, F: Forearc,*  
 263 *And RDR: Ridgeward dipping reflectors interpreted as*  
 264 *widespread detachment faults formed at the slow-*  
 265 *spreading mid-Atlantic ridge (Marcaillou et al., 2021).*  
 266 *The location of the MCS lines is shown in the inset map*  
 267 *as thick red lines.*

268

269



270 Southeast of longitude -61°W, both the seismic reflections and bathymetric features separate  
 271 the NLA prism into an inner and outer zone (Figure 4). Northwest of this longitude, only the  
 272 inner zone appears to be visible (see Ant01 and 06 in Laurencin et al., 2019). The outer part  
 273 consists of small sets of subparallel reflections separated by planes of closely spaced landward

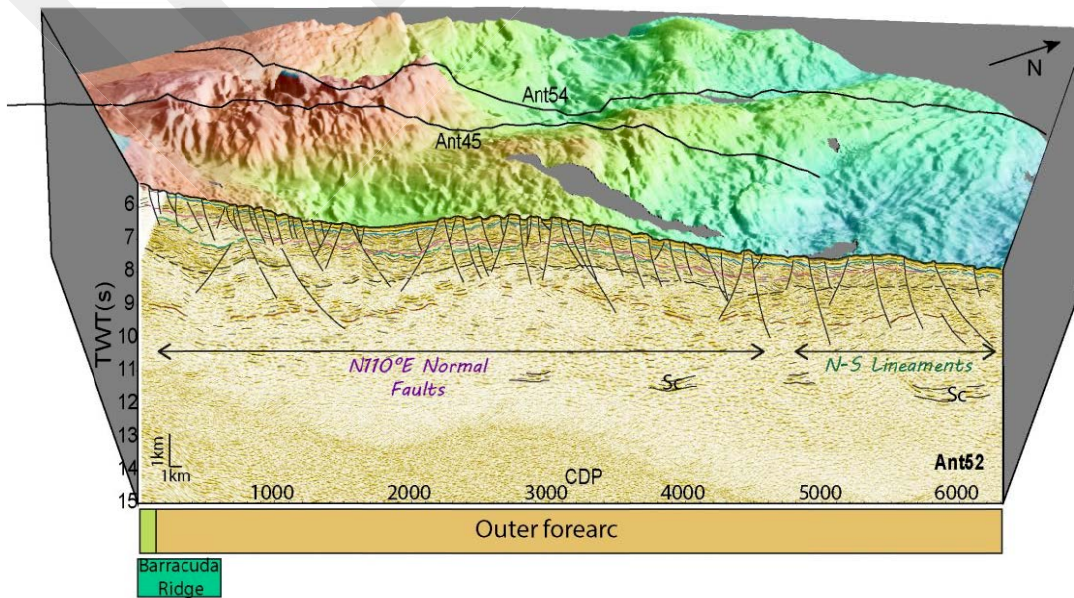
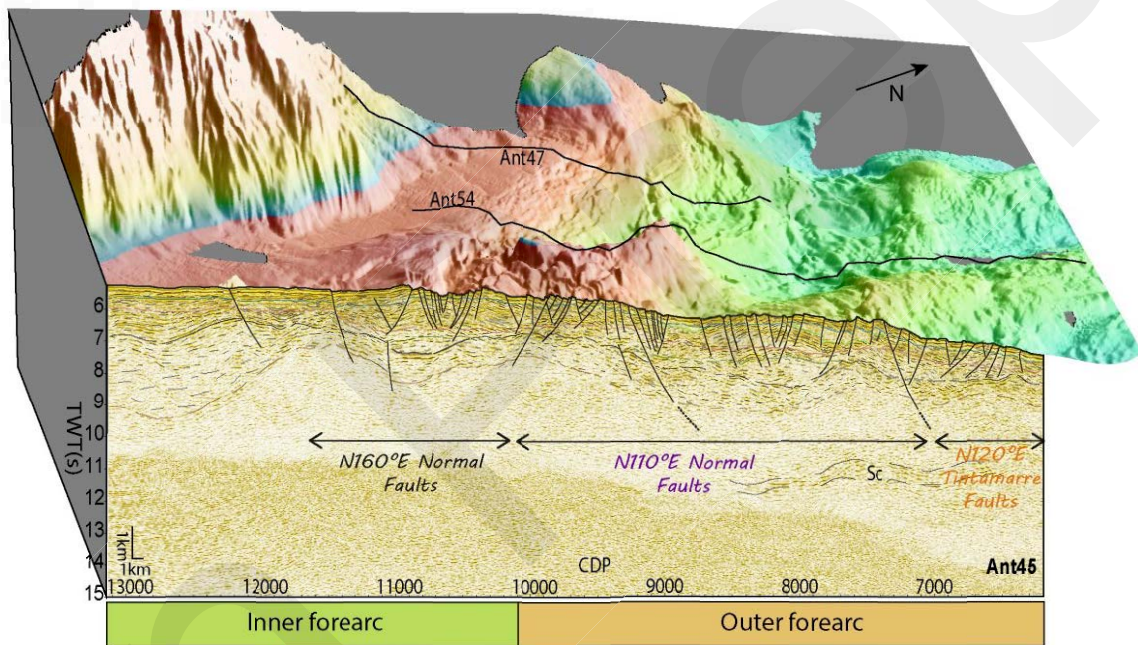
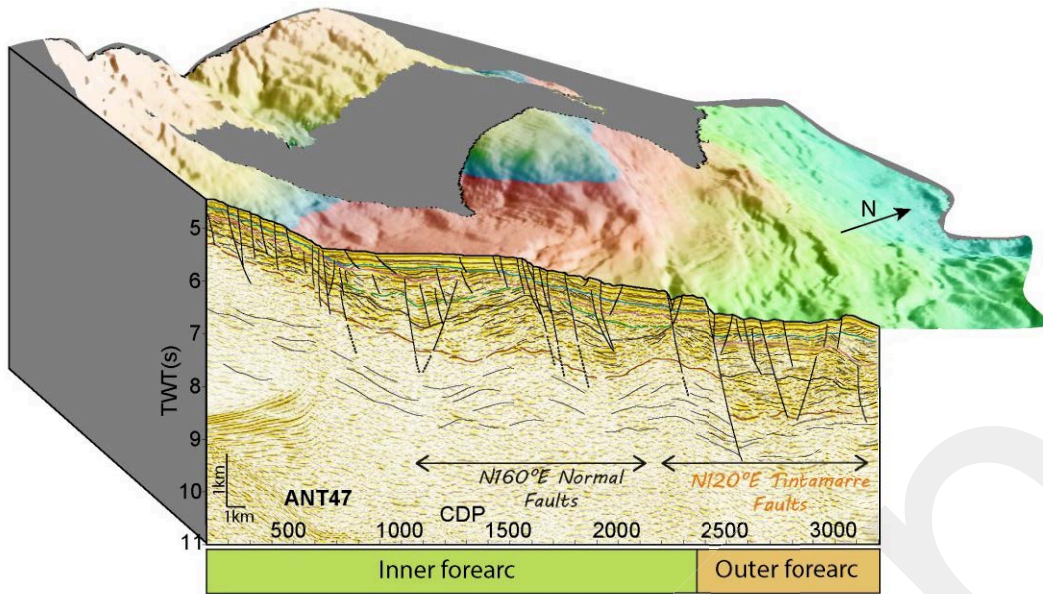
274 dipping reflectors that drape from the seafloor to the decollement. This zone varies in distance  
275 from few kilometres to ~10 km. The inner part is relatively less reflective but also consist of  
276 planes of landward dipping reflectors that are largely spaced. They vary in distance from few  
277 kilometres to ~20 km. The thickness of the landward boundary of the prism varies from ~2.5 –  
278 3.0 stwt in all the seismic lines. On the seafloor, the topography of the prism nearly follows the  
279 horst and graben structures of the downgoing plate. The decollement level that bounds the base  
280 of the prism appears almost at the top of the sediment pile on the oceanic plate up to the trench,  
281 and less than half of the sediments in the trench appears to be accreted to the margin. Thus, the  
282 prism shows very narrow thrusts in the frontal part, and small imbricate stacks of sediment  
283 scrapped off the incoming trench sequence that decreases progressively northwards.

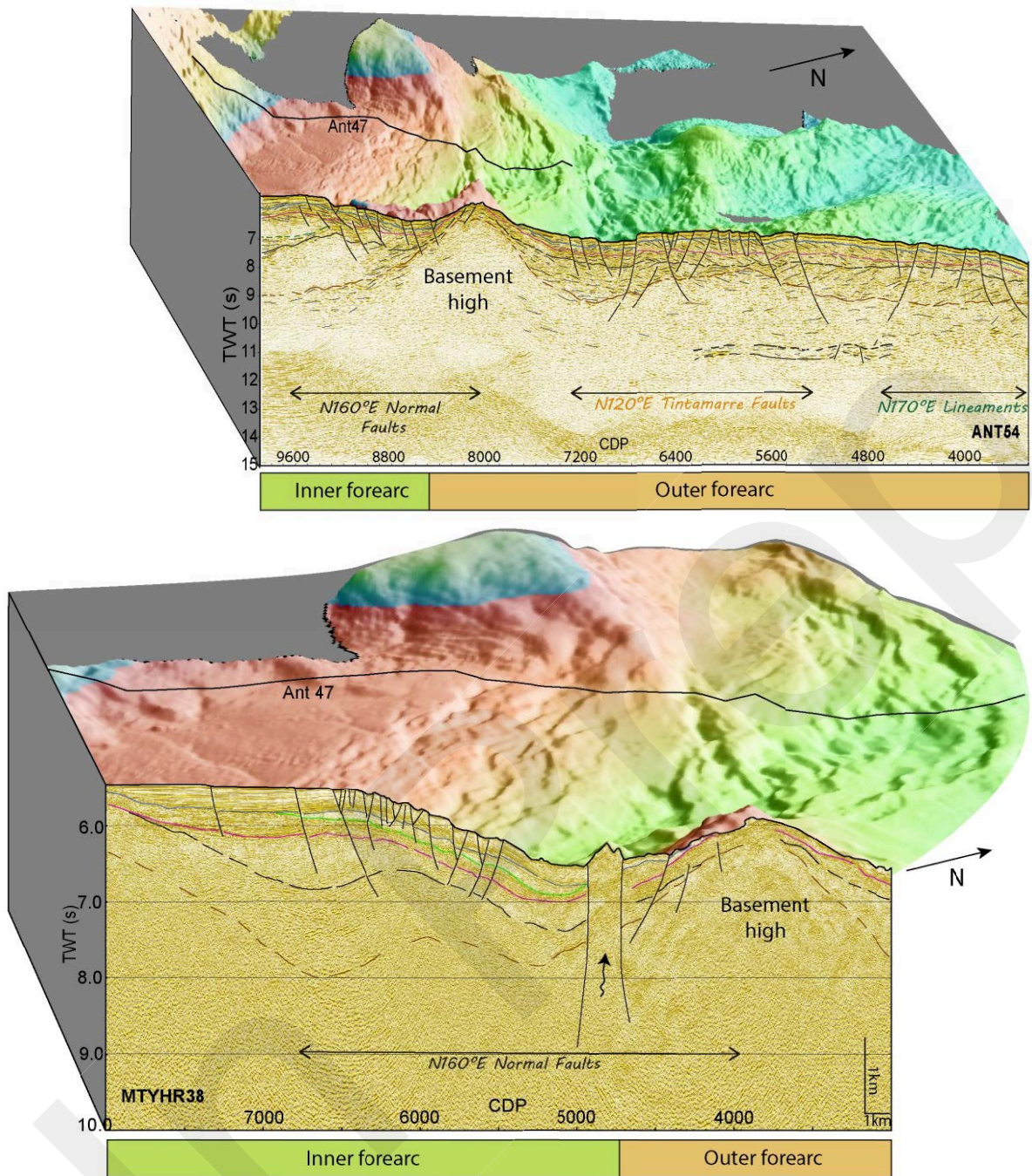
#### 284 **4.2.3 The Inner and Outer Forearc structures**

285 Joint interpretation of MCS lines and high-resolution bathymetry of the NLA forearc within  
286 our study area capture series of sea-bottom scalps, and faults identified on the seismic section.  
287 They include sea-bottom lineaments, deep-rooted extensional faults, series of basement highs  
288 and mound-like seafloor morphologies (Figure 5 and 6).

289 Trenchward, from 18.2°N to the Barracuda Ridge, the outer forearc is characterized by a set of  
290 N140° - 170°E trending sigmoid seafloor lineament series, that rotates to a N – S trending series  
291 to the south of the Barracuda Ridge (Ant52 at CDP 4500-6200 in Figure 5 and dark green lines  
292 in Figure 2). Between the inner and outer forearc, the N120°E Tintamarre Faults (orange lines  
293 in Figure 2) described in Boucard et al., (2021), terminates into a set of N160°E normal faults  
294 (black lines in Figure 2). South of the Tintamarre Faults (orange lines), the N160°E faults rotate  
295 to a N110°E faults (purple lines in Figure 2) subparallel to parallel to the Barracuda ridge  
296 through the outer forearc and the prism. These N110°E faults intersect the N – S lineament  
297 series in the outer forearc, separating a less rough seafloor morphology north of the Barracuda  
298 ridge with a very rough seafloor south of the ridge (Figure 1 & 2). On the seismic sections,  
299 these normal faults dip in both seaward and landward directions, and cuts through the seafloor,  
300 forming series of closely spaced grabens and half grabens (Figure 5 and line MTYHR40 in the  
301 supplementary materials). Displacement of seismic reflectors along these normal faults where  
302 they are largest reach ~0.18 stwt, for instance at CDP 7000 in MTYHR40 (supplementary  
303 material).

304

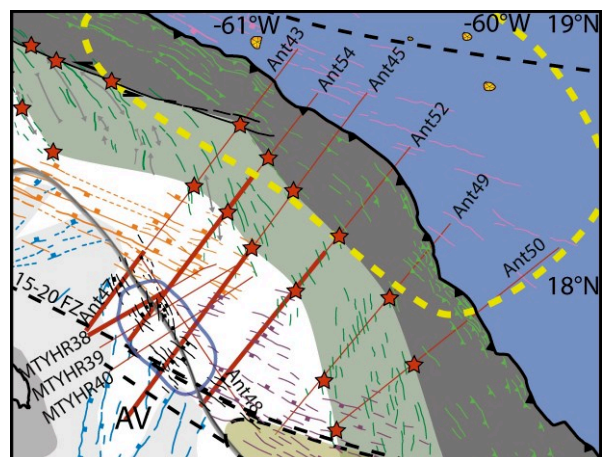




306

307 *Figure 5: 3-D seismic bathymetric view of the*  
 308 *forearc along dip lines Ant47, 45, 52, 54, and*  
 309 *MTYHR38. The N160°E - N110°E normal*  
 310 *extensional faults show collapse of the seafloor,*  
 311 *and form graben and half graben structures.*  
 312 *The black arrow on MTYHR38 show fluid*  
 313 *escape pathway to the seafloor. All the MCS*  
 314 *profiles are located in a NE – SW direction from*  
 315 *the trench. The inset map shows the exact*  
 316 *segment of the shown profiles (thick red).*  
 317 *See fig 2 for map legends.*

318



319 The high amplitude and low frequency reflector of the top of the margin basement divides the  
320 sedimentary units from the low frequency, low amplitude, and chaotic reflections of the margin  
321 basement. The basement topography dips trench-wards, with the basement crust thinning in  
322 this same direction. The basement shows prominent topographic highs. In line 45, moderate  
323 basement high apexes are located at CDP 8600, 10000 and 11500 (Figure 5). In line Ant54  
324 (Figure 5) and Ant48, the basement culminates at 3,750 m dominating the inner forearc close  
325 to the Antigua Valley (Figure 2 and Ant54 CDP 7700-8600 in Figure 5). These uplifts could be  
326 a part of the Antigua spur separated by the trench perpendicular extensions. The N160°-110°E  
327 normal faults fracture this basement high, where we observe mud volcanoes and pockmark at  
328 the seafloor (Figure 6 and line MTYHR38 in Figure 5). The top of the basement is at 9.5 stwt  
329 (for instance CDP 8000-8500 in Ant45) at the deepest and 5.3 stwt (CDP 1-100 in Ant47) at  
330 the shallowest. Seaward, the upper plate basement terminates at the backstop's seaward edge,  
331 and the contact between the backstop and the prism is detectable by the sharp downward  
332 deflection of reflectors from the top of the upper plate basement, the abrupt change in stacking  
333 velocity, or the strike slip Bunce fault (Figure 3 and supplementary material).

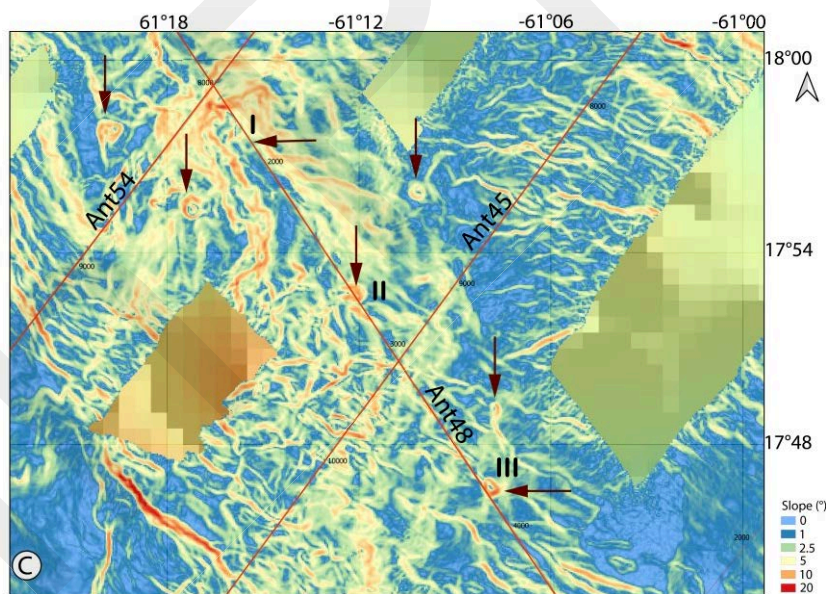
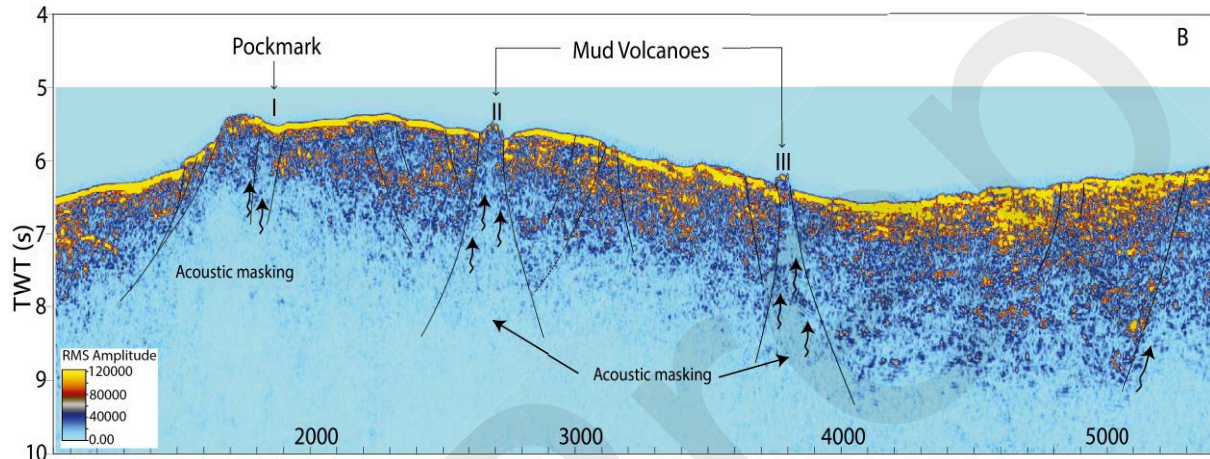
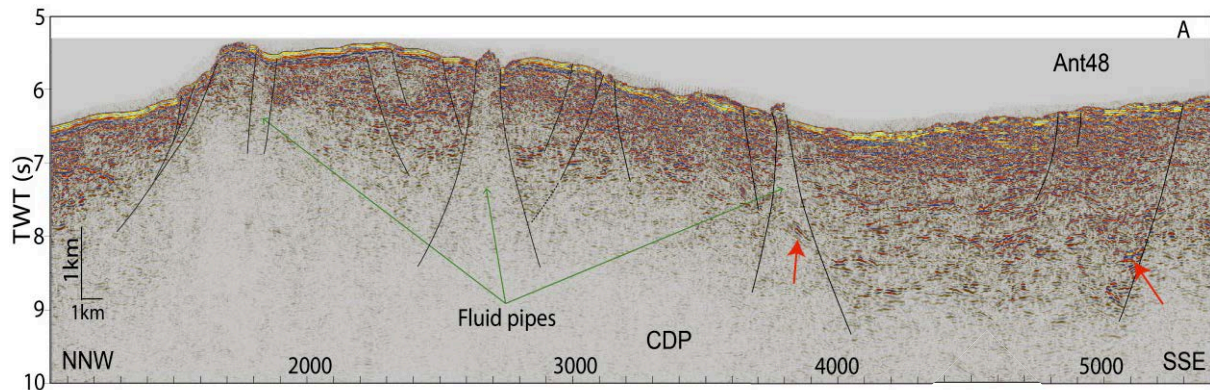
#### 334 ***4.3 Fluid Indicators from Acoustic Anomalies***

335 We present in this section, series of acoustic anomalies from the seismic data that show  
336 evidence of fluid occurrence up to the seafloor (Figure 6). These includes low amplitude  
337 transparent zones, discontinuous reflections, and high amplitude-reverse polarity reflections.

338 MCS lines in the study zone show striking features of low amplitude transparent and  
339 discontinuous reflections that form acoustic pipe structures (fluid pipes). At least three of these  
340 fluid pipes were observed between the inner and outer forearc, with acoustic masking zones at  
341 the base (Figure 6a and b). The fluid pipes extend from 9 – 9.5 stwt depth in the margin  
342 basement up to the seafloor (Figure 6a and Figure 5 at CDP 4800 in line MTYHR38). They  
343 thus have a vertical length of 2.7 – 3.5 stwt, ~3.3 – ~4.3 km considering our velocity model. On  
344 the seafloor, the upper limits of these fluid pipes correspond with pockmarks and volcano-shape  
345 domes that we observe on the bathymetric map, which dominate this region of the forearc  
346 (brown arrows in Figure 6c).

347

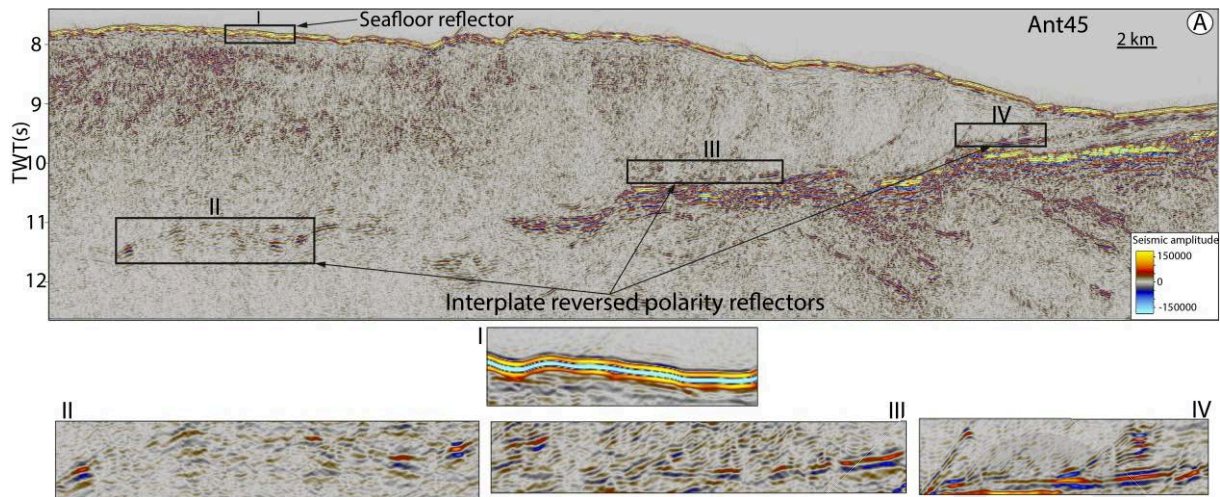




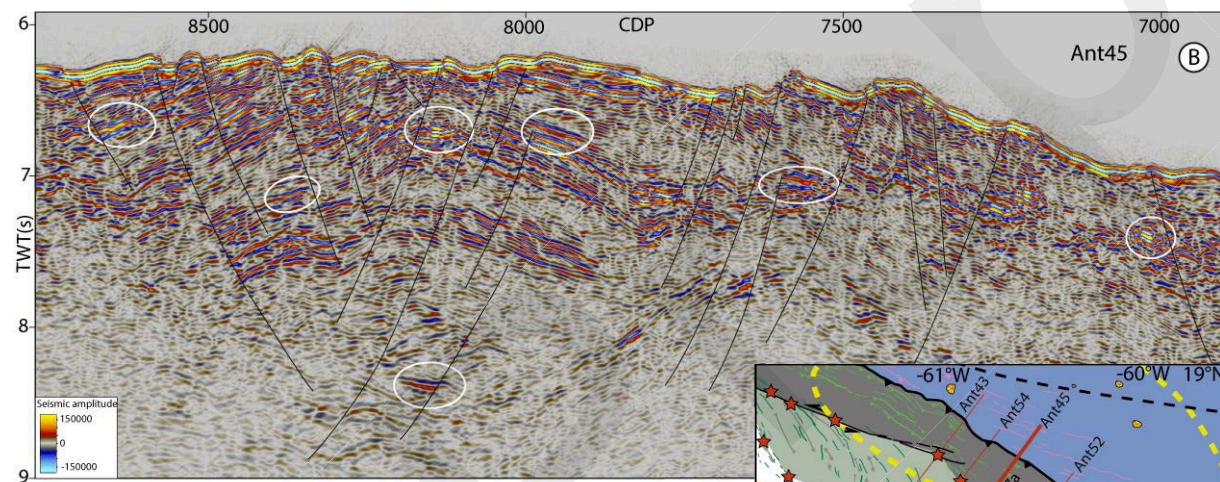
348

349

350 *Figure 6: Acoustic anomalies observed on MCS data as indicators of fluid occurrence. (a) Fluid*  
 351 *pipes rising up to the seafloor to form pockmarks and mud volcanoes. The red arrows show*  
 352 *tilted bright amplitude reflectors with reversed polarity and high RMS amplitude close to deep-*  
 353 *rooted faults. (b) Acoustic masking zones below the fluid pipes. The black zig-zag arrows*  
 354 *represent fluid migration pathways. (c) Slope map of the bathymetry showing areas with domes*  
 355 *and V-shape depression on the seafloor consistent with the MCS data (circular shapes pointed*  
 356 *by the brown arrows). Similar features are also observed in the surrounding area on the*  
 357 *bathymetric map.*



358



359

360 *Figure 7: Bright amplitude reversed polarity reflectors*  
 361 *observed along (a) the decollement reflector and (b) at*  
 362 *shallow layers along N160° - N110° normal faults that*  
 363 *form grabens and half grabens (indicated by the white ellipses). The black boxes in A represent*  
 364 *the positions of the closed-up views shown in I, II, III, and IV. (I) show the polarity of the*  
 365 *seafloor, while (II, III, and IV) show the polarity at several positions along the interplate, which*  
 366 *is different from the observed seafloor polarity. The inset map indicates the position of the*  
 367 *shown portions on line Ant45.*

368

369 Another striking feature observed in the seismic data is the presence of high amplitude  
 370 anomalous reflections, which may not be related to stratigraphic layers. These reflectors have  
 371 reversed polarity compared to the seafloor. They are present in the decollement at shallow  
 372 depths below the accretionary prism, as well as at greater depth close to the top of the oceanic  
 373 crust (Figure 7a). It was difficult there to locate the decollement reflection, but this reverse

374 polarity clearly indicates the negative impedance contrast associated to subducting sediments  
375 that have lower velocities and densities than the overlying crustal material of the forearc crust.  
376 Fluid-rich sediments of the decollement have particularly low-impedance values responsible  
377 for this clear negative reflection polarity (e.g. Bangs et al., 2015). We also observe such reverse  
378 polarity reflections within the forearc sedimentary units at deep stratigraphic layers, and at  
379 depth close to the planes of deep-rooted faults as tilted reflectors (red arrows in Figure 6a).  
380 They also occur close to normal faults that form graben and half graben structures within the  
381 shallow units (white ellipses in Figure 7b). The tilted reflectors with reversed polarity at depth  
382 close to planes of deep-rooted faults sometimes occur directly below the pockmarks and  
383 volcanic-shape domes on the seafloor (Figure 6), while the reverse polarity reflectors in the  
384 shallow units (Figure 7b) also occur closely below the location of the decollement reflectors at  
385 depth with reversed polarity.

## 386 **5.0 Discussions**

### 387 ***5.1 The NLA trench and the Frontal prism deformations***

388 In the NLA, the dominant tectonic regime at the margin front varies from South to North. Along  
389 the trench segment running from the Barracuda Ridge northern flank up-to the Jacksonville  
390 patch north-western end, a moderate thickness of trench sediment and a relatively smooth  
391 oceanic basement favour accretion of thin sediment layers along closely-spaced en-serie thrusts  
392 (OP in Figure 4). This short frontal accretion is visible from dip-line K in Laigle et al., (2013)  
393 to line Ant43. Farther north, the decreasing sediment thickness and the rougher seafloor spiked  
394 with seamounts and elongated ridges generate an irregular tectonic regime with numerous  
395 evidences of frontal erosion. Locally, small-scale accumulation of sediment in the trench  
396 triggers an accretion phase, which is likely to be transient. As a result, to the North of the  
397 Barracuda Ridge, the prism records decreasing frontal accretion and increasingly dominating  
398 erosion that is controlled by variation in the dominant tectonic regime.

399 In contrast, to the Central and Southern Lesser Antilles, where long-term accretion has resulted  
400 in voluminous accretionary prism, ~150 km-wide and up to 10-km-thick between the Barracuda  
401 and Tiburon Ridges (Laigle et al., 2013; Bangs et al., 1990) and up-to ~300-400-km-wide and  
402 ~12-18-km-thick to the South of the Tiburon Rise (Westbrook et al., 1988). This variation in  
403 the LA prism is largely attributed to the effect of the topographic ridges (Barracuda and Tiburon  
404 ridges) that developed during the Miocene and Pleistocene respectively (Pichot et al., 2012),  
405 and the uneven supply of sediments from south to north, which also has an influence on the  
406 topographic reliefs that is exposed on the subducting oceanic crust. The variation may also be

407 related to the collision of the Bahamas Bank from the Eocene (Mann, 1999; Legendre et al.,  
408 2018), since rocks of the accretionary prism, dated to the Cretaceous has been found in the  
409 Dominican Republic (Goncalves et al., 2015) and in Cuba (Hinsbergen et al., 2009). It is likely  
410 that this collision destroyed the prism north of Cuba and Hispaniola, and possibly impacted the  
411 prism size farther east in the NLA.

412 Thus, we propose that the accretionary prism north of the Barracuda Ridge in the LASZ is likely  
413 eroding diachronously since the Eocene. The collision of the Bahamas Bank on the northern  
414 Caribbean margin in the Eocene (Mann, 1999) led to frontal erosion of the accretionary prism  
415 in the Greater Antilles and frontal erosion in the NLA. Prior to this time, sediment supply  
416 sources were likely from the Venezuela and Guyana Plateau in the south (e.g. (Wright, 1984;  
417 Xie et al., 2010), and the supply of terrigenous sediments, precisely through the Orinoco and  
418 Amazonian Rivers has remained consistent. As at Miocene, the Tiburon Rise, followed by the  
419 Barracuda Ridge in Early Pleistocene uplifted, and has been sweeping south beneath the margin  
420 (Pichot et al., 2012). These two topographic highs may have been eroding the deformation front  
421 since their subduction. Evidence of topographic highs locally causing frontal erosion has been  
422 documented along the Middle American convergent margin (e.g. Ranero & Von Huene, 2000),  
423 and in Costa Rica (e.g. von Huene et al., 2004). Moreover, the relief of these ridges forms  
424 barrier to the propagation of sediments (Westbrook, 1982), giving rise to the deflection of  
425 bottom currents (Deville et al., 2015), and reducing the rate of sediment supply northwards.  
426 This uneven distribution of sediments from south to north is consistent with the current oceanic  
427 and trench sediment fill in the LASZ. Thus, in the southern LA, thick sediment-fill in the trench  
428 up-to 10km smooths the rough topography of the subducting oceanic lithosphere and favours  
429 development of wide and thick accretionary prism (Westbrook, 1982), while thin to very thin  
430 trench-fill-sediments  $< 0.3\text{km}$  in the north is not enough to smooth the subducting lithosphere  
431 and favours erosion.

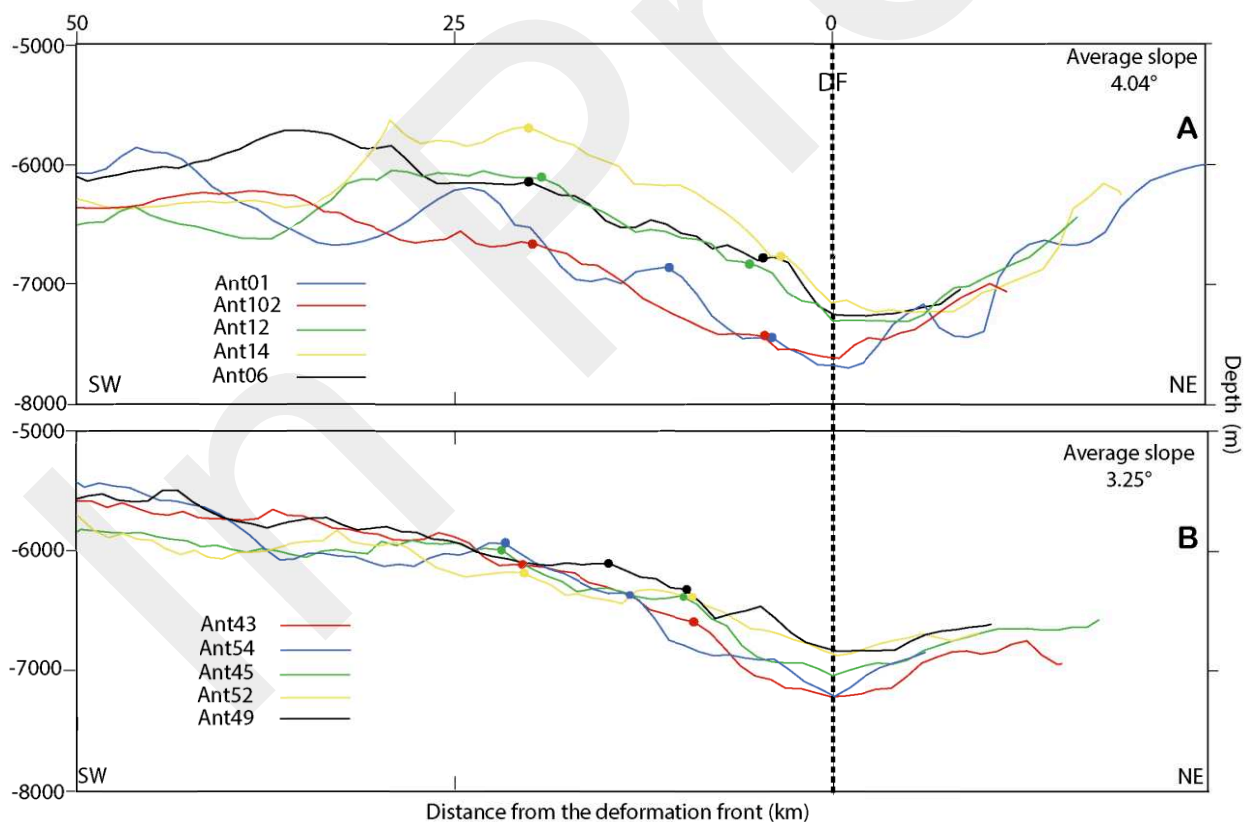
## 432 ***5.2 The forearc slope and taper angle***

433 The study of forearc geometries has been used to infer tectonic erosion in other subduction  
434 zones (e.g. Clift & Vannucchi, 2004; Noda, 2016; Kopp et al., 2006). These studies have shown  
435 that at subduction zones undergoing tectonic erosion, the outer wedge slope and taper angles  
436 are high, usually  $>3^\circ$  and  $>10^\circ$  respectively.

437 Using the method described in Noda, (2016), we calculate the outer wedge slope angle based  
438 on bathymetric tracks along our trench-normal MCS lines (Figure 8). The calculated slope angle

439 for each line is an average value of the inner and middle prism, which constitute the outer  
 440 wedge. We record values of the slope angles that vary with an increasing slope trend from south  
 441 to north of the study area from an average of  $3.25^\circ$  in B consisting of the inner and outer prism  
 442 to  $4.04^\circ$  in A consisting of only the inner prism (Figure 8). However, we estimate an average  
 443 value of slope angle of  $3.65^\circ$  to represent an overall trend of the outer wedge slope in the NLA.  
 444 Thus, with an average dip of  $\sim 8^\circ$  for the oceanic crust beneath the prism at less than 50 km  
 445 distance from the trench (Laurencin et al., 2018), we calculate a taper of  $\sim 11.65^\circ$  for the NLA  
 446 wedge.

447 These calculated values for the forearc slope angle and the taper are rather low, but lie within  
 448 estimated ranges for erosive margins (e.g. Clift & Vannucchi, 2004; Noda, 2016). The values  
 449 differ from those measured along the southern LA where the trench sediment-fill is thicker and  
 450 the accretionary wedge longer (e.g. Clift and Vannucchi, 2004) indicating that the entire margin  
 451 cannot be considered accretionary anymore. In contrast our data shows that there is a variation  
 452 from north to south of the LA margin, and the margin is dominantly erosive in the NLA.



453  
 454 *Figure 8: Display of bathymetric tracks in the NLA margin across dip MCS profiles from the*  
 455 *oceanic domain to 50 km distance from the deformation front. The forearc slope angle*  
 456 *calculated here is the average value of slope angles of the frontal and middle prism. The dots*  
 457 *on the bathymetric tracks are points used in the calculation. DF- Deformation front. See the*  
 458 *location of the MCS lines in Figure 1.*

### 459 ***5.3 Margin subsidence and forearc crustal thinning***

460 As shown in previous studies (e.g. Boucard et al., 2021; Cornée et al., 2021), the rate of forearc  
461 subsidence have been estimated to be up to 0.34 mm/yr since the middle Miocene ~16Ma. This  
462 estimation is based on the current depth of the earliest Mid-Miocene sub-aerial unconformity  
463 UB2, which occurs at up to 7stwt in dip seismic reflection lines located west of Longitude –  
464 61°W. To the south of this longitude and as far south as the Barracuda Ridge, we observe similar  
465 unconformity UB2 surface on trench-normal seismic lines (Figure 3 and supplementary  
466 material). This surface occurs even at greater depth of up to 7.5stwt, and increases progressively  
467 to 8stwt along the trenchward tilted segment of the margin (From CDP 3000 to 4000 in line  
468 Ant43 for instance - Figure 3 and supplementary material). The unconformity can be traced  
469 from the inner forearc to the backstop. Considering P wave velocity  $V_p$  of 1.7 to 2.5 km/s in  
470 the sedimentary column, we can estimate a maximum forearc subsidence of 0.44 mm/yr where  
471 UB2 is the deepest (8 stwt), close to the Barracuda Ridge trailing flank. We propose that the  
472 southward sweeping of the barracuda topographic high locally increases the regional margin  
473 basal erosion along the N110°E normal faults segments (Ant45 in Figure 5 and MTYHR40 in  
474 the supplementary material). Therefore, this local increase in subsidence maybe associated to  
475 the subducting impact of the Ridge at this location. These observations therefore suggests  
476 increasing widespread margin subsidence that affects thousands of square kilometres of the  
477 NLA margin, similar to those observed in the central (De Min et al., 2015; Leclerc et al., 2014;  
478 Leclerc & Feuillet, 2019), and PRVI margins (Grindlay et al., 2005).

479 At convergent margins, forearc subsidence can result from several phenomena, such as, crustal  
480 thinning by forearc extension, basal erosion, or changes in slab dip (Noda, 2016; Karig et al.,  
481 1979). The extensional faults including the Tintamarre Faults (Boucard et al., 2021), and the  
482 N110°E - N160°E faults that cuts through the margin forearc likely accommodates extension  
483 due to subsidence of the margin. The Tintamarre Faults are oriented parallel to the trench and  
484 are generated by trench perpendicular extensions (Boucard et al., 2021). On the other hand, the  
485 N110°E - N160°E faults rotate southward from nearly parallel to the trench (N160°E) in the  
486 Barbuda Valley to oblique to the trench, and sub-parallel to the Barracuda Ridge (N110°E)  
487 along its trailing flank. These faults thus likely rotated to accommodate the oblique subduction  
488 and southward sweeping of the Barracuda ridge (Figure 2 & 6). Like the Tintamarre Faults,  
489 they offset the seafloor, cutting through the recent sedimentary units. Moreover, they form  
490 series of grabens and half grabens with tilted fault walls, likely generated in the wake of the  
491 subduction of the topographic ridge bounded by the 15-20 fracture zone. A significant feature

492 of these forearc extensional faults in the NLA margin is that they are associated with a major  
493 crustal thinning (Figure 6 and supplementary material). North of longitude  $-61^{\circ}\text{W}$ , basement  
494 thinning along the Tintamarre fault zone is estimated to be up to 50% locally (Boucard et al.,  
495 2021). We estimate similar values ( $\sim 48 - 50\%$ ), for instance in Ant45 between CDP 7800 -  
496 9800, and Ant52 between CDP 1 - 2800, along the zones of the  $\text{N}110^{\circ}\text{E} - \text{N}160^{\circ}\text{E}$  faults.  
497 Displacement along these major faults is calculated to vary between  $\sim 0.15$  to  $\sim 0.68$  km where  
498 they are highest (for instance at CDP 7000 - 8000 in MTYHR40), while the unconformity UB2  
499 surface, deposited in Mid-Miocene  $\sim 16\text{Ma}$  (Boucard et al., 2021) is currently at the depth of  
500  $\sim 7$  km. Thus, the displacement along these faults is not enough to account for the degree of  
501 subsidence and basement thinning that occur throughout the NLA forearc margin.

502 In subduction margins where the finite displacement of normal, extensional faults and  
503 associated crustal thinning cannot account for the measured forearc subsidence, it is likened to  
504 an erosive margin, for example, in the Japan outer forearc (Von Huene & Lallemand, 1990;  
505 Boston et al., 2017). Studies on the processes that result to the large-scale, long-term margin  
506 subsidence in the LASZ suggests tectonic erosion (e.g. De Min et al., 2015; Boucard et al.,  
507 2021) and slab rollback on the basis of GNSS data (e.g. van Rijsingen et al., 2022). As a result,  
508 at a regional scale, several mechanisms may be responsible for the LA margin subsidence,  
509 which is likely increased in the NLA because of subduction basal erosion.

#### 510 ***5.4 Fluid migration***

511 Both the seismic and bathymetric data within the study zone show evidence of fluid presence  
512 at different structural levels and active faults from the plate interface, through the overriding  
513 plate up-to the seafloor (Figure 6). The upward flow of fluids in seismic data is characterized  
514 by the presence of shallow outcropping conduits, which are imaged as sub-vertical, circular,  
515 and narrow acoustic masking zones occurring as acoustic-pipe-structures (e.g. Saritas et al.,  
516 2018; Andreassen et al., 2007; Hustoft et al., 2007). These fluid pipes have a direct relationship  
517 with the formation of mud volcanoes/ or pockmarks on the seafloor. While pockmarks occur as  
518 V-shaped depression structures (e.g. Judd & Hovland, 2007), mud volcanoes appear in the form  
519 of positive domed structures due to the upward migration of low-density materials (e.g. Saritas  
520 et al., 2018). In addition, the high amplitude, reversed polarity reflectors observed close to the  
521 normal faults that dominate this margin (Figure 7b) likely show presence of fluids along the  
522 fault planes. Moreover, previous studies based on wide-angle derived velocity anomaly  
523 (Klingelhoefer et al., 2018), and positive thermal anomaly (Ezenwaka et al., 2022) within the

524 forearc ~70 km northwest of this zone also suggested warm fluid upward migration through  
525 these faults, up-to the seafloor.

526 The reflector of the decollement level has high amplitude and reverse polarity (Figure 7a)  
527 indicative of fluids from sediments accumulated within the subduction channel (Bangs et al.,  
528 2015). Studies has shown that high porosity and high fluid content can be maintained along the  
529 fault if there is delayed consolidation of the fault zone, and subducting sediments beneath the  
530 fault zone (e.g. Bangs et al., 2014; 2010; Tobin & Saffer, 2009; Sage et al., 2006).

531 The reverse polarity for the decollement reflector discontinuously extends beneath the outer  
532 forearc ~70 km from the trench possibly due to subducting sediment compaction and decreasing  
533 fluid content. It is unlikely that the subducting sediment compaction is the only source of fluids,  
534 which migrate through the margin pathways system. Moreover, the structures observed in the  
535 seismic and bathymetric data that support upward fluid migration occur in the outer forearc, at  
536 least > 100 km from the deformation front. Based on thermal models of the NLA subduction  
537 margin, Ezenwaka et al., (2022) predicts that the subducted sediments will reach 150°C,  
538 consistent with the thermal limit for driving clay mineral dehydration (Moore & Saffer, 2001),  
539 at the depth of 25 km and distance of 110 km from the deformation front. They also predicted  
540 the dehydration of the slab at 70 - 80 km depth for metamorphosed Mid-oceanic ridge basalt,  
541 and 140 – 160 km for seperntinized-exhumed mantle. It is thus likely that a combination of  
542 fluids released at several depths by deserpentination, eclogitization, and clay mineral  
543 compaction and dehydration collectively contribute to the hydration of the margin depth and  
544 fluid upward percolation system.

#### 545 ***5.5 Link between the fluids and forearc tectonic deformations***

546 Various seismic lines show basement highs covered by thin and deformed sediments (Ant48,  
547 54 and MTYHR38 in Figure 6) and separated by prominent normal faults consisting of the  
548 southward end of the N120°E Tintamarre Fault, and the N160°E - N110°E faults. Some of these  
549 faults fracture the sediment down to the upper plate basement, indicating that they are deeply  
550 rooted. The location of mud volcanoes and pockmarks above fault structured basement high  
551 strikingly indicates that the deformation pattern favours the collection of fluids and its migration  
552 up to the seafloor.

553 The Lesser Antilles subduction margin is a region that is dominated by massive circulating  
554 fluids originating from depths (e.g. Marcaillou et al., 2021; Bie et al., 2022; Ezenwaka et al.,  
555 2022). We propose that the deeply rooted faults collect deep fluids possibly provided by the



556 plate interface and act as major fluid pathways through the interplate. Some of these faults  
557 segment structure the basement topographic high and likely drives fluids toward the pockmark  
558 and mud volcanoes preferentially located on top of these basement bulges. As a result, the over-  
559 pressured fluids penetrate the thin sediment units to form mound-like structures on the seafloor.  
560 Where a decrease in the shear strength of the overlying sediment and static instability occurs  
561 (e.g. Hovland & Judd, 1988), they result to blowout and slumps on the seafloor, forming the  
562 pockmarks.

563 Numerous indications of fluid pathways and storage in the vertical dimension that we record in  
564 this study suggest a potential widespread fluid circulation, which is in agreement with  
565 observations from heat flow data (Ezenwaka et al., 2022) and Wide-Angle velocity models  
566 (Klingelhoefer et al., 2018) at less than 70 km north of this study location. If we extrapolate the  
567 idea that the entire NLA forearc is widely invaded by fluids, flowing upward up-to the seafloor,  
568 this widespread pervasive fluid circulation may be playing a significant role in its long-term  
569 tectonic deformation. In other subduction zones, like the Chilean margin (VonHuene et al.,  
570 2004), over-pressured fluids expelled from depth has been interpreted to favour hydrofracturing  
571 and basal erosion. Following the characteristic evidence of subsidence and erosions that we  
572 have recorded in the NLA margin, in addition to its tectonic deformation patterns and  
573 widespread fluid circulations, we propose a mechanism for subduction erosion in this margin  
574 that would favour basal hydrofracturing by fluids.

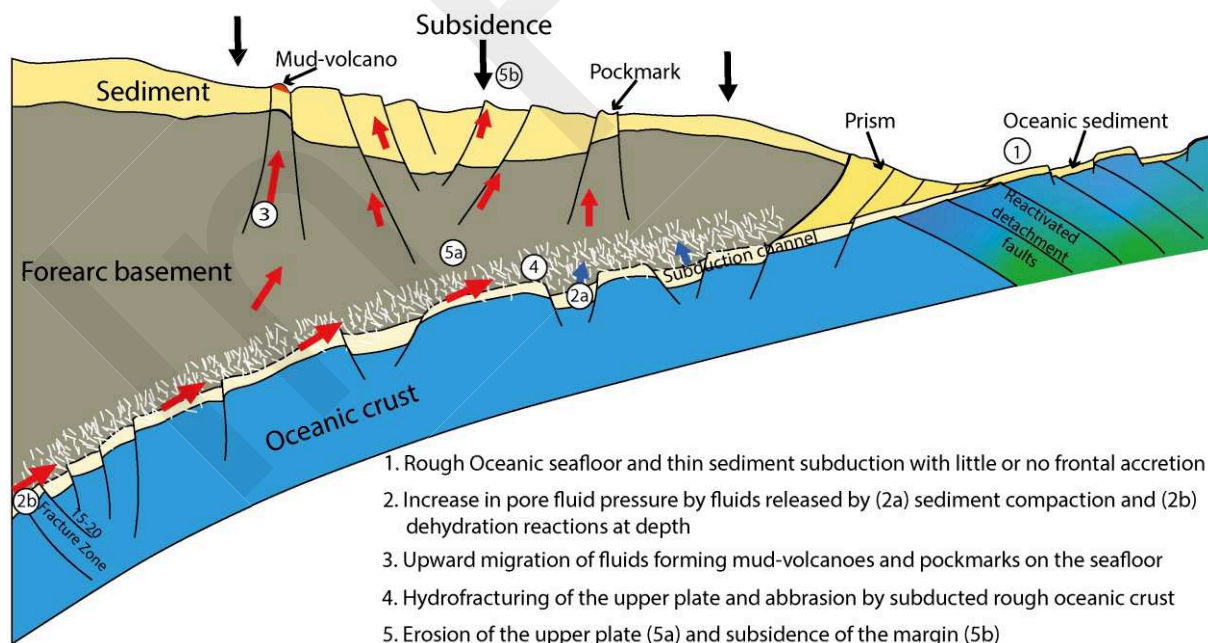
### 575 ***5.6 Mechanism of subduction erosion in the NLA margin***

576 Our model for the process of subduction erosion in the NLA margin is based on the nature of  
577 the subducting oceanic lithosphere, the extent of fluid circulation within the subduction zone,  
578 the volume of trench-fill sediment that subducts within the subduction channel, the subducting  
579 Barracuda ridge bounded by the 15-20 fracture zone, and the Jacksonville FZ at the trench.

580 The oceanic basement that subducts beneath the NLA margin was formed at a slow-spreading  
581 ridge, and consist of dispersed patches of exhumed and highly hydrated mantle rocks that can  
582 be deeply and pervasively fractured by widespread detachment faults (e.g. in the Jacksonville  
583 patch, Marcaillou et al., 2021). As the plate approaches the trench and subducts, these  
584 detachment faults might be reactivated by plate bending and allows downward fluid  
585 percolations (Ezenwaka et al., 2022). In addition, the orientation of the Jacksonville FZ almost  
586 parallel to the trench immediately northwest of the patch likely favour its reactivation at plate  
587 bending, allowing further fluid percolations and creating rough seafloor morphology. In the  
588 trench, the decollement level is located at the top of the thin trench-fill-sediments and allows

589 sediment subduction with little or no frontal accretion. As the oceanic lithosphere subducts,  
 590 pore pressure within the slab increases due to metamorphic reactions and increasing lithostatic  
 591 pressure. Moreover, at greater depth in the subduction, the highly hydrated oceanic crust and  
 592 the 15-20 crustal scale Fracture zone may release additional amount of fluid by dehydration  
 593 into the plate interplate damaged zone (Ezenwaka et al., 2022). These fluids possibly migrate  
 594 updip through the interplate damaged zone, increase the local pore fluid pressure and reduce  
 595 effective stress (Moreno et al., 2014). Overpressure fluids are likely to triggers margin  
 596 hydrofracturing before being collected by deep-rooted upper plate forearc faults. The fluids  
 597 then migrate upwards (in a continuous or transient way) up to the seafloor. Evidence of fluids  
 598 released by high-temperature venting along normal faults are present in the outer forearc in the  
 599 NLA subduction margin. Presence of these fluids have been inferred to indicate elevated fluid  
 600 pressure in subduction zones (e.g. Hensen et al., 2004). The consistent hydrofracturing of the  
 601 upper plate and its abrasion by the subducted rough oceanic crust may dislodge basement  
 602 materials into the subduction channel, and produce subsidence and thinning of the upper plate's  
 603 forearc crust (Figure 9). The eroded fragments of the upper plate may be accommodated by the  
 604 subducted grabens within the subduction channel, and the active interface thrust will constantly  
 605 migrate upwards as proposed by VonHuene et al., (2004).

606



607

608 *Figure 9: Sketch of the proposed mechanism of subduction erosion within the northern Lesser*  
 609 *Antilles subduction zone.*

610 This mechanism may have been acting long before the initiation and interaction of the  
611 Barracuda ridge with the NLA subduction margin, and we have explored several scenarios to  
612 arrive at this conclusion. First, forearc margin subsidence in the NLA began from the Mid-  
613 Miocene  $\sim 15$  Ma (Boucard et al., 2021), while the Barracuda ridge uplift is dated Early  
614 Pleistocene  $\sim 2.3$  Ma according to Pichot et al., (2012). The Barracuda Ridge cannot therefore  
615 be responsible for the onset of this margin subsidence that began more than 12 Ma before its  
616 emplacement. If we consider a plate convergence motion of  $20 \text{ mmyr}^{-1}$  towards  $S74^\circ W$   
617 (DeMets et al., 2010), and the Barracuda ridge trending WNW-ESE at  $\sim N110^\circ E$ , then the  
618 ridge-normal sweeping rate will be  $\sim 11.7 \text{ km/myr}$ . The covered trench-normal displacement  
619 of the BR since its emplacement is  $\sim 27 \text{ km}$ . In other words, BR ridge has migrated over a  
620 distance equivalent to its width since its creation at 2.3 Ma. One would need to triple its age to  
621 have an ending interaction with the imbricated backstop and to quadruple it for starting it, at  $\sim 9$   
622 Ma.

623 Secondly, in the forearc, at the eastern flank of the Antigua Valley, the  $N160^\circ E - N110^\circ E$  faults  
624 (black – purple lines in Figure 2) show typical attributes of rotated faults, and forearc collapsing  
625 that follow the southward sweeping ridge. Imprints of these faults on the bathymetry are  
626 observed up-to the ridge but terminate just before the southern flank of the ridge, indicating  
627 their association with the subducting topographic high. They are furthermore located at the  
628 distance range closely consistent with the ridge emplacement 2.3 Ma, with their northern extent  
629 at about a ridge-width distance from the present ridge's northern flank. These faults are not  
630 present farther NW beyond the western wall of Antigua valley, possibly because of the Barbuda  
631 spur hampering to observe any evidence of the ridge interaction with the margin in the inner  
632 forearc. However, in the outer forearc, they are completely non-existent. Hence, at a vertical  
633 distance of  $\sim 40 \text{ km}$  from the northern flank of the ridge to the northernmost extent of these  
634 faults at lat.  $18^\circ N$ , it will require  $\sim 3.4 \text{ Ma}$  for the ridge to cover this distance.

635 According to plate reconstruction models (Muller & Smith, 1993; Muller et al., 1999), the  
636 Barracuda Ridge uplift was due to convergence between the North and South American plates.  
637 The ridge has been linked to the western continuation of the 15-20 fracture zone (Roest &  
638 Collette, 1986), which subducts and sweeps south beneath the margin since 10 Myr (McCann  
639 & Sykes, 1984). Based on the age of the ridge uplift at the trench  $\sim 2.3 \text{ Ma}$  (Pichot et al., 2012),  
640 and the extent of its structural imprint on the forearc, we propose that the concentration of strain  
641 and displacement to accommodate the North and South American plate motion likely affected  
642 the forearc domain earlier than at the eastern flank where the ridge is located in the oceanic

643 domain. At last, we infer that the Barracuda ridge interacted only with a portion of the margin  
644 below lat. 18°N and does not contribute to the erosion occurring earlier than ~3.4 Ma. Recent  
645 observations of subsidence from micro-atolls (Philibosian et al., 2022) and GNSS data  
646 (VanRijsingin et al., 2022) collected over the past ~100 yrs has estimated an increased rate of  
647 subsidence up to 1-2 mm/yr. Moreover, geological records (Cornée et al., 2021) has also  
648 observed variations in long-term subsidence rates in the LA.

649 However, the Marathon FZ has been subducting beneath the LA margin since 30Ma (Braszus  
650 et al., 2021), while the Tiburon Rise began uplifting since Mid-Late Miocene (Pichot et al.,  
651 2012). Although we cannot predict the location of the Tiburon Ridge at its initiation, it is very  
652 likely that this ridge has been partly impacting the margin and contributing to its erosion in the  
653 NLA since Mid-Miocene. The ridge act as barrier to sediment supply to the north, thus, giving  
654 rise to the rough oceanic seafloor that subduct at that location, which favours both frontal and  
655 basal erosions.

## 656 **6.0 Conclusions**

657 Fluid flow processes such as fluid pipes and deep-rooted faults on the MCS and high-resolution  
658 seismic, with direct links to mud volcanoes and pockmarks on seafloor bathymetry dominate  
659 our study location in the NLA margin. The massive occurrence of fluids as imaged here,  
660 consistently with previous investigations confirms a forearc margin that is invaded by fluids,  
661 likely originating from depths.

662 In addition, we have also observed similar to other tectonic investigations northwest of our  
663 study area, large-scale forearc subsidence and basement thinning along normal extensional  
664 faults, rough oceanic seafloor, low trench sediment fill, and a narrow accretionary prism  
665 characterised by slope and taper angles with values within the limits of global erosive margins.  
666 Our data show the imprint of the southward sweeping Barracuda Ridge beneath the forearc, and  
667 highlight its possible northernmost interaction with the forearc margin, which cannot account  
668 for the entire margin-wide extent and age of erosion and subsidence.

669 We propose a mechanism for subduction erosion in this margin related to the subduction of a  
670 rough oceanic basement, and vigorous fluid circulation along the plate interface that causes  
671 elevated pore fluid pressure and hydrofracturing of the upper plate. Fluids are introduced into  
672 the subduction zone through sediments in the subduction channel, and crust dehydration at  
673 depths. These fluids migrate updip, penetrating extensional fractures in the upper plate and

674 dislodging its materials into the subduction channel grabens. This activity results to the thinning  
675 of the upper plate's crust and causes subsidence of the margin.

676 Based on our proposed mechanism, fluid impacted features dominated the basal erosion long  
677 before the interaction of the Barracuda ridge with the margin. We conclude that the effects of  
678 the ridge formation began beneath the forearc at the latitude of Antigua Valley earlier than at  
679 the trench, and the ridge interaction likely affected only a portion of the margin below this  
680 latitude at a recent time.

681

682

683

684

685

686

687

688

689

690

691

692

693

694

695

696

697

698

699

700

701 **References**

- 702 Andreassen, K., Nilssen, E. G., & Ødegaard, C. M. (2007). Analysis of shallow gas and fluid  
703 migration within the Plio-Pleistocene sedimentary succession of the SW Barents Sea  
704 continental margin using 3D seismic data. *Geo-Marine Letters*, 27(2), 155–171.  
705 <https://doi.org/10.1007/s00367-007-0071-5>
- 706 Bangs, N. L. B., Westbrook, G. K., Ladd, J. W., & Buhl, P. (1990). Seismic velocities from the  
707 Barbados Ridge Complex: Indicators of high pore fluid pressures in an accretionary  
708 complex. *Journal of Geophysical Research: Solid Earth*, 95(B6), 8767–8782.  
709 <https://doi.org/https://doi.org/10.1029/JB095iB06p08767>
- 710 Bangs, N. L., Christeson, G. L., & Shipley, T. H. (2003). Structure of the Lesser Antilles  
711 subduction zone backstop and its role in a large accretionary system. *Journal of*  
712 *Geophysical Research: Solid Earth*, 108(B7). <https://doi.org/10.1029/2002jb002040>
- 713 Bangs, N. L., Hornbach, M. J., Moore, G. F., & Park, J.-O. (2010). Massive methane release  
714 triggered by seafloor erosion offshore southwestern Japan. *Geology*, 38(11), 1019–1022.  
715 <https://doi.org/10.1130/G31491.1>
- 716 Bangs, N. L., McIntosh, K. D., Silver, E. A., Kluesner, J. W., & Ranero, C. R. (2015). Fluid  
717 accumulation along the Costa Rica subduction thrust and development of the seismogenic  
718 zone. *Journal of Geophysical Research: Solid Earth*, 120(1), 67–86.  
719 <https://doi.org/https://doi.org/10.1002/2014JB011265>
- 720 Bie, L., Hicks, S., Rietbrock, A., Goes, S., Collier, J., Rychert, C., Harmon, N., & Maunder, B.  
721 (2022). Imaging slab-transported fluids and their deep dehydration from seismic velocity  
722 tomography in the Lesser Antilles subduction zone. *Earth and Planetary Science Letters*,  
723 586, 117535. <https://doi.org/10.1016/j.epsl.2022.117535>
- 724 Boston, B., Moore, G. F., Nakamura, Y., & Kodaira, S. (2017). Forearc slope deformation  
725 above the Japan Trench megathrust: Implications for subduction erosion. *Earth and*  
726 *Planetary Science Letters*, 462, 26–34. <https://doi.org/10.1016/j.epsl.2017.01.005>
- 727 Boucard, M., Marcaillou, B., Lebrun, J. F., Laurencin, M., Klingelhoefer, F., Laigle, M.,  
728 Lallemand, S., Schenini, L., Graindorge, D., Cornée, J. J., Münch, P., Philippon, M., &  
729 the, A. (2021). Paleogene V-Shaped Basins and Neogene Subsidence of the Northern  
730 Lesser Antilles Forearc. *Tectonics*, 40(3), 1–18. <https://doi.org/10.1029/2020TC006524>

- 731 Braszus, B., Goes, S., Allen, R., Rietbrock, A., Collier, J., Harmon, N., Henstock, T., Hicks, S.,  
732 Rychert, C. A., Maunder, B., van Hunen, J., Bie, L., Blundy, J., Cooper, G., Davy, R.,  
733 Kendall, J. M., Macpherson, C., Wilkinson, J., & Wilson, M. (2021). Subduction history  
734 of the Caribbean from upper-mantle seismic imaging and plate reconstruction. *Nature*  
735 *Communications*, 12(1). <https://doi.org/10.1038/s41467-021-24413-0>
- 736 Calais, É., Symithe, S., Mercier de Lépinay, B., & Prépetit, C. (2016). Plate boundary  
737 segmentation in the northeastern Caribbean from geodetic measurements and Neogene  
738 geological observations. *Comptes Rendus - Geoscience*, 348(1), 42–51.  
739 <https://doi.org/10.1016/j.crte.2015.10.007>
- 740 Clift, P., & Vannucchi, P. (2004). Controls on tectonic accretion versus erosion in subduction  
741 zones: Implications for the origin and recycling of the continental crust. *Reviews of*  
742 *Geophysics*, 42(2). <https://doi.org/10.1029/2003RG000127>
- 743 Cooper, G. F., Macpherson, C. G., Blundy, J. D., Maunder, B., Allen, R. W., Goes, S., Collier,  
744 J. S., Bie, L., Harmon, N., Hicks, S. P., Iveson, A. A., Prytulak, J., Rietbrock, A., Rychert,  
745 C. A., Davidson, J. P., Cooper, G. F., Macpherson, C. G., Blundy, J. D., Maunder, B., ...  
746 Wilson, M. (2020). Variable water input controls evolution of the Lesser Antilles volcanic  
747 arc. *Nature*, 582(7813), 525–529. <https://doi.org/10.1038/s41586-020-2407-5>
- 748 Cornée, J. J., Münch, P., Philippon, M., BouDagher-Fadel, M., Quillévéré, F., Melinte-  
749 Dobrinescu, M., Lebrun, J. F., Gay, A., Meyer, S., Montheil, L., Lallemand, S.,  
750 Marcaillou, B., Laurencin, M., Legendre, L., Garroq, C., Boucard, M., Beslier, M. O.,  
751 Laigle, M., Schenini, L., ... Marivaux, L. (2021). Lost islands in the northern Lesser  
752 Antilles: possible milestones in the Cenozoic dispersal of terrestrial organisms between  
753 South-America and the Greater Antilles. *Earth-Science Reviews*, 217(October 2020).  
754 <https://doi.org/10.1016/j.earscirev.2021.103617>
- 755 Davy, R. G., Collier, J. S., Henstock, T. J., Rietbrock, A., Goes, S., Blundy, J., Harmon, N.,  
756 Rychert, C., Macpherson, C. G., Van Hunen, J., Kendall, M., Wilkinson, J., Davidson, J.,  
757 Wilson, M., Cooper, G., Maunder, B., Bie, L., Hicks, S., Allen, R., ... Labahn, E. (2020).  
758 Wide-Angle Seismic Imaging of Two Modes of Crustal Accretion in Mature Atlantic  
759 Ocean Crust. *Journal of Geophysical Research: Solid Earth*, 125(6), 1–21.  
760 <https://doi.org/10.1029/2019JB019100>
- 761 De Min, L., Lebrun, J. F., Cornée, J. J., Münch, P., Léticée, J. L., Quillévéré, F., Melinte-

- 762 Dobrinescu, M., Randrianasolo, A., Marcaillou, B., & Zami, F. (2015). Tectonic and  
763 sedimentary architecture of the Karukéra spur: A record of the Lesser Antilles fore-arc  
764 deformations since the Neogene. *Marine Geology*, 363, 15–37.  
765 <https://doi.org/10.1016/j.margeo.2015.02.007>
- 766 DeMets, C., Gordon, R. G., & Argus, D. F. (2010). Geologically current plate motions.  
767 *Geophysical Journal International*, 181(1), 1–80. [https://doi.org/10.1111/j.1365-  
768 246X.2009.04491.x](https://doi.org/10.1111/j.1365-246X.2009.04491.x)
- 769 Deville, E., Mascle, A., Callec, Y., Huyghe, P., Lerat, O., Mathieu, X., Pedron de Carillo, C.,  
770 Patriat, M., Pichot, T., Loubrieux, B., & Granjeon, D. (2015). *Tectonics and sedimentation  
771 interactions in the east Caribbean subduction zone : An overview from the Orinoco delta  
772 and the Barbados accretionary prism*. 64(June), 76–103.  
773 <https://doi.org/10.1016/j.marpetgeo.2014.12.015>
- 774 Dominguez, S., Malavieille, J., & Lallemand, S. E. (2000). Deformation of accretionary wedges  
775 in response to seamount subduction: Insights from sandbox experiments. *Tectonics*, 19(1),  
776 182–196. <https://doi.org/10.1029/1999TC900055>
- 777 Evain, M., Galve, A., Charvis, P., Laigle, M., Kopp, H., Bécel, A., Weinzierl, W., Hirn, A.,  
778 Flueh, E. R., & Gallart, J. (2013). Structure of the Lesser Antilles subduction forearc and  
779 backstop from 3D seismic refraction tomography. *Tectonophysics*, 603, 55–67.  
780 <https://doi.org/10.1016/j.tecto.2011.09.021>
- 781 Ezenwaka, K., Marcaillou, B., Laigle, M., Klingelhofer, F., Lebrun, J. F., Paulatto, M., Biari,  
782 Y., Rolandone, F., Lucazeau, F., Heuret, A., Pichot, T., & Bouquerel, H. (2022).  
783 Thermally-constrained fluid circulation and seismicity in the Lesser Antilles subduction  
784 zone. *Earth and Planetary Science Letters*, 597, 117823.  
785 <https://doi.org/10.1016/j.epsl.2022.117823>
- 786 Goncalves, P., Guillot, S., Lardeaux, J., Nicollet, C., Lepinay, B. M. De, Goncalves, P., Guillot,  
787 S., Lardeaux, J., Goncalves, P., Guillot, S., Lardeaux, J., Nicollet, C., & De, B. M. (2015).  
788 *Thrusting and sinistral wrenching in a pre-Eocene HP-LT Caribbean accretionary wedge  
789 ( Samaná Peninsula , Dominican Republic ) Thrusting and sinistral wrenching in a pre-  
790 Eocene HP-LT Caribbean accretionary wedge ( Samana Peninsula , Dominican Republic  
791 ). 13*, 119–122. <https://doi.org/10.1080/09853111.2000.11105368>
- 792 Grindlay, N. R., Carolina, N., & Dolan, J. F. (2005). *Neotectonics and subsidence of the*



- 793        *northern Puerto Rico – Virgin Islands margin in response to the oblique subduction of*  
794        *high-standing ridges.* 31–60.
- 795 Hensen, C., Wallmann, K., Schmidt, M., Ranero, C. R., & Suess, E. (2004). Fluid expulsion  
796        related to mud extrusion off Costa Rica—A window to the subducting slab. *Geology*,  
797        32(3), 201–204. <https://doi.org/10.1130/G20119.1>
- 798 Hinsbergen, D. J. J. Van, Iturralde-vinent, M. A., Geffen, P. W. G. Van, & Garc1, A. (2009).  
799        *Structure of the accretionary prism , and the evolution of the Paleogene northern " ey ,*  
800        *Cuba Caribbean subduction zone in the region of Camagu.* 31, 1130–1144.  
801        <https://doi.org/10.1016/j.jsg.2009.06.007>
- 802 Hovland, M., & Judd, A. G. (1988). Seabed pockmarks and seepages. Impact on geology,  
803        biology and marine environment. In *Graham and Trotman Ltd., London* (Vol. 6, pp. 2–3).
- 804 Hustoft, S., Mienert, J., Bünz, S., & Nouzé, H. (2007). *High-resolution 3D-seismic data*  
805        *indicate focussed fluid migration pathways above polygonal fault systems of the mid-*  
806        *Norwegian margin.* 245, 89–106. <https://doi.org/10.1016/j.margeo.2007.07.004>
- 807 Jany I, I., Scanlon, K. M., & Mauffret, A. (1990). Geological Interpretation of Combined  
808        Seabeam, Gloria and Seismic Data from Anegada Passage (Virgin Islands, North  
809        Caribbean). *Marine Geophysical Researches*, 12, 173–196.
- 810 Judd, A., & Hovland, M. (2007). *Seabed Fluid Flow: The Impact on Geology, Biology and the*  
811        *Marine Environment.* Cambridge University Press. [https://doi.org/DOI:](https://doi.org/DOI:10.1017/CBO9780511535918)  
812        [10.1017/CBO9780511535918](https://doi.org/DOI:10.1017/CBO9780511535918)
- 813 Karig, D. E., Suparka, S., Moore, G. F., & Hehanussa, P. E. (1979). Structure and cenozoic  
814        evolution of the sunda arc in the central Sumatra region. *Deep Sea Research Part B.*  
815        *Oceanographic Literature Review*, 26(12), 776–777.  
816        [https://doi.org/https://doi.org/10.1016/0198-0254\(79\)90715-5](https://doi.org/https://doi.org/10.1016/0198-0254(79)90715-5)
- 817 Klingelhoefer, F., & Marcaillou, B. (2022). *MANTA-RAY cruise, RV L'Atalante.*  
818        <https://doi.org/https://doi.org/10.17600/18002498>
- 819 Klingelhoefer, F., Marcaillou, B., Laurencin, M., Biari, Y., Laigle, M., Graindorge, D., Evain,  
820        M., Lebrun, J.-F., & Paulatto, M. (2018). Relation Between the Nature of the Subducting  
821        Plate, Heat Flow and Fluid Escape Structures at the Lesser Antilles Island arc. *American*  
822        *Geophysical Union Fall Meeting, Wahsington, DC, USA, T22B-04*, 10–14.

- 823 Kopp, H., Flueh, E. R., Petersen, C. J., Weinrebe, W., Wittwer, A., & Scientists, M. (2006).  
824 The Java margin revisited: Evidence for subduction erosion off Java. *Earth and Planetary*  
825 *Science Letters*, 242(1–2), 130–142. <https://doi.org/10.1016/j.epsl.2005.11.036>
- 826 Laigle, M., Becel, A., de Voogd, B., Sachpazi, M., Bayrakci, G., Lebrun, J. F., & Evain, M.  
827 (2013). Along-arc segmentation and interaction of subducting ridges with the Lesser  
828 Antilles Subduction forearc crust revealed by MCS imaging. *Tectonophysics*, 603, 32–54.  
829 <https://doi.org/10.1016/j.tecto.2013.05.028>
- 830 Laigle, M., Lebrun, J.-F., & Hirn, A. (2007). *SISMANTILLES 2 cruise, RV L'Atalante*.  
831 <https://doi.org/https://doi.org/10.17600/7010020>
- 832 Lallemand, S. E., Schnürle, P., Malavieille, J. (1994). Coulomb theory applied to accretionary  
833 and nonaccretionary wedges: Possible causes for tectonic erosion and/or frontal accretion.  
834 *Journal of Geophysical Research*, 1994, 99(B6), pp.12033-12055
- 835 Laurencin, M., Graindorge, D., Klingelhofer, F., Marcaillou, B., & Evain, M. (2018).  
836 Influence of increasing convergence obliquity and shallow slab geometry onto tectonic  
837 deformation and seismogenic behavior along the Northern Lesser Antilles zone. *Earth and*  
838 *Planetary Science Letters*, 492, 59–72. <https://doi.org/10.1016/j.epsl.2018.03.048>
- 839 Laurencin, M., Marcaillou, B., Graindorge, D., Klingelhofer, F., Lallemand, S., Laigle, M., &  
840 Lebrun, J. F. (2017). The polyphased tectonic evolution of the Anegada Passage in the  
841 northern Lesser Antilles subduction zone. *Tectonics*, 36(5), 945–961.  
842 <https://doi.org/10.1002/2017TC004511>
- 843 Laurencin, M., Marcaillou, B., Graindorge, D., Lebrun, J. F., Klingelhofer, F., Boucard, M.,  
844 Laigle, M., Lallemand, S., & Schenini, L. (2019). The Bunce Fault and Strain Partitioning  
845 in the Northern Lesser Antilles. *Geophysical Research Letters*, 46(16), 9573–9582.  
846 <https://doi.org/10.1029/2019GL083490>
- 847 Leclerc, F., & Feuillet, N. (2019). *Quaternary coral reef complexes as powerful markers of*  
848 *long-term subsidence related to deep processes at subduction zones : Insights from Les*  
849 *Saintes ( Guadeloupe , French West Indies ).* 15(4), 983–1007.
- 850 Leclerc, F., Feuillet, N., Cabioch, G., Deplus, C., Lebrun, J. F., Bazin, S., Beauducel, F.,  
851 Boudon, G., LeFriant, A., De Min, L., & Melezan, D. (2014). The Holocene drowned reef  
852 of Les Saintes plateau as witness of a long-term tectonic subsidence along the Lesser  
853 Antilles volcanic arc in Guadeloupe. *Marine Geology*, 355, 115–135.

- 854 <https://doi.org/10.1016/j.margeo.2014.05.017>
- 855 Legendre, L., Philippon, M., Münch, P., Leticée, J. L., Noury, M., Maincent, G., Cornée, J. J.,  
856 Caravati, A., Lebrun, J. F., & Mazabraud, Y. (2018). Trench Bending Initiation: Upper  
857 Plate Strain Pattern and Volcanism. Insights From the Lesser Antilles Arc, St. Barthelemy  
858 Island, French West Indies. *Tectonics*, 37(9), 2777–2797.  
859 <https://doi.org/10.1029/2017TC004921>
- 860 Mann, P. (1999). Chapter 1 Caribbean sedimentary basins: classification and tectonic setting  
861 from jurassic to present. In P. B. T.-S. B. of the W. Mann (Ed.), *Caribbean Basins* (Vol.  
862 4, pp. 3–31). Elsevier. [https://doi.org/https://doi.org/10.1016/S1874-5997\(99\)80035-5](https://doi.org/https://doi.org/10.1016/S1874-5997(99)80035-5)
- 863 Mann, P., & Burke, K. (1984). Neotectonics of the Caribbean. *Reviews of Geophysics*, 22(4),  
864 309–362. <https://doi.org/10.1029/RG022i004p00309>
- 865 Mann, P., Hippolyte, J.-C., Grindlay, N. R., & Abrams, L. J. (2005). Neotectonics of southern  
866 Puerto Rico and its offshore margin. In P. Mann (Ed.), *Active Tectonics and Seismic*  
867 *Hazards of Puerto Rico, the Virgin Islands, and Offshore Areas* (Vol. 385, p. 0).  
868 Geological Society of America. <https://doi.org/10.1130/0-8137-2385-X.173>
- 869 Marcaillou, B., & Klingelhoefer, F. (2013a). *ANTITHESIS-1-Leg1 Cruise, RV L'Atalante*.  
870 <https://doi.org/doi:10.17600/13010070>
- 871 Marcaillou, B., & Klingelhoefer, F. (2013b). *ANTITHESIS-1-Leg2 Cruise, RV Pourquoi Pas?*  
872 <https://doi.org/doi:10.17600/13030100>
- 873 Marcaillou, B., & Klingelhoefer, F. (2016). *ANTITHESIS-3 Cruise, RV Pourquoi Pas?*  
874 <https://doi.org/doi:10.17600/16001700>
- 875 Marcaillou, B., Klingelhoefer, F., Laurencin, M., J-f, L., Laigle, M., Schenini, S., Gay, L.,  
876 Boucard, M., & Graindorge, D. (2013). *Pervasive detachments in slow spreading oceanic*  
877 *basement subducting beneath the poorly-coupled Antilles Margin*. 1–15.
- 878 Marcaillou, B., Klingelhoefer, F., Laurencin, M., Lebrun, J.-F., Laigle, M., Lallemand, S.,  
879 Schenini, L., Gay, A., Boucard, M., Ezenwaka, K., & Graindorge, D. (2021). Pervasive  
880 detachment faults within the slow spreading oceanic crust at the poorly coupled Antilles  
881 subduction zone. *Communications Earth & Environment*, 2(1).  
882 <https://doi.org/10.1038/s43247-021-00269-6>
- 883 Masson, D. G., & Scanlon, K. M. (1991). The neotectonic setting of Puerto Rico. *GSA Bulletin*,

884 103(1), 144–154. <https://doi.org/10.1130/0016-7606>

885 Mccann, W. R., & Sykes, L. R. (1984). section is also characterized by both interplate Antilles  
886 and to the north of Puerto Rico . Both anomalies , bathymetric trends , and the pattern of  
887 descending slab and , therefore , westerly striking Puerto Rico trench where the North  
888 American plate mov. *Main*, 89(4), 4493–4519.

889 Montheil, L., Philippon, M., Münch, P., Camps, P., Vaes, B., Cornée, J.-J., Poidras, T., van  
890 Hinsbergen D.J.J. (2023). Paleomagnetic rotations in the northeastern Caribbean region  
891 reveal major intraplate deformation since the Eocene. *Tectonics*, 42, e2022TC007706.  
892 <https://doi.org/10.1029/2022TC007706>

893 Moore, J. C., & Saffer, D. (2001). Updip limit of the seismogenic zone beneath the accretionary  
894 prism of Southwest Japan: An effect of diagenetic to low-grade metamorphic processes  
895 and increasing effective stress. *Geology*, 29(2), 183–186. <https://doi.org/10.1130/0091-7613>

897 Moreno, M., Haberland, C., Oncken, O., Rietbrock, A., Angiboust, S., & Heidbach, O. (2014).  
898 Locking of the Chile subduction zone controlled by fluid pressure before the 2010  
899 earthquake. *Nature Geoscience*, 7(4), 292–296. <https://doi.org/10.1038/ngeo2102>

900 Muller, R. D., & Smith, W. H. F. (1993). Deformation of the oceanic crust between the North  
901 American and South American plates. *Journal of Geophysical Research*, 98(B5), 8275–  
902 8291. <https://doi.org/10.1029/92JB02863>

903 Müller, R.D., Cande, S.C., Royer, J.-Y., Roest, W.R., Maschenkov, S., 1999. New constraints  
904 on the Late Cretaceous/Tertiary plate tectonic evolution of the Caribbean. In: Mann, P.  
905 (Ed.), *Caribbean Basins. Sedimentary Basins of the World*, 4. Elsevier Science,  
906 Amsterdam, pp. 39–55.

907 Noda, A. (2016). Forearc basins: Types, geometries, and relationships to subduction zone  
908 dynamics. *Bulletin of the Geological Society of America*, 128(5–6), 879–895.  
909 <https://doi.org/10.1130/B31345.1>

910 Philibosian, B., Feuillet, N., Weil-Accardo, J., Jacques, E., Guihou, A., Mériaux, A. S.,  
911 Anglade, A., Saurel, J. M., & Deroussi, S. (2022). 20th-century strain accumulation on the  
912 Lesser Antilles megathrust based on coral microatolls. *Earth and Planetary Science  
913 Letters*, 579, 117343. <https://doi.org/10.1016/j.epsl.2021.117343>

- 914 Philippon, M., van Hinsbergen, D. J. J., Boschman, L. M., Gossink, L. A. W., Cornée, J. J.,  
915 BouDagher-Fadel, M., Léticée, J. L., Lebrun, J. F., & Munch, P. (2020). Caribbean intra-  
916 plate deformation: Paleomagnetic evidence from St. Barthélemy Island for post-Oligocene  
917 rotation in the Lesser Antilles forearc. *Tectonophysics*, 777.  
918 <https://doi.org/10.1016/j.tecto.2020.228323>
- 919 Pichot, T., Patriat, M., Westbrook, G. K., Nalpas, T., Gutscher, M. A., Roest, W. R., Deville,  
920 E., Moulin, M., Aslanian, D., & Rabineau, M. (2012). The Cenozoic tectonostratigraphic  
921 evolution of the Barracuda Ridge and Tiburon Rise, at the western end of the North  
922 America-South America plate boundary zone. *Marine Geology*, 303–306, 154–171.  
923 <https://doi.org/10.1016/j.margeo.2012.02.001>
- 924 Ranero, C. R., & Von Huene, R. (2000). Subduction erosion along the Middle America  
925 convergent margin. *Nature*, 404(6779), 748–752. <https://doi.org/10.1038/35008046>
- 926 Reid, J.A., Plumley, P.W., Schellekens, J.H. (1991). Paleomagnetic evidence for late Miocene  
927 counterclockwise rotation of north coast carbonate sequence, Puerto Rico. *Geophys. Res.*  
928 *Lett.* 18 (3), 565–568
- 929 Roest, W. R., & Collette, B. J. (1986). The Fifteen Twenty Fracture Zone and the North  
930 American-South American plate boundary. *Journal of the Geological Society, London*, 9,  
931 833–843.
- 932 Sage, F., Collot, J.-Y., & Ranero, C. R. (2006). Interplate patchiness and subduction-erosion  
933 mechanisms: Evidence from depth-migrated seismic images at the central Ecuador  
934 convergent margin. *Geology*, 34(12), 997–1000. <https://doi.org/10.1130/G22790A.1>
- 935 Saritas, H., Çifçi, G., Géli, L., Thomas, Y., Marsset, B., Henry, P., Grall, C., & Rochat, A.  
936 (2018). Gas occurrence and shallow conduit systems in the Western Sea of Marmara : a  
937 review and new acoustic evidence. *Geo-Marine Letters*, 38, 385–402.  
938 <https://doi.org/https://doi.org/10.1007/s00367-018-0547-5>
- 939 Scholl, D. W., & Von Huene, R. (2009). Implications of estimated magmatic additions and  
940 recycling losses at the subduction zones of accretionary (non-collisional) and collisional  
941 (suturing) orogens. *Geological Society Special Publication*, 318, 105–125.  
942 <https://doi.org/10.1144/SP318.4>
- 943 Stern, C. R. (2011). Subduction erosion: Rates, mechanisms, and its role in arc magmatism and  
944 the evolution of the continental crust and mantle. *Gondwana Research*, 20(2–3), 284–308.

- 945 <https://doi.org/10.1016/j.gr.2011.03.006>
- 946 Stern, R. J., & Scholl, D. W. (2010). Yin and yang of continental crust creation and destruction  
947 by plate tectonic processes. *International Geology Review*, 52(1), 1–31.  
948 <https://doi.org/10.1080/00206810903332322>
- 949 Tobin, H. J., & Saffer, D. M. (2009). Elevated fluid pressure and extreme mechanical weakness  
950 of a plate boundary thrust, Nankai Trough subduction zone. *Geology*, 37(8), 679–682.  
951 <https://doi.org/10.1130/G25752A.1>
- 952 Van Fossen, M.C., Channell, J.E., Schellekens, J.H. (1989). Paleomagnetic evidence for  
953 Tertiary anticlockwise rotation in southwest Puerto Rico. *Geophys. Res. Lett.* 16 (8), 819–  
954 822
- 955 van Rijnsingen, E. M., Calais, E., Jolivet, R., de Chabaliér, J.-B., Robertson, R., Ryan, G. A., &  
956 Symithe, S. (2022). Ongoing tectonic subsidence in the Lesser Antilles subduction zone.  
957 *Geophysical Journal International*, 319–326. <https://doi.org/10.1093/gji/ggac192>
- 958 Von Huene, R., & Lallemand, S. (1990). Tectonic erosion along the Japan and Peru convergent  
959 margins. *GSA Bulletin*, 102(6), 704–720. <https://doi.org/10.1130/0016-7606>
- 960 von Huene, R., Ranero, C. R., & Vannucchi, P. (2004). Generic model of subduction erosion.  
961 *Geology*, 32(10), 913–916. <https://doi.org/10.1130/G20563.1>
- 962 von Huene, R., & Scholl, D. W. (1991). Observations at convergent margins concerning  
963 sediment subduction, subduction erosion, and the growth of continental crust. *Reviews of*  
964 *Geophysics*, 29(3), 279–316. <https://doi.org/10.1029/91RG00969>
- 965 Westbrook, G. K. (1982). The Barbados Ridge Complex: Tectonics of a mature forearc system.  
966 *Geological Society Special Publication*, 10(Saunders 1979), 275–290.  
967 <https://doi.org/10.1144/GSL.SP.1982.010.01.18>
- 968 Westbrook, G. K., Ladd, J. W., Buhl, P., Bangs, N., & Tiley, G. J. (1988). Cross section of an  
969 accretionary wedge: Barbados Ridge complex. *Geology*, 16(7), 631–635.  
970 <https://doi.org/10.1130/0091-7613>
- 971 Wright, A. (1984). Sediment Distribution and Depositional Processes Operating in The Lesser  
972 Antilles Intraoceanic Island Arc, Eastern Caribbean. Biju-Duval B., Moore J.C., *et*  
973 *al.* (Eds.), Initial Reports of the Deep-Sea Drilling Project, Vol. 78 A, U.S. Gov. Print.  
974 Off, Washington, DC, pp. 301-324

975 Xie, X., Mann, P., & Escalona, A. (2010). Regional provenance study of Eocene clastic  
976 sedimentary rocks within the South America – Caribbean plate boundary zone using  
977 detrital zircon geochronology. *Earth and Planetary Science Letters*, 291(1–4), 159–171.  
978 <https://doi.org/10.1016/j.epsl.2010.01.009>

979

in Prep

## Supplementary Material:

### Mechanism of tectonic erosion at the Northern Lesser Antilles margin

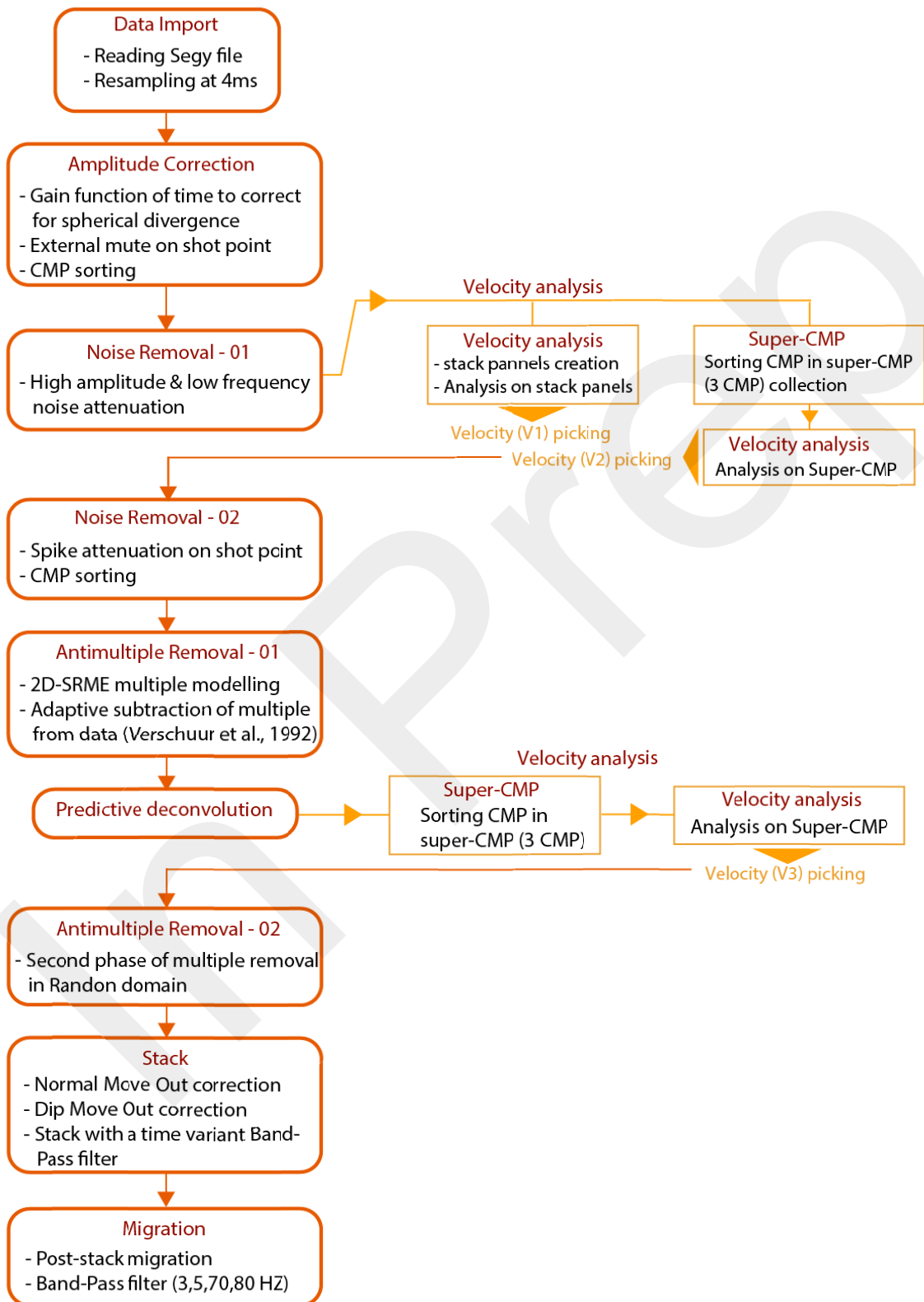


Figure 1: The workflow adopted in the image processing of the multichannel seismic data.



| <b>Survey</b>                         | <b>Antithesis 3</b> | <b>Manta-Ray (HR)</b> |
|---------------------------------------|---------------------|-----------------------|
| <b>Source volume (in<sup>3</sup>)</b> | 6500                | 320                   |
| <b>Shot spacing</b>                   | 150 m               | 10 s                  |
| <b>Rate of shot (s)</b>               | 1 shot/min          | 6 shots/min           |
| <b>Acquisition speed (Kn)</b>         | 5                   | 5                     |
| <b>Traces number</b>                  | 720                 | 480                   |
| <b>Traces spacing (m)</b>             | 6.25                | 6.25                  |
| <b>Record time (s)</b>                | 20                  | 9-13                  |
| <b>Data sampling (ms)</b>             | 2                   | 2                     |

*Table 1: Acquisition parameters of the seismic reflection during the Antithesis 1 and 3, and Manta-Ray cruises. See § 2.3.1 of Laigle et al., (2013) for the acquisition parameters of Sismantilles 2 survey.*

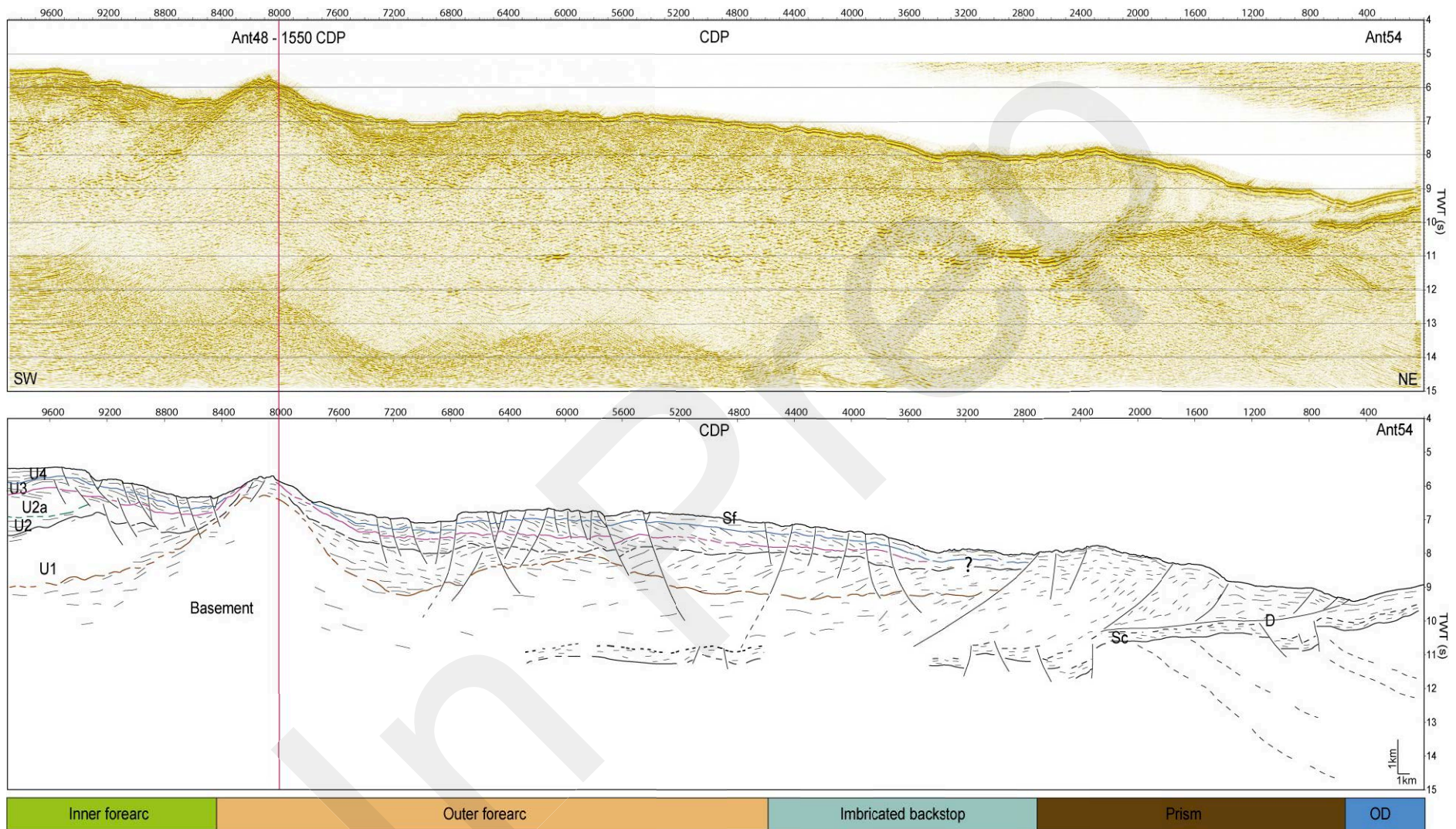


Figure 2: Structural and stratigraphic interpretations on line Ant54. D – Decollement, Sf – Seafloor, Sc – Subduction channel. U1 – U4 are interpreted seismic stratigraphic layers. UB0 – UB3 represent seismic stratigraphic surfaces. See Fig 1 in the text for the locations of the seismic lines.

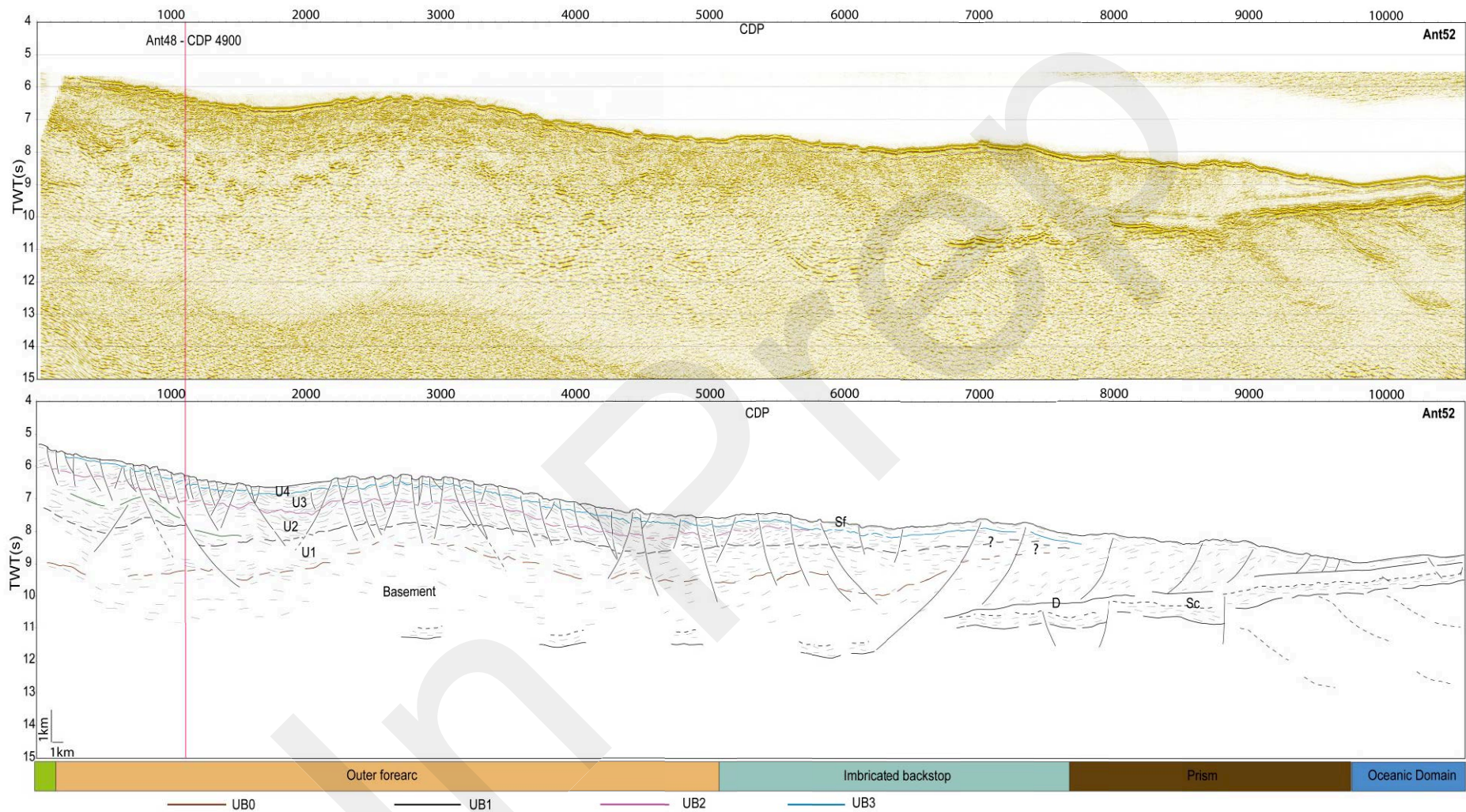


Figure 3: Structural and stratigraphic interpretations on line Ant52.

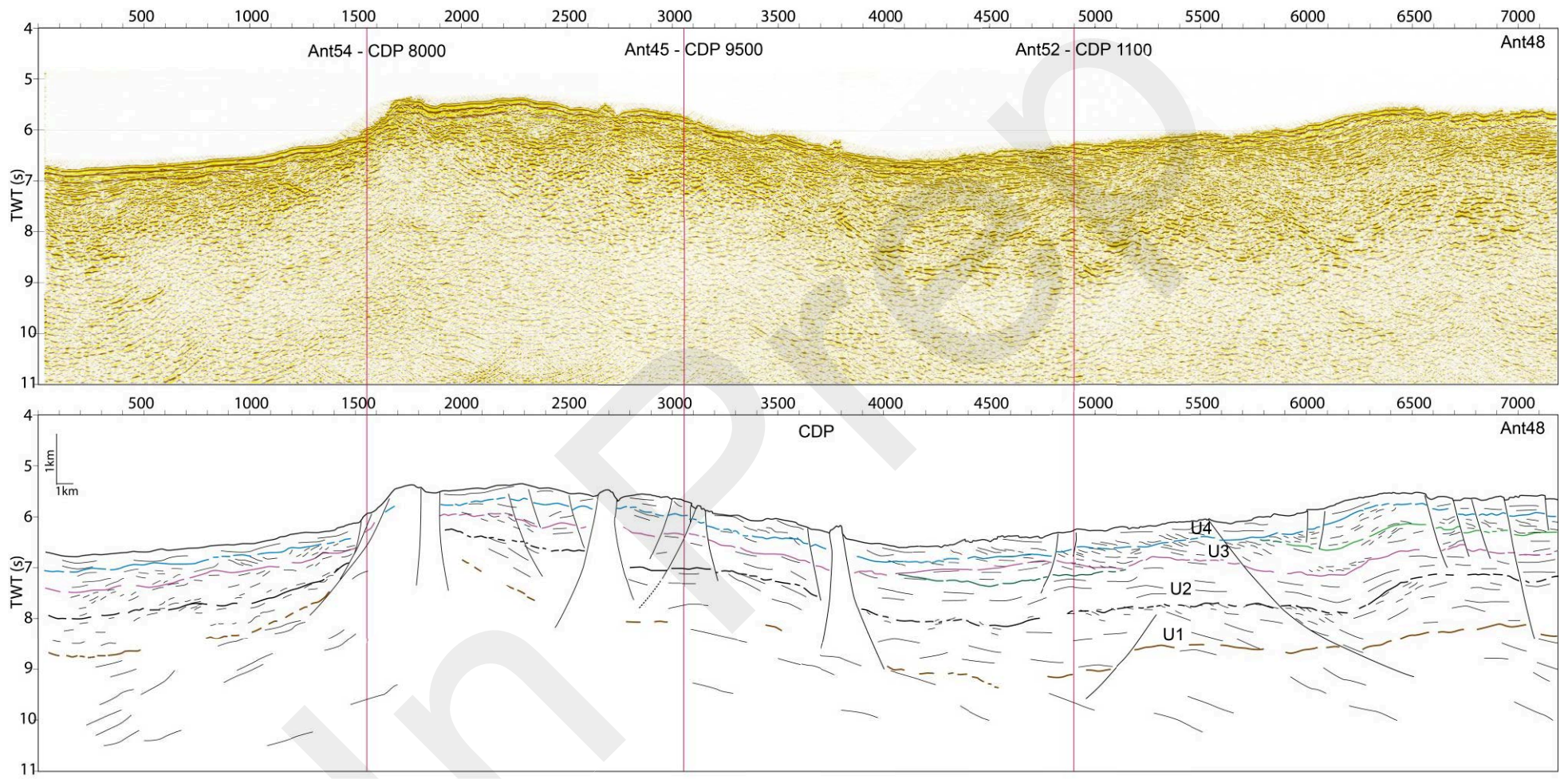


Figure 4: Structural and stratigraphic interpretations on line Ant48. The red vertical lines are the intersections of dip lines Ant54, 45, and 52 with strike line Ant48.

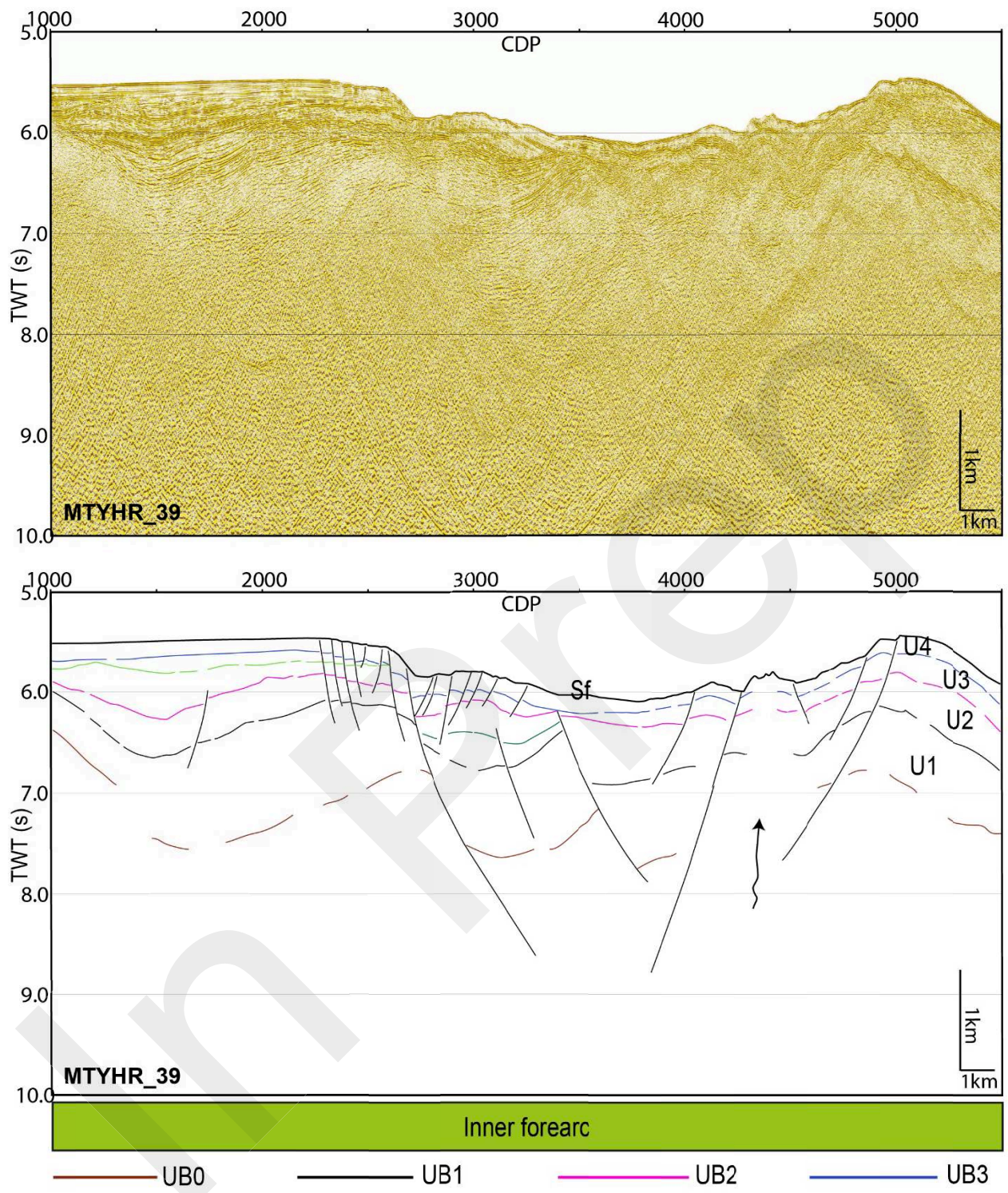


Figure 5: Structural and stratigraphic interpretations on line MTYHR39.

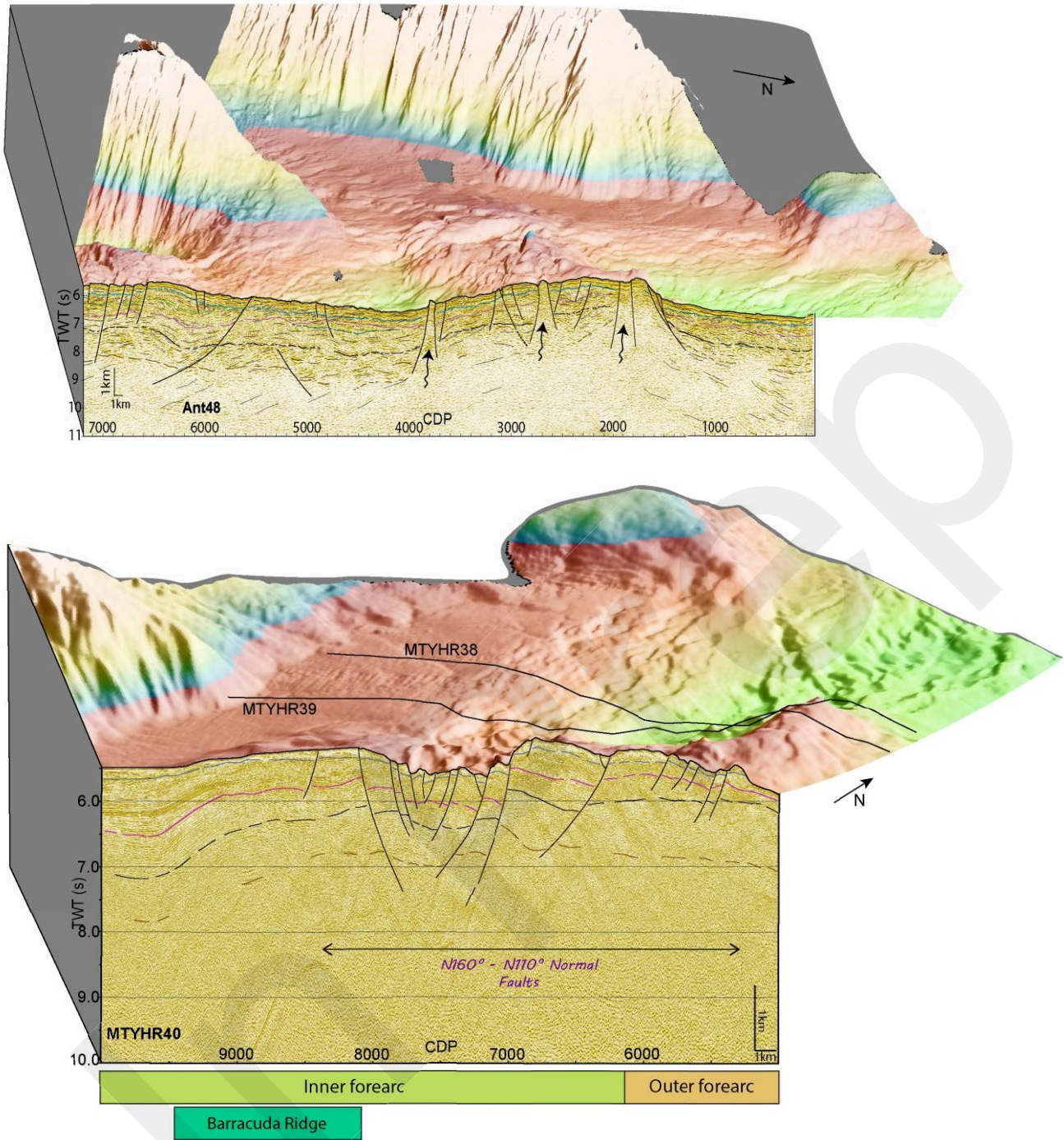
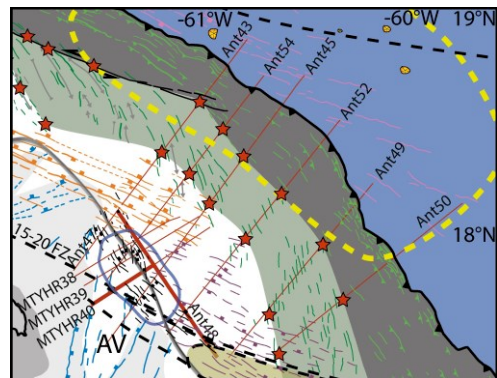


Figure 6: 3D seismic bathymetric view of the forearc along strike line Ant48 and dip High-resolution line MTYHR40. Notice how the N160° - N110° normal faults cut through the uplifted basement and the collapse of the forearc forming graben and half grabens. The black arrows in Ant48 show fluid pathways to the seafloor where they form mud volcanoes and pockmarks. The inset map shows the exact segment of the shown profiles (thick red)



# Chapter 5

## 5.0 Summary and Conclusions

The Lesser Antilles is an end-member subduction zone, which undergoes the subduction of a complex oceanic lithosphere. The oceanic crust, which formed at slow-spreading Mid-Atlantic Ridge where poor magma production favours tectonically dominated crusts (e.g. Cannat et al., 2006; Escartín et al., 2008), consist of patches of exhumed, serpentinized peridotites, with varying amount of gabbro bodies (Ildefonse et al., 2007; Zitkar et al., 2019; Davy et al., 2020; Marcaillou et al., 2021). Before the trench, numerous sub-parallel trans-oceanic fracture zones may deeply fracture and hydrate the oceanic crust and mantle (Hensen et al., 2019). Some of them are sub-parallel to the Barracuda and the Tiburon Ridges, which originate from ongoing deformation of the North and South American diffuse plate boundary, 2.3 and 10 Myr ago respectively (Patriat et al., 2011). In the Central Lesser Antilles, the subduction of those oceanic basement ridges oblique to the margin deeply fractures the forearc (Laigle et al, 2013), while the subducting fracture zones have been considered to generate vigorous dewatering and fluid circulations at depth (Cooper et al., 2020, Marcaillou et al., 2021).

In the Northern Lesser Antilles, the subducted portions of sub-parallel-to-the-trench “ridge-and-fracture” systems are expected to drastically impact there the tectonic pattern, the thermal structure and the seismic activity. This segment is therefore an excellent environment to study the effects of subducting patches of tectonically-dominated crust, and vigorous fluid circulation on the thermal structure, tectonic deformation, and seismicity along subduction zones.

Using MCS, bathymetry, heat-flow, and improved local offshore earthquake locations, acquired during 3 oceanographic campaigns (Marcaillou & Klingelhoefer, 2013a; Marcaillou & Klingelhoefer, 2013b; Marcaillou & Klingelhoefer, 2016; Laigle et al., 2007; Klingelhoefer & Marcaillou, 2022), we characterized the nature of the crust, the margin temperature, circulating fluid pathways, and the geometry of the main structural interfaces and faults of both the forearc and prism domains. The new constraints obtained on these different elements has helped to answer the questions that was raised in this study. We propose that fluids associated to structural heterogeneities (ridges and faults) strongly impact 1/ the subduction thermal structure, generating thermal anomalies compared to the conductive heat transfer, 2/ the seismogenic behaviour by locally decreasing the interplate coupling, and 3/ the margins tectonic deformation, inducing subsidence and erosion of the margin. The results are summarized in the following sections.

### **5.0.1 Tectonically-dominated oceanic crust in the Northern Lesser Antilles**

MCS and bathymetric data highlight strong heterogeneities between the oceanic crust of the Jacksonville patch, and those located northwest and southeast of this patch. The oceanic crust at the trench, northwest and southeast of the patch present structural and morphological characteristics, which are similar to a typical layer 2/3 magmatic crust found in oceanic crust at other subduction zones worldwide. Contrastingly, in the patch, we observe distinct reflection patterns in the oceanic crust, which occur as Ridgeward-Dipping-Reflectors (RDRs) based on estimations of their true dip directions (N60° - 90°E). Wide-Angle Seismic velocity model reveals that the basement in this patch show a single layer velocity from top to bottom with a constant velocity gradient. This crust is interpreted to correspond to exhumed and serpentized rocks, formed at the tectonically dominated portion of the slow-spreading Mid-Atlantic Ridge. Based on the RMS amplitude analysis, we show that the RDRs represent widespread pervasive detachment faults, which formed at the ridge axis and might be reactivated during plate bending to favour fluid percolation, rock alterations, and serpentization reactions. These pervasive detachment faults have a different orientation than the so-called plate-bending faults of the outer rise, which has similar orientation with the Jacksonville and 15-20 FZ lying almost parallel to the trench at that location. We envisage that the Jacksonville FZ is reactivated at the trench by plate bending, and so does the 15-20 FZ ~20–25 Ma ago (Braszus et al., 2021) due to their sub-parallel orientations to the trench. Serpentinized exhumed mantle rocks have been identified in the Puerto Rico trench by petrological analysis (Klein et al., 2017) and in the oceanic crust between Barracuda and Tiburon Ridges from Wide-Angle seismic imaging (Davy et al., 2020) Our study highlights for the first time, the presence of a tectonically dominated crust at the trench and beneath the margin front of a subduction zone.

### **5.0.2 Thermal structure of the margin**

The thermal modelling of the Lesser Antilles subduction zone is constrained with heat-flow data collected along two trench-normal profiles, at latitudes of 15-16°N and 18-19°N. This modelling shows that heat transfer anomalies across the margin is influenced by heat advection due to circulating fluids in a contrasted way between the two locations. At the Central Lesser Antilles (15-16°N), an insulated hydrothermal circulation dominates in the trench and the margin front, with warm fluid up-dip migration up to the trench, where thick and continuous trench sediments do not favour cold fluid percolation. In contrast, at the Northern Lesser Antilles (18-19°N), a ventilated hydrothermal circulation is active at two complementary sites: first, downward cold fluid percolation is possible along two plate-bending reactivated major



oceanic structures: first, the trench-parallel fracture zones such as the Jacksonville FZ, which presently deeply marks the sea-bottom morphology, or the Fifteen-Twenty FZ, 20-25 Myr ago (see movie of Braszus et al., 2021); second, the detachment faults in the trench promoting hydrothermal cooling in the margin front, and warm fluid upward migration at the forearc along deep-rooted faults causing hydrothermal warming in the forearc.

Compared to previous conductive models (Gutscher et al., 2013), modelling hydrothermal circulation results in an updip limit of the thermally-defined seismogenic zone located 10 km farther landward in the Northern Lesser Antilles, and 15 km seaward in the Central Lesser Antilles. Based on the depth of the forearc Moho which intersects the interplate fault at similar depths with the updip limits of the seismogenic zone (Hyndman et al., 1997), the crustal–crustal contact of the seismogenic portion in the north becomes almost non-existent. However, this estimation is only based on temperature in relation to chemical and mechanical changes associated with clay mineral transitions (Moore & Saffer, 2001). Considering the rough oceanic seafloor and low trench fill sediment subducting in the northern Lesser Antilles, we cannot rule out the possibility of a crustal-crustal contact.

### **5.0.3 Impact of subducting heterogeneities and associated fluids on seismogenesis**

At the northern Lesser Antilles margin, uneven spatial distribution and low seismic activities are recorded over a long period of time, with a seismic gap which likely exist between Barbuda and the Virgin Islands. Moreover, seismic coupling is still unresolved with diverging views of a coupled (e.g. Philibosian et al., 2022), to partially coupled (Manaker et al., 2008), and decoupled or low coupling plate interface (Symithe et al., 2015; van Rijsingen et al., 2021; van Rijsingen et al., 2022).

Based on the thermal model interpretations, the absence of thrust earthquakes at the interplate crustal part in this northern margin segment is likely due to the location of the updip limit (150°C) of the seismogenic zone that almost intersect with the forearc moho at depth. In addition, evidence of fluid circulation from heat-flow anomalies has established that at the Northern Lesser Antilles, the subduction of exhumed, serpentized mantle rocks and the 15-20 Fracture Zone hydrates the subduction zone at depth. Upward fluid circulation suggested by the thermal model will also contribute to unclamp the plate interface, favouring low interplate coupling.

Downdip of the subduction, the serpentized forearc mantle will favour stable sliding and aseismic slip (e.g. Hyndman et al., 1997). Although this hypothesis has been complicated by up

to Mw ~5 thrust earthquakes occurring at greater depths in the subduction zones, for instance in the Central Lesser Antilles (Laigle et al., 2013), the subduction of exhumed, serpentinized mantle portions at the top of the subducting plate will impede rupture nucleation or propagation (Scholz, 1998). Our study shows that with respect to the plate convergence direction, the location of the Jacksonville Patch is consistent with the portion of the margin where few seismic activities has been recorded and low interplate coupling (Manaker et al., 2008; Symithe et al., 2015; Van Rijnsingen et al., 2021; 2022) have been estimated in the Northern Lesser Antilles. Subduction of oceanic fabrics similar to the Jacksonville patch at depth likely favours stable sliding and contribute significantly to the megathrust weakness and low seismic activities of this region.

Thus, the interpretation developed in this thesis therefore suggests that, the combined influence of temperature, fluids and subducting heterogeneities strongly contribute to the low interplate seismicity and seismic gap of the Barbuda to Virgin Island segment, leading to seismological heterogeneities in the Northern Lesser Antilles.

At last, we identified depths of metamorphic dehydrations for composition of subducting oceanic crust that can vary from mid-oceanic basalts (Kirby et al., 1996; Hacker et al., 2003) to serpentinized exhumed mantle (Wunder & Schreyer, 1997; Ulmer & Trommsdorff, 1995; Ferrand, 2019). Within the slab at this cold subduction zone they are expected to occur at 70 – 80 km and 140 – 160 km respectively. Using seismicity distributions and models offshore Martinique in the Central Lesser Antilles, we show that these dehydration reactions within the slab and upper plate mantle correspond to the locations of intraslab and supraslab seismicity clusters, establishing the link between temperature, fluids, and seismicity.

#### **5.0.4 Tectonic impact of structural heterogeneities and associated fluids**

The data, modelling and interpretations included in this thesis suggest that the subduction of a heterogeneous basement, partly consisting of hydrated mantle rocks along detachment planes, plate-bending reactivated fracture zones, and topographic reliefs would trigger vigorous fluids circulation which invade the damaged forearc crust of the Northern Lesser Antilles subduction zone. Using MCS and bathymetric data, we analysed the structural features to understand the tectonic impacts of these subducting structural heterogeneities and associated fluid circulation.

At the trench, sediment thickness decreases from the north of the Barracuda Ridge to the Anegada Passage. We imaged a short frontal prism that decreases in width northwards, showing evidence of very short accretion that disappears northwest of the Jacksonville Patch. Thin

trench-fill sediments and rough oceanic seafloor creates frontal erosion of the margin that increases northwards. The low trench sedimentation rate is, at least partly, due to the uplift of the Barracuda and Tiburon Ridges that reduces northward migration of sediments from the South American Rivers (Westbrook, 1982). As a result, the trench fill is much thicker and seafloor smoother to the south of the Barracuda ridge (Pichot et al., 2012) than to the North. Forearc slope and taper angles that we calculated for the Northern Lesser Antilles lies within the values estimated for erosive margins (e.g. Clift & Vannucchi, 2004; Noda, 2016). We thus conclude that the margin north of the Barracuda Ridge in the Northern Lesser Antilles is erosive and differ from its counterpart in the south of Tiburon Rise, which is widely considered as an end-member accretionary margin.

MCS and bathymetric data along the forearc highlights several seafloor lineaments, with shallow and deep-rooted faults within the inner and outer forearc domains. The most significant being the N160° - N110° normal faults that form grabens and half grabens, with minor rotational blocks and collapsing. These faults follow the trend of the Barracuda Ridge, and their northward extent that disappears just northeast of the Antigua Valley likely marks the initiation of the Barracuda uplift beneath the forearc, 2.3 Myr ago (Pichot et al 2012). Consistently with the observations of fluid circulations from the heat-flow data, we imaged fluid related features on the MCS and bathymetry, such as fluid pipes, volcanoes and pockmarks on the seafloor, and reverse polarity along the decollement and deep structures. We established that the structural patterns in the forearc consisting of basement highs and deep-rooted faults favour the movement of fluids along pathways up to the seafloor, suggesting that the fluids originate from depths. At last, we record widespread margin subsidence similar to those of other studies (De Min et al., 2015; Boucard et al., 2021; Leclerc & Feuillet, 2019), which cannot be explained by the displacement along the normal faults only.

Following these observations, we conclude that the margin north of the Barracuda Ridge is undergoing subduction erosion, in which fluid hydrofracturing is likely to play a significant role. Although the Barracuda Ridge interacts with the margin north of the Lesser Antilles, our estimations based on the time of uplift according to (Pichot et al., 2012) suggests that it cannot be the cause of the erosion that began long before its initiation. However, the Tiburon Rise likely impacts with the margin and contributes to its erosion since Mid-Miocene. It acts as a barrier to northward sediment transport, allowing the development of rough seafloor. This roughness is enhanced northward by the sea-bottom morphology of the plate-blending reactivated, trench sub-parallel fracture zones, and favours both frontal and basal erosion.

## 5.1 Future work

The interpretations presented in this thesis focusses on describing the impact of subducting heterogeneities and fluid on the Northern Lesser Antilles margin tectonic deformation and seismogenesis. The results suggest that the combined influence of subducted oceanic fracture zones, patches of tectonically-dominated crust consisting of exhumed and hydrated mantle rocks, and fluid flow contribute significantly to low interplate coupling and low thrust earthquakes in this region. It further highlights that the subduction of ridges, rough oceanic basement, and vigorous fluid circulation favour frontal and basal erosion in this margin segment. Based on the results, one subduction feature that significantly impacts this margin seismicity and tectonic deformation are fluids brought in by the incoming plate. The RDRs and possibly the plate-bending reactivated oceanic Jacksonville FZ at the trench are sites for downward fluid percolations. Therefore, a possible future study target is to map their full outcropping extent at the basement top, and quantify their potential scarp (not impacting the seafloor morphology). In addition, the fluid content of these reactivated faults needs to be characterized.

Secondly, upward fluid migration along deeply-rooted faults are recorded within the overriding plate, and fluid-related features such as pockmarks and mud-volcanoes are present on the seafloor. Therefore, the nature and fluid contents of the overriding plate need to be investigated in order to estimate the fluid budget within this end member subduction zone.

The Manta-Ray campaign dataset which contains new dip MCS lines across the margin, high-resolution seismic lines in the forearc, and 3D ocean-bottom seismometer array before the trench at the oceanic domain will be useful for the purpose of these new investigations.

## References

- Boucard, M., Marcaillou, B., Lebrun, J. F., Laurencin, M., Klingelhoefer, F., Laigle, M., Lallemand, S., Schenini, L., Graindorge, D., Cornée, J. J., Münch, P., Philippon, M., & the, A. (2021). Paleogene V-Shaped Basins and Neogene Subsidence of the Northern Lesser Antilles Forearc. *Tectonics*, *40*(3), 1–18. <https://doi.org/10.1029/2020TC006524>
- Braszus, B., Goes, S., Allen, R., Rietbrock, A., Collier, J., Harmon, N., Henstock, T., Hicks, S., Rychert, C. A., Maunder, B., van Hunen, J., Bie, L., Blundy, J., Cooper, G., Davy, R., Kendall, J. M., Macpherson, C., Wilkinson, J., & Wilson, M. (2021). Subduction history of the Caribbean from upper-mantle seismic imaging and plate reconstruction. *Nature Communications*, *12*(1). <https://doi.org/10.1038/s41467-021-24413-0>
- Cannat, M., Sauter, D., Mendel, V., Ruellan, E., Okino, K., Escartin, J., Combier, V., & Baala, M. (2006). Modes of seafloor generation at a melt-poor ultraslow-spreading ridge. *Geology*, *34*(7), 605–608. <https://doi.org/10.1130/G22486.1>
- Clift, P., & Vannucchi, P. (2004). Controls on tectonic accretion versus erosion in subduction zones: Implications for the origin and recycling of the continental crust. *Reviews of Geophysics*, *42*(2). <https://doi.org/10.1029/2003RG000127>
- Cooper, G. F., Macpherson, C. G., Blundy, J. D., Maunder, B., Allen, R. W., Goes, S., Collier, J. S., Bie, L., Harmon, N., Hicks, S. P., Iveson, A. A., Prytulak, J., Rietbrock, A., Rychert, C. A., Davidson, J. P., Cooper, G. F., Macpherson, C. G., Blundy, J. D., Maunder, B., ... Wilson, M. (2020). Variable water input controls evolution of the Lesser Antilles volcanic arc. *Nature*, *582*(7813), 525–529. <https://doi.org/10.1038/s41586-020-2407-5>
- Davy, R. G., Collier, J. S., Henstock, T. J., Rietbrock, A., Goes, S., Blundy, J., Harmon, N., Rychert, C., Macpherson, C. G., Van Hunen, J., Kendall, M., Wilkinson, J., Davidson, J., Wilson, M., Cooper, G., Maunder, B., Bie, L., Hicks, S., Allen, R., ... Labahn, E. (2020a). Wide-Angle Seismic Imaging of Two Modes of Crustal Accretion in Mature Atlantic Ocean Crust. *Journal of Geophysical Research: Solid Earth*, *125*(6), 1–21. <https://doi.org/10.1029/2019JB019100>
- Davy, R. G., Collier, J. S., Henstock, T. J., Rietbrock, A., Goes, S., Blundy, J., Harmon, N., Rychert, C., Macpherson, C. G., Van Hunen, J., Kendall, M., Wilkinson, J., Davidson, J., Wilson, M., Cooper, G., Maunder, B., Bie, L., Hicks, S., Allen, R., ... Labahn, E. (2020b). Wide-Angle Seismic Imaging of Two Modes of Crustal Accretion in Mature Atlantic Ocean Crust. *Journal of Geophysical Research: Solid Earth*, *125*(6). <https://doi.org/10.1029/2019JB019100>
- De Min, L., Lebrun, J. F., Cornée, J. J., Münch, P., Léticée, J. L., Quillévéré, F., Melinte-Dobrinescu, M., Randrianasolo, A., Marcaillou, B., & Zami, F. (2015). Tectonic and sedimentary architecture of the Karukéra spur: A record of the Lesser Antilles fore-arc deformations since the Neogene. *Marine Geology*, *363*, 15–37. <https://doi.org/10.1016/j.margeo.2015.02.007>
- Escartín, J., Smith, D. K., Cann, J., Schouten, H., Langmuir, C. H., & Escrig, S. (2008). Central role of detachment faults in accretion of slow-spreading oceanic lithosphere. *Nature*, *455*(7214), 790–794. <https://doi.org/10.1038/nature07333>

- Ferrand, T. P. (2019). Seismicity and mineral destabilizations in the subducting mantle up to 6 GPa, 200 km depth. *Lithos*, 334–335, 205–230. <https://doi.org/10.1016/j.lithos.2019.03.014>
- Gutscher, M.-A., Westbrook, G. K., Marcaillou, B., Graindorge, D., Gailler, A., Pichot, T., & Maury, R. C. (2013). How wide is the seismogenic zone of the Lesser Antilles forearc? In *Bull. Soc. géol. France* (Vol. 184, Issue 2).
- Hacker, B. R., Peacock, S. M., Abers, G. A., & Holloway, S. D. (2003). Subduction factory 2. Are intermediate-depth earthquakes in subducting slabs linked to metamorphic dehydration reactions? *Journal of Geophysical Research: Solid Earth*, 108(B1). <https://doi.org/10.1029/2001jb001129>
- Hensen, C., Duarte, J. C., Vannucchi, P., Mazzini, A., Lever, M. A., Terrinha, P., Géli, L., Henry, P., Villinger, H., Morgan, J., Schmidt, M., Gutscher, M. A., Bartolome, R., Tomonaga, Y., Polonia, A., Gràcia, E., Tinivella, U., Lupi, M., Çağatay, M. N., ... Nuzzo, M. (2019). Marine transform faults and fracture zones: A joint perspective integrating seismicity, fluid flow and life. In *Frontiers in Earth Science* (Vol. 7, pp. 1–29). Frontiers Media S.A. <https://doi.org/10.3389/feart.2019.00039>
- Hyndman, R. D., Yamano, M., & Oleskevich, D. A. (1997). The seismogenic zone of subduction thrust faults. *Island Arc*, 6(3), 244–260. <https://doi.org/10.1111/j.1440-1738.1997.tb00175.x>
- Ildefonse, B., Blackman, D. K., John, B. E., Ohara, Y., Miller, D. J., MacLeod, C. J., Abe, N., Abratis, M., Andal, E. S., Andréani, M., Awaji, S., Beard, J. S., Brunelli, D., Charney, A. B., Christie, D. M., Delacour, A. G., Delius, H., Drouin, M., Einaudi, F., ... Zhao, X. (2007). Oceanic core complexes and crustal accretion at slow-spreading ridges. *Geology*, 35(7), 623–626. <https://doi.org/10.1130/G23531A.1>
- Kirby, S., Engdahl, E. R., & Denlinger, R. (1996). Intermediate-depth intraslab earthquakes and arc volcanism as physical expressions of crustal and uppermost mantle metamorphism in subducting slabs. *Geophysical Monograph Series*, 96, 195–214. <https://doi.org/10.1029/GM096p0195>
- Klein, F., Marschall, H. R., Bowring, S. A., Humphris, S. E., & Horning, G. (2017). Mid-ocean ridge serpentinite in the Puerto Rico Trench: From seafloor spreading to subduction. *Journal of Petrology*, 58(9), 1729–1754. <https://doi.org/10.1093/petrology/egx071>
- Klingelhoefer, F., & Marcaillou, B. (2022). *MANTA-RAY* cruise, *RV L'Atalante*. <https://doi.org/https://doi.org/10.17600/18002498>
- Laigle, M., Hirn, A., Sapin, M., Bécel, A., Charvis, P., Flueh, E., Diaz, J., Lebrun, J. F., Gesret, A., Raffaele, R., Galvé, A., Evain, M., Ruiz, M., Kopp, H., Bayrakci, G., Weinzierl, W., Hello, Y., Lépine, J. C., Viodé, J. P., ... Nicolich, R. (2013). Seismic structure and activity of the north-central Lesser Antilles subduction zone from an integrated approach: Similarities with the Tohoku forearc. In *Tectonophysics* (Vol. 603, pp. 1–20). <https://doi.org/10.1016/j.tecto.2013.05.043>
- Laigle, M., Lebrun, J.-F., & Hirn, A. (2007). *SISMANTILLES 2* cruise, *RV L'Atalante*. <https://doi.org/https://doi.org/10.17600/7010020>

- Leclerc, F., & Feuillet, N. (2019). *Quaternary coral reef complexes as powerful markers of long-term subsidence related to deep processes at subduction zones : Insights from Les Saintes ( Guadeloupe , French West Indies )*. 15(4), 983–1007.
- Manaker, D. M., Calais, E., Freed, A. M., Ali, S. T., Przybylski, P., Mattioli, G., Jansma, P., Prépetit, C., & De Chabaliér, J. B. (2008). Interseismic plate coupling and strain partitioning in the Northeastern Caribbean. *Geophysical Journal International*, 174(3), 889–903. <https://doi.org/10.1111/j.1365-246X.2008.03819.x>
- Marcaillou, B., & Klingelhoefer, F. (2013a). *ANTITHESIS-1-Leg1 Cruise, RV L'Atalante*. <https://doi.org/doi:10.17600/13010070>
- Marcaillou, B., & Klingelhoefer, F. (2013b). *ANTITHESIS-1-Leg2 Cruise, RV Pourquoi Pas?* <https://doi.org/doi:10.17600/13030100>
- Marcaillou, B., & Klingelhoefer, F. (2016). *ANTITHESIS-3 Cruise, RV Pourquoi Pas?* <https://doi.org/doi:10.17600/16001700>
- Marcaillou, B., Klingelhoefer, F., Laurencin, M., Lebrun, J.-F., Laigle, M., Lallemand, S., Schenini, L., Gay, A., Boucard, M., Ezenwaka, K., & Graindorge, D. (2021). Pervasive detachment faults within the slow spreading oceanic crust at the poorly coupled Antilles subduction zone. *Communications Earth & Environment*, 2(1). <https://doi.org/10.1038/s43247-021-00269-6>
- Noda, A. (2016). Forearc basins: Types, geometries, and relationships to subduction zone dynamics. *Bulletin of the Geological Society of America*, 128(5–6), 879–895. <https://doi.org/10.1130/B31345.1>
- Patriat, M., Pichot, T., Westbrook, G. K., Umler, M., Deville, E., Bénard, F., Roest, W. R., & Loubrieu, B. (2011). Evidence for Quaternary convergence across the North America-South America plate boundary zone, east of the Lesser Antilles. *Geology*, 39(10), 979–982. <https://doi.org/10.1130/G32474.1>
- Philibosian, B., Feuillet, N., Weil-Accardo, J., Jacques, E., Guihou, A., Mériaux, A. S., Anglade, A., Saurel, J. M., & Deroussi, S. (2022). 20th-century strain accumulation on the Lesser Antilles megathrust based on coral microatolls. *Earth and Planetary Science Letters*, 579, 117343. <https://doi.org/10.1016/j.epsl.2021.117343>
- Pichot, T., Patriat, M., Westbrook, G. K., Nalpas, T., Gutscher, M. A., Roest, W. R., Deville, E., Moulin, M., Aslanian, D., & Rabineau, M. (2012). The Cenozoic tectonostratigraphic evolution of the Barracuda Ridge and Tiburon Rise, at the western end of the North America-South America plate boundary zone. *Marine Geology*, 303–306, 154–171. <https://doi.org/10.1016/j.margeo.2012.02.001>
- Scholz, C. H. (1998). Earthquakes and friction laws. In *NATURE* (Vol. 391).
- Symithe, S., Calais, E., De Chabaliér, J. B., Robertson, R., & Higgins, M. (2015). Current block motions and strain accumulation on active faults in the Caribbean. *Journal of Geophysical Research: Solid Earth*, 120(5), 3748–3774. <https://doi.org/10.1002/2014JB011779>

- Szitkar, F., Dymant, J., Petersen, S., Bialas, J., Klischies, M., Graber, S., Klaeschen, D., Yeo, I., & Murton, B. J. (2019). Detachment tectonics at Mid-Atlantic Ridge 26°N. *Scientific Reports*, 9(1), 0–8. <https://doi.org/10.1038/s41598-019-47974-z>
- Ulmer, P., & Trommsdorff, V. (1995). Serpentine stability to mantle depths and subduction-related magmatism. *Science*, 268(5212), 858–861. <https://doi.org/10.1126/science.268.5212.858>
- van Rijsingen, E. M., Calais, E., Jolivet, R., de Chabalier, J. B., Jara, J., Symithe, S., Robertson, R., & Ryan, G. A. (2021). Inferring Interseismic Coupling Along the Lesser Antilles Arc: A Bayesian Approach. *Journal of Geophysical Research: Solid Earth*, 126(2), 1–21. <https://doi.org/10.1029/2020JB020677>
- van Rijsingen, E. M., Calais, E., Jolivet, R., de Chabalier, J.-B., Robertson, R., Ryan, G. A., & Symithe, S. (2022). Ongoing tectonic subsidence in the Lesser Antilles subduction zone. *Geophysical Journal International*, 319–326. <https://doi.org/10.1093/gji/ggac192>
- Westbrook, G. K. (1982). The Barbados Ridge Complex: Tectonics of a mature forearc system. *Geological Society Special Publication*, 10(Saunders 1979), 275–290. <https://doi.org/10.1144/GSL.SP.1982.010.01.18>
- Wunder, B., & Schreyer, W. (1997). Antigorite: High-pressure stability in the system MgO-SiO<sub>2</sub>-H<sub>2</sub>O (MSH). *Lithos*, 41(1–3), 213–227. [https://doi.org/10.1016/s0024-4937\(97\)82013-0](https://doi.org/10.1016/s0024-4937(97)82013-0)